Universidade do Minho
Escola de Ciências

Joana Catarina Pereira Guedes

Studies on apoptosis regulation: the role of N-terminal acetylation and the N-degron pathways

june de 2022

Studies on apoptosis regulation: the role of N-terminal acetylation and the N-degron pathways
Joana Catarina Pereira Guedes
UMinho | 2022

Universidade do Minho
Escola de Ciências

Joana Catarina Pereira Guedes

Studies on apoptosis regulation: the role of N-terminal acetylation and the N-degron pathways

Doctoral Thesis in Biology
Doctoral Program in Molecular and Environmental Biology
Branch of Cellular Biology and Health

Work supervised by:
Professora Doutora Manuela Côrte-Real
Doutor Rafael Aldabe

june de 2022

ACKNOWLEDGEMENTS

Quase a terminar uma longa e importante etapa, existem muitas pessoas a quem tenho e devo agradecer por de uma forma ou de outra terem sido essenciais ao longo desta caminhada.

À minha orientadora, professora Manuela Côrte-Real, por tudo o que deu de si por mim nesta tese. Por todas as horas no zoom a partilhar conhecimento, por todo o apoio mesmo quando estava em Espanha, e, sobretudo, porque sempre me mostrou que tudo valia pena e nunca me deixou baixar os braços. Sou imensamente grata em tê-la como orientadora! Ao meu co-orientador, Rafael Aldabe, muchas gracias por haberme recibido en Pamplona y por todo lo que me has enseñado en el labo. Muchas gracias por siempre te preocupares por mí... ha sido un placer trabajar contigo. Obrigada por confiarem no meu trabalho e por toda a disponibilidade, fosse semana ou fim-de-semana. Muito, muito obrigada! O mérito é também vosso.

Não posso deixar de agradecer à professora Susana, por todo o apoio e por todo o seu contributo nesta tese sempre com ideias e críticas construtivas. Quero também agradecer à Carmela Giglione e toda a equipa, que tão prontamente se disponibilizaram a ajudar-nos com toda a parte da proteómica. Não menos importante, ao Stéphen, por estar sempre disponível para nos ajudar mesmo na incerteza do resultado final. Muito obrigada!

Agradeço também à Fundação para a Ciência e Tecnologia pelo financiamento através das bolsas SFRH/BD/132070/2017 e COVID/BD/151956/2021.

E como sozinhos nunca somos ninguém, por detrás desta tese houve toda uma equipa e uma rede de apoio que sempre me suportou. Aos meus colegas da Micro I, em especial à Fi, Cátia, Vitória e ao António, agradeço a partilha, o espírito de equipa, a boa disposição e por verem sempre algo positivo mesmo num mau resultado. Um obrigado muito especial ao Gusto e à Clau, os meus parceirões deste PhD, por sermos porto de abrigo uns dos outros nesta aventura. A todas as outras pessoas do DB pela constante entreajuda e todos os sorrisos trocados nos corredores que, por vezes, tanta força davam. Obrigada ao CBMA e a todo o pessoal técnico por me terem acolhido, em especial ao Sr. Luís que tantos balões de meio autoclavou às 8h30 da manhã para que nunca me faltasse nada para trabalhar, e à Inês, à Dona Manuela e Dona Isabel. A mis compis del labo 4.04, que durante 1 año y 8 meses me recibieron como sí siempre hubiera pertenecido allí. ¡Agradezco todo lo bien que me han hecho, la ayuda en el labo y por todos las cerves y copas que nos tomamos fuera del trabajo! Muchas gracias a Jasmine y Bea, por todas las horas enseñándome todo y por toda la ayuda para que el proyecto salga adelante. A mi Andrea,

le tengo que dar las gracias, por tanto. Ha sido mi mayor apoyo en el labo (y fuera), nunca me ha largado da mano, y fue la mejor partner que podría haber pedido.

E porque rodearmo-nos de amigos torna tudo muito mais fácil, posso orgulhosamente dizer que tenho os melhores. Devo-lhes a minha sanidade mental! Gabo-lhes a paciência que sempre tiveram para me aturarem e ser-lhes-ei eternamente grata por tudo. Ao "Gang Machado" Fi, TT, Cátia, Matias, Beli, Taxti, Nuno, António, Carlinha, Rita; às "Nódoas" Fi, Gusto, Anabela, Clau; às "Choquinhas" Fi e Catarina; aos meus afilhadinhos Pipa, Balta e Tiago; ao Flores e ao Ginger; aos grossos da Supremus Crossfit; aos "Los de Siempre" y a mis chicas bonitas Andrea, Aina e Montse. Obrigada por fazerem parte da minha vida e por serem luz no meu caminho.

Porque o melhor fica sempre para o fim, tenho também de agradecer a toda a minha família. Somos o que somos pelos pilares que temos por detrás de nós e eu tenho um orgulho imenso em fazer parte desta superfamília. Obrigada a todos, tios, primos, padrinhos, tiveram todos sem exceção um grande contributo neste caminho. Em especial, aos meus pais, sou-lhes imensamente grata por todos os valores e educação que me deram e, mesmo não entendendo bem esta profissão, sempre me apoiaram e sempre me deram colo quando precisava. Ao Zé, meu mano crescido, obrigada por te preocupares sempre comigo, por me entenderes cada vez melhor. Não esquecerei nunca a tua visita quando estava em Pamplona! Ao meu avôzinho, tenho-lhe um amor que não cabe em mim e é a minha maior inspiração.

Obrigada a todos vocês que tornaram este caminho mais fácil e a chegada mais prazerosa!

A todos vocês, dedico este trabalho.

STATEMENT OF INTEGRITY

I hereby declare having conducted this academic work with integrity. I confirm that I have not used plagiarism or any form of undue use of information or falsification of results along the process leading to its elaboration.

I further declare that I have fully acknowledged the Code of Ethical Conduct of the University of Minho.

ABSTRACT

STUDIES ON APOPTOSIS REGULATION:

THE ROLE OF N-TERMINAL ACETYLATION AND THE N-DEGRON PATHWAYS

N-terminal (Nt)-acetylation has arisen as a highly multifunctional protein modification. The eight currently known eukaryotic N-terminal acetyltransferases (NATs) mediate Nt-acetylation of a wide range of proteins, resulting in the Nt-acetylome. NatB, composed of the catalytic subunit Naa20 and the auxiliary subunit Naa25, is after NatA the second major contributor to the Nt-acetylome. In spite of the well-known role of NatB-mediated Nt-acetylation on biological processes, such as actin cytoskeleton and cell proliferation, its impact on apoptosis is still poorly elucidated, in particular regarding its effect on protein stability and degradation through the recognition of specific residues at the N-terminus. Herein, we sought to assess the impact of NatB-mediated Nt-acetylation on apoptosis regulation. We show that inactivation of the NatB catalytic subunit Naa20 in mouse embryonic fibroblasts (MEFs) reduces the Nt-acetylation of about one third of the identified NatB substrates. As the inactivation of Naa20 is unable to eliminate Nt-acetylation of NatB substrates, another enzyme or paralog likely fills its absence. Moreover, $Naa20^{-/-}$ MEFs exhibit a significant reduction in protein levels of procaspase-8, -9, -3 and of Bid, associated with a decreased susceptibility to etoposide and TNF-α plus SMAC/DIABLO mimetics that, in this later case, was partially reverted by silencing the E3 ubiquitin protein ligase UBR4, a N-recognin of the Arg/N-degron pathway. We also show through an *in silico* systematic search that the main apoptotic components are NATs and N-recognins substrates, suggesting a complex interplay between Nt-acetylation and degradation by N-degron pathways with a relevant impact on apoptosis modulation. Additionally, a novel yeast-based system to study Bax regulation under conditions mimicking its function in the cellular context, was developed. Cell death in response to acetic acid was reverted by Bcl-xL, but not by its truncated form Bcl-xLΔC. Yet, in the absence of NatB-mediated Nt-acetylation, Bax was unstable, and though Bcl-xL protects Bax from degradation it does not protect cells from the loss of plasma membrane integrity. Altogether, the work developed brought novel insights supporting the relevance of NatB-mediated Nt-acetylation for cellular proteostasis and proper function of apoptosis.

Keywords: Apoptosis, NatB, N-degron pathways, N-terminal acetylation

RESUMO

ESTUDOS SOBRE A REGULAÇÃO DA APOPTOSE:

O PAPEL DA ACETILAÇÃO E DAS VIAS DE DEGRADAÇÃO N-TERMINAL

A acetilação N-terminal tem surgido como uma modificação proteica altamente multifuncional. As oito acetiltransferases (NATs) atualmente conhecidas em eucariotas medeiam a acetilação de uma vasta gama de proteínas no seu N-terminal, resultando no acetiloma. A NatB, composta pela subunidade catalítica Naa20 e pela subunidade auxiliar Naa25, é a seguir à NatA, a que mais contribui para o acetiloma. Apesar do seu conhecido papel em vários processos celulares, como o citoesqueleto de actina e proliferação celular, o seu impacto na apoptose está ainda pouco elucidado, em particular o seu efeito na estabilidade e degradação de proteínas através do reconhecimento de resíduos específicos no seu N-terminal. Nesta tese, procurámos avaliar o impacto da acetilação N-terminal mediada pela NatB na regulação da apoptose. Dado que a inativação da Naa20 em fibroblastos embrionários de rato (MEFs) reduziu apenas para cerca de um terço a acetilação do N-terminal dos substratos da NatB identificados, outra enzima ou parálogo deve colmatar a sua ausência. Além disso, Naa20$^{-/-}$ MEFs exibiram uma redução significativa nos níveis de procaspase-8, -9 e -3 e de Bid, associada a uma diminuição da suscetibilidade das células ao etoposídeo e TNF-α suplementado com SMAC/DIABLO que, neste último caso, foi parcialmente revertida através do silenciamento da E3 ubiquitin ligase UBR4, uma N-recognina da via de degradação Arg. Através de uma pesquisa sistemática *in silico*, mostrámos que os principais componentes das vias apoptóticas são substratos das NATs e das N-recogninas, suportando uma relação complexa entre a acetilação N-terminal e a degradação pelas vias N-degron com impacto na modulação da apoptose. Foi ainda desenvolvido um sistema para estudar a regulação de Bax na levedura em condições que mimetizam a sua função em contexto celular. A morte celular em resposta ao ácido acético foi revertida pela Bcl-xL, mas não pela Bcl-xLΔC. Contudo, na ausência de acetilação mediada pela NatB, Bax mostrou-se instável e, embora a Bcl-xL proteja Bax da degradação, não protege as células da perda de integridade da membrana plasmática. Resumindo, o trabalho trouxe novos conhecimentos que suportam a importância da acetilação mediada pela NatB na proteostase celular e correto funcionamento da apoptose.

Palavras-chave: Apoptose, NatB, Vias dos N-degrons, Acetilação N-terminal

TABLE OF CONTENTS

OUTPUTS

Peer-reviewed publications

- Joana P. Guedes*, Vitória Baptista*, Cátia Santos-Pereira, Maria João Sousa, Stéphen Manon, Susana R. Chaves, Manuela Côrte-Real (2022) Acetic acid triggers cytochrome *c* release in yeast heterologously expressing human Bax. *Apoptosis*. doi: 10.1007/s10495-022-01717-0

  *Both authors contributed equally

- Joana P. Guedes*, Jean Baptiste Boyer*, Jasmin Elurbide*, Beatriz Carte, Virginie, Laila, Thierry Meinnel, Carmela Giglione, Manuela Côrte-Real#, Rafael Aldabe#. NatB-mediated Nt-acetylation warrants cellular proteostasis and proper function of apoptosis *(manuscript in preparation).*

  *# authors contributed equally

- Joana P. Guedes, Manuela Côrte-Real. Interplay between Nt-acetylation and N-degron pathways in the modulation of apoptosis *(manuscript in preparation).*

Oral communications

- Joana P. Guedes, Manuela Côrte-Real, Rafael Aldabe (2021) "Unveiling the role of NatB-mediated N-terminal acetylation in apoptosis regulation". II International Meeting of the Portuguese Society of Genetics (IMPSG), Vila Real, Portugal.

Poster communications

- Joana Guedes, Vitória Baptista, Cátia Pereira, Maria João Sousa, Stéphen Manon, Susana Chaves, Manuela Côrte-Real (2021) "Acetic acid as a trigger to activate human Bax heterologously expressed in yeast". 15th International Congress on Yeasts meets the 30th International Conference on Yeast Genetics and Molecular Biology (ICY 15 meets 30 ICYGMB), August, Vienna, Austria.

Other activities

- Joana P. Guedes, Rafael Aldabe, Manuela Côrte-Real (2021) "Bax regulation by N-terminal acetylation in yeast and MEFs cells". Seminar presentation, 12th Edition of the Advanced course on "Mammalian and Yeast as Complementary Cell Models in Programmed Cell Death and Autophagy", Braga, Portugal

Internship abroad

- Centro de Investigación Médica Aplicada (CIMA), Universidad de Navarra; February 4st 2019 – October 2nd 2020, Pamplona, Spain

Peer-reviewed scientific publications, oral and poster communications not included in this thesis:

- Cátia Santos-Pereira, Joana P. Guedes, Débora Ferreira, Lígia R. Rodrigues, Manuela Côrte-Real (2022) Lactoferrin perturbs intracellular trafficking, disrupts cholesterol-rich lipid rafts and inhibits glycolysis of highly metastatic cancer cells harbouring plasmalemmal V-ATPase *(submitted to International Journal of Biological Macromolecules).*
- Joana P. Guedes, Cátia S. Pereira, Lígia R. Rodrigues, Manuela Côrte-Real (2017) "Molecular mechanism underlying the anticancer activity of Lactoferrin in highly metastatic cancer cell lines". 2nd Joint Workshop of the PhD Programs in Applied and Environmental Microbiology (DP_AEM) and Molecular and Environmental Biology (PDBMA), Braga, Portugal *(oral communication).*
- Joana P. Guedes, Cátia S. Pereira, Lígia R. Rodrigues and Manuela Côrte-Real (2018) "The highly metastatic prostate cancer PC-3 and osteosarcoma MG-63 cell lines are sensitive to bovine lactoferrin". IV Symposium of the Doctoral Program in Applied and Environmental Biology, Braga, Portugal *(poster presentation).*

LIST OF ABBREVIATIONS

7-AAD	7-Amino-Actinomycin D
Ac-CoA	Acetyl-Coenzyme A
ACN	Acetonitrile
Ad5CMVCre	Recombinant adenovirus expressing Cre recombinase
AdEmpty	Adenovirus Empty
AKT	Protein Kinase B
APAF1	Apoptotic Protease-Activating factor 1
ATE1	Arginyl-tRNA-protein Transferase 1
Aβ	β-Amyloid Peptide
BSA	Bovine Serum Albumin
CFUs	Colony Forming Units
cyt *c*	cytochrome *c*
DIAP1	*Drosophila melanogaster* Inhibitor of Apoptosis 1
DMEM	Dulbecco's Modified Eagle Medium
EDTA	Ethylenediamine Tetraacetic Acid
EGTA	Ethylene Glycol Tetraacetic Acid
ER	Endoplasmic Reticulum
ERK	Extracellular signal-Regulated Kinase
EV	Empty Vector
FA	Formic Acid
FBS	Fetal Bovine Serum
FDR	False Discovery Rate
GSK3β	Glycogen Synthase Kinase 3β
HYPK	Huntingtin-interacting protein K
IAP	Inhibitor of Apoptosis
iMet	initiator Methionine
KO	Knockout
LFQ	label free quantification
MEFs	Mouse Embryonic Fibroblasts

MetAPs	Methionine Aminopeptidases
MOM	Mitochondrial Outer Membrane
MOMP	Mitochondrial Outer Membrane Permeabilization
MS	Mass Spectrometry
MYL9	Myosin regulatory light chain 9
NATs	N-terminal Acetyltransferases
NME	N-terminal methionine excision
NO	Nitric Oxide
NTA or **Nt-acetylation**	N-terminal acetylation
Ntan1	N-terminal asparagine deamidase 1
Ntaq1	N-terminal glutamine deamidase 1
OD640	Optical Density at 640 nm
P/S	Penicillin/Streptomycin
PBS	Phosphate-Buffered Saline
PBST	Phosphate-Buffered Saline with 0.1% Tween® 20 detergent
PCR	Polymerase Chain Reaction
PFN2	Profilin 2
PGK1	Phosphoglycerate kinase 1
PI	Propidium Iodide
PKCξ	Protein Kinase Cξ
PMSF	Phenylmethylsulfonyl fluoride
PS	Phosphatidylserine
PTMs	Post-Translational Modifications
PVDF	Polyvinylidene Difluoride
ROS	Reactive Oxygen Species
RT	Room Temperature
SCX-LC	Solid Cation Exchange-Liquid Chromatography
SDS	Sodium Dodecyl Sulfate
SILProNAQ	Stable Isotope Labelling Protein N-terminal Acetylation Quantification
SMAC/DIABLO	Second mitochondria-derived activator of caspase/Direct inhibitor of apoptosis-binding protein
t-BID	truncated BID

TBST	Tris-Buffered Saline with 0.1% Tween® 20 detergent
TNF-α	Tumor necrosis factor-alpha
UBR	Ubiquitin protein ligase
WT	Wild Type
YPD	Yeast Extract-Peptone-Dextrose

LIST OF FIGURES

LIST OF TABLES

CHAPTER 1

Motivation, Aims and Thesis Outline

1.1. Motivation

N-terminal (Nt)-acetylation has been established as a highly abundant and multifunctional protein modification, acetylating a wide range of proteins. In fact, your favourite protein is most probably Nt-acetylated in its N-terminus [1,2]. Actually, owing to several advances in the field, this protein modification is no longer viewed as a negligible modification, but instead it has become of great interest, emerging as a crucial component in many biological pathways. Apoptosis, a type of regulated cell death conserved across eukaryotic organisms, is crucial to ensure the maintenance of normal physiology and tissue function by elimination of damaged, dysfunctional or unnecessary cells [3,4]. However, despite its beneficial biological role, unbalanced apoptosis has been implicated in a diversity of abnormal functions and in the progression and development of diseases. For instance, Parkinson's and Alzheimer's diseases, as well as the development of cancer result from an excessive or deficient apoptosis, respectively. Therefore, to avoid the occurrence of these diseases and maintain cellular homeostasis, the proper function and regulation of apoptosis is of paramount importance. Although in recent years Nt-acetylation has been implicated in apoptosis, whether and how this protein modification can be exploited to regulate this key cellular process is far from an answer.

Another emerging hot topic is the relation between Nt-acetylation and protein degradation by N-degron pathways. It has always been widely known that Nt-acetylation is involved in the protein stability and turnover [5–8]. The discovery that both unacetylated or acetylated destabilizing residues in the protein N-terminus (N-degrons) and the creation of conditional N-degrons brought into debate how N-acetylation and degradation via N-degron pathways warrant cellular proteostasis. Despite several studies showed that Nt-acetylation or N-degron pathways can individually affect the apoptotic cell death, the impact of their interplay on apoptosis regulation is far from being elucidated. Aiming to understand how these processes can interact to regulate apoptosis, we thus sought to further exploit the interplay between Nt-acetylation and N-degron pathway and predict its impact on apoptosis modulation.

As curiosity, this year will take place an EMBO workshop entitled "Protein termini: From mechanisms to biological impact", where topics like protein N-termini and its major roles in proteostasis and as biological regulators will be discussed. This highlights how emerging and relevant these issues are.

1.2. Aims

The increasing relevance of Nt-acetylation in several biological processes has rendered this protein modification of great interest. Given the lack of extensive studies around the NatB-mediated Nt-

acetylation and apoptosis, and taking into account that the link between Nt-acetylation and protein degradation is an emerging hot topic, the main research aims of this thesis were:

- to cover the *in vivo* NatB N-terminome and proteome in Naa20$^{-/-}$ Mouse Embryonic Fibroblasts (MEFs) lacking the catalytic subunit NAA20 by performing a quantitative N-terminomic and proteomic analysis;
- to elucidate how Nt-acetylation impacts cellular proteostasis, and in particular apoptosis, by studying its effect on the main apoptotic proteins and cell susceptibility to different apoptotic stimuli, in Naa20$^{-/-}$ MEFs;
- to predict the impact of the interplay between Nt-acetylation and N-degron pathways on apoptosis modulation by performing an *in silico* systematic analysis to assess the potential of the main apoptotic proteins to be Nt-acetylated and degraded by N-degron pathways;
- to further highlight the mechanisms underlying Bax regulation under conditions mimicking the natural Bax function in the cellular context by addressing Bax activation and its interaction with its regulators such as Bcl-xL, Bcl-xLΔC and Rim11p in yeast cells expressing human Bax;
- to dissect the role of Bax Nt-acetylation on its stability, interaction with Bcl-xL and on acetic acid-induced death of yeast cells expressing human Bax.

1.3. Thesis Outline

The present thesis was structured in the following chapters (Figure 1.1):

- **Chapter 1:** provides an overview of the motivation, aims and the outline of the thesis.
- **Chapter 2:** presents a comprehensive overview on the different topics covered in the present thesis. It starts with a brief explanation of the Nt-acetylation followed by a detailed description regarding the N-terminal acetyltransferases (NATs), their biological significance, regulation, and crosstalk with other protein modifications, as well as the relation between Nt-acetylation and degradation by the N-degron pathways. Afterwards, the state of the art on apoptosis and on its regulation is provided. Finally, the interplay between Nt-acetylation and apoptosis, and between N-degron pathways and apoptosis is included.
- **Chapter 3:** describes the study performed to assess the impact of NatB-mediated Nt-acetylation on cellular proteostasis and proper function of apoptosis. MEFs depleted for the NatB catalytic subunit NAA20 were generated for the first time, and used to perform a quantitative N-

terminomics and proteomic analysis. The effect of NAA20 inactivation on actin cytoskeleton, cell proliferation, and more specifically on apoptosis is covered. The results described in this chapter unveil new clues on the interplay between NatB-mediated Nt-acetylation and the Arg/N-degron pathway on apoptosis modulation. These findings may pave the way towards novel therapeutic strategies for diseases associated with apoptosis dysfunctions.

- **Chapter 4:** presents an *in silico* systematic search towards the main components of the apoptotic machinery in order to assess the potential impact of Nt-acetylation and N-degron pathways and of their interplay on apoptosis regulation. Full-length proteins as well as their fragments generated by caspase- or calpain-mediated proteolytic cleavage are evaluated regarding their potential to be targets of Nt-acetylation and of degradation via N-degron pathways. Herein, novel insights on the high complexity of the interplay between the Nt-acetylation and degradation by N-degron pathways, and of its impact on apoptosis modulation are discussed.

- **Chapter 5:** includes de work performed to develop a yeast model to further understand the regulation of Bax under conditions closely resembling the natural Bax function in the cellular context. Heterologous expression of human wild type Bax in yeast *Saccharomyces cerevisiae* was used to study the activation of Bax in response to an exogenous stimulus, and assess Bax interaction with its regulators. A novel simple yeast-based system for ectopic Bax expression, associated with the Bax-mediated cyt *c* release in response to a sub-lethal dose of acetic acid, was developed. This tool will allow to screen for novel Bax regulators.

- **Chapter 6:** the role of Nt-acetylation of Bax mediated by Nat3p on the regulation of Bax function is ascertained. *S. cerevisiae* lacking Nat3p is used as a model organism to study the stability of Bax, of its interaction with Bcl-xL as well as of the susceptibility of Bax expressing cells to a sub-lethal concentration of acetic acid. The results obtained in this chapter contribute to decipher the impact of Bax Nt-acetylation on Bax function and its regulation and highlight the importance of the protein Nt-acetylation in cellular stress responses.

- **Chapter 7:** summarizes the conclusions of the work developed throughout this thesis and discusses future perspectives based on the open questions left by the present work.

- **Appendix:** at the end of the thesis, an appendix containing supplementary information is included.

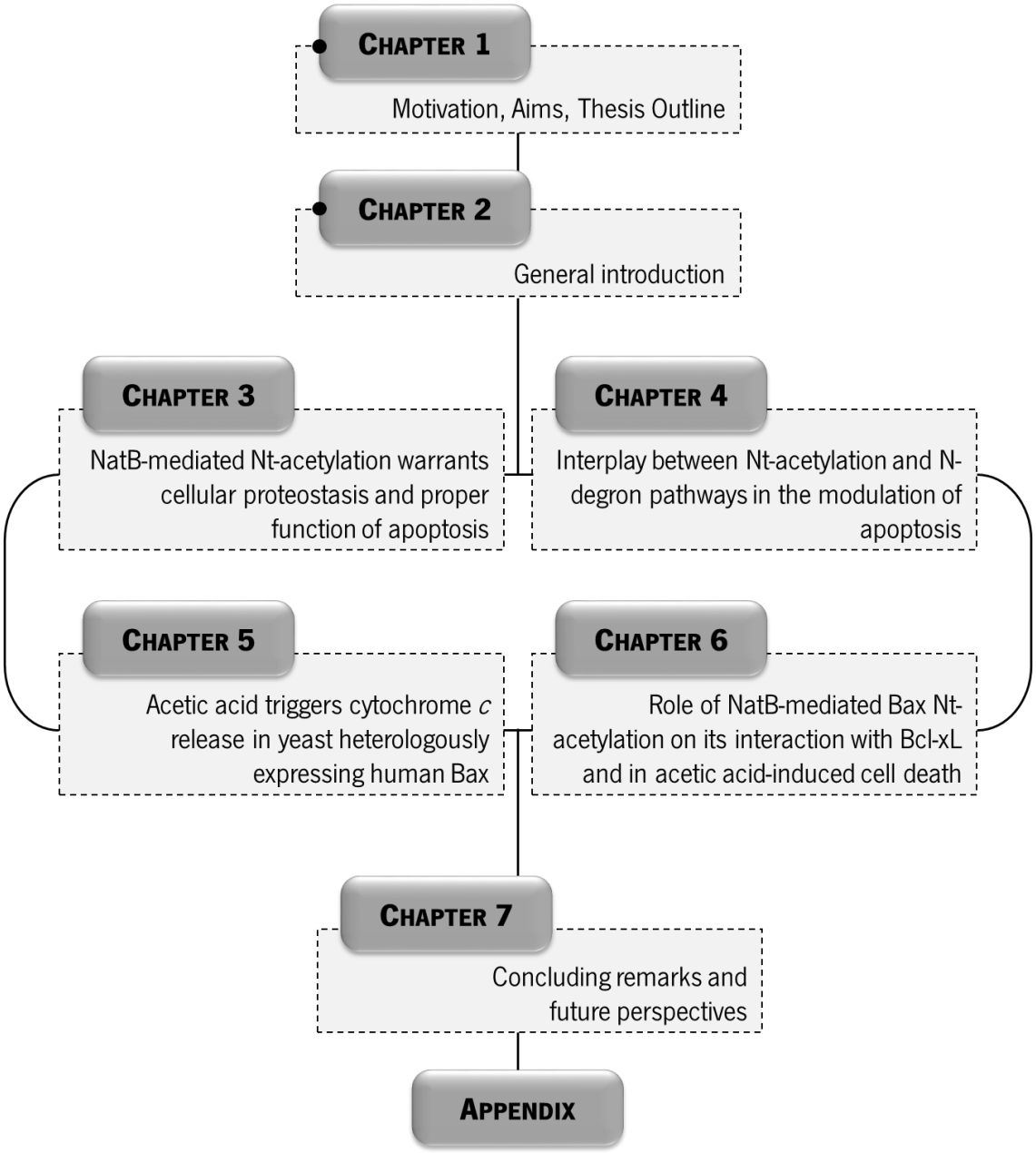

Figure 1.1: Schematic overview of the thesis outline.

References

1. Deng S, Marmorstein R. Protein N-Terminal Acetylation: Structural Basis, Mechanism, Versatility, and Regulation. Trends Biochem Sci. 2021;46: 15–27. doi:10.1016/j.tibs.2020.08.005

2. Aksnes H, Ree R, Arnesen T. Co-translational, Post-translational, and Non-catalytic Roles of N-Terminal Acetyltransferases. Mol Cell. 2019;73: 1097–1114. doi:10.1016/j.molcel.2019.02.007

3. Bertheloot D, Latz E, Franklin BS. Necroptosis, pyroptosis and apoptosis: an intricate game of cell death. Cell Mol Immunol. 2021;18: 1106–1121. doi:10.1038/s41423-020-00630-3

4. Galluzzi L, Vitale I, Aaronson SA, Abrams JM, Adam D, Agostinis P, et al. Molecular mechanisms of cell death: Recommendations of the Nomenclature Committee on Cell Death 2018. Cell Death

Differ. 2018;25: 486–541. doi:10.1038/s41418-017-0012-4

5. Hershko A, Heller H, Eytan E, Kaklij G, Rose IA. Role of the α-amino group of protein in ubiquitin-mediated protein breakdown. Proc Natl Acad Sci U S A. 1984;81: 7021–7025. doi:10.1073/pnas.81.22.7021

6. Linster E, Forero Ruiz FL, Miklankova P, Ruppert T, Mueller J, Armbruster L, et al. Cotranslational N-degron masking by acetylation promotes proteome stability in plants. Nat Commun. 2022;13: 810(1–12). doi:10.1038/s41467-022-28414-5

7. Hwang CS, Shemorroy A, Varshavsky A. N-Terminal Acetylation of Cellular Proteins Creates Specific Degradation Signals. Bone. 2010;327: 973–977. doi:doi:10.1126/science.1183147

8. Kats I, Khmelinskii A, Kschonsak M, Huber F, Knieß RA, Bartosik A, et al. Mapping Degradation Signals and Pathways in a Eukaryotic N-terminome. Mol Cell. 2018;70: 488–501. doi:10.1016/j.molcel.2018.03.033

CHAPTER 2

General Introduction

This chapter comprises parts of the following publication:

Joana P. Guedes, Manuela Côrte-Real (2022) **Interplay between Nt-acetylation and N-degron pathways in the modulation of apoptosis** *(manuscript in preparation)*

2.1. Protein N-terminal acetylation

Most eukaryotic proteins undergo co- and/or post-translational modifications (PTMs), important events that regulate the function, interaction and localization of proteins, hence contributing to the diversification of the proteome [1]. Some of the protein modifications more extensively studied in the last years have been phosphorylation, glycosylation, ubiquitination, hydroxylation, methylation, SUMOylation and acetylation. Acetylation is one of the most common *in vivo* protein modification resulting in multiple effects at the protein level, tissue differentiation and organism development [2]. Protein acetylation may occur through the covalent addition of an acetyl group from acetyl coenzyme A to the ε-amino group of lysine residues (N-ε-acetylation), catalyzed by lysine acetyltransferases (KATs) [2,3] or to the α-amino group of the N-terminus of proteins (N-terminal-α-acetylation), catalyzed by N-terminal acetyltransferases (NATs). In particular, N-terminal (Nt)-acetylation has arisen as a highly multifunctional co- and/or post-translational protein modification. The eight currently known eukaryotic NATs mediate Nt-acetylation of a wide range of proteins, resulting in the Nt-acetylome [4,5]. It is estimated that 80-90% of the human proteome is Nt-acetylated (Nt-acetylome) while it only represents 50-70% of the yeast proteome [3,6,7]. In contrast to N-ε-acetylation, N-terminal deacetylases (NDACs) have not been identified, so Nt-acetylation can be considered an irreversible process [5,8].

2.1.1. N-terminal acetyltransferases and N-terminal acetylome

Nt-acetylation has been established as a highly abundant and regulated protein modification in eukaryotic cells. In fact, a majority of the proteome is Nt-acetylated, including soluble cytosolic proteins and transmembrane proteins [6,9]. The intracellular distribution of the eight known eukaryotic members of the NAT family vary from cytosolic and ribosome associated (NatA, NatB, NatC, NatD and NatE) to Golgi membrane (NatF), organelle lumen (NatG) and cytosolic but non-ribosomal (NatH) (Figure 2.1) [3,5]. The first five ribosome-associated NATs (NatA to NatE) are highly conserved among eukaryotes and, except for NatD and NatH, all of them are formed by a catalytic and a regulatory subunit, both required for the optimal enzymatic activity of the NAT complex [5]. Each NAT acetylates the N-terminus of a specific subset of proteins based on their N-terminal amino acid sequence, usually of the first two amino acid residues (see Table A1, Appendix, to check the amino acid code). It has been possible to identify several NAT substrates and their specificities through different approaches including N-terminal combined fractional diagonal chromatograph (COFRADIC) [10,11], stable-isotope protein N-terminal acetylation quantification (SILProNAQ) [12], mass spectrometry and *in vitro* NAT assay [8], among others. In the case of NatA and NatD, whose substrate´s second amino acid is relatively small, the initiator

methionine (iMet) is cleaved by methionine aminopeptidases (MetAPs) before acetylation [13]. On the other hand, iMet-retaining N termini are modified by other NATs, which add an acetyl group to the iMet [6,13–15]. Interestingly, owing to the NATs´s substrate specificity, proteins can be fully or partially acetylated, existing in both acetylated and unacetylated forms. Moreover, not all the predicted NAT substrates are in fact acetylated *in vivo.* For instance, Helbig *et al.* experimentally confirmed 59 new substrates of the yeast NatB from a total of 756 N-terminal acetylated proteins, which are only 8% of the 16% theoretical NatB substrates [16]. The NATs so far identified, besides differing in their substrate specificity may also differ in their subcellular localization and subunit composition. Nevertheless, some NATs exhibit overlapping substrate profiles thus showing a redundancy between them.

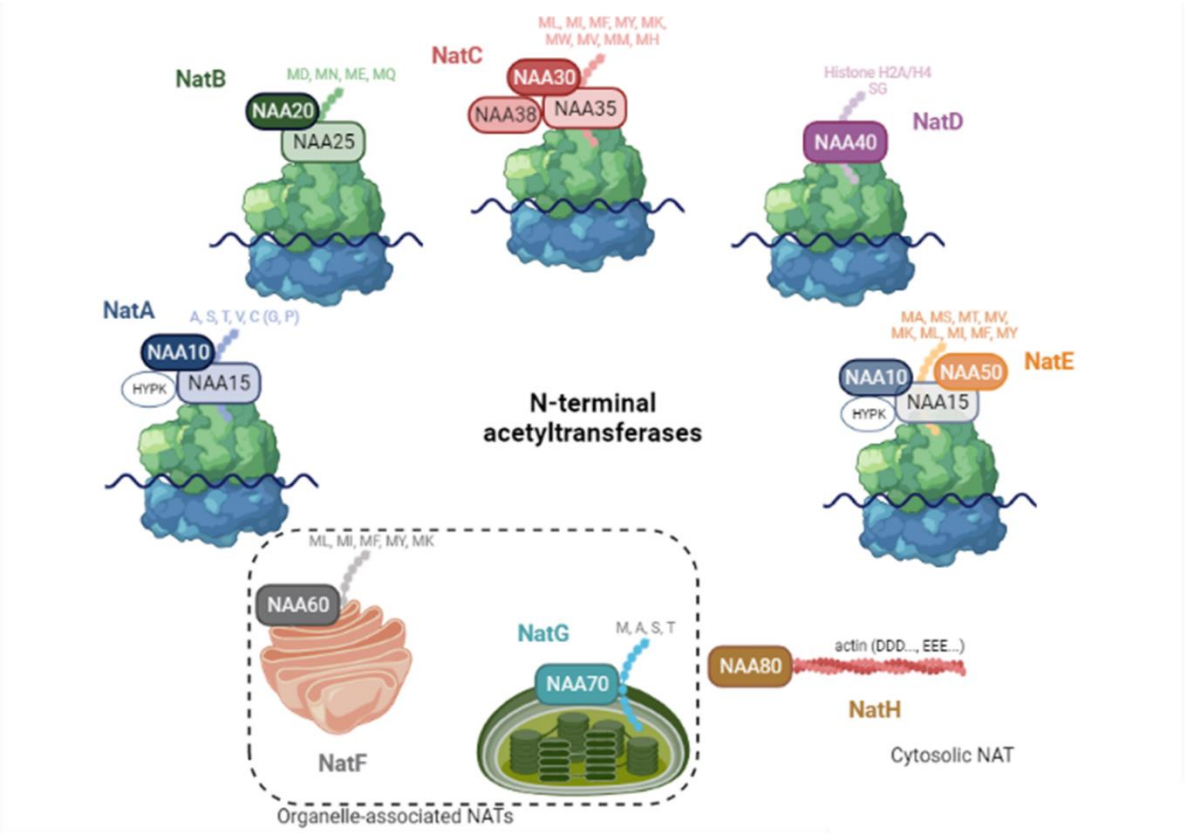

Figure 2.1: The eukaryotic N-terminal acetyltransferases. Schematic overview of the currently eight eukaryotic NATs. NatA-NatE are cytosolic and ribosome associated-NATs, NatF and NatG are organelle-associated NATs (Golgi membrane and chloroplast lumenal, respectively) and NatH is a cytosolic but non-ribosomal or organelle NAT. All NATs are composed of a catalytic subunit (darker color) and in case of NatA, NatB, NatC and NatE of a regulatory subunit (lighter color). Each NAT acetylates specific protein N-terminal amino acid sequences; NatD and NatH are highly selective NATs due to its specificity for histones H2A/H4 and actin isoforms, respectively. Created with BioRender.com.

The human NatA complex is composed of a catalytic subunit NAA10 and an auxiliary subunit NAA15 (Figure 2.1) [14,17,18]. For an optimal enzymatic activity of the complex, NAA15 may act as a

ribosomal anchor by contacting with the ribosome and in the modulation of NAA10 substrate specificity [19,20]. Furthermore, the Huntingtin-interacting protein K (HYPK), a chaperone-like protein, seems to be stably associated with NatA, being reported as an important component for proper NatA-mediated Nt-acetylation of cellular proteins [21]. This complex co-translationally acetylates protein N-termini starting with A-, S-, T-, V- and C-. Interestingly, Gly (G) and Pro (P) N-terminal proteins are rarely or almost never acetylated, respectively [5,6]. Furthermore, NatA accounts for 46% of the human proteome, though only 38% corresponds to Nt-acetylated proteins and the remaining 8% to unacetylated proteins [3]. The NatB complex is composed of the catalytic subunit NAA20 and the auxiliary/ribosomal subunit NAA25, whose catalytic site of NAA20 is specialized to anchor the large cellular pool to Met-acidic/hydrophilic N-termini (MD-, MN-, ME-, and MQ-) substrates [22,23]. Although NatB only covers nearly 21% of the human proteome, NatB substrates are almost fully Nt-acetylated [23], in contrast to other NATs. The NatC complex, the third of the major NATs, acetylates proteins with Met-hydrophobic/amphipathic N-termini (ML- MI-, MF-, MY-, MK-, MW-, MV-, MM- and MH-) to a different degree [24,25]. This complex comprises three subunits: the catalytic subunit NAA30, the ribosomal anchor NAA35 and the small auxiliary subunit NAA38, identified in both *Saccharomyces cerevisiae* and human NatC with a potential role in RNA binding [5,26]. NatD, the only human ribosomal NAT without a known ribosomal subunit, is solely composed of the catalytic subunit NAA40. Being a highly selective NAT, its catalytic site specifically accommodates histones H2A and H4 (SG- starting) [27–29]. The NatE complex, formed by the catalytic subunit NAA50, physically interacts with the NatA complex [30–32]. In this association, NAA50 is anchored to the ribosome and might then act on the rare NatA-type N-termini for which the iMet has not been removed by MetAPs. On the other hand, NAA50 may have independent functions from NatA, acting alone toward Met-hydrophobic N-termini [30,32]. Though these five NATs are considered as parts of the co-translational machinery common to all eukaryotes, recent studies have identified more specialized NATs with post-translational activity and specific to some eukaryotic species. In fact, NatF and NatG comprise the first organelle-associated NATs. NatF is an organellar NAT with the catalytic subunit NAA60 anchored to the cytosolic side of the Golgi membrane through its C-terminal extension. There, it specifically acts on transmembrane proteins acetylating ML-, MI-, MF-, MY- and MK- residues [33,34]. It is present in multicellular eukaryotes like animals and plants but not in unicellular yeast. Curiously, NatC, NatE and NatF together cover nearly 28% of the human proteome, in which 21% corresponds to Nt-acetylated proteins and 7% to unacetylated proteins, meaning that these NATs are responsible for acetylating 21% of the proteome [3]. NatG is a chloroplast lumenal-associated NAT composed only of a catalytic subunit NAA70. NAA70 is localized to the chloroplast stroma, and is responsible for Nt-acetylation of the portion

of these chloroplast lumen proteins (M-, A-, S- and T-) [35]. Recently, the NATs family became more complete with the discovery of NatH. NatH, composed only of a catalytic subunit NAA80, acts post-translationally in the cytosol, making it the unique non-ribosome or organelle-associated NAT. Similarly to NatD, NatH is a highly selective NAT, acetylating all six isoforms of actin, one of the most abundant cytosolic proteins [36]. Interestingly, for the NAA80-mediated actin Nt-acetylation, processing requires two steps: (i) in a first phase, which is common to all eukaryotes, NatB carries out the co-translational Nt-acetylation of the two cytoplasmic β- and γ–actin isoforms (class I), while Nt-acetylation of the four muscle actin isoforms (class II) is achieved by NatA after iMet excision; (ii) afterwards, the Nt-acetylation post-translational step is mediated by NatH (specific for animals) only after the removal of the Ac-Nt by an unknown acetylmethionine aminopeptidase [36]. Interestingly, profilin 2 (PFN2), an actin binding protein affecting cytoskeleton structure, has been associated with NAA80 to promote efficient acetylation of the actin N-terminus [37].

Although NATs are conserved between species, the same is not true for all their substrates, meaning that a NAT deletion phenotype observed in one organism may not apply to other organisms [16]. Currently, new approaches with increased quantitative coverage of *in vivo* Nt-acetylation sites by taking advantage of faster and more sensitive mass spectrometers will help to clarify these issues. Besides some technical limitations that can still be overcome, the discrepancy between the predicted NATs substrates and those experimentally confirmed may be explained, as discussed hereafter (section 2.2), by protein destabilization created by Nt-acetylation which leads to their subsequent degradation.

2.1.2. Effects of protein N-terminal acetylation and its biological significance

Despite being a ubiquitous process, the biological significance of Nt-acetylation only recently has begun to be understood. Considering the large number of proteins undergoing Nt-acetylation, it is not surprising that this protein modification can have quite different effects on the function of proteins. In fact, Nt-acetylation may affect the protein function at several levels, such as interfering with the interaction with other proteins, complex formation, aggregation and correct folding, as well as in protein subcellular localization, or through protein-protein interactions or direct protein-membrane interactions [3,5] (Figure 2.2). In general, Nt-acetylation has been ascribed as conferring protein stability, but less often, it has also been reported to enhance protein turnover through proteasomal degradation pathway. Moreover, it has an impact at the cell level such as in morphology and migration rates as well as actin polymerization, among other cellular functions (reviewed by [5,38]). So, Nt-acetylation may impact the proteome dynamics with implications in normal development processes. It could therefore been anticipated that

misregulation of the Nt-acetylation machinery leads to severe diseases such as cancer [39,40], neurodegenerative diseases and cardiovascular disorders (reviewed by [5,40].

Regarding protein-protein interactions, it was shown that NatB is involved in the interaction of angiogenesis-related proteins. Indeed, the Nt-acetylation mediated by NatB of phosducin-like 3 (PDCL3), an identified chaperone protein involved in the regulation of vascular endothelial growth factor receptor 2 (VEGFR-2), negatively affects the interaction with VEGFR-2, as the Nt-acetylation destabilizes PDCL3 [41]. Concerning protein targeting, Nt-acetylation has been proven to be crucial for proper localization of two different Golgi-associated proteins, Arl3 [42,43] and Grh1 [44]. In the absence of NatC-mediated Nt-acetylation, these proteins lose their Golgi localization and accumulate in the cytoplasm. On the other hand, Forte and colleagues discovered that protein Nt-acetylation inhibits ER translocation both *in vivo* and *in vitro* [45]. Another example is the finding that the Nt-acetylation of protein abrogates the import of proteins into the ER through the SRP-independent pathway using the Sec62 translocation channel [3]. Recently, it was shown that the Nt-acetylation mediated by the NatB maintains Bax in an inactive conformation in the cytosol of yeast and MEF cells [46]. The presence or absence of Nt-acetylation may be a central factor in protein folding and aggregation. In fact, NatA-depleted yeast cells show an accumulation of misfolded proteins and increased levels of chaperones [47]. Furthermore, Nt-acetylation has a protective role against α-Synuclein oligomerization and aggregation in Parkinson's disease, by disrupting intermolecular hydrogen bonds important for α-Syn oligomerization [48,49]. Also, huntingtin (Htt) protein seems to become prone to aggregation in the absence of Nt-acetylation. Importantly, HYPK, the subunit that stably interacts with NatA, can also exhibit chaperone-like properties preventing Huntingtin aggregation [21,50]. In fact, knockdown of HYPK or NAA10 resulted in increased aggregation of Huntingtin protein, which is found in patients with Huntington's disease. Recently, this phenotype was corroborated through the evidence of the *in vitro* NatA-mediated Nt-acetylation of the Htt protein [50].

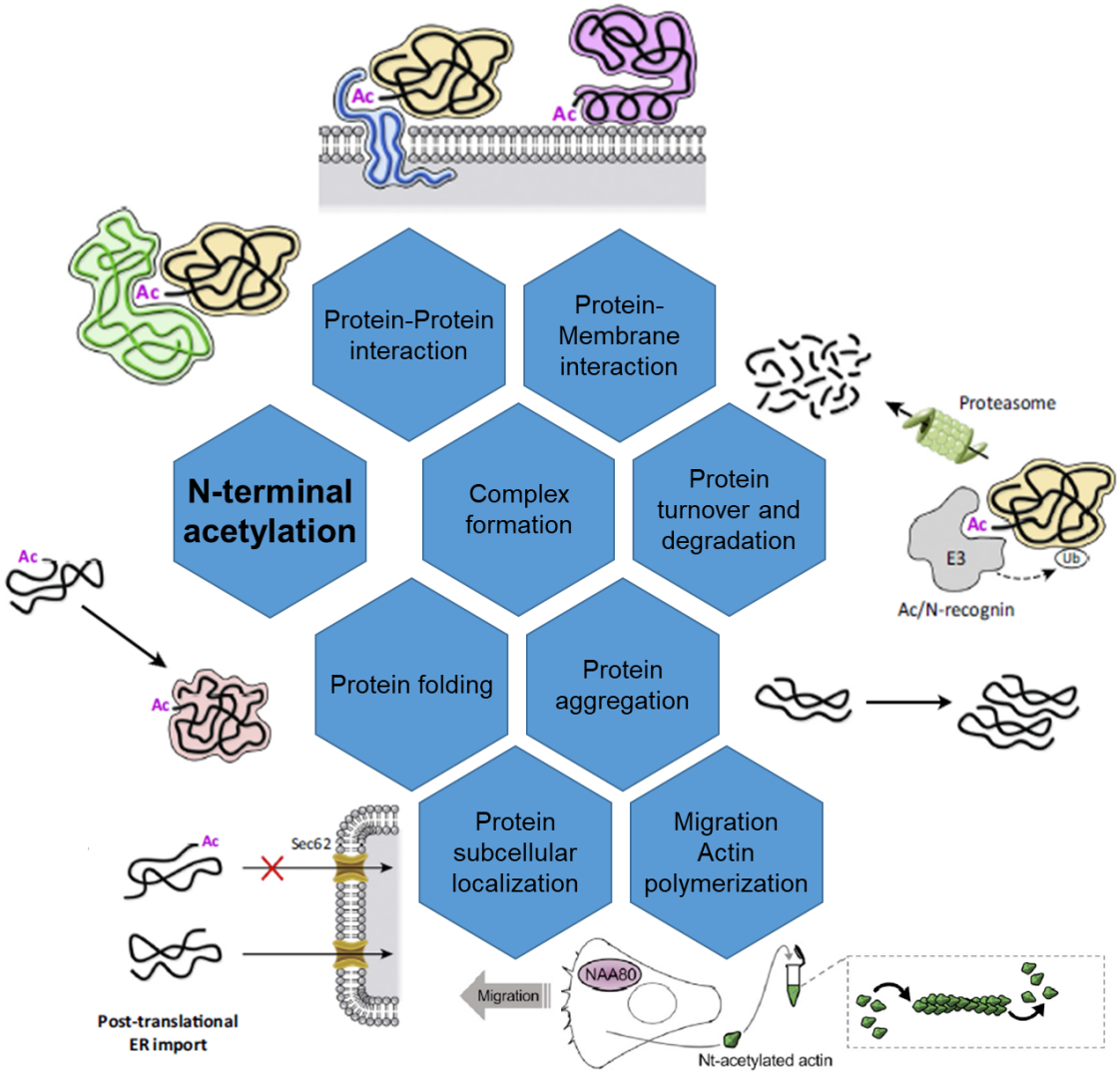

Figure 2.2: Nt-acetylation may affect the protein function at several levels. Summary of the effects of Nt-acetylation on proteins. This protein modification may be involved in the protein-protein interactions or direct protein-membrane interactions, in the complex formation, protein subcellular localization, aggregation and proper folding, as well as in the protein turnover. At the cell level, NatH-mediated Nt-acetylation of actin may affect the cell morphology, the migration rates and actin polymerization. Adapted from [3,5].

The effects on cell morphology and migration rates as well as actin polymerization have emerged with the discovery of the recent actin-highly selective NatH. The lack of actin Nt-acetylation mediated by NAA80 increases filopodia and lamellipodia, promotes cell migration and decreases actin polymerization rates [36,38]. Although Nt-acetylation affects all these biological processes, its involvement in the protein stability and degradation has been questioned. As this topic is covered in this thesis, it will be discussed in detail in the section 2.2.

2.1.3.Regulation of N-terminal acetylation

Nt-acetylation was initially thought to be a constitutive and static modification. However, it was later found that NATs can be regulated both at the protein synthesis and activity levels. Indeed, it was shown that Nt-acetylation levels change in response to different conditions such as drought stress in plants [51] and calorie restriction in yeasts [52] through downregulation of NatA and NatD, respectively. As abovementioned, HYPK stably interacts with NatA for an optimal NatA enzymatic activity towards some substrates such as protein PEST proteolytic signal-containing nuclear protein (PCNP), and exhibits chaperone-like properties preventing Huntingtin aggregation. In contrast, a recent study showed that HYPK associates with human NatA complex to negatively regulate its activity, but not the NatA activity of *Schizosaccharomyces pombe* [53]. Furthermore, structural and biochemical evidence revealed that HYPK can also form a stable complex with NatE to downregulate its activity. HYPK binding to NatA blocks the targeting of NAA50 to NatA and reduces the binding affinity of HYPK and NAA50 [54].

As aforementioned, NAA80 activity is regulated by the actin chaperone profilin [37,55]. In fact, enzymatic assays revealed that PFN2 binds to NAA80 through a proline-rich loop increasing the intrinsic catalytic activity of NAA80 and, consequently, promoting the binding between NAA80 and actin and subsequently its acetylation.

Furthermore, acetyl coenzyme A (Ac-CoA) availability may also regulate Nt-acetylation [56]. In cancer cells, Yi and colleagues proposed Ac-CoA as a signaling molecule that affects apoptotic sensitivity by regulating Nt-acetylation. Indeed, overexpression of Bcl-xL, an anti-apoptotic protein of the Bcl-2 family, causes a reduction of Ac-CoA levels and, consequently, of Nt-acetylated proteins. Nevertheless, increased levels of Ac-CoA are able to restore Nt-acetylation sensitizing cells to apoptosis. Contrarily, in yeast cells, fluctuations in Ac-CoA do not affect the Nt-acetylation state. In fact, despite a strong decrease in Ac-CoA levels upon starvation, yeast cells maintain their global Nt-acetylation levels [57].

2.1.4. Crosstalk with other modifications

Even though the majority of eukaryotic proteome is Nt-acetylated, the N-termini can be modified by other processing enzymes which opens a functional interplay between different modifications at the N-terminus. Nt-methyl-, Nt-propionyl-, Nt-myristoyl-, Nt-palmitoyltransferases may covalently attach a methyl, propionyl, myristoyl and palmitoyl group, respectively, to the α-amino group of the protein N-terminus. Also, ubiquitin ligases are able to modify N-termini through ubiquitination [58]. As a result, in the last years, the interaction between Nt-acetylation and the other protein Nt-modifications have been described. For instance, a recent report provides insights into the interplay between Nt-acetylation and Nt-

myristoylation demonstrating that both Nt-modifications may compete for the same N-termini [59]. Importantly, this study showed that Gly-starting N-termini can in general only undergo Nt-myristoylation instead of Nt-acetylation, but also that specific proteins can dually exist in either Nt-acetylated or Nt-myristoylated states. The same happens with Ser-starting myosin regulatory light chain 9 (MYL9) that exhibits *in vivo* both Nt-acetylation and Nt-methylation states. MYL9 was the first confirmed protein showing that NATs and N-terminal methyltransferases can have overlapping substrates depending on its origin tissue [60]. Curiously, these two states of MYL9 showed to be associated with different cellular roles. In fact, Nt-acetylation of MYL9 promotes increased phosphorylation at serine 19 associated with increased cytoplasmic activity of MYL9. In turn, exclusive MYL9 Nt-methylation not only enhances DNA binding and stimulates its nuclear role as a transcription factor, but also negatively affects interactions between the MYL9 N-terminus and cytoskeletal proteins [61]. NatD-mediated histone H4 Nt-acetylation also interacts with methylation. Schiza and colleagues found that the H4 Nt-acetylation triggers the blockade of histone H4 arginine 3 methylation by inhibiting Hmt1 methyltransferase activity *in vitro* [62]. On the other hand, another group found a suppression of histone H4 serine 1 phosphorylation associated with the Nt-acetylation of H4, repressing the expression of transcription factors [63]. Recently, a study described a remarkable inverse correlation between Nt-acetylation and Nt-ubiquitination. Among the proteins analyzed, Pro- and Val-starting N-termini proteins, whose N-termini are known to rarely be Nt-acetylated, showed to undergo a preferred Nt-ubiquitination instead of Nt-acetylation [64]. In the following section, the relation of these latter Nt-modifications will be discussed. In conclusion, the different Nt-modifications and the crosstalk between them contribute to the complexity and functional diversity of the proteome, with impact on protein regulation, cellular signaling and pathogenesis.

2.2. The mammalian N-degron pathways: the involvement of N-terminal acetylation

For several decades it was thought that Nt-acetylation could contribute to protein stability *in vivo* [65,66] and avoid protein degradation. In 2010, Hwang and colleagues discovered that Nt-acetylation was also able to create N-degrons that are targeted for degradation through the N-end rule proteolytic system [67]. The “N-end rule” concept arose 36 years ago with the discovery of some destabilizing residues at the protein N-terminal, generating short-lived proteins [68,69]. Actually, advances in this field have revealed that all 20 amino acids of the genetic code can act as N-degrons (Figure 2.3) [70]. Recently, the earlier term “N-end rule” was replaced by N-degron, renaming thus the N-end rule pathways to N-degron pathways [70].

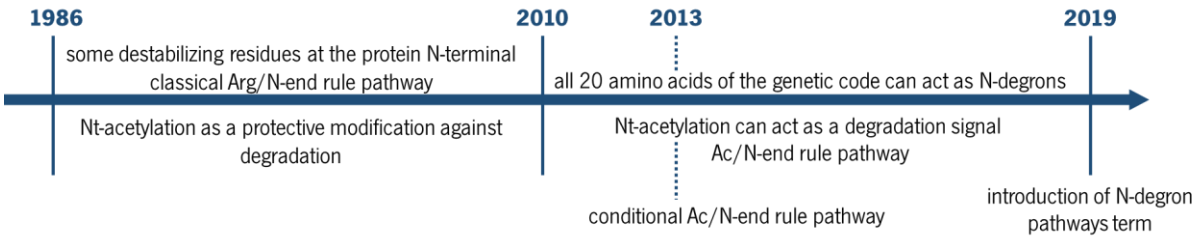

Figure 2.3: Evolution of the "N-end rule" concept and the involvement of Nt-acetylation on protein degradation. The "N-end rule" concept was introduced in 1986 by Bachmair and colleagues with the discovery of some destabilizing unacetylated N-terminal residues called N-degrons. Until 2010, Nt-acetylation was considered to play a protective role against protein degradation. However, this concept was changed by the discovery of a different branch of N-end rule pathway, designated Ac/N-end rule pathway, by creating destabilizing Nt-acetylated residues, the Ac/N-degrons in contrast to the Arg/N-degrons. In 2013, some features and processes involving Ac/N-degrons and conferring protection against protein degradation raised the concept of conditional Ac/N-degrons. Actually, all 20 amino acids of the genetic code can act as N-degrons and the N-end rule concept has been replaced by N-degron pathways.

In mammals, the proteolytic system targeting N-degrons englobes three different branches: the classical Arg/N-degron pathway, Ac/N-degron pathway and Gly/N-degron pathway (Figure 2.4). All the three pathways are implicated in fine-tuning diverse biological functions, including in the: elimination of misfolded proteins; control of subunit´s stoichiometry, repression of neurodegeneration, regulation of apoptosis, autophagy, chromosome repair, cohesion/segregation, G proteins, cytoskeleton-involved proteins and cell migration, among others [70,71].

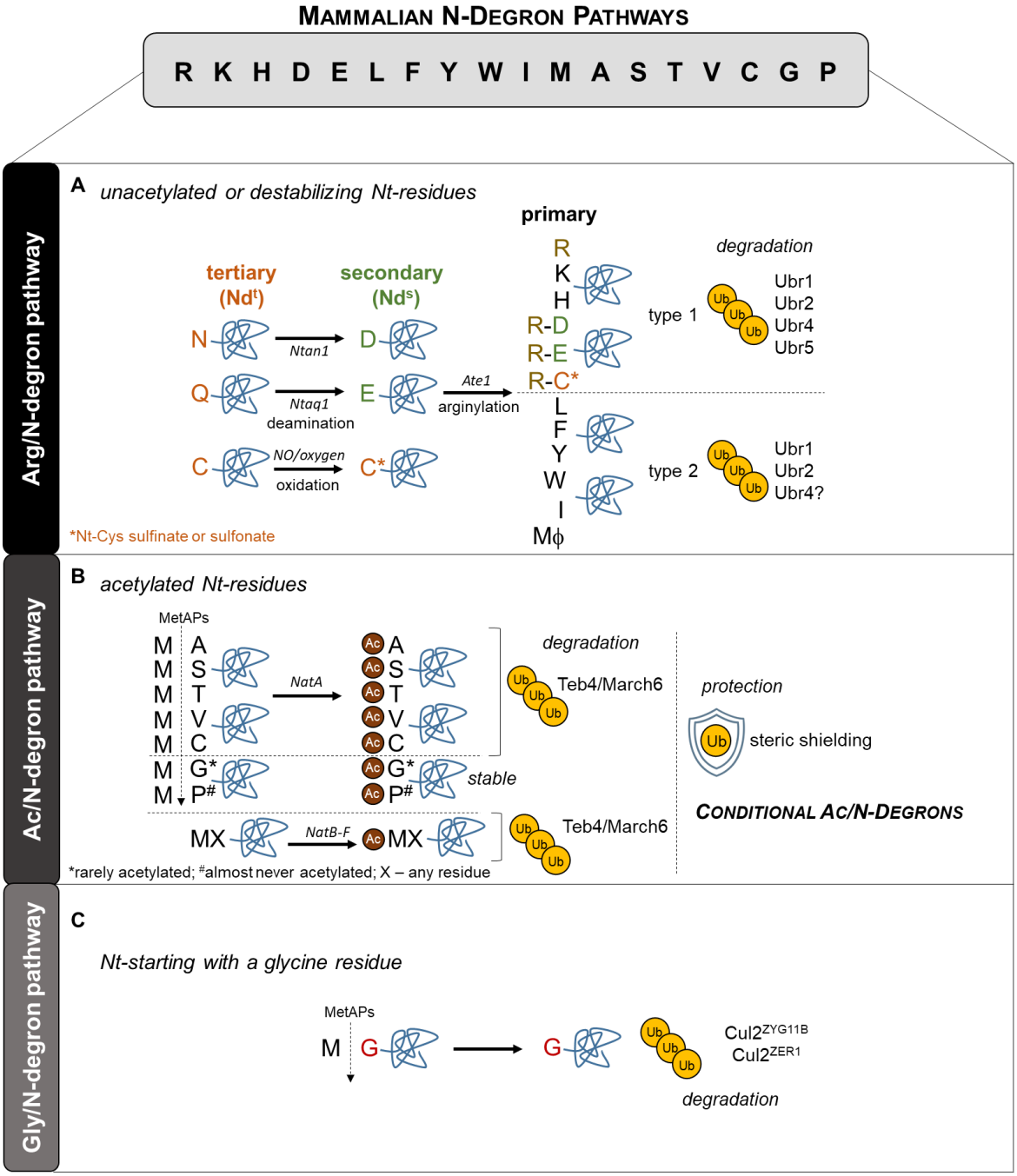

Figure 2.4: The three mammalian N-degron pathways. All 20 amino acids of the genetic code can act as N-degrons. **(A)** The classical Arg/N-degron pathway targets unacetylated or destabilizing N-terminal tertiary, secondary and primary residues. The tertiary Nt-N, -Q and -C residues undergo enzymatic Nt-deamination and oxidation by Ntan1, Ntaq1 and NO/oxygen, respectively. The secondary Nt-D and Nt-E residues are exposed to the enzymatic arginylation catalyzed by Ate1. Primary residues are assembled into two groups: type-1 substrates recognized by the UBR box domain of UBR1, UBR2, UBR4 and UBR5 and type-2 recognized by the N-domain of UBR1, UBR2 and probably by UBR4 (unknown mechanism). Mϕ - methionine followed by a hydrophobic residue. **(B)** The Ac/N-degron pathway targets Nt-acetylated residues A-, S-, T-, V-, C- and MX- (where X is any amino acid residue) to the degradation through Teb4/March6. Protection mediated by steric shielding creates conditional Ac/N-degrons. **(C)** The Gly/N-degron pathway triggers the degradation of residues with glycine (G) at the

N-terminal after MetAPs cleavage. Two related Cullin-E3 ligases, $Cul2^{ZYG11B}$ and $Cul2^{ZER1}$, redundantly act to be the N-recognins of this pathway. Adapted from [70,72].

The Arg/N-degron pathway directly targets unacetylated or destabilizing N-terminal primary residues such as Nt-R, Nt-K, Nt-H (type-1 substrates) and Nt-L, Nt-F, Nt-Y, Nt-W, Nt-I, or Nt-M followed by a bulk hydrophobic residue (type-2 substrates). The tertiary Nt-N and Nt-Q residues, and the secondary Nt-D and Nt-E residues, are recognized by Arg/N-recognins after enzymatic Nt-deamination followed by Nt-arginylation, and arginylation, respectively. In eukaryotes that produce nitric oxide (NO), the Nt-C residue is also considered a tertiary destabilizing Nt-residue after NO-mediated oxidation followed by arginylation [68,73–78]. In animals, plants and yeasts, Nt-deamination of Nt-N and Nt-Q is mediated by Nt-N-specific Nt^N-amidase (Ntan1) and Nt-Q-specific Nt^Q-amidase (Ntaq1), respectively [75,79]. Nt-arginylation of Nt-E and Nt-D residues is mediated by mammalian and yeast ATE1 R-transferase, which catalyzes the conjugation of the Arg to their α-amino group [75,80]. The E3 ubiquitin protein ligases UBR1, UBR2, UBR4 and UBR5 have emerged as the main Arg/N-recognins. UBR1 and UBR2 have a similar sequence and share only ≈80-residue UBR domains with UBR4 and UBR5 (reviewed by [81]). Notably, while the N-degron of type-1 substrates is recognized by the UBR box domain of the UBR1, UBR2, UBR4 and UBR5, type-2 substrates, containing large hydrophobic N-terminal residues, are recognized by the N-domain of UBR1 and UBR2 E3 ubiquitin ligases [81–83]. Although no N-domain has been identified for UBR4, studies has reported that it can also bind type-2 N-degrons [83,84]. Small molecules, di-peptides, heterovalent ligands and bioactive compounds have been tested and used as potential inhibitors of UBR E3 ligases. For instance, Di-peptides displaying an L-conformation [85] and heterovalent ligands [86,87] have been developed to mimic N-degrons and compete for binding to UBR E3 ligases N-recognins, therefore, avoiding binding to their substrates. While di-peptides are prone to be unstable, likely due to cleavage by endopeptidases, and the effective inhibition can only be achieved at high concentrations [85], the lipid based heterovalent inhibitor RFC11 seems to be protected from proteolytic degradation [87]. In fact, RFC11 compound binds N-recognins sites and block type-1 and type-2 N-degron activities [86]. Furthermore, a combined treatment of RFC11 with the natural naphthoquinone compound shikonin, in a stable receptor-targeted liposomal formulation, showed to exhibit antitumor effects by stabilizing and upregulating the short-lived apoptotic protein RIPK1 through the inhibition of UBR1 E3 ligase [87].

The Ac/N-degron pathway, in contrast to the Arg/N-degron pathway, triggers the degradation of the Nt-acetylated residues M-, A-, S-, T-, V- and C- through the Teb4/March6 E3 Ub ligases [67,78,88,89].

However, most Nt-acetylated proteins remain stable and long-lived [88–90]. This contradiction may be explained by a steric shielding of the targeted Nt-acetylated proteins. Remarkably, the interaction between the target protein with its partner, or the assembly within a protein complex after rapid sequestration results in a steric shielding of the Ac/N-degron, creating conditional Ac/N-degrons and, consequently, providing an explanation for the stability and long-lived Nt-acetylated proteins. For instance, Nt-Ac-Cog1, -Hcn1 and -Rgs2, short-lived Ac/N-degron substrates, can be long-lived by co-overexpressing Cog2/Cog3, Cut9 or Gαq, respectively or when their Ac/N-degrons are sterically shielded by their partners [91,92]. Moreover, the Nt-acetyl group usually enhances the thermodynamic stability of the protein complex [93]. The binding to a molecular chaperone, particularly the Hsp90 system, also proved to be protective for target proteins. In fact, a study revealed that weakening of the *S. cerevisiae* Hsp90 system makes long-lived proteins to short-lived, because of their rapid degradation by the Arg/N-degron pathway [94]. In addition, the degradation of Nt-acetylated proteins appears to be important in the protein quality control and protein complexes stoichiometry. Interestingly, an elegant and comprehensive study using high-throughput multiplexed stability profiling in yeast dissected the key factors modulating the N-terminal dependent protein degradation [90]. Although this analysis confirms the specific involvement of the N-degron pathways in protein turnover, it also suggests that, globally, Nt-acetylation is rarely recognized as a degron. While substrates acetylated by NatA (C-, S-, V-, G-, A- and T-) and NatB (MN-, MD-, ME-, MQ-) are mostly stable due to their basic, polar and uncharged residues, NatC substrates (MW, ML, MF, MI) are mostly unstable due to their hydrophobic residues. In fact, in the absence of the catalytic subunit of NatC NAA30 or of Ac/N-degron E3 ligase Doa10 the stability of NatC substrates was recovered. This supported the interpretation that the overall hydrophobicity of the N-terminal amino acid residue is the main factor of degron strength rather than the acetylation status [90]. In this line, Kim and colleagues demonstrated a functional complementarity between Arg/N-degron and Ac/N-degron pathways by the discovery of Nt-Met-hydrophobic residues as degrons for both pathways. While unacetylated Met is recognized by UBR1 and degraded via the Arg/N-degron pathway, acetylated Met is targeted by Doa10/Not4 for Ac/N-degron-mediated degradation [76]. Moreover, N-terminal acetylation was found to directly prevent the protein degradation by UBR1, or prevent the removal of the iMet, and thus preclude UBR1-mediated degradation [90]. Recent studies have corroborated the general protective role of Nt-acetylation against protein degradation in HeLa human cells [95] and specifically against UBR4-mediated degradation in *D. melanogaster* [96].

The Gly/N-degron pathway comprises the most recent branch of the N-degron pathway in which two related Cullin-E3 ligases, $Cul2^{ZYG11B}$ and $Cul2^{ZER1}$, redundantly act to target N-termini starting with

G- residue [97]. While $Cul2^{ZYG11B}$ recognizes just Nt-G and the following residue, $Cul2^{ZER1}$ preferentially recognize amino acids with bulky side chains after the Nt-G. The control of myristoylation and the degradation of protein fragments generated by caspase cleavage during apoptosis are pointed as two potential physiological roles for this pathway.

2.3. Apoptosis: a regulated type of cell death

Apoptosis, a type of regulated cell death conserved across eukaryotic organisms, has been the subject of extensive studies for the past decades and, for most of this time, was considered the only type of regulated of cell death. Apoptosis is crucial to ensure the maintenance of normal physiology and tissue function by elimination of damaged, dysfunctional or unnecessary cells. However, despite its beneficial biological role, unbalanced apoptosis has been implicated in a diversity of abnormal functions and in the progression and development of diseases. While excessive levels of apoptosis have been associated with neurodegenerative disorders such as Parkinson's and Alzheimer's diseases, a deficit in apoptosis levels have been related to the development of cancer and autoimmune diseases [98,99].

Cells committed into apoptotic cell death undergo several morphological and biochemical alterations namely cytoplasmic shrinkage, nucleus and chromatin condensation (pyknosis), nuclear fragmentation (karyorrhexis), chromatin dissolution (karyolysis) and plasma membrane blebbing, while preserving plasma membrane integrity [100]. This process culminate with the formation of small vesicles, the so-called apoptotic bodies, which are engulfed by immune neighboring cells through phagocytosis and, then, degraded within lysosomes (reviewed by [99]). Other hallmarks of apoptosis include caspases activation, loss of mitochondrial membrane potential, mitochondrial outer membrane permeabilization (MOMP) followed by the release of cytochrome *c* (cyt *c*) from mitochondria to the cytosol, exposure of phosphatidylserine (PS) and reactive oxygen species (ROS) accumulation [98,99,101]. The apoptotic cascade comprises two phases: initiation and execution. The term "execution" refers to the biochemical processes that truly cause the cellular demise and the initiation phase corresponds to the signal transducer events that trigger the execution mechanisms.

2.3.1. Extrinsic *versus* intrinsic apoptotic pathways

Cells commit into apoptosis through two major pathways referred to as the extrinsic and intrinsic pathways (Figure 2.5). The extrinsic or death-receptor pathway is triggered in response to external stimuli and involves the binding of a ligand to a transmembrane death receptor on the cell surface. FAS, TNFR

and TRAILR are the best known and characterized death receptors with FASL, TNF-alpha (TNF-α) and TRAIL as their respective ligands (reviewed by [98,99,102]). Upon activation by the ligands, the death receptors oligomerized to allow the assembly and formation of signaling complexes, namely the multiprotein death-inducing signaling complex (DISC), involving the cytosolic FAS-associated via death domain (FADD) or the TNFR1-associated death domain (TRADD) proteins and procaspase-8/-10 [103,104]. Procaspase-8/-10 maturation and activation involves a cascade of events, in which the first step entails the binding to FADD/TRADD at the DISC, allowing its homodimerization and consequent activation by autoproteolytic cleavage [105]. Importantly, the activation of procaspase-8/-10 can be regulated by a caspase-like protein – c-FLIP, also present in the DISC [106]. The short variant c-FLIP (c-$FLIP_S$) and its long counterpart (c-$FLIP_L$) inhibit and activate procaspase-8, respectively. After caspase-8/-10 activation, the execution stage of the extrinsic pathway can follow two different ways: (1) direct cleavage and activation of procaspase-3 and -7, which triggers apoptosis induction and (2) cleavage of BID by caspase-8 generating t-BID. t-BID then translocates to mitochondria, where it functions as a BH3-only activator to trigger BAX/BAK-mediated MOMP and the subsequent events underlying the intrinsic pathway [107]. In this way, a crosstalk between the extrinsic and the intrinsic pathways is established.

The intrinsic or mitochondrial pathway is triggered by dysregulation/imbalance in the intracellular homeostasis caused by environmental perturbations. This includes genotoxic damage (DNA damage and irradiation), cellular organelles damage (Endoplasmic Reticulum (ER) stress and mitochondrial damage), activated oncogenes, hypoxia, growth factor deprivation and excessive mitogenic stimulation [99,108]. Notably, although other forms of cell death are being discovered and described, the intrinsic apoptosis pathway is physiologically dominant, promoting the demise of more than 60 billions of our cells per day [109]. The critical step of this pathway is the release of cyt *c* following MOMP, which is regulated by a fine balance between the pro-apoptotic and the anti-apoptotic members of the B cell lymphoma 2 (BCL-2) family. While the anti-apoptotic members harbor four BCL-2 homology domains (BH1 to BH4), the pro-apoptotic proteins comprise two different sets of proteins: multidomain members, which encompass BH1, BH2 and BH3 domains, and BH3-only members [110]. The BH1, BH2 and BH3 domains form a hydrophobic groove where the BH3 domain of the same or of another family member can bind [111], allowing in this way the formation of homodimers and heterodimers [112].

The anti-apoptotic members comprise the proteins BCL-2, BCL-XL, BCL-W, MCL-1 and BFL-1, while BAX, BAK, BOK and the BH3-only proteins (BID, PUMA, BIM, NOXA, BAD, BMF1 and HRK) constitute the pro-apoptotic proteins of the BCL-2 family [113]. Of these proteins, t-BID, PUMA and BIM are referred to as potent “activators” of BAX and BAK, whereas NOXA, BAD, BMF1 and HRK are called

"sensitizers" and are involved in the inhibition of anti-apoptotic proteins [114]. In healthy cells, BAX is mainly located in the cytosol but it is also in equilibrium with the mitochondrial outer membrane (MOM) where it is loosely bound [115]. However, in response to apoptotic stimuli, inactive BAX changes from a cytosolic monomeric globular conformation to an extended mitochondrial membrane embedded conformation after which it can become fully active. The structure of cytosolic BAX revealed by nuclear magnetic resonance (NMR) showed a globular structure composed by nine α helices, with the hydrophobic α-helix 5 at the protein core, forming a compacted structure that encloses the hydrophobic C-terminal. In BAX native conformation, the α-helix 9 containing the C-terminal and a transmembrane domain (TM) occupies the hydrophobic groove, masking the BH3 domain, located in α-helix 2, explaining its mostly cytosolic localization. Under apoptotic stimuli, BAX C-terminal α-helix 9 is displaced and inserted into OMM and, then, BH3 domain becomes exposed to facilitate hetero- and homo-oligomerization [116,117]. Besides α-helix 9, other domains can also modulate Bax localization. In fact, a specific sequence comprising the first 20 amino acids of BAX known as Apoptosis Regulating Targeting (ART) identified at its N-terminal domain has been shown to maintain BAX in an inactive conformation. Thus, its displacement increases BAX OMM insertion ability, demonstrating the importance of the N-terminal sequence of BAX in determining its subcellular localization [116,118]. BH3-only proteins transiently interact with inactive BAX, BAK and BOK, activating it, to promote a series of conformational changes followed by protein dimerization and oligomerization. The oligomers form large ring-like structures in the MOM, named pores, culminating in the MOMP (reviewed by [119]). Importantly, MOMP is counteracted by anti-apoptotic proteins through the inhibition of BAX and BAK by the BCL-2 anti-apoptotic members: either by preventing its oligomerization and pore formation or by sequestering BH3-only "activators" or "sensitizers" [111,120,121]. As a consequence of MOMP, apoptogenic factors, including cyt *c* and second mitochondria-derived activator of caspase/direct inhibitor of apoptosis-binding protein (SMAC/DIABLO), are released from the mitochondria intermembrane space to the cytosol [108]. When in the cytosol, cyt *c* promotes the assembly of a supramolecular complex known as apoptosome, composed of itself, oligomerized apoptotic protease-activating factor 1 (APAF1) and procaspase-9. This complex is responsible for activating procaspase-9 [122]. Active caspase-9 cleaves and activates the executioner procaspase-3 and -7, which in turn cleave other procaspases leading to the amplification of the apoptotic cascade [108]. The execution stage culminates in diverse apoptosis-related events, among them, DNA fragmentation [123], PS exposure [124,125] and apoptotic bodies formation [126]. Similar to the anti-apoptotic BCL-2 proteins, members of the inhibitor of apoptosis (IAP) protein family, such as XIAP and c-IAP1/2, antagonize the apoptotic cascade by blocking caspases activity [127,128].

Nonetheless, the association of SMAC/DIABLO with these IAPs can prevent this blockade, promoting caspases activation by the apoptosome [129,130].

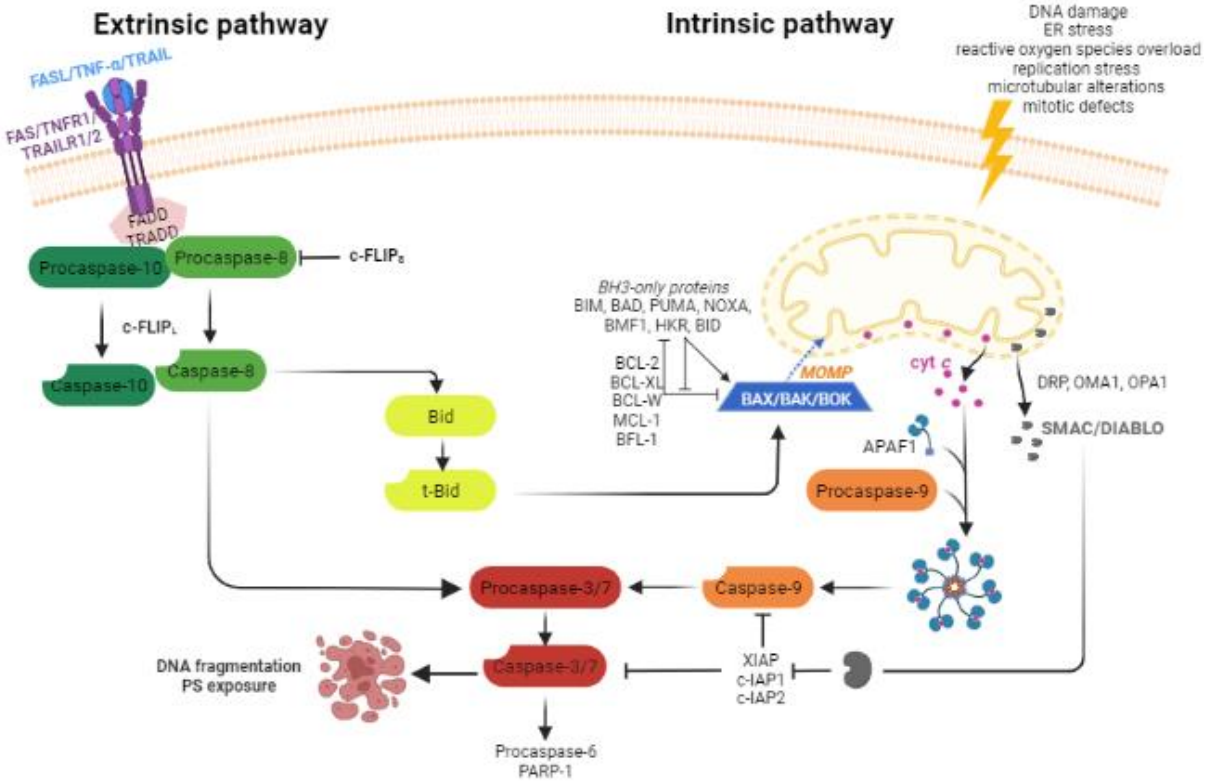

Figure 2.5: Extrinsic and intrinsic apoptotic pathways. The extrinsic pathway is initiated by the binding of a ligand (FASL, TNF-α and TRAIL) to their respective death receptor (FAS, TNFR, TRAILR), resulting in the activation of the initiator caspase-8 through the cytosolic FAS-associated via death domain (FADD) or the TNFR1-associated death domain (TRADD), that then activates the effector caspases triggering the apoptosis. In the intrinsic pathway, activated BH3-only proteins bind and activate BAX, BAK and BOK by inhibiting anti-apoptotic BCL-2 proteins. Mitochondrial outer membrane permeabilization (MOMP) is triggered and thus cytosolic apoptogenic factors such as cyt *c* and SMAC/DIABLO, are released from the mitochondria to the cytosol. In the cytosol, cyt *c* together with Apaf1 and procaspase-9 forms the apoptosome complex, which in turn activate procaspase-9 and, consequently, activates the effector caspases, leading to apoptosis. SMAC/DIABLO inhibits the XIAP, c-IAP1 and -2. The crosstalk between extrinsic and intrinsic pathway occurs through t-Bid protein generated by the cleavage of Bid mediated by caspase-8. Created with BioRender.com.

2.3.2. Regulation of apoptosis

In order to maintain cell homeostasis, the components of the apoptotic cell death are subjected to a highly coordinated regulation, otherwise, several disorders can develop. BCL-2 family proteins have been implicated as the central key regulators of intrinsic apoptosis. Balanced levels of pro- and anti-apoptotic BCL-2 proteins and their binding affinities may largely determine cell fate decisions between

death and life. This careful balance can be tightly modulated by protein interactions, posttranslational modifications and proteolytic cleavage [112,131–133].

- *Regulation by interaction between BCL-2 family members*

As abovementioned, the anti-apoptotic proteins can block apoptosis by binding and sequestering BAX and BAK or BH3-only activators/sensitizers [111,120,121]. This interaction depends on a hydrophobic binding groove formed by BH1, BH2, and BH3 domains [131,134]. Initially, the original rheostat model proposed that the ratio of pro-apoptotic to anti-apoptotic proteins determined the cell's fate [135]. Given the multiple and complex interactions between the expanded family of Bcl-2 proteins, it is now believed that the fate of the cells is mostly determined by the interactions between all of them, which in turn are determined by their relative abundance and affinities. Similarly to the rheostat model, if the interactions result in MOMP, the cell is irreversibly committed to death [112].

Despite inhibiting BAX function, under physiological conditions, BCL-2 and BCL-XL can help BAX-addressing toward mitochondria, "priming" BAX for further activation upon an apoptotic stimulus [111,136]. Indeed, BH3-mimetic molecule ABT-737 was more efficient to induce apoptosis in BAX and BCL-XL-co-expressing cells than in cells only expressing BAX [137,138]. Using HeLa cells, it was demonstrated that even under conditions in which BCL-XL inhibits Bax function, BCL-XL can promote BAX translocation to mitochondria [139]. Additionally, it is known that overexpression of BCL-XL stimulates not only BAX translocation to the mitochondria, but also its retrotranslocation to the cytosol, suggesting that BCL-XL plays a fundamental role in BAX localization, and in the regulation of BAX mitochondrial content [110,138,140]. However, since BAX activation blocks shuttling into the cytosol, active BAX is not retrotranslocated [140]. Curiously, it has been further discovered that a mutant BCL-XL deleted of the C-terminal α-helix (BCL-XLΔC) was not able to retrotranslocate BAX from the mitochondria to the cytosol, indicating an important role of the BCL-XL C-terminal during this process [138,141]. Importantly, the inhibitory effect of BCL-2 and BCL-XL on BAX activation seems to be distinct, as they induce different conformation changes on BAX: while BCL-2 leads to BAX oligomerization but inhibits its insertion into the outer mitochondrial membrane and its permeabilization [121,141], BCL-XL favors the insertion but not the oligomerization [110,138]. Another hypothesis of Bax regulation through anti-apoptotic BCL-2 proteins is the competition between BCL-XL and BAX for binding to MOM and t-BID, in liposomes or in isolated mitochondria [142]. Regarding BH3-only proteins, its binding to the anti-apoptotic proteins or the pro-apoptotic BAX/BAK proteins is highly selective, exhibiting, therefore, different binding affinities for each of them (reviewed in [99,112,143]). For instance, BID, BIM and PUMA strongly bind any anti-apoptotic proteins; BAD preferentially interacts with BCL-2, BCL-XL and BCL-W; NOXA prefers MCL-1 and BFL-1;

and HRK preferentially inhibits BCL-XL. Moreover, while BID preferentially activates BAK, BIM preferentially activates BAX [144–146]. Some studies have suggested constitutively active forms of BAX and BAK controlled by the anti-apoptotic machinery, with MOMP being triggered when activate Bax and BAK are liberated from the anti-apoptotic proteins by BH3 "sensitizers" proteins. In this case, MOMP occurs in the absence of a physical interaction namely between BH3 "sensitizers" and BAX/BAK [147,148]. Interestingly, the activation of BAX and BAK has been observed even without BH3-only activators. Indeed, although these proteins are required for direct activation of BAX and BAK, other direct regulators and interactors may exist in their absence [149,150].

- *Regulation by post-translational modifications*

The stability, localization and function of BCL-2 proteins can be directly regulated by PTMs including phosphorylation/dephosphorylation, ubiquitination, myristoylation, deamination, acetylation and proteolytic cleavage (reviewed by [133]). However, several reports studying PTMs have not been independently confirmed or, in some cases, describe opposite effects. Examples of apoptotic proteins which undergo different PTMs, the targeted residues as well as the outcome on the protein function are illustrated in Table 2.1.

Regarding protein phosphorylation level, and in particular of the members of the BCL-2 family, it must be taken into account that it results from the balance of kinases and phosphatases acting on serine, threonine and tyrosine residues [133]. Some studies have demonstrated that the phosphorylation of BCL-2 at S70 may be required to positively regulate its anti-apoptotic function by enhancing dimerization with BAX and, consequently, suppress apoptosis [151,152]. More recently, it was found a conformation change in the loop domain of BCL-2 associated with the phosphorylation at S70, which strongly increases the affinity and binding of BCL-2 to BAK and BIM. As consequence, these pro-apoptotic proteins are sequestered, enhancing the protection against apoptosis [153]. In contrast, the multisite phosphorylation at T69, S70, and S87 has been proposed to inactivate BCL-2 during the G2/M phase of the cell cycle, inducing apoptosis [154,155]. These contradictory effects have also been noticed for BCL-XL. In response to microtubule inhibitors, BCL-XL maintains its anti-apoptotic function after phosphorylation at S63 but the dephosphorylation may trigger apoptosis [156]. The phosphorylation of BCL-XL mediated by PINK1, a mitochondrial protein kinase, significantly protects cells from apoptotic cell death by impairing its pro-apoptotic N-terminal cleavage, upon mitochondrial depolarization [157]. Conversely, another study suggested that this phosphorylation plays a pro-apoptotic role by restricting the ability of BCL-XL to bind BAX [158].

In the case of BAX, phosphorylation mainly occurs in residues of both its N- and C-termini compromising its binding abilities and the induction of apoptosis [142]. Several studies have reported the phosphorylation of BAX at S184 as one of the most prominent due to its localization in the C-terminal α-helix 9, whose movement is crucial for BAX activation [159]. Indeed, the phosphorylation of this residue mediated by the AKT (protein kinase B) or Protein Kinase Cξ (PKCξ) is known to inhibit BAX through a conformational change that prevents BAX translocation, in neutrophils [160,161] and in a mouse embryonic fibroblasts (MEFs) cell line [162]. In support of these results, the AKT-activated BAX S184 phosphorylation was also observed in A549 human lung cancer cells, in the presence of nicotine. Nicotine favours BAX phosphorylation, which abrogates the cisplatin-induced BAX translocation and MOM insertion, increasing cell survival and chemoresistance [163]. Furthermore, Protein Phosphatase 2A-mediated dephosphorylation of BAX at S184 increases its pro-apoptotic activity [164]. Later, these findings were corroborated using mutants at S184 in MEF or lung cancer H157 cells. Non-phosphorylated BAX mutant S184A allows the conformational change that exposes the 6A7 epitope in the N-terminal, important for BAX activation, operating, therefore, as an active form of BAX. Inversely, a phosphomimetic BAX mutant S184E is not able to insert into the MOM as consequence of a mobility-shift. This suggests that the conformational change conferred by S184 site phosphorylation may directly inactivate the pro-apoptotic function of BAX [165]. Unexpectedly, Simonyan *et al.*, found that the point mutation S184D results in BAX activation in yeast cells heterologously co-expressing AKT and human BAX, indicating that the regulation of BAX by AKT may not simply be a cytosolic sequestration of phosphorylated BAX. Moreover, authors point a more tightly regulation of phosphorylated BAX by BCL-XL [166]. Glycogen Synthase Kinase 3β (GSK3β), another kinase, regulates the activity of BAX through the *in vitro* and *in vivo* direct phosphorylation in another residue site - S163, localized in the loop between α-helices 8 and 9. This phosphorylation promotes the addressing of BAX to mitochondria in HEK293 cells, thereby inducing apoptotic cell death [167]. In contrast with the aforementioned results with BAX-S184A and S184E mutants, the non-phosphorylatable S163A and the phosphomimetic S163D does not significantly alter the apoptotic activity of BAX and its localization in yeast cells [165]. These results suggest that the phosphorylation at S184 displays a more prominent role than the S163 phosphorylation in the modulation of pro-apoptotic function of BAX. Interestingly, the conjugation of the S163D mutant with a P168A/S60A double mutant (inactive but susceptible to conformational changes), results in a strong stimulation of BAX targeting and activation, when compared with S163D alone [111,168]. Nonetheless, GSK3β can be itself phosphorylated and consequently inactivated by AKT. Hence, AKT may inhibit BAX through two different ways: either directly via phosphorylation of S184 or indirectly by preventing the phosphorylation of S163

as consequence of the inactivated GSK3β [111,168]. Another identified phosphorylation site is the Threonine 167 (T167). In human hepatoma HepG2 cells, under stress conditions, c-Jun NH2-terminal kinase or p38 kinase are able to promote the phosphorylation of BAX-T167. As consequence, BAX undergoes a conformational change that exposes the N- and C-terminal domains, increasing its translocation to MOM and activation and thus its killing activity [169].

Besides BCL-2 family proteins, caspases have also been reported as target of phosphorylation, which typically causes inactivation. For instance, procaspase-9 can be phosphorylated at S196 by AKT or RAS (rat sarcoma) [170], at T125 by extracellular signal-regulated kinase (ERK) or cyclin-dependent kinase 1 (CDK1) [171] and at S144 by PKCξ [172] preventing its activation by the impairment of apoptosome formation and, then, restraining the intrinsic apoptotic pathway. Similarly, ERK was shown to phosphorylate procaspase-8 at S387 resulting in the inhibition of its activity and apoptosis induced by TRAIL [173]. Additionally, caspase-8 maturation is regulated via phosphorylation at Y380 [174]. Moreover, p38-MAPK phosphorylates and inhibits the active caspase-8 and caspase-3 at S364 and S150, respectively [175]. Procaspase-7 can also undergo phosphorylation at S30, T173 and S239 by p21-activated kinase 2 which inhibits its activity and decreases apoptosis [176]. Only a single phosphorylation site has been reported for procaspase-6. ARK5 kinase phosphorylates procaspase-6 at S257 leading to its inactivation and the suppression of AKT-dependent cell death mediated by death receptors [177].

Besides phosphorylation, Nt-acetylation has also been described to regulate BAX localization and activity [46]. In previous studies, BAX was one of the Nt-acetylated protein identified in human proteomic analysis [178,179]. As BAX (MDGSGE-) displays one of the amino acid sequence targeted by NatB at the N-terminal (MD-), it was predicted to be NatB substrate. More recently, our group confirmed that BAX is Nt-acetylated by yNaa20p and that its Nt-acetylation is critical to keep BAX in its cytosolic and inactive conformation in yeast and MEF cells [46]. In addition, under basal conditions, the inactivation of *Naa20* favors the targeting of BAX to mitochondria but it is not able to activate it and trigger cyt *c* release. Accordingly, the same phenotype is observed with the knockout of the catalytic subunit NAA20 in MEF cells (results described in detail in Chapter 3).

In addition to these PTMs, it was found that the E3 ubiquitin ligase SCFFBW7 governs cellular apoptosis by ubiquitinating MCL-1 after GSK3β-mediated phosphorylation. In fact, MCL-1 undergoes *in vivo* and *in vitro* phosphorylation by GSK3β at multiple sites (S159, T163, S64 and S121) and the inactivation of these phosphorylation sites impairs the targeting of MCL-1 for degradation by SCFFBW7 *in vivo*, suggesting that GSK3-dependent phosphorylation of MCL-1 is necessary for the interaction of MCL-

1 with SCFFBW7 [180]. In the present thesis, we propose that procaspase-8 and procaspase-9 are also prone to degradation by E3 ubiquitin ligases (results described in detail in Chapter 3).

Table 2.1: Regulation of apoptotic proteins by post-translational modifications (PTM). *n.i. not identified*

PROTEIN	PTM	RESIDUE	OUTCOME	REFERENCE
BCL-2	Phosphorylation	S70	inhibition of apoptosis	[151–155]
		S70, T69, S87	induction of apoptosis	
BCL-XL	Phosphorylation	S63	inhibition of apoptosis	[156]
		S63	inhibition of apoptosis	[157]
		S63	induction of apoptosis	[158]
	Dephosphorylation	S63	induction of apoptosis	[156]
MCL-1	Phosphorylation Ubiquitination	S159, T163, S64, S121	inhibition of apoptosis	[180]
BAX	Phosphorylation	S184	inhibition of apoptosis	[160–163]
	Phosphorylation	S163, T167	induction of apoptosis	[167,169]
	Dephosphorylation	S184	induction of apoptosis	[164]
	Nt-acetylation	N-terminal (MD-)	prevention of mitochondrial targeting	[46]
PROCASPASE-9	Phosphorylation	S196, T125, S144	inhibition of apoptosis	[170–172]
	Ubiquitination	*n.i.*	inhibition of apoptosis	in this study
PROCASPASE-8	Phosphorylation	S387	inhibition of apoptosis	[173]
	Phosphorylation	Y380	maturation of caspase-8	[174]
	Ubiquitination	*n.i.*	inhibition of apoptosis	in this study
CASPASE-8	Phosphorylation	S364	inhibition of caspase-8	[175]
CASPASE-3	Phosphorylation	S150	inhibition of caspase-3	[175]
PROCASPASE-7	Phosphorylation	S30, T173, S239	decrease of apoptosis	[176]
PROCASPASE-6	Phosphorylation	S257	inhibition of apoptosis	[177]

The proteolytic processing may regulate the cellular activity, localization and turnover of the apoptotic proteins by selective cleavage mediated by caspases, calpains, cathepsins and granzymes [132,181–184]. In contrast with other posttranslational modification, the proteolytic cleavage results, in a large part, in protein fragments displaying pro-apoptotic functions, which allows a rapid and efficient execution of apoptosis. Of note, while caspases display a specificity towards aspartate residues [132], the preferred residues for calpains were initially identified as lysine, tyrosine and arginine after the cleavage site (P1 position) [184] but recently several other calpain cleavage sites were identified [185]. Regarding the BCL-2 family proteins, in general, the cleavage of both anti- and pro-apoptotic proteins converts them into fragments with pro-apoptotic functions. Specifically, in the case of pro-apoptotic proteins, their functions are strongly increased, which results in the amplification of the apoptotic cascade. For instance, the cleavage of the unstructured loop domain of BCL-2 at D34 by caspase-3 results in a fragment without the N-terminal BH4 domain, critical for the anti-apoptotic role of BCL-2 [186]. Indeed, this Nt-cleaved form, so-called ΔN34, was shown to induce apoptosis by stimulating cyt *c* release. Caspase-8 was found to cleave BCL-2 in an adjacent site (D31), also generating a truncated fragment with pro-apoptotic activity [187]. BCL-XL is also cleaved by caspase-3 at D61 and D76, generating the corresponding ΔN61 and ΔN76 truncated fragments, which were implicated in pore formation and permeabilization of lipid vesicles, respectively [188,189]. Moreover, both fragments stimulate the release of cyt *c* when incubated with isolated rat mitochondria. Additionally, under hypoxia conditions, BCL-XL can also be cleaved by calpains, at A60 residue, producing a potently proapoptotic C-terminal fragment [190]. MCL-1 is another anti-apoptotic protein which undergoes proteolytic cleavage by caspase-3, at D127 and D157. The fragments generated, ΔN127 and ΔN157, fail to exert anti-apoptotic activity and are found to increase its binding to the pro-apoptotic BIM, as well as to promote the direct interaction with t-BID, BAK and BAX [191–193]. Valero *et al.*, noticed that BFL-1 is cleaved by a calpain between BH4 and BH3 domain at F71 residue, promoting apoptosis through α5/α9-mediated MOM permeabilization [194,195]. Interestingly, the same calpain was found to cleave BAX at D33 generating the p18 fragment with mitochondrial localization and pro-apoptotic function [196]. In contrast to full-length BAX, the cleaved fragment is not able to bind BCL-2. However, BCL-2 overexpression can block calpain activation to hinder BAX cleavage. Although p18 BAX accelerates stress-induced apoptosis, this fragment may be rapidly degraded by a cathepsin-like protease [197]. Besides cleavage at D33, BAX cleavage between Q28 and G29 by calpain results in the $tBAX_{29}$ fragment, identified to enhance the pro-apoptotic function of BAX [198]. Similarly, BAK is also cleaved by a calpain at two different recognition sites R42 localized at the end of the BH4 domain and at R87 within the BH3 domain [139]. In response

to different stimulus, caspase-3 was found to cleave BAD at D14 and D29 generating fragments more potent to induce apoptosis than the full-length BAD [199,200]. BID is mainly cleaved by caspase-8 at D59 generating the truncated t-BID fragment associated to the induction of mitochondrial dysfunction, cyt *c* release, cell shrinkage and nuclear condensation [201]. During UV radiation associated with a cytotoxic drug, caspase-3 is also able to cleave BID at D59 [202]. In response to cisplatin, calpain cleaves BID between G70 and R71 triggering the release of cyt *c* from mitochondria [203]. The isoform Bim_{EL} is N-terminally cleaved by caspase-3 at D13 in the initiation phase of both intrinsic and extrinsic apoptotic pathways. The cleaved fragment exhibits an increased affinity to BCL-2 and, consequently, an increased apoptosis [204].

Interestingly, the majority of procaspases can undergo self-activation. Indeed, procaspase-9 can also be cleaved by itself or by caspase-3 [205,206]; procaspase-3 is cleaved by itself and by caspase-8, -9 and -10 [207]; procaspase-7 undergoes proteolytic cleavage via caspase-3, -8, -9 and -10 and calpains [208–210]; procaspase-6 is cleaved by itself and by caspase-3 [211,212]; procaspase-10 is self-activated [213,214]; and procaspase-8 is cleaved through auto-processing or by caspase-9 [215]. PARP was shown to be cleaved at D214 by caspase-3 and caspase-7 resulting in a fragment with increased rate of cell death [216]. Curiously, the cleavage of APAF1 at D271 by caspase-3 results in a p30 N-terminal fragment with anti-apoptotic functions. In fact, APAF1 p30 fragment is not able to trigger the activation of effector caspases due to the impairment of the apoptosome assemblage, as a result of unfolded or inappropriately oligomerized APAF1 [217].

2.4. Apoptosis and Nt-acetylation

Nt-acetylation has been implicated in several cellular processes including apoptosis [2,3,40]. Despite there are few studies reporting the involvement of Nt-acetylation on the regulation of apoptosis, it is known that the deregulation of NATs or their respective subunits may affect apoptotic cell death. So far, NatA, NatB, NatC and NatD are the only NAT enzymes referred in the literature that were shown to interfere with apoptosis through their role in Nt-acetylation [2,3,40]. Interestingly, these studies have associated both anti- and pro-apoptotic roles to Nt-acetylation.

- *NatA and apoptosis*

The most studied NAT, NatA, mainly exhibits an anti-apoptotic role. Indeed, knockdown of the NatA subunits (NAA10 or NAA15) was shown to induce apoptosis in HeLa cells and sensitize them to the pro-apoptotic stimulus daunorubicin [218]. This effect seems to be dependent on a functional p53 since

knockdown of NAA10 induces apoptosis in human colon carcinoma HCT116 $p53^{(+/+)}$ cells but not in HCT116 $p53^{(-/-)}$ [219]. Another study reported that loss of NAA10 in HCT116 cells promotes formation of double-strand DNA breaks, a type of DNA damage that activates the γH2A.X/Chk2 module that initiates DNA damage signaling. The activation of γH2A.X/Chk2 is independent of p53 status but may lead to activation of the pathway in cells with functional p53, through p53 phosphorylation at Ser15 [219]. Recently, Yang and colleagues showed that miRNAs targeting NAA10 mRNA for degradation promote apoptosis in SW480 and SW620 colon cancer cells, preventing the tumorigenesis of colon cancer cells *in vitro* and *in vivo* [220]. In addition, the miRNA miR-342 decreases the overexpression of NAA10 observed in acute myeloid leukaemia patients, both at gene and protein levels, repressing cell proliferation and increasing cell apoptosis [221]. In another report, NAA10 was shown to modulate the MCL-1 expression, an anti-apoptotic protein and a member of the BCL-2 family of proteins, which are key regulators of apoptosis. In that study, the authors found that NAA10 inhibits apoptosis through RelA/p65-regulated MCL-1 expression, and NAA10 knockdown sensitized colon cancer cells to anticancer drug-induced apoptosis [222]. Furthermore, in the human neuroblastoma cell line SH-SY5Y, Hsp70 NAA10-mediated acetylation protected cells from doxorubicin-induced cell death by sequestering APAF1, inhibiting caspase-3/PARP cleavage, thus preventing apoptosis [223]. Recently, the depletion of NatA by RNAi in HeLa cells was found to generate endogenous SMAC mimetics that cause inactivation and downregulation of IAPs, ultimately triggering apoptosis [95]. Another study conducted in an oxygen-glucose deprivation (OGD) *in vitro* model and middle cerebral artery occlusion (MCAO) *in vivo* rat model, showed that apoptosis is significantly increased after silencing of NAA10 (siNAA10) in response to sevoflurane, an inhaled anesthetic reported to have a neuroprotective effect on cerebral ischemia/reperfusion. In accordance, expression of cleaved caspase-3 in MCAO rats and OGD group was also strongly increased in the same conditions, suggesting that NAA10 downregulation is able to attenuate the neuroprotective effect of sevoflurane in the MCAO model [224]. Altogether, these findings emphasize the involvement of NAA10 on apoptosis inhibition. However, some studies showed an opposite role for NAA10 in apoptosis regulation. NatA was identified as an apoptotic regulator in a genome-wide RNA interference (RNAi) screen in *Drosophila melanogaster* cells in response to DNA damage. This finding prompted to posit that hNaa10p links cell metabolism to apoptosis induction in cancer cells. In fact, hNaa10p depletion caused resistance to apoptosis by repressing caspase-2, -3 and -9 activities in cells where DNA damage was induced. Thus, hNaa10p may be required for caspase activation during apoptosis, promoting cell death and, therefore, holding a pro-apoptotic role [56,225]. More recently, a study correlated NAA10 overexpression with a more prominent chemotherapeutic effect of cisplatin in

oral squamous cell carcinoma. In fact, while high levels of NAA10 enhance cell sensitivity to cisplatin, NAA10 knockdown decreases it. Accordingly, upregulation of NAA10 reduced the expression of the anti-apoptotic BCL-2 protein. This effect was further confirmed *in vivo* in nude mouse xenograft model [226].

- *NatB and apoptosis*

Knockdown studies of the NatB enzymatic complex or its subunits have identified this complex as an essential component for apoptosis regulation. Indeed, knockdown of NAA20 decreased the proliferation of HeLa cells through cell cycle arrest in G2/M and increased susceptibility to the pro-apoptotic agent and proteasome inhibitor MG132 [227]. Depletion of NAA20 also promoted up-regulation of the pro-apoptotic p53 and anti-proliferative p21, and phosphorylation of p53 at Ser15. In a similar study, the same authors observed a clear induction of apoptosis in HepG2 and Hep3B cells expressing *hNAA20* siRNA in response to the treatment with MG132. This effect was correlated with a reduction in the protein levels of the anti-apoptotic protein BCL-2 [228]. Additionally, as referred in 2.3.2, it was found that inactivation of the regulatory subunit NAA25 in MEFs leads to translocation of the pro-apoptotic protein Bax from the cytosol to mitochondria and sensitized MEFs to MG132 [46]. However, as discussed in chapter 3, inactivation of the catalytic subunit NAA20 in MEF cells affects differently their susceptibility to apoptosis but in a stimulus-dependent way.

- *NatC and apoptosis*

So far, knockdown studies of the NatC complex have suggested that this NAT only displays anti-apoptotic functions. For instance, knockdown of NAA30 induced p53-dependent apoptosis in colon carcinoma cells. In fact, NAA30 knockdown was found to increase the p53 levels and its phosphorylation at Ser37, which, in turn, up-regulates downstream pro-apoptotic effectors such as Noxa, KILLER/DR5 and FAS. The same phenotype was observed for HeLa cells [25]. Furthermore, knockdown of NatC subunits led to reduced DNA synthesis, increased cells with sub-G0/G1 DNA content, double-stranded DNA breaks, PARP cleavage promoting growth arrest and likely caspase-dependent cell death. In agreement with this data, Varland and colleagues demonstrated, more recently, that overexpression of NAA30 is able to increase cell viability through apoptosis inhibition [229]. In fact, NAA30 overexpression decreased PARP and α-Fodrin cleavage, two well-studied caspase targets and apoptotic markers. On the other hand, in accordance with previous studies, these authors found increased levels not only of p53 but also of the p53 phosphorylated at Ser15. Decreased levels of cyclin D1, a key regulator of cell proliferation, were also observed upon NAA30 overexpression. In spite of these apparently opposing effects, the authors point to a stronger anti-apoptotic than pro-apoptotic effect responsible for the

increased viability of NAA30-overexpressing cells. Altogether, these outcomes suggest that NatC-mediated acetylation may affect the balance between cell survival and apoptosis.

- *NatD and apoptosis*

Like some of the other NATs, NatD can exhibit either pro- or anti-apoptotic roles. Indeed, NatD complex and the acetyltransferase NAA40 have been identified as critical regulators of the expression of specific genes controlling apoptosis and tumorigenesis. For instance, Liu *et al.* found that NAA40, named as Patt1 in this study, was strongly downregulated in hepatocellular carcinoma tissues conferring a protection from apoptosis in Chang liver cells. Moreover, NAA40 overexpression or upregulation sensitized hepatoma cancer cells to apoptosis induction by chemotherapeutic drugs, therefore displaying a pro-apoptotic effect on these cells, which was dependent on its acetyltransferase activity [230]. In contrast, another study evidenced an anti-apoptotic role by a showing that NAA40 knockdown decreases cell survival and increases apoptosis by either activating the mitochondrial caspase-9-mediated apoptotic pathway, or through a p53-independent mechanism [231].

- *NatH and apoptosis*

As result the recent discovery of NatH, its biological function and mechanism of mediated actin Nt-acetylation are poorly understood and, consequently, its role on apoptosis regulation is still unknown. However, there is evidence of a close connection between apoptosis and the actin machinery although this interaction is not well elucidated [232–234]. Besides actin, several actin-binding proteins were found to play vital roles during the apoptotic process [234,235]. Interestingly, actin appears to be an essential regulator or target in both intrinsic and extrinsic apoptotic pathways. For instance, actin was shown to be required to stimulate death receptors like TNF-α or CD44 to trigger the downstream apoptotic response in Jurkat cells [235]. Another example is the association between F-actin and the pro-apoptotic factor BCL-2 family protein BMF1. Upon a cellular stress, adhesion to the F-actin cytoskeleton is disrupted and BMF1 is translocated to the mitochondria prompting the apoptotic cascade [236]. The involvement of actin on apoptosis was, recently, reviewed by Ren and colleagues, where the important role of actin and actin-binding proteins in apoptosis regulation was greatly highlighted [237]. Taking this evidence into account, it is likely that NatH-mediated Nt-acetylation of actin affects apoptosis induction, and future studies will certainly enlighten the role of this highly selective NAT in apoptosis.

2.5. Apoptosis and N-degron pathways

As mentioned in the previous sections, apoptosis is one of the processes regulated by the N-degron pathways. During the apoptotic process, ~1000 different proteins in a mammalian cell undergo proteolytic cleavage mediated by active caspases and calpains to possibly generate pro-apoptotic fragments that act as apoptosis enhancers. In some cases, these fragments bear destabilizing Nt-residues [70,81]. For instance, a major anti-apoptotic function of the Arg/N-degron pathway through its ability to selectively degrade these pro-apoptotic fragments has been suggested [238–241]. Accordingly, there are studies demonstrating that the inhibition of N-degron pathways, or the knockdown of its components, enhance the cell sensitivity to apoptosis [238]. Indeed, caspase-mediated cleavage of *D. melanogaster* inhibitor of apoptosis 1 (DIAP1) converts the more stable Pro-DIAP1 into the highly unstable Asn-DIAP1, a possible target of N-degron pathways. Loss of *ate1*, the Arg-RNA protein transferase that catalyzes Nt-arginylation required for subsequent ubiquitination, markedly increased the levels of DIAP1, which were unexpectedly associated with apoptosis induction. This apparent contradiction (i.e. that the impairment of DIAP1 degradation results in a failure of DIAP1 to inhibit apoptosis), was explained by its inability to regulate caspases [238]. In another study, the pro-apoptotic fragments Cys-RIPK1, Cys-TRAF1, Asp-BRCA1, Leu-LIMK1, Tyr-NEDD9, Arg-BID, Asp-BCL-XL, Arg-BIM_{EL}, Asp-EPHA4, and Tyr-MET, identified as having destabilizing Nt-residues, were shown to be short-lived due to their degradation via Arg/N-degron pathway, highlighting the anti-apoptotic role of this pathway [240]. Notably, metabolic stabilization of the receptor-interacting serine/threonine protein kinase 1 (RIPK1), key regulator of TNF-mediated apoptosis and necroptosis, through substitution of the Cys- residue by Val-, increased the levels of caspase-3 activation, and partial ablation of the Arg/N-degron pathway sensitized the cells to apoptosis. Altogether these studies suggest that this specific N-degron pathway plays an active role in inhibiting cell death.

Conversely, additional studies showed that the N-degron machinery is able to induce cell death [242] and degrade anti-apoptotic protein fragments [243]. For instance, Eldeeb and colleagues demonstrated how the Arg/N-degron pathway can exhibit a pro-apoptotic function [243]. These authors showed that the N-terminal truncated LynΔN, generated by proteolytic caspase cleavage of the Lyn tyrosine kinase, bear a Nt-Leu destabilizing residue targeted for degradation, making it a Arg-N-degron substrate. Moreover, they found that inhibition of the proteasome by MG132 or the knockdown of UBR1 and UBR2 ubiquitin E3 ligases result in the escape from degradation and, therefore, in the stabilization of LynΔN. As LynΔN protein expression triggers imatinib resistance in chronic myelogenous leukemia K562 cells, its degradation by N-degron pathway was shown to decrease cell viability and, consequently, increase the susceptibility to imatinib. Later, Kumar and colleagues reinforced the specific pro-apoptotic

role of Ate1p and arginylation in response to a lethal stressor. In the presence of a stress, the cellular levels of Ate1p and arginylation activity increased, which directly promoted cell death. In fact, the lack of *ATE1* gene in both *S. cerevisiae* and MEFs greatly attenuated cellular sensitivity to cell death-inducing stress conditions [242], which contradicts the anti-apoptotic role for ATE1 and arginylation previously proposed [238–240].

Different studies also addressed the role of degradation of non-proteolytic processed proteins through the N-degron pathway on apoptosis regulation. Recently, a study showed an enhancement on the effect of apoptosis-inducing drugs *in vitro* and *in vivo* through the knockdown of the Arg/N-degron components [244]. In both Hepa cells and spontaneous mouse model of hepatocellular carcinoma, a combined treatment of staurosporine or doxorubicin with reduced doses of siRNA against UBR1, UBR2, UBR4 and UBR5 resulted in an increase in the percentage of apoptotic cells. However, this study did not identify the possible apoptotic proteins affected by the N-degron pathway. In another study, the β-amyloid peptide (Aβ), inducer of neuronal cell death involved in the processes of neurodegeneration in Alzheimer's disease, was shown to exert its pro-apoptotic effect through the inhibition of the Arg/N-degron pathway. Aβ peptides interact with ATE1 to decrease its enzymatic activity and, therefore, prevent ATE1-mediated arginylation, triggering the apoptotic effects of Aβ peptides [245]. This evidence points to a mutual regulation of Arg/N-degron pathway and apoptosis. In fact, a mutual suppression between this pathway and the apoptotic machinery was suggested, which is supported by the fact that active caspases can downregulate the Arg/N-degron pathway. Effectively, ATE1 and UBR1 cleavage was shown to be mediated by specific activated caspases, which, in turn, leads to the functional inactivation of Arg/N-degron pathway [240]. Recently, a study of the RIPK1, showed that its ubiquitination on Lys376 is mainly mediated by the E3 ubiquitin ligases cIAP1/2. Mutation of RIPK1 (K376R) in primary MEFs remarkably inhibits ubiquitination of RIPK1, and consequently promotes both apoptosis and necroptosis in response to TNF-α. Indeed, cleaved caspase-3 and phosphorylated MLKL, a pseudokinase that plays a key role in TNF-induced necroptosis, are clearly detected in RIPK1$^{K376R/K376R}$ cells [246]. Altogether, these examples attribute an important role of the N-degron pathway in the critical balance between several pro- and anti-apoptotic proteins.

While the Arg/N-degron pathway has been associated with apoptosis regulation, the same is not applicable for the Ac/N-degron pathway. Indeed, its main functions include quality control and the regulation of stoichiometry of protein complexes *in vivo*. Despite the controversy around Nt-acetylation and degradation, Nt-acetylated residues are rarely recognized as Ac/N-degrons as they can be hidden by proper protein folding, interaction with partners or by integration in a protein complex generating

conditional Ac/N-degrons [89–92]. These different ways of protection can be compromised by delayed or defective folding of a protein's N-terminal domain, or by a delay in the partner sequestration or integration in the cognate protein complex that can be caused by different cellular stresses, increasing the probability of protein degradation [247]. As apoptosis can be triggered in response to different stresses, it is plausible that Ac/N-degron pathway has a role in apoptosis modulation. Interestingly, Gly/N-degron pathway is associated with the degradation of the fragments resulting from caspase cleavage [97]. Indeed, approximately one third of the human caspase cleavage sites results in the exposure of a glycine residue at the N-terminal. Therefore, the Gly/N-recognins ZYG11B and ZER1 were shown to target many caspases cleaved fragments for degradation, pointing to an important role of the Gly/N-degron pathway in the regulation of apoptosis.

References

1. Young NL, Plazas-Mayorca MD, Garcia BA. Systems-wide proteomic characterization of combinatorial post-translational modification patterns. Expert Rev Proteomics. 2010;7: 79–92. doi:10.1586/epr.09.100
2. Drazic A, Myklebust LM, Ree R, Arnesen T. The world of protein acetylation. Biochim Biophys Acta - Proteins Proteomics. 2016;1864: 1372–1401. doi:10.1016/j.bbapap.2016.06.007
3. Aksnes H, Drazic A, Marie M, Arnesen T. First Things First: Vital Protein Marks by N-Terminal Acetyltransferases. Trends Biochem Sci. 2016;41: 746–760. doi:10.1016/j.tibs.2016.07.005
4. Deng S, Marmorstein R. Protein N-Terminal Acetylation: Structural Basis, Mechanism, Versatility, and Regulation. Trends Biochem Sci. 2021;46: 15–27. doi:10.1016/j.tibs.2020.08.005
5. Aksnes H, Ree R, Arnesen T. Co-translational, Post-translational, and Non-catalytic Roles of N-Terminal Acetyltransferases. Mol Cell. 2019;73: 1097–1114. doi:10.1016/j.molcel.2019.02.007
6. Arnesen T, Van Damme P, Polevoda B, Helsens K, Evjenth R, Colaert N, et al. Proteomics analyses reveal the evolutionary conservation and divergence of N-terminal acetyltransferases from yeast and humans. Proc Natl Acad Sci. 2009;106: 8157–8162. doi:10.1073/pnas.0901931106
7. Van Damme P, Arnesen T, Gevaert K. Protein alpha-*N*-acetylation studied by N-terminomics. FEBS J. 2011;278: 3822–3834. doi:10.1111/j.1742-4658.2011.08230.x
8. Ree R, Varland S, Arnesen T. Spotlight on protein N-terminal acetylation. Exp Mol Med. 2018;50: 1–13. doi:10.1038/s12276-018-0116-z
9. Aksnes H, Hole K, Arnesen T. Molecular, Cellular, and Physiological Significance of N-Terminal Acetylation. Int Rev Cell Mol Biol. 2015;316: 267–305. doi:10.1016/bs.ircmb.2015.01.001
10. Gevaert K, Goethals M, Martens L, Van Damme J, Staes A, Thomas GR, et al. Exploring proteomes and analyzing protein processing by mass spectrometric identification of sorted N-terminal peptides. Nat Biotechnol. 2003;21: 566–569. doi:10.1038/nbt810
11. Staes A, Impens F, Damme P Van, Ruttens B, Goethals M, Demol H, et al. Selecting protein N-

terminal peptides by combined fractional diagonal chromatography. Nat Protoc. 2011;6: 1130–1141. doi:10.1038/nprot.2011.355

12. Bienvenut W V., Giglione C, Meinnel T. SILProNAQ: A Convenient Approach for Proteome-Wide Analysis of Protein N-Termini and N-Terminal Acetylation Quantitation. Protein Terminal Profiling: Methods and Protocols, Methods in Molecular Biology. 2017. pp. 17–34. doi:10.1007/978-1-4939-6850-3

13. Frottin F, Martinez A, Peynot P, Mitra S, Holz RC, Giglione C, et al. The proteomics of N-terminal methionine cleavage. Mol Cell Proteomics. 2006;5: 2336–2349. doi:10.1074/mcp.M600225-MCP200

14. Mullen JR, Kayne PS, Moerschell RP, Tsunasawa S, Gribskov M, Colavito-Shepanski M, et al. Identification and characterization of genes and mutants for an *N*-terminal acetyltransferase from yeast. EMBO J. 1989;8: 2067–2075. doi:https://doi.org/10.1002/j.1460-2075.1989.tb03615.x

15. Polevoda B, Norbeck J, Takakura H, Blomberg A, Sherman F. Identification and specificities of N-terminal acetyltransferases from *Saccharomyces cerevisiae*. EMBO J. 1999;18: 6155–6168. doi:10.1093/emboj/18.21.6155

16. Helbig AO, Rosati S, Pijnappel PWWM, van Breukelen B, Timmers MHTH, Mohammed S, et al. Perturbation of the yeast N-acetyltransferase NatB induces elevation of protein phosphorylation levels. BMC Genomics. 2010;11: 685(1–15). doi:10.1186/1471-2164-11-685

17. Arnesen T, Anderson D, Baldersheim C, Lanotte M, Varhaug JE, Lillehaug JR. Identification and characterization of the human ARD1-NATH protein acetyltransferase complex. Biochem J. 2005;386: 433–443. doi:10.1042/BJ20041071

18. Park EC, Szostak JW. ARD1 and NAT1 proteins form a complex that has N-terminal acetyltransferase activity. EMBO J. 1992;11: 2087–2093. doi:10.1002/j.1460-2075.1992.tb05267.x

19. Van Damme P. Charting the N-terminal acetylome: A comprehensive map of human NatA substrates. Int J Mol Sci. 2021;22: 10692(1–17). doi:10.3390/ijms221910692

20. Liszczak G, Goldberg JM, Foyn H, Petersson EJ, Arnesen T, Marmorstein R. Molecular basis for N-terminal acetylation by the heterodimeric NatA complex. Nat Struct Mol Biol. 2013;20: 1098–1105. doi:10.1038/nsmb.2636

21. Arnesen T, Starheim KK, Van Damme P, Evjenth R, Dinh H, Betts MJ, et al. The Chaperone-Like Protein HYPK Acts Together with NatA in Cotranslational N-Terminal Acetylation and Prevention of Huntingtin Aggregation. Mol Cell Biol. 2010;30: 1898–1909. doi:10.1128/mcb.01199-09

22. Starheim KK, Arnesen T, Gromyko D, Ryningen A, Varhaug JE, Lillehaug JR. Identification of the human Nα-acetyltransferase complex B (hNatB): A complex important for cell-cycle progression. Biochem J. 2008;415: 325–331. doi:10.1042/BJ20080658

23. Van Damme P, Lasa M, Polevoda B, Gazquez C, Elosegui-Artola A, Kim DS, et al. N-terminal acetylome analyses and functional insights of the N-terminal acetyltransferase NatB. Proc Natl Acad Sci U S A. 2012;109: 12449–12454. doi:10.1073/pnas.1210303109

24. Van Damme P, Kalvik T V., Starheim KK, Jonckheere V, Myklebust LM, Menschaert G, et al. A role for human N-alpha acetyltransferase 30 (Naa30) in maintaining mitochondrial integrity. Mol Cell Proteomics. 2016;15: 3361–3372. doi:10.1074/mcp.M116.061010

25. Starheim KK, Gromyko D, Evjenth R, Ryningen A, Varhaug JE, Lillehaug JR, et al. Knockdown of Human Nα-Terminal Acetyltransferase Complex C Leads to p53-Dependent Apoptosis and Aberrant Human Arl8b Localization. Mol Cell Biol. 2009;29: 3569–3581. doi:10.1128/mcb.01909-08

26. Grunwald S, Hopf LVM, Bock-Bierbaum T, Lally CCM, Spahn CMT, Daumke O. Divergent architecture of the heterotrimeric NatC complex explains N-terminal acetylation of cognate substrates. Nat Commun. 2020;11: 5506(1–14). doi:10.1038/s41467-020-19321-8

27. Magin RS, Liszczak GP, Marmorstein R. The molecular basis for Histone H4- and H2A-specific amino-terminal acetylation by NatD. Structure. 2015;23: 332–341. doi:10.1016/j.str.2014.10.025

28. Hole K, van Damme P, Dalva M, Aksnes H, Glomnes N, Varhaug JE, et al. The human N-Alpha-acetyltransferase 40 (hNaa40p/hNatD) is conserved from yeast and N-terminally acetylates histones H2A and H4. PLoS One. 2011;6: e24713(1-11). doi:10.1371/journal.pone.0024713

29. Song OK, Wang X, Waterborg JH, Sternglanz R. An Nαacetyltransferase responsible for acetylation of the N-terminal residues of histones H4 and H2A. J Biol Chem. 2003;278: 38109–38112. doi:10.1074/jbc.C300355200

30. Evjenth R, Hole K, Karlsen OA, Ziegler M, Amesen T, Lillehaug JR. Human Naa50p (Nat5/San) displays both protein Nα- and Nε-acetyltransferase activity. J Biol Chem. 2009;284: 31122–31129. doi:10.1074/jbc.M109.001347

31. Arnesen T, Anderson D, Torsvik J, Halseth HB, Varhaug JE, Lillehaug JR. Cloning and characterization of hNAT5/hSAN: An evolutionarily conserved component of the NatA protein N-α-acetyltransferase complex. Gene. 2006;371: 291–295. doi:10.1016/j.gene.2005.12.008

32. Van Damme P, Hole K, Gevaert K, Arnesen T. N-terminal acetylome analysis reveals the specificity of Naa50 (Nat5) and suggests a kinetic competition between N-terminal acetyltransferases and methionine aminopeptidases. Proteomics. 2015;15: 2436–2446. doi:10.1002/pmic.201400575

33. Aksnes H, Goris M, Strømland Ø, Drazic A, Waheed Q, Reuter N, et al. Molecular determinants of the N-Terminal acetyltransferase Naa60 anchoring to the Golgi membrane. J Biol Chem. 2017;292: 6821–6837. doi:10.1074/jbc.M116.770362

34. Aksnes H, Van Damme P, Goris M, Starheim KK, Marie M, Støve SI, et al. An organellar Nα-acetyltransferase, Naa60, acetylates cytosolic N termini of transmembrane proteins and maintains golgi integrity. Cell Rep. 2015;10: 1362–1374. doi:10.1016/j.celrep.2015.01.053

35. Dinh T V., Bienvenut W V., Linster E, Feldman-Salit A, Jung VA, Meinnel T, et al. Molecular identification and functional characterization of the first N-alpha-acetyltransferase in plastids by global acetylome profiling. Proteomics. 2015;15: 2426–2435. doi:10.1002/pmic.201500025

36. Drazic A, Aksnes H, Marie M, Boczkowska M, Varland S, Timmerman E, et al. NAA80 is actin's N-terminal acetyltransferase and regulates cytoskeleton assembly and cell motility. Proc Natl Acad Sci U S A. 2018;115: 4399–4404. doi:10.1073/pnas.1718336115

37. Ree R, Kind L, Kaziales A, Varland S, Dai M, Richter K, et al. PFN2 and NAA80 cooperate to efficiently acetylate the N-terminus of actin. J Biol Chem. 2020;295: 16713–16731. doi:10.1074/jbc.RA120.015468

38. Aksnes H, Marie M, Arnesen T, Drazic A. Actin polymerization and cell motility are affected by NAA80-mediated posttranslational N-terminal acetylation of actin. Commun Integr Biol. 2018;11:

1–5. doi:10.1080/19420889.2018.1526572

39. Myklebust LM, Van Damme P, Støve SI, Dörfel MJ, Abboud A, Kalvik T V., et al. Biochemical and cellular analysis of Ogden syndrome reveals downstream Nt-acetylation defects. Hum Mol Genet. 2015;24: 1956–1976. doi:10.1093/hmg/ddu611

40. Kalvik T V., Arnesen T. Protein N-terminal acetyltransferases in cancer. Oncogene. 2013;32: 269–276. doi:10.1038/onc.2012.82

41. Srinivasan S, Chitalia V, Meyer RD, Hartsough E, Mehta M, Harrold I, et al. Hypoxia-induced expression of phosducin-like 3 regulates expression of VEGFR-2 and promotes angiogenesis. Angiogenesis. 2015;18: 449–462. doi:10.1007/s10456-015-9468-3

42. Setty SRG, Strochlic TI, Tong AHY, Boone C, Burd CG. Golgi targeting of Arf-like GTPase Arl3p requires its Nα-acetylation and the integral membrane protein Sys1p. Nat Cell Biol. 2004;6: 414–419. doi:10.1038/ncb1121

43. Behnia R, Panic B, Whyte JRC, Munro S. Targeting of the Arf-like GTPase Arl3p to the Golgi requires N-terminal acetylation and the membrane protein Sys1p. Nat Cell Biol. 2004;6: 405–413. doi:10.1038/ncb1120

44. Behnia R, Barr FA, Flanagan JJ, Barlowe C, Munro S. The yeast orthologue of GRASP65 forms a complex with a coiled-coil protein that contributes to ER to Golgi traffic. J Cell Biol. 2007;176: 255–261. doi:10.1083/jcb.200607151

45. Forte GMA, Pool MR, Stirling CJ. N-terminal acetylation inhibits protein targeting to the endoplasmic reticulum. PLoS Biol. 2011;9: e1001073. doi:10.1371/journal.pbio.1001073

46. Alves S, Neiri L, Chaves SR, Vieira S, Trindade D, Manon S, et al. N-terminal acetylation modulates Bax targeting to mitochondria. Int J Biochem Cell Biol. 2018;95: 35–42. doi:10.1016/j.biocel.2017.12.004

47. Holmes WM, Mannakee BK, Gutenkunst RN, Serio TR. Loss of amino-terminal acetylation suppresses a prion phenotype by modulating global protein folding. Nat Commun. 2014;5: 4383(1–11). doi:10.1038/ncomms5383

48. Ruzafa D, Hernandez-Gomez YS, Bisello G, Broersen K, Morel B, Conejero-Lara F. The influence of N-terminal acetylation on micelle-induced conformational changes and aggregation of α-Synuclein. PLoS One. 2017;12: 1–24. doi:10.1371/journal.pone.0178576

49. Bu B, Tong X, Li D, Hu Y, He W, Zhao C, et al. N-Terminal Acetylation Preserves α-Synuclein from Oligomerization by Blocking Intermolecular Hydrogen Bonds. ACS Chem Neurosci. 2017;8: 2145–2151. doi:10.1021/acschemneuro.7b00250

50. Gottlieb L, Guo L, Shorter J, Marmorstein R. N-alpha-acetylation of Huntingtin protein increases its propensity to aggregate. J Biol Chem. 2021;297: 101363(1–12). doi:10.1016/j.jbc.2021.101363

51. Linster E, Stephan I, Bienvenut W V., Maple-Grødem J, Myklebust LM, Huber M, et al. Downregulation of N-terminal acetylation triggers ABA-mediated drought responses in *Arabidopsis*. Nat Commun. 2015;6: 7640(1–13). doi:10.1038/ncomms8640

52. Molina-Serrano D, Schiza V, Demosthenous C, Stavrou E, Oppelt J, Kyriakou D, et al. Loss of Nat4 and its associated histone H4 N-terminal acetylation mediates calorie restriction-induced longevity. EMBO Rep. 2016;17: 1829–1843. doi:10.15252/embr.201642540

53. Gottlieb L, Marmorstein R. Structure of Human NatA and Its Regulation by the Huntingtin

Interacting Protein HYPK. Structure. 2018;26: 925–935. doi:10.1016/j.str.2018.04.003

54. Deng S, McTiernan N, Wei X, Arnesen T, Marmorstein R. Molecular basis for N-terminal acetylation by human NatE and its modulation by HYPK. Nat Commun. 2020;11: 1–14. doi:10.1038/s41467-020-14584-7

55. Rebowski G, Boczkowska M, Drazic A, Ree R, Goris M, Arnesen T, et al. Mechanism of actin N-terminal acetylation. Sci Adv. 2020;6: eaay8793(1-14). doi:10.1126/sciadv.aay8793

56. Yi CH, Pan H, Seebacher J, Jang IH, Hyberts SG, Heffron GJ, et al. Metabolic regulation of protein N-alpha-acetylation by Bcl-xL promotes cell survival. Cell. 2011;146: 607–620. doi:10.1016/j.cell.2011.06.050

57. Varland S, Aksnes H, Kryuchkov F, Impens F, Van Haver D, Jonckheere V, et al. N-terminal acetylation levels are maintained during acetyl-CoA deficiency in *Saccharomyces cerevisiae*. Mol Cell Proteomics. 2018;17: 2309–2323. doi:10.1074/mcp.RA118.000982

58. Varland S, Osberg C, Arnesen T. N-terminal modifications of cellular proteins: The enzymes involved, their substrate specificities and biological effects. Proteomics. 2015;15: 2385–2401. doi:10.1002/pmic.201400619

59. Castrec B, Dian C, Ciccone S, Ebert CL, Bienvenut W V., Le Caer JP, et al. Structural and genomic decoding of human and plant myristoylomes reveals a definitive recognition pattern. Nat Chem Biol. 2018;14: 671–679. doi:10.1038/s41589-018-0077-5

60. Petkowski JJ, Schaner Tooley CE, Anderson LC, Shumilin IA, Balsbaugh JL, Shabanowitz J, et al. Substrate specificity of mammalian N-terminal α-amino methyltransferase NRMT. Biochemistry. 2012;51: 5942–5950. doi:10.1021/bi300278f

61. Nevitt C, Tooley JG, Schaner Tooley CE. N-terminal acetylation and methylation differentially affect the function of MYL9. Biochem J. 2018;475: 3201–3219. doi:10.1042/BCJ20180638

62. Schiza V, Molina-Serrano D, Kyriakou D, Hadjiantoniou A, Kirmizis A. N-alpha-terminal Acetylation of Histone H4 Regulates Arginine Methylation and Ribosomal DNA Silencing. PLoS Genet. 2013;9: e1003805(1-12). doi:10.1371/journal.pgen.1003805

63. Ju J, Chen A, Deng Y, Liu M, Wang Y, Wang Y, et al. NatD promotes lung cancer progression by preventing histone H4 serine phosphorylation to activate Slug expression. Nat Commun. 2017;8: 928(1–14). doi:10.1038/s41467-017-00988-5

64. Akimov V, Barrio-Hernandez I, Hansen SVF, Hallenborg P, Pedersen AK, Bekker-Jensen DB, et al. UbiSite approach for comprehensive mapping of lysine and n-terminal ubiquitination sites. Nat Struct Mol Biol. 2018;25: 631–640. doi:10.1038/s41594-018-0084-y

65. Jörnvall H. Acetylation of protein N-terminal amino groups structural observations on α-amino acetylated proteins. J Theor Biol. 1975;55: 1–12. doi:10.1016/S0022-5193(75)80105-6

66. Hershko A, Heller H, Eytan E, Kaklij G, Rose IA. Role of the α-amino group of protein in ubiquitin-mediated protein breakdown. Proc Natl Acad Sci U S A. 1984;81: 7021–7025. doi:10.1073/pnas.81.22.7021

67. Hwang C-S, Shemorry A, Varshavsky A. N-Terminal Acetylation of Cellular Proteins Creates Specific Degradation Signals. Science. 2010;327: 973–977. doi:10.1126/science.1183147

68. Bachmair A, Finley D, Varshavsky A. In vivo half-life of a protein is a function of its amino-terminal residue. Science. 1986;234: 179–186. doi:10.1126/science.3018930

69. Varshavsky A. The N-end rule: Functions, mysteries, uses. Proc Natl Acad Sci U S A. 1996;93: 12142–12149. doi:10.1073/pnas.93.22.12142

70. Varshavsky A. N-degron and C-degron pathways of protein degradation. Proc Natl Acad Sci U S A. 2019;116: 358–366. doi:10.1073/pnas.1816596116

71. Vu TTM, Mitchell DC, Gygi SP, Varshavsky A. The Arg/N-degron pathway targets transcription factors and regulates specific genes. Proc Natl Acad Sci U S A. 2020;117: 31094–31104. doi:10.1073/pnas.2020124117

72. Timms RT, Koren I. Tying up loose ends: The N-degron and C-degron pathways of protein degradation. Biochem Soc Trans. 2020;48: 1557–1567. doi:10.1042/BST20191094

73. Nguyen KT, Kim JM, Park SE, Hwang CS. N-terminal methionine excision of proteins creates tertiary destabilizing N-degrons of the Arg/N-end rule pathway. J Biol Chem. 2019;294: 4464–4476. doi:10.1074/jbc.RA118.006913

74. Bachmair A, Varshavsky A. The degradation signal in a short-lived protein. Cell Press. 1989;56: 1019–1032. doi:10.1016/0092-8674(89)90635-1

75. Varshavsky A. The N-end rule pathway and regulation by proteolysis. Protein Sci. 2011;20: 1298–1345. doi:10.1002/pro.666

76. Kim HK, Kim RR, Oh JH, Cho H, Varshavsky A, Hwang CS. The N-terminal methionine of cellular proteins as a degradation signal. Cell. 2014;156: 158–169. doi:10.1016/j.cell.2013.11.031

77. Kim JM, Seok OH, Ju S, Heo JE, Yeom J, Kim DS, et al. Formyl-methionine as an N-degron of a eukaryotic N-end rule pathway. Science. 2018;362: 1–19. doi:10.1126/science.aat0174

78. Nguyen KT, Mun SH, Lee CS, Hwang CS. Control of protein degradation by N-terminal acetylation and the N-end rule pathway. Exp Mol Med. 2018;50: 91(1–8). doi:10.1038/s12276-018-0097-y

79. Wang H, Piatkov KI, Brower CS, Varshavsky A. Glutamine-Specific N-Terminal Amidase, a Component of the N-End Rule Pathway. Mol Cell. 2009;34: 686–695. doi:10.1016/j.molcel.2009.04.032

80. Kwon YT, Kashina AS, Davydov I V., Hu RG, An JY, Seo JW, et al. An essential role of N-terminal arginylation in cardiovascular development. Science. 2002;297: 96–99. doi:10.1126/science.1069531

81. Kim JG, Shin HC, Seo T, Nawale L, Han G, Kim BY, et al. Signaling pathways regulated by UBR box-containing E3 ligases. Int J Mol Sci. 2021;22: 8323(1–23). doi:10.3390/ijms22158323

82. Choi WS, Jeong BC, Joo YJ, Lee MR, Kim J, Eck MJ, et al. Structural basis for the recognition of N-end rule substrates by the UBR box of ubiquitin ligases. Nat Struct Mol Biol. 2010;17: 1175–1181. doi:10.1038/nsmb.1907

83. Tasaki T, Zakrzewska A, Dudgeon DD, Jiang Y, Lazo JS, Kwon YT. The substrate recognition domains of the N-end rule pathway. J Biol Chem. 2009;284: 1884–1895. doi:10.1074/jbc.M803641200

84. Tasaki T, Kim ST, Zakrzewska A, Lee BE, Kang MJ, Yoo YD, et al. UBR box N-recognin-4 (UBR4), an N-recognin of the N-end rule pathway, and its role in yolk sac vascular development and autophagy. Proc Natl Acad Sci U S A. 2013;110: 3800–3805. doi:10.1073/pnas.1217358110

85. Sriram S, Lee JH, Mai BK, Jiang Y, Kim Y, Yoo YD, et al. Development and characterization of monomeric N-end rule inhibitors through *in vitro* model substrates. J Med Chem. 2013;56: 2540–

2546. doi:10.1021/jm400046q

86. Min JL, Pal K, Tasaki T, Roy S, Jiang Y, Jee YA, et al. Synthetic heterovalent inhibitors targeting recognition E3 components of the N-end rule pathway. Proc Natl Acad Sci U S A. 2008;105: 100–105. doi:10.1073/pnas.0708465105

87. Agarwalla P, Banerjee R. N-end rule pathway inhibition assists colon tumor regression via necroptosis. Mol Ther - Oncolytics. 2016;3: 16020. doi:10.1038/mto.2016.20

88. Eldeeb MA, Fahlman RP, Ragheb MA, Esmaili M. Does N-Terminal Protein Acetylation Lead to Protein Degradation? BioEssays. 2019;41: 1800167(1–10). doi:10.1002/bies.201800167

89. Lee KE, Heo JE, Kim JM, Hwang CS. N-terminal acetylation-targeted N-end rule proteolytic system: The Ac/N-end rule pathway. Mol Cells. 2016;39: 169–178. doi:10.14348/molcells.2016.2329

90. Kats I, Khmelinskii A, Kschonsak M, Huber F, Knieß RA, Bartosik A, et al. Mapping Degradation Signals and Pathways in a Eukaryotic N-terminome. Mol Cell. 2018;70: 488–501. doi:10.1016/j.molcel.2018.03.033

91. Park SE, Kim J-M, Seok OH, Cho H, Wadas B, Kim S-Y, et al. Control of mammalian G protein signaling by N-terminal acetylation and the N-end rule pathway. Science. 2015;347: 1249–1252. doi:10.1126/science.aaa3844

92. Shemorry A, Hwang CS, Varshavsky A. Control of Protein Quality and Stoichiometries by N-Terminal Acetylation and the N-End Rule Pathway. Mol Cell. 2013;50: 540–551. doi:10.1016/j.molcel.2013.03.018

93. Scott DC, Monda JK, Bennett EJ, Harper JW, Schulman BA. N-terminal acetylation acts as an avidity enhancer within an interconnected multiprotein complex. Science. 2011;334: 674–678. doi:10.1126/science.1209307

94. Oh JH, Hyun JY, Varshavsky A. Control of Hsp90 chaperone and its clients by N-terminal acetylation and the N-end rule pathway. Proc Natl Acad Sci U S A. 2017;114: E4370–E4379. doi:10.1073/pnas.1705898114

95. Mueller F, Friese A, Pathe C, Da Silva RC, Rodriguez KB, Musacchio A, et al. Overlap of NatA and IAP substrates implicates N-terminal acetylation in protein stabilization. Sci Adv. 2021;7: eabc8590(1-14). doi:10.1126/sciadv.abc8590

96. Sheng Z, Du W. NatB regulates Rb mutant cell death and tumor growth by modulating EGFR/MAPK signaling through the N-end rule pathways. PLoS Genet. 2020;16: e1008863(1-25). doi:10.1371/journal.pgen.1008863

97. Timms RT, Zhang Z, Rhee DY, Harper JW, Koren I, Elledge SJ. A glycine-specific N-degron pathway mediates the quality control of protein N-myristoylation. Science. 2019;365: eaaw4912. doi:10.1126/science.aaw4912

98. Bertheloot D, Latz E, Franklin BS. Necroptosis, pyroptosis and apoptosis: an intricate game of cell death. Cell Mol Immunol. 2021;18: 1106–1121. doi:10.1038/s41423-020-00630-3

99. Galluzzi L, Vitale I, Aaronson SA, Abrams JM, Adam D, Agostinis P, et al. Molecular mechanisms of cell death: Recommendations of the Nomenclature Committee on Cell Death 2018. Cell Death Differ. 2018;25: 486–541. doi:10.1038/s41418-017-0012-4

100. Kerr JFR, Wyllie AH, Currie AR. Apoptosis: a basic biological phenomenon with wideranging implications in tissue kinetics. Br J Cancer. 1972;26: 239–257. doi:10.1038/bjc.1972.33

101. Galluzzi L, Bravo-San Pedro JM, Vitale I, Aaronson SA, Abrams JM, Adam D, et al. Essential versus accessory aspects of cell death: Recommendations of the NCCD 2015. Cell Death Differ. 2015;22: 58–73. doi:10.1038/cdd.2014.137

102. Ashkenazi A, Salvesen G. Regulated cell death: signaling and mechanisms. Annu Rev Cell Dev Biol. 2014;30: 337–356. doi:10.1146/annurev-cellbio-100913-013226

103. Medema JP, Scaffidi C, Kischkel FC, Shevchenko A, Mann M, Krammer PH, et al. FLICE is activated by association with the CD95 death-inducing signaling complex (DISC). EMBO J. 1997;16: 2794–2804. doi:10.1093/emboj/16.10.2794

104. Muzio M, Chinnaiyan AM, Kischkel FC, O'Rourke K, Shevchenko A, Ni J, et al. FLICE, a novel FADD-homologous ICE/CED-3-like protease, is recruited to the CD95 (Fas/APO-1) death–inducing signaling complex. Cell. 1996;85: 817–827. doi:10.1016/s0092-8674(00)81266-0

105. Oberst A, Pop C, Tremblay AG, Blais V, Denault JB, Salvesen GS, et al. Inducible dimerization and inducible cleavage reveal a requirement for both processes in caspase-8 activation. J Biol Chem. 2010;285: 16632–16642. doi:10.1074/jbc.M109.095083

106. Hughes MA, Powley IR, Jukes-Jones R, Horn S, Feoktistova M, Fairall L, et al. Co-operative and Hierarchical Binding of c-FLIP and Caspase-8: A Unified Model Defines How c-FLIP Isoforms Differentially Control Cell Fate. Mol Cell. 2016;61: 834–849. doi:10.1016/j.molcel.2016.02.023

107. Huang K, Zhang J, O'Neill KL, Gurumurthy CB, Quadros RM, Tu Y, et al. Cleavage by Caspase 8 and Mitochondrial Membrane Association Activate the BH3-only Protein Bid during TRAIL-induced Apoptosis. J Biol Chem. 2016;291: 11843–11851. doi:10.1074/jbc.M115.711051

108. Green DR, Llambi F. Cell death signaling. Cold Spring Harb Perspect Biol. 2015;7: a006080(1-24). doi:10.1101/cshperspect.a006080

109. Cotter TG. Apoptosis and cancer: The genesis of a research field. Nat Rev Cancer. 2009;9: 501–507. doi:10.1038/nrc2663

110. Renault TT, Dejean LM, Manon S. A brewing understanding of the regulation of Bax function by Bcl-xL and Bcl-2. Mech Ageing Dev. 2016;161: 201–210. doi:10.1016/j.mad.2016.04.007

111. Renault TT, Manon S. Bax: Addressed to kill. Biochimie. 2011;93: 1379–1391. doi:10.1016/j.biochi.2011.05.013

112. Kale J, Osterlund EJ, Andrews DW. BCL-2 family proteins: Changing partners in the dance towards death. Cell Death Differ. 2018;25: 65–80. doi:10.1038/cdd.2017.186

113. Gross A, McDonnell JM, Korsmeyer SJ. BCL-2 family members and the mitochondria in apoptosis. Genes Dev. 1999;13: 1899–1911. doi:10.1101/gad.13.15.1899

114. Letai A, Bassik MC, Walensky LD, Sorcinelli MD, Weiler S, Korsmeyer SJ. Distinct BH3 domains either sensitize or activate mitochondrial apoptosis, serving as prototype cancer therapeutics. Cancer Cell. 2002;2: 183–192. doi:10.1016/S1535-6108(02)00127-7

115. Schellenberg B, Wang P, Keeble JA, Rodriguez-Enriquez R, Walker S, Owens TW, et al. Bax Exists in a Dynamic Equilibrium between the Cytosol and Mitochondria to Control Apoptotic Priming. Mol Cell. 2013;49: 959–971. doi:10.1016/j.molcel.2012.12.022

116. Cartron PF, Priault M, Oliver L, Meflah K, Manon S, Vallette FM. The N-terminal end of Bax contains a mitochondrial-targeting signal. J Biol Chem. 2003;278: 11633–11641. doi:10.1074/jbc.M208955200

117. Wolter KG, Hsu Y Te, Smith CL, Nechushtan A, Xi XG, Youle RJ. Movement of Bax from the cytosol to mitochondria during apoptosis. J Cell Biol. 1997;139: 1281–1292. doi:10.1083/jcb.139.5.1281

118. Cartron PF, Moreau C, Oliver L, Mayat E, Meflah K, Vallette FM. Involvement of the N-terminus of Bax in its intracellular localization and function. FEBS Lett. 2002;512: 95–100. doi:10.1016/S0014-5793(02)02227-5

119. Kalkavan H, Green DR. MOMP, cell suicide as a BCL-2 family business. Cell Death Differ. 2018;25: 46–55. doi:10.1038/cdd.2017.179

120. Lee EF, Grabow S, Chappaz S, Dewson G, Hockings C, Kluck RM, et al. Physiological restraint of Bak by Bcl-xL is essential for cell survival. Genes Dev. 2016;30: 1240–1250. doi:10.1101/gad.279414.116

121. Renault TT, Teijido O, Antonsson B, Dejean LM, Manon S. Regulation of Bax mitochondrial localization by Bcl-2 and Bcl-xL: Keep your friends close but your enemies closer. Int J Biochem Cell Biol. 2013;45: 64–67. doi:10.1016/j.biocel.2012.09.022

122. Li P, Nijhawan D, Budihardjo I, Srinivasula SM, Ahmad M, Alnemri ES, et al. Cytochrome c and dATP-dependent formation of Apaf-1/caspase-9 complex initiates an apoptotic protease cascade. Cell. 1997;91: 479–489. doi:10.1016/S0092-8674(00)80434-1

123. Nagata S. DNA degradation in development and programmed cell death. Annu Rev Immunol. 2005;23: 853–875. doi:10.1146/annurev.immunol.23.021704.115811

124. Martin SJ, Finucane DM, Amarante-Mendes GP, O'Brien GA, Green DR. Phosphatidylserine externalization during CD95-induced apoptosis of cells and cytoplasts requires ICE/CED-3 protease activity. J Biol Chem. 1996;271: 28753–28756. doi:10.1074/jbc.271.46.28753

125. Naito M, Nagashima K, Mashima T, Tsuruo T. Phosphatidylserine externalization is a downstream event of interleukin- 1β -converting enzyme family protease activation during apoptosis. Blood. 1997;89: 2060–2066. doi:10.1182/blood.v89.6.2060

126. Coleman ML, Sahai EA, Yeo M, Bosch M, Dewar A, Olson MF. Membrane blebbing during apoptosis results from caspase-mediated activation of ROCK I. Nat Cell Biol. 2001;3: 339–346. doi:10.1038/35070009

127. Eckelman BP, Salvesen GS, Scott FL. Human inhibitor of apoptosis proteins: Why XIAP is the black sheep of the family. EMBO Rep. 2006;7: 988–994. doi:10.1038/sj.embor.7400795

128. Graber TE, Holcik M. Distinct roles for the cellular inhibitors of apoptosis proteins 1 and 2. Cell Death Dis. 2011;2: e135(1-3). doi:10.1038/cddis.2011.20

129. Verhagen AM, Ekert PG, Pakusch M, Silke J, Connolly LM, Reid GE, et al. Identification of DIABLO, a mammalian protein that promotes apoptosis by binding to and antagonizing IAP proteins. Cell. 2000;102: 43–53. doi:10.1016/S0092-8674(00)00009-X

130. Du C, Fang M, Li Y, Li L, Wang X. Smac, a mitochondrial protein that promotes cytochrome c-dependent caspase activation by eliminating IAP inhibition. Cell. 2000;102: 33–42. doi:10.1016/S0092-8674(00)00008-8

131. Czabotar PE, Lessene G, Strasser A, Adams JM. Control of apoptosis by the BCL-2 protein family: Implications for physiology and therapy. Nat Rev Mol Cell Biol. 2014;15: 49–63. doi:10.1038/nrm3722

132. Crawford ED, Wells JA. Caspase substrates and cellular remodeling. Annu Rev Biochem. 2011;80:

1055–1087. doi:10.1146/annurev-biochem-061809-121639

133. Letai A, Kutuk O. Regulation of Bcl-2 Family Proteins by Posttranslational Modifications. Curr Mol Med. 2008;8: 102–118. doi:10.2174/156652408783769599

134. Lalier L, Vallette F, Manon S. Bcl-2 Family Members and the Mitochondrial Import Machineries: The Roads to Death. Biomolecules. 2022;12: 162(1–19). doi:10.3390/biom12020162

135. Korsmeyer SJ, Shutter JR, Veis DJ, Merry DE, Oltvai ZN. Bcl-2/Bax: a rheostat that regulates an anti-oxidant pathway and cell death. Semin Cancer Biol. 1993;4: 327–332.

136. Teijido O, Dejean L. Upregulation of Bcl2 inhibits apoptosis-driven BAX insertion but favors BAX relocalization in mitochondria. FEBS Lett. 2010;584: 3305–3310. doi:10.1016/j.febslet.2010.07.002

137. Gautier F, Guillemin Y, Cartron PF, Gallenne T, Cauquil N, Le Diguarher T, et al. Bax Activation by Engagement with, Then Release from, the BH3 Binding Site of Bcl-xL. Mol Cell Biol. 2011;31: 832–844. doi:10.1128/mcb.00161-10

138. Renault TT, Teijido O, Missire F, Ganesan YT, Velours G, Arokium H, et al. Bcl-xL stimulates Bax relocation to mitochondria and primes cells to ABT-737. Int J Biochem Cell Biol. 2015;64: 136–146. doi:10.1016/j.biocel.2015.03.020

139. Llambi F, Moldoveanu T, Tait SWG, Bouchier-Hayes L, Temirov J, McCormick LL, et al. A Unified Model of Mammalian BCL-2 Protein Family Interactions at the Mitochondria. Mol Cell. 2011;44: 517–531. doi:10.1016/j.molcel.2011.10.001

140. Edlich F, Banerjee S, Suzuki M, Cleland MM, Arnoult D, Wang C, et al. Bcl-xL retrotranslocates Bax from the mitochondria into the cytosol. Cell. 2011;145: 104–116. doi:10.1016/j.cell.2011.02.034

141. Todt F, Cakir Z, Reichenbach F, Youle RJ, Edlich F. The C-terminal helix of Bcl-xL mediates Bax retrotranslocation from the mitochondria. Cell Death Differ. 2013;20: 333–342. doi:10.1038/cdd.2012.131

142. Billen LP, Kokoski CL, Lovell JF, Leber B, Andrews DW. Bcl-XL inhibits membrane permeabilization by competing with Bax. PLoS Biol. 2008;6: 1268–1280. doi:10.1371/journal.pbio.0060147

143. Singh R, Letai A, Sarosiek K. Regulation of apoptosis in health and disease: the balancing act of BCL-2 family proteins. Nat Rev Mol Cell Biol. 2019;20: 175–193. doi:10.1038/s41580-018-0089-8

144. Moldoveanu T, Grace CR, Llambi F, Nourse A, Fitzgerald P, Gehring K, et al. BID-induced structural changes in BAK promote apoptosis. Nat Struct Mol Biol. 2013;20: 589–597. doi:10.1038/nsmb.2563

145. Sarosiek KA, Chi X, Bachman JA, Sims JJ, Montero J, Patel L, et al. BID preferentially activates BAK while BIM preferentially activates BAX, affecting chemotherapy response. Mol Cell Biol. 2013;51: 751–765. doi:10.1016/j.molcel.2013.08.048

146. Gavathiotis E, Suzuki M, Davis ML, Pitter K, Bird GH, Katz SG, et al. BAX activation is initiated at a novel interaction site. Nature. 2008;455: 1076–1081. doi:10.1038/nature07396

147. Willis SN, Chen L, Dewson G, Wei A, Naik E, Fletcher JI, et al. Proapoptotic Bak is sequestered by Mcl-1 and Bcl-xL, but not Bcl-2, until displaced by BH3-only proteins. Genes Dev. 2005;19: 1294–1305. doi:10.1101/gad.1304105

148. O'neill KL, Huang K, Zhang J, Chen Y, Luo X. Inactivation of prosurvival Bcl-2 proteins activates Bax/Bak through the outer mitochondrial membrane. Genes Dev. 2016;30: 973–988. doi:10.1101/gad.276725.115

149. Brahmbhatt H, Uehling D, Al-awar R, Leber B, Andrews D. Small molecules reveal an alternative mechanism of Bax activation. Biochem J. 2016;473: 1073–1083. doi:10.1042/BCJ20160118

150. Chen HC, Kanai M, Inoue-Yamauchi A, Tu HC, Huang Y, Ren D, et al. An interconnected hierarchical model of cell death regulation by the BCL-2 family. Nat Cell Biol. 2015;17: 1270–1281. doi:10.1038/ncb3236

151. Deng X, Ruvolo P, Carr B, May WS. Survival function of ERK1/2 as IL-3-activated, staurosporine-resistant Bcl2 kinases. 2000;97: 1578–1583. doi:10.1073/pnas.97.4.1578

152. Deng X, Gao F, Flagg T, May WS. Mono- and multisite phosphorylation enhances Bcl2's antiapoptotic function and inhibition of cell cycle entry functions. Proc Natl Acad Sci U S A. 2004;101: 153–158. doi:10.1073/pnas.2533920100

153. Dai H, Ding H, Meng XW, Lee SH, Schneider PA, Kaufmann SH. Contribution of Bcl-2 phosphorylation to bak binding and drug resistance. Cancer Res. 2013;73: 6998–7008. doi:10.1158/0008-5472.CAN-13-0940

154. Vantieghem A, Xu Y, Assefa Z, Piette J, Vandenheede JR, Merlevede W, et al. Phosphorylation of Bcl-2 in G2/M phase-arrested cells following photodynamic therapy with hypericin involves a CDK1-mediated signal and delays the onset of apoptosis. J Biol Chem. 2002;277: 37718–37731. doi:10.1074/jbc.M204348200

155. Yamamoto K, Ichijo H, Korsmeyer SJ. BCL-2 is phosphorylated and inactivated by an ASK1/Jun N-terminal protein kinase pathway normally activated at G(2)/M. Mol Cell Biol. 1999;19: 8469–8478. doi:10.1128/MCB.19.12.8469

156. Du L, Lyle CS, Chambers TC. Characterization of vinblastine-induced Bcl-xL and Bcl-2 phosphorylation: Evidence for a novel protein kinase and a coordinated phosphorylation/ dephosphorylation cycle associated with apoptosis induction. Oncogene. 2005;24: 107–117. doi:10.1038/sj.onc.1208189

157. Arena G, Gelmetti V, Torosantucci L, Vignone D, Lamorte G, De Rosa P, et al. PINK1 protects against cell death induced by mitochondrial depolarization, by phosphorylating Bcl-xL and impairing its pro-apoptotic cleavage. Cell Death Differ. 2013;20: 920–930. doi:10.1038/cdd.2013.19

158. Upreti M, Galitovskaya EN, Chu R, Tackett AJ, Terrano DT, Granell S, et al. Identification of the major phosphorylation site in Bcl-xL induced by microtubule inhibitors and analysis of its functional significance. J Biol Chem. 2008;283: 35517–35525. doi:10.1074/jbc.M805019200

159. Suzuki M, Youle RJ, Tjandra N. Structure of Bax: Coregulation of Dimer Formation and Intracellular Localization. Cell. 2000;103: 645–654. doi:http://dx.doi.org/10.1016/S0092-8674(00)00167-7

160. Gardai SJ, Hildeman DA, Frankel SK, Whitlock BB, Frasch SC, Borregaard N, et al. Phosphorylation of Bax Ser184 by Akt regulates its activity and apoptosis in neutrophils. J Biol Chem. 2004;279: 21085–21095. doi:10.1074/jbc.M400063200

161. Yamaguchi H, Wang HG. The protein kinase PKB/Akt regulates cell survival and apoptosis by inhibiting Bax conformational change. Oncogene. 2001;20: 7779–7786. doi:10.1038/sj.onc.1204984

162. Xin M, Gao F, May WS, Flagg T, Deng X. Protein kinase Czeta abrogates the proapoptotic function of Bax through phosphorylation. J Biol Chem. 2007;282: 21268–21277. doi:10.1074/jbc.M701613200

163. Xin M, Deng X. Nicotine inactivation of the proapoptotic function of Bax through phosphorylation. J Biol Chem. 2005;280: 10781–10789. doi:10.1074/jbc.M500084200

164. Xin M, Deng X. Protein phosphatase 2A enhances the proapoptotic function of Bax through dephosphorylation. J Biol Chem. 2006;281: 18859–18867. doi:10.1074/jbc.M512543200

165. Wang Q, Sun SY, Khuri F, Curran WJ, Deng X. Mono- or double-site phosphorylation distinctly regulates the proapoptotic function of Bax. PLoS One. 2010;5: e13393(1-8). doi:10.1371/journal.pone.0013393

166. Simonyan L, Renault TT, Da Costa Novais MJ, Sousa MJ, Côrte-Real M, Camougrand N, et al. Regulation of Bax/mitochondria interaction by AKT. FEBS Lett. 2016;590: 13–21. doi:10.1002/1873-3468.12030

167. Linseman DA, Butts BD, Precht TA, Phelps RA, Le SS, Laessig TA, et al. Glycogen synthase kinase-3β phosphorylates bax and promotes its mitochondrial localization during neuronal apoptosis. J Neurosci. 2004;24: 9993–10002. doi:10.1523/JNEUROSCI.2057-04.2004

168. Arokium H, Ouerfelli H, Velours G, Camougrand N, Vallette FM, Manon S. Substitutions of potentially phosphorylatable serine residues of bax reveal how they may regulate its interaction with mitochondria. J Biol Chem. 2007;282: 35104–35112. doi:10.1074/jbc.M704891200

169. Kim BJ, Ryu SW, Song BJ. JNK- and p38 kinase-mediated phosphorylation of Bax leads to its activation and mitochondrial translocation and to apoptosis of human hepatoma HepG2 cells. J Biol Chem. 2006;281: 21256–21265. doi:10.1074/jbc.M510644200

170. Cardone MH, Roy N, Stennicke HR, Salvesen GS, Franke TF, Stanbridge E, et al. Regulation of cell death protease caspase-9 by phosphorylation. Science. 1998;282: 1318–1321. doi:10.1126/science.282.5392.1318

171. Allan LA, Clarke PR. Phosphorylation of Caspase-9 by CDK1/Cyclin B1 protects mitotic cells against apoptosis. Mol Cell. 2007;26: 301–310. doi:10.1016/j.molcel.2007.03.019

172. Brady SC, Allan LA, Clarke PR. Regulation of Caspase 9 through Phosphorylation by Protein Kinase C Zeta in Response to Hyperosmotic Stress. Mol Cell Biol. 2005;25: 10543–10555. doi:10.1128/mcb.25.23.10543-10555.2005

173. Mandal R, Raab M, Matthess Y, Becker S, Knecht R, Strebhardt K. PERK 1/2 inhibit Caspase-8 induced apoptosis in cancer cells by phosphorylating it in a cell cycle specific manner. Mol Oncol. 2014;8: 232–249. doi:10.1016/j.molonc.2013.11.003

174. Cursi S, Rufini A, Stagni V, Condò I, Matafora V, Bachi A, et al. Src kinase phosphorylates Caspase-8 on Tyr380: A novel mechanism of apoptosis suppression. EMBO J. 2006;25: 1895–1905. doi:10.1038/sj.emboj.7601085

175. Alvarado-Kristensson M, Melander F, Leandersson K, Rönnstrand L, Wernstedt C, Andersson T. p38-MAPK Signals Survival by Phosphorylation of Caspase-8 and Caspase-3 in Human Neutrophils. J Exp Med. 2004;199: 449–458. doi:10.1084/jem.20031771

176. Li X, Wen W, Liu K, Zhu F, Malakhova M, Peng C, et al. Phosphorylation of caspase-7 by p21-activated protein kinase (PAK) 2 inhibits chemotherapeutic drug-induced apoptosis of breast cancer cell lines. J Biol Chem. 2011;286: 22291–22299. doi:10.1074/jbc.M111.236596

177. Velázquez-Delgado EM, Hardy JA. Phosphorylation regulates assembly of the caspase-6 substrate-binding groove. Structure. 2012;20: 742–751. doi:10.1016/j.str.2012.02.003

178. Gauci S, Helbig AO, Slijper M, Krijgsveld J, Heck AJR, Mohammed S. Lys-N and trypsin cover complementary parts of the phosphoproteome in a refined SCX-based approach. Anal Chem. 2009;81: 4493–4501. doi:10.1021/ac9004309

179. Vaca Jacome AS, Rabilloud T, Schaeffer-Reiss C, Rompais M, Ayoub D, Lane L, et al. N-terminome analysis of the human mitochondrial proteome. Proteomics. 2015;15: 2519–2524. doi:10.1002/pmic.201400617

180. Inuzuka H, Shaik S, Onoyama I, Gao D, Tseng A, Maser RS, et al. SCFFBW7 regulates cellular apoptosis by targeting MCL1 for ubiquitylation and destruction. Nature. 2011;471: 104–109. doi:10.1038/nature09732

181. Chwieralski CE, Welte T, Bühling F. Cathepsin-regulated apoptosis. Apoptosis. 2006;11: 143–149. doi:10.1007/s10495-006-3486-y

182. Heibein JA, Goping IS, Barry M, Pinkoski MJ, Shore GC, Green DR, et al. Granzyme B-mediated cytochrome c release is regulated by the Bcl-2 family members Bid and Bax. J Exp Med. 2000;192: 1391–1401. doi:10.1084/jem.192.10.1391

183. Sutton VR, Wowk ME, Cancilla M, Trapani JA. Caspase activation by granzyme B is indirect, and caspase autoprocessing requires the release of proapoptotic mitochondrial factors. Immunity. 2003;18: 319–329. doi:10.1016/S1074-7613(03)00050-5

184. Tompa P, Buzder-Lantos P, Tantos A, Farkas A, Szilágyi A, Bánóczi Z, et al. On the sequential determinants of calpain cleavage. J Biol Chem. 2004;279: 20775–20785. doi:10.1074/jbc.M313873200

185. Liu ZX, Yu K, Dong J, Zhao L, Liu Z, Zhang Q, et al. Precise prediction of calpain cleavage sites and their aberrance caused by mutations in cancer. Front Genet. 2019;10: 715(1–13). doi:10.3389/fgene.2019.00715

186. Cheng EH-Y, Kirsch DG, Clem RJ, Ravi R, Kastan MB, Bedi A, et al. Conversion of Bcl-2 to a Bax-like Death Effector by Caspases. Science. 1997;278: 1966–1968. doi:10.1126/science.278.5345.1966

187. Zhu J, Yang Y, Wu J. Bcl-2 cleavages at two adjacent sites by different caspases promote cisplatin-induced apoptosis. Cell Res. 2007;17: 441–448. doi:10.1038/cr.2007.36

188. Fujita N, Nagahashi A, Nagashima K, Rokudai S, Tsuruo T. Acceleration of apoptotic cell death after the cleavage of Bcl-XL protein by caspase-3-like proteases. Oncogene. 1998;17: 1295–1304. doi:10.1038/sj.onc.1202065

189. Basañez G, Zhang J, Chau BN, Maksaev GI, Frolov VA, Brandt TA, et al. Pro-apoptotic Cleavage Products of Bcl-xL Form Cytochrome *c*-conducting Pores in Pure Lipid Membranes. J Biol Chem. 2001;276: 31083–31091. doi:10.1074/jbc.M103879200

190. Nakagawa T, Yuan J. Cross-talk between two cysteine protease families: Activation of caspase-12 by calpain in apoptosis. J Cell Biol. 2000;150: 887–894. doi:10.1083/jcb.150.4.887

191. Weng C, Li Y, Xu D, Shi Y, Tang H. Specific cleavage of Mcl-1 by caspase-3 in tumor necrosis factor-related apoptosis-inducing ligand (TRAIL)-induced apoptosis in Jurkat leukemia T cells. J Biol Chem. 2005;280: 10491–10500. doi:10.1074/jbc.M412819200

192. Herrant M, Jacquel A, Marchetti S, Belhacène N, Colosetti P, Luciano F, et al. Cleavage of Mcl-1

by caspases impaired its ability to counteract Bim-induced apoptosis. Oncogene. 2004;23: 7863–7873. doi:10.1038/sj.onc.1208069

193. Ménoret E, Gomez-Bougie P, Surget S, Trichet V, Oliver L, Pellat-Deceunynck C, et al. Mcl-1128-350 fragment induces apoptosis through direct interaction with Bax. FEBS Lett. 2010;584: 487–492. doi:10.1016/j.febslet.2009.11.094

194. Valero JG, Cornut-Thibaut A, Jugé R, Debaud AL, Giménez D, Gillet G, et al. μ -calpain conversion of antiapoptotic Bfl-1 (BCL2A1) into a prodeath factor reveals two distinct alpha-helices inducing mitochondria-mediated apoptosis. PLoS One. 2012;7: e28620(1-12). doi:10.1371/journal.pone.0038620

195. Kucharczak JF, Simmons MJ, Duckett CS, Gélinas C. Constitutive proteasome-mediated turnover of Bfl-1/A1 and its processing in response to TNF receptor activation in FL5.12 pro-B cells convert it into prodeath factor. Cell Death Differ. 2005;12: 1225–1239. doi:10.1038/sj.cdd.4401684

196. Wood DE, Thomas A, Devi LA, Berman Y, Beavis RC, Reed JC, et al. Bax cleavage is mediated by calpain during drug-induced apoptosis. Oncogene. 1998;17: 1069–1078. doi:10.1038/sj.onc.1202034

197. Cao X, Deng X, May WS. Cleavage of Bax to p18 Bax accelerates stress-induced apoptosis, and a cathepsin-like protease may rapidly degrade p18 Bax. Blood. 2003;102: 2605–2614. doi:10.1182/blood-2003-01-0211

198. Toyota H, Yanase N, Yoshimoto T, Moriyama M, Sudo T, Mizuguchi J. Calpain-induced Bax-cleavage product is a more potent inducer of apoptotic cell death than wild-type Bax. Cancer Lett. 2003;189: 221–230. doi:10.1016/S0304-3835(02)00552-9

199. So YS, Chen YB, Ivamovska I, Ranger AM, Hong SJ, Dawson VL, et al. BAD is a pro-survival factor prior to activation of its pro-apoptotic function. J Biol Chem. 2004;279: 42240–42249. doi:10.1074/jbc.M406775200

200. Condorelli F, Salomoni P, Cotteret S, Cesi V, Srinivasula SM, Alnemri ES, et al. Caspase Cleavage Enhances the Apoptosis-Inducing Effects of BAD. Mol Cell Biol. 2001;21: 3025–3036. doi:10.1128/MCB.21.9.3025–3036.2001

201. Li H, Zhu H, Xu CJ, Yuan J. Cleavage of BID by caspase 8 mediates the mitochondrial damage in the Fas pathway of apoptosis. Cell. 1998;94: 491–501. doi:10.1016/S0092-8674(00)81590-1

202. Slee EA, Keogh SA, Martin SJ. Cleavage of BID during cytotoxic drug and UV radiation-induced apoptosis occurs downstream of the point of Bcl-2 action and is catalysed by caspase-3: A potential feedback loop for amplification of apoptosis-associated mitochondrial cytochrome c release. Cell Death Differ. 2000;7: 556–565. doi:10.1038/sj.cdd.4400689

203. Mandic A, Viktorsson K, Strandberg L, Heiden T, Hansson J, Linder S, et al. Calpain-Mediated Bid Cleavage and Calpain-Independent Bak Modulation: Two Separate Pathways in Cisplatin-Induced Apoptosis. Mol Cell Biol. 2002;22: 3003–3013. doi:10.1128/mcb.22.9.3003-3013.2002

204. Chen D, Zhou Q. Caspase cleavage of BimEL triggers a positive feedback amplification of apoptotic signaling. Proc Natl Acad Sci U S A. 2004;101: 1235–1240. doi:10.1073/pnas.0308050100

205. Li P, Zhou L, Zhao T, Liu X, Zhang P, Liu Y, et al. Caspase-9: Structure, mechanisms and clinical application. Oncotarget. 2017;8: 23996–24008. doi:10.18632/oncotarget.15098

206. Würstle ML, Laussmann MA, Rehm M. The central role of initiator caspase-9 in apoptosis signal transduction and the regulation of its activation and activity on the apoptosome. Exp Cell Res.

2012;318: 1213–1220. doi:10.1016/j.yexcr.2012.02.013

207. Ponder KG, Boise LH. The prodomain of caspase-3 regulates its own removal and caspase activation. Cell Death Discov. 2019;5: 56(1–10). doi:10.1038/s41420-019-0142-1

208. Gafni J, Cong X, Chen SF, Gibson BW, Ellerby LM. Calpain-1 cleaves and activates caspase-7. J Biol Chem. 2009;284: 25441–25449. doi:10.1074/jbc.M109.038174

209. Denault JB, Salvesen GS. Human Caspase-7 Activity and Regulation by Its N-terminal Peptide. J Biol Chem. 2003;278: 34042–34050. doi:10.1074/jbc.M305110200

210. Srinivasula SM, Ahmad M, Fernandes-Alnemri T, Alnemri ES. Autoactivation of procaspase-9 by Apaf-1-mediated oligomerization. Mol Cell. 1998;1: 949–957. doi:10.1016/S1097-2765(00)80095-7

211. Inoue S, Browne G, Melino G, Cohen GM. Ordering of caspases in cells undergoing apoptosis by the intrinsic pathway. Cell Death Differ. 2009;16: 1053–1061. doi:10.1038/cdd.2009.29

212. Klaiman G, Champagne N, LeBlanc AC. Self-activation of Caspase-6 *in vitro* and *in vivo*: Caspase-6 activation does not induce cell death in HEK293T cells. Biochim Biophys Acta. 2009;1793: 592–601. doi:10.1016/j.bbamcr.2008.12.004

213. Zhu S, Hsu AP, Vacek MM, Zheng L, Schäffer AA, Dale JK, et al. Genetic alterations in caspase-10 may be causative or protective in autoimmune lymphoproliferative syndrome. Hum Genet. 2006;119: 284–294. doi:10.1007/s00439-006-0138-9

214. Shin MS, Kim HS, Kang CS, Park WS, Kim SY, Lee SN, et al. Inactivating mutations of *CASP10* gene in non-Hodgkin lymphomas. Blood. 2002;99: 4094–4099. doi:10.1182/blood.V99.11.4094

215. Hoffmann JC, Pappa A, Krammer PH, Lavrik IN. A New C-Terminal Cleavage Product of Procaspase-8, p30, Defines an Alternative Pathway of Procaspase-8 Activation. Mol Cell Biol. 2009;29: 4431–4440. doi:10.1128/mcb.02261-07

216. Boulares AH, Yakovlev AG, Ivanova V, Stoica BA, Wang G, Iyer S, et al. Role of poly(ADP-ribose) polymerase (PARP) cleavage in apoptosis. J Biol Chem. 1999;274: 22932–22940. doi:10.1074/jbc.274.33.22932

217. Bratton SB, Walker G, Roberts DL, Cain K, Cohen GM. Caspase-3 cleaves Apaf-1 into an ~ 30 kDa fragment that associates with an inappropriately oligomerized and biologically inactive ~ 1.4 MDa apoptosome complex. Cell Death Differ. 2001;8: 425–433. doi:10.1038/sj.cdd.4400834

218. Arnesen T, Gromyko D, Pendino F, Ryningen A, Varhaug JE, Lillehaug JR. Induction of apoptosis in human cells by RNAi-mediated knockdown of hARD1 and NATH, components of the protein N-α -acetyltransferase complex. Oncogene. 2006;25: 4350–4360. doi:10.1038/sj.onc.1209469

219. Gromyko D, Arnesen T, Ryningen A, Varhaug JE, Lillehaug JR. Depletion of the human Nα -terminal acetyltransferase A induces p53-dependent apoptosis and p53-independent growth inhibition. Int J Cancer. 2010;127: 2777–2789. doi:10.1002/ijc.25275

220. Yang H, Li Q, Niu J, Li B, Jiang D, Qingmei ZW, et al. microRNA-342-5p and miR-608 inhibit colon cancer tumorigenesis by targeting NAA10. Oncotarget. 2015;7: 2709–2720. doi:10.18632/oncotarget.6458

221. Wang H, He H, Yang C. miR-342 suppresses the proliferation and invasion of acute myeloid leukemia by targeting Naa10p. Artif Cells, Nanomedicine Biotechnol. 2019;47: 3671–3676. doi:10.1080/21691401.2019.1596930

222. Xu H, Jiang B, Meng L, Ren T, Zeng Y, Wu J, et al. N-α -acetyltransferase 10 protein inhibits apoptosis through RelA/p65-regulated MCL1 expression. Carcinogenesis. 2012;33: 1193–1202. doi:10.1093/carcin/bgs144

223. Park YH, Seo JH, Park JH, Lee HS, Kim KW. Hsp70 acetylation prevents caspase-dependent/independent apoptosis and autophagic cell death in cancer cells. Int J Oncol. 2017;51: 573–578. doi:10.3892/ijo.2017.4039

224. Xu K, Zhang Y. Down-regulation of NAA10 mediates the neuroprotection induced by sevoflurane preconditioning via regulating ERK1/2 phosphorylation. Neurosci Lett. 2021;755: 135897. doi:10.1016/j.neulet.2021.135897

225. Yi CH, Sogah DK, Boyce M, Degterev A, Christofferson DE, Yuan J. A genome-wide RNAi screen reveals multiple regulators of caspase activation. J Cell Biol. 2007;179: 619–626. doi:10.1083/jcb.200708090

226. Sun L, Wang K, Peng L, Zhang J, Yang J, Zhao J, et al. Naa10p enhances chemosensitivity to cisplatin in oral squamous cell carcinoma cells. Cancer Manag Res. 2021;13: 1843–1851. doi:10.2147/CMAR.S296783

227. Ametzazurra A, Larrea E, Civeira MP, Prieto J, Aldabe R. Implication of human N-alpha-acetyltransferase 5 in cellular proliferation and carcinogenesis. Oncogene. 2008;27: 7296–7306. doi:10.1038/onc.2008.332

228. Ametzazurra A, Gázquez C, Lasa M, Larrea E, Prieto J, Aldabe R. Characterization of the human N-alpha-terminal acetyltransferase B enzymatic complex. BMC Proc. 2009;3: 1–7. doi:10.1186/1753-6561-3-s6-s4

229. Varland S, Myklebust LM, Goksøyr SØ, Glomnes N, Torsvik J, Varhaug JE, et al. Identification of an alternatively spliced nuclear isoform of human N-terminal acetyltransferase Naa30. Gene. 2018;644: 27–37. doi:10.1016/j.gene.2017.12.019

230. Liu Z, Liu Y, Wang H, Ge X, Jin Q, Ding G, et al. Patt1, a novel protein acetyltransferase that is highly expressed in liver and downregulated in hepatocellular carcinoma, enhances apoptosis of hepatoma cells. Int J Biochem Cell Biol. 2009;41: 2528–2537. doi:10.1016/j.biocel.2009.08.009

231. Pavlou D, Kirmizis A. Depletion of histone N-terminal-acetyltransferase Naa40 induces p53-independent apoptosis in colorectal cancer cells via the mitochondrial pathway. Apoptosis. 2016;21: 298–311. doi:10.1007/s10495-015-1207-0

232. Gourlay CW, Ayscough KR. The actin cytoskeleton: A key regulator of apoptosis and ageing? Nat Rev Mol Cell Biol. 2005;6: 583–589. doi:10.1038/nrm1682

233. Moss DK, Lane JD. Microtubules: forgotten players in the apoptotic execution phase. Trends Cell Biol. 2006;16: 330–338. doi:10.1016/j.tcb.2006.05.005

234. Desouza M, Gunning PW, Stehn JR. The actin cytoskeleton as a sensor and mediator of apoptosis. Bioarchitecture. 2012;2: 75–87. doi:10.4161/bioa.20975

235. Franklin-Tong VE, Gourlay CW. A role for actin in regulating apoptosis/programmed cell death: Evidence spanning yeast, plants and animals. Biochem J. 2008;413: 389–404. doi:10.1042/BJ20080320

236. Grespi F, Soratroi C, Krumschnabel G, Sohm B, Ploner C, Geley S, et al. BH3-only protein Bmf mediates apoptosis upon inhibition of CAP-dependent protein synthesis. Cell Death Differ.

2010;17: 1672–1683. doi:10.1038/cdd.2010.97

237. Ren W, Zhao W, Cao L, Huang J. Involvement of the Actin Machinery in Programmed Cell Death. Front Cell Dev Biol. 2021;8: 634849(1–15). doi:10.3389/fcell.2020.634849

238. Ditzel M, Wilson R, Tenev T, Zachariou A, Paul A, Deas E, et al. Degradation of DIAP1 by the N-end rule pathway is essential for regulating apoptosis. Nat Cell Biol. 2003;5: 467–473. doi:10.1038/ncb984

239. Xu Z, Payoe R, Fahlman RP. The C-terminal proteolytic fragment of the breast cancer susceptibility type 1 protein (BRCA1) is degraded by the N-end rule pathway. J Biol Chem. 2012;287: 7495–7502. doi:10.1074/jbc.M111.301002

240. Piatkov KI, Brower CS, Varshavsky A. The N-end rule pathway counteracts cell death by destroying proapoptotic protein fragments. Proc Natl Acad Sci U S A. 2012;109: E1839–E1847. doi:10.1073/pnas.1207786109

241. Eldeeb MA, Fahlman RP. Phosphorylation impacts N-end rule degradation of the proteolytically activated form of BMX kinase. J Biol Chem. 2016;291: 22757–22768. doi:10.1074/jbc.M116.737387

242. Kumar A, Birnbaum MD, Patel DM, Morgan WM, Singh J, Barrientos A, et al. Posttranslational arginylation enzyme Ate1 affects DNA mutagenesis by regulating stress response. Cell Death Dis. 2016;7: e2378(1-16). doi:10.1038/cddis.2016.284

243. Eldeeb MA, Fahlman RP. The anti-apoptotic form of tyrosine kinase Lyn that is generated by proteolysis is degraded by the N-end rule pathway. Oncotarget. 2014;5: 2714–2722. doi:10.18632/oncotarget.1931

244. Leboeuf D, Abakumova T, Prikazchikova T, Rhym L, Anderson DG, Zatsepin TS, et al. Downregulation of the Arg/N-degron Pathway Sensitizes Cancer Cells to Chemotherapy *In Vivo*. Mol Ther. 2020;28: 1092–1104. doi:10.1016/j.ymthe.2020.01.021

245. Kechko OI, Petrushanko IY, Brower CS, Adzhubei AA, Moskalev AA, Piatkov KI, et al. Beta-amyloid induces apoptosis of neuronal cells by inhibition of the Arg/N-end rule pathway proteolytic activity. Aging (Albany NY). 2019;11: 6134–6152. doi:10.18632/aging.102177

246. Zhang X, Zhang H, Xu C, Li X, Li M, Wu X, et al. Ubiquitination of RIPK1 suppresses programmed cell death by regulating RIPK1 kinase activation during embryogenesis. Nat Commun. 2019;10: 4158. doi:10.1038/s41467-019-11839-w

247. Hwang CS, Shemorry A, Auerbach D, Varshavsky A. The N-end rule pathway is mediated by a complex of the RING-type Ubr1 and HECT-type Ufd4 ubiquitin ligases. Nat Cell Biol. 2010;12: 1177–1185. doi:10.1038/ncb2121

CHAPTER 3

NatB-mediated Nt-acetylation warrants cellular proteostasis and proper function of apoptosis

This chapter is adapted from the following publication:

Joana P. Guedes*, Jean Baptiste Boyer*, Jasmin Elurbide*, Beatriz Carte, Virginie, Laila, Thierry Meinnel, Carmela Giglione#, Manuela Côrte-Real#, Rafael Aldabe# **NatB-mediated Nt-acetylation warrants cellular proteostasis and proper function of apoptosis.** *Manuscript in preparation*

*# Authors contributed equally

3.1. Background

NatB is the second major contributor to the Nt-acetylome being responsible for the fully acetylation of 21% of human and 15% of yeast proteome, unlike substrates of other NATs that are only partially acetylated [1–3]. Inactivation or downregulation of any of the NatB subunits affects enzymatic activity reducing the N-terminal modification on NatB substrates. In particular, inactivation of NatB in yeast and *Arabidopsis thaliana* blocks Nt-acetylation of most of its substrates [2,3], whereas in *Caenorhabditis elegans* the partial acetylation of NatB substrates is still observed in the null mutants indicating that other NATs could modify these substrates [1]. The deregulation of NatB complex or its subunits has been shown to affect several cellular processes namely actin cytoskeleton [3–7], cell proliferation [4,8,9] and apoptosis [4,8,10]. However, contrarily to NatA, the impact of NatB-mediated Nt-acetylation with respect to apoptosis regulation has been poorly exploited (see Chapter 2, section 2.4 for detailed information).

Recently, our previous studies found that inactivation of *Naa25* in MEFs increases the levels of pro-apoptotic protein Bax in mitochondria and sensitized MEFs to the apoptotic inducer MG132. Additionally, Bax was shown to be a NatB substrate [10]. Taking into account the nature of the second amino acid, several apoptotic proteins can also be predicted as NatB substrates. Given these evidences, in the present chapter we sought to further explore the impact of Nt-acetylation on the regulation of apoptosis using immortalized MEFs with conditional inactivation of the NatB catalytic subunit Naa20. As in MEFs the biological role of NatB has been assessed after total depletion of *Naa25* [10], herein we aimed to achieve a total depletion of *Naa20*. The proper and efficient inactivation was confirmed by monitoring the cell proliferation and actin cytoskeleton, as performed in other organisms. Moreover, the impact of the total depletion of *Naa20* on the Nt-acetylome and proteome was also evaluated. The effect of the absence of Naa20 on apoptosis regulation was assessed by monitoring the protein and gene level expression of a set of apoptotic proteins that are predicted or confirmed as substrates of NatB, before and after exposing MEF cells to different apoptotic stimuli. In line with the abovementioned roles of NatB, it has also been demonstrated the dual effect of Nt-acetylation on protein stability and degradation (see Chapter 2, section 2.2 for detailed information). So far, to our knowledge the interplay between Nt-acetylation and N-degron pathways, and its impact on apoptosis regulation, has not been addressed. To try fill this gap, we aimed to identify the N-recognins that target the apoptotic proteins for degradation and determine the apoptotic final outcome when Naa20 is inactivated.

3.2. Materials and Methods

3.2.1. Generation of Naa20 knockout mice

Knockout mice were generated using the clone created by The Knockout Mouse Project (KOMP) targeting Naa20 ($Naa20^{tm1a(KOMP)Wtsi}$) that was employed for blastocyst microinjection and generation of chimeric mice. Chimeric mice were mated with C57BL6/J mice, and germ-line transmission of targeted alleles was detected by Polymerase Chain Reaction (PCR). B6;129S-$Naa20^{tm1a(KOMP)Wtsi}$ mice were crossed with the strain B6;J-Tg(ACTFLPe)9205Dym/J to inactivate Naa20 mutation, as Naa20 inactivation is embryonic lethal in homozygosity, selecting animals without the Flpe transgene. These animals were backcrossed more than 10 times into the C57BL6/J background. All experiments were performed according to the protocols approved by the Institutional Animal Care and Use Committe (CEEA) of University of Navarra.

3.2.2. Establishment of mouse embryonic fibroblast cell strains

MEFs were obtained from $Naa20^{tm1a(KOMP)Wtsi}$ transgenic mice where *Naa20* can be inactivated if Cre recombinase is expressed. Embryos isolated from de uterus of the pregnant mice were transferred to petri dishes with sterile Phosphate-Buffered Saline (PBS - 1.37 M NaCl, 2.7 mM KCl, 10 mM Na_2HPO_4, 1.8 mM KH_2PO_4, pH 7.4). Head and internal organs were removed from the embryos. Each embryo was transferred to a well of a 6-well plate with Trypsin/Ethylenediamine Tetraacetic Acid (EDTA), and plates were incubated for 30 min at 37 °C. Then, embryos were pulled through an 18-gauge needle to disaggregate them to obtain isolated fibroblast. Obtained cells were grown in a 100 mm-petri dish with DMEM (Dulbecco's Modified Eagle Medium) supplemented with 10% of fetal bovine serum (FBS) and 1% of penicillin/streptomycin (P/S). When the cells were confluent, they were re-plated in 60 mm-petri dishes and next day they were immortalized by retroviral infection with a recombinant virus expressing the large T antigen of the SV40 virus and zeocin resistance gene. The infection process was repeated after 24 h to increase the efficiency. When the plate was confluent, cells were harvested and plated in 100 mm-petri dishes. 48 h later zeocin (200 μg/ml) was added to the plates for selection of T-antigen expressing cells. Cells were incubated with the medium with the antibiotic replacing every two days the medium to remove death cells and refresh antibiotic. When clear isolated cell clones were observed, they were harvested with a micropipette and plated in 96 well plates to be grown separately. Each clone was amplified and once they were established, they were used for experimental assays.

3.2.3. Inactivation of *Naa20* gene in MEFs

The inactivation of *Naa20* gene is achieved with a recombinant adenovirus expressing CRE recombinase – Ad5CMVCre (Multiplicity of Infection 2000). As infection negative control an adenovirus empty (AdEmpty, Multiplicity of Infection 2000) was used. Cells were plated in 6-well plates (6.25×10^4 cells/ml). The day after, cells were inoculated with Ad5CMVCre in DMEM supplemented with 2% FBS and 1% P/S, and 24 h later, regular DMEM was added to the cells. After 2 days of infection, cells were tripsinized and re-plated in 6.25×10^4 cells/ml (AdEmpty) and 1.25×10^5 cells/ml (Ad5CMVCre). 5 days post-infection, the same procedure was performed with the following cell concentrations - 1.75×10^5 cells/ml (AdEmpty) and 2.5×10^5 cells/ml (Ad5CMVCre). The next day, cells were harvested for the different experimental assays.

3.2.4. Real-Time PCR assay

Total RNAs were extracted with Maxwell® RSC simplyRNA Kit (Promega). Reverse transcription was performed as previously reported [11]. Real-Time PCRs were performed with iQ SYBR Green supermix (Bio-Rad) in a CFX96 Real-Time System (Bio-Rad), using specific primers for each gene: Naa20 WT F 5' CCTTCACCTGCGACGACCTGTT, Naa20 WT R 5' GGAATTCAGGGGCGACAGAG; Histone F 5' AAAGCCGCTCGCAAGAGTGCG, Histone R 5' ACTTGCCTCCTGCAAAGCAC; Procaspase-3 F 5'TACATGGGAGCAAGTCAGTGG, Procaspase-3 R 5'CACATCCGTACCAGAGCGAG; Procaspase-8 F 5'TCAGAAGAAGTGAGCGAGTTGG, Procaspase-8 R 5'ATCCTCGATCTTCCCCAGCA; Procaspase-9 F 5'GGGAAGATCAGGGGACATGC, Procaspase-9 R 5'TCTTGGCAGTCAGGTCGTTC; Apaf1 F 5'CTCCTTGGACGACAGCCATT, Apaf1 R 5'AAACACGCGTGGTAAACAGC; Bax F 5'ACCAAGAAGCTGAGCGAGTG, Bax R 5'ATGGTTCTGATCAGCTCGGG; Bid F 5' GGCGTCTGCGTGGTGATTC and Bid R 5' CCAGTAAGCTTGCACAGGCA. The amount of each transcript was quantified by the formula: $2ct(\beta\text{–Histone})\text{–}ct(gene)$, with ct being the point at which the fluorescence rises substantially above the background fluorescence.

3.2.5. Cell proliferation assay

Cells were grown as previously described in 3.2.3 section. The counting of cell number was performed 2, 3, 4, 5 and 6 days after post-infection and four wells per condition/per day were used. Cell number detection was achieved using a TC20™ Automated Cell Counter (Bio-Rad).

3.2.6. Immunofluorescence and confocal microscopy

For immunofluorescence experiments, cells were seeded in 6-well plates containing glass coverslips. 6 days post-infection, cells were fixed with 4% paraformaldehyde (16% Formaldehyde Solution, Thermo Scientific) for 15 min at room temperature (RT). After rinsing with 1× PBS, cells were permeabilized with 0.1% Triton X-100 (Sigma) during 15 min at RT and then washed. Following this process, cells were incubated with the anti-α-vinculin (V9131, SIGMA) and Alexa Fluor 488-Phalloidin (Invitrogen) in 1× Tris-Buffered Saline with 0.1% Tween® 20 detergent (TBST) with 3% Bovine Serum albumin (BSA) for 30 min, 37 °C. Subsequently, cells were washed and incubated with anti-mouse IgG Cy3 conjugated developed in sheep (Sigma) or anti-rabbit IgG Alexa488 conjugate developed in donkey (Molecular Probes), during 30 min at 37 °C. After mounting the coverslip in Vectashield mounting medium with DAPI (Vector Laboratories), samples were maintained at 4 °C until visualization. Images were acquired with an Axiovert 200M confocal LSM 510 META Zeiss microscope using a 40× objective.

3.2.7. FITC Annexin V/7-AAD (AV/7-AAD) assay

Apoptosis was detected using FITC-Annexin V (BioLegend) and 7-Amino-Actinomycin D (7-AAD) (BD Pharmingen™). 5 x 10^5 cells per condition were harvested, rinsed with 1× PBS and incubated with FITC-Annexin V (1:20) in annexin binding buffer (10 mm HEPES pH 7.4, 150 mm NaCl, 2.5 mm $CaCl_2$ in PBS pH 7.4), for 15 min in the dark, at RT. Cells were then centrifuged and resuspended with cold FACS buffer containing 7-AAD (1:50). Acquisition was performed by flow cytometry.

3.2.8. Flow cytometry analysis

Flow cytometry analysis was performed with a six-color BD FACSCanto II Flow Cytometer (BD) equipped with a 488-nm blue and 633-nm red lasers. FITC-Annexin was detected by blue laser and 7-AAD fluorescence (PerCP-Cy5-5-A) was detected in the far-red range of the spectrum (650 nm long-pass filter). For each sample, 10 000 events were evaluated. Data are processed using FlowJo software (version 7.6).

3.2.9. Apoptosis induction assays

Cells were seeded in 6-well plates, infected and six days post-infection treated with 50 μM etoposide, 100 ng/ml TNF-α plus 500 nM SMAC, 5 μM of MG132 and 5 ng/μl of tunicamycin for 0, 8, 12 and 24 h. At each time point, cells were harvested and collected for protein extraction for further analysis by western blot.

3.2.10. MEFs fractionation

Cells were grown as descried above and six days post-infection, cells were harvested (basal conditions) or treated with 50 μM etoposide and 5 μM MG13 for 12 h and 8 h, respectively. After, 6.6 x 10^6 cells per condition were harvested and cell fractionation was performed using a Cell fractionation kit (Abcam AB109719) following the manufacturers' guidelines. 1 x 10^6 cells per condition was used for total extracts. 4× Laemmli Sample Buffer (Bio-Rad) plus β-mercaptoethanol with 2% Sodium Dodecyl Sulfate (SDS) (Bio-Rad) supplemented with Tris-HCl 0.5 M pH 7.4 and protease inhibitors was used to collect cellular fractions. GAPDH and COX IV were used as cytosolic and mitochondrial controls, respectively. Protein bands were quantified Image Studio Lite Software System – LI-COR.

3.2.11. E3 ubiquitin ligases silencing by siRNAs

Cells were seeded in 6-wll plates and infected the day after. After 2 days, cells were tripsinized and re-plated as described previously in 3.2.3 section. Cells were tripsinized and re-plated 4 days post-infection in a final concentration of 1.5 x 10^5 cells/ml to transfect the siRNAs with cells in suspension. Lipofectamine® RNAiMAX Transfection Reagent (Invitrogen, 13778) was used according to manufacturer's instructions to transfect the following siRNAs: siRNA Silencer™ Select Negative Control No. 1 (Thermo Scientific, 4390843), Silencer® Select Ubr1 siRNA (Thermo Scientific, 4390771-s75706), Silencer® Select Ubr2 siRNA (Thermo Scientific, 4390771-s104948), Silencer® Select Ubr4 siRNA (Thermo Scientific, 4390771-s87462), Silencer® Select Cnot4 siRNA (Thermo Scientific, 4390771-s79257) and Silencer® Select March6 siRNA (Thermo Scientific, 4390771-s104524). Transfected cells were collected 48 h post-transfection for western blot or treated with apoptotic inducers for further western blot analysis.

3.2.12. Protein extraction

Cells were harvested and 2× Laemmli Sample Buffer (Bio-Rad) plus β-mercaptoethanol with 2% SDS (Bio-Rad) supplemented with Tris-HCl 0.5 M pH 7.4 and protease inhibitors – 1 mM phenylmethylsulfonyl fluoride (PMSF), 0.001 mg/ml Aprotinin, 1 mM Sodium Orthovanadate and 1 mM Sodium Pyrophosphate (Roche) was used to collect cell lysates. The soluble protein concentration was normalized using Revert staining with Revert 700 Total Protein Stain (LI-COR) through Image Studio Lite Software – LI-COR.

3.2.13. Western blot analysis

Protein samples were separated by SDS polyacrylamide gel electrophoresis and transferred onto nitrocellulose membranes (Bio-Rad). Next, to avoid non-specific interactions, membranes were blocked in 5% BSA or 5% non-fat milk in 1× TBST for 30 min at RT with agitation. Membranes were then incubated 1 h with agitation at RT with primary antibodies, namely mouse monoclonal anti-GAPDH (AbD serotec) and rabbit polyclonal anti-Nat5 (Naa20, ProteinTech). Rabbit polyclonal anti-Caspase-3, anti-cleaved Caspase-3, anti-cleaved Caspase-9, anti-cleaved Caspase-8, anti-Caspase-6, anti-Bax, rabbit monoclonal anti-Caspase-8, anti-Cyt *c*, anti-Apaf1, anti-COX IV, anti-cleaved PARP, anti-SMAC/DIABLO, mouse polyclonal anti-Bid and mouse monoclonal anti-caspase-9 were all purchased from Cell Signaling. Subsequently, membranes were incubated 1 h with agitation at RT with secondary antibodies anti-mouse IgG or anti-rabbit IgG (Cell Signaling). Chemiluminescence detection was performed using the ECL Ultra detection system (Lumigen) and an Odyssey® Fc Imaging System (LI-COR).

3.2.14. Proteomic approach

For proteomic analysis, protein was extracted from cell pellet with a total protein extraction buffer with 50 mM HEPES/NaOH pH 7.2, 1.5 mM $MgCl_2$, 1 mM Ethylene Glycol Tetraacetic Acid (EGTA), 10% glycerol, 1% Triton and a protease inhibitor mix (1 mM PMSF, 1 μg/mL Aprotinin, 1 mM Orthovanadate and 1 mM Sodium Pyrophosphate). The homogenates were incubated at 4 °C for 30 min with shaking. The supernatants were separated from the insoluble fraction by centrifugation at 15000 ×*g* at 4 °C for 30 min and used to determine protein concentration using the Bradford protocol [12]. After, 1 mg of proteins was denaturated in 6 M Guanidine-HCl, 50 mM Tris-HCl (pH 8) and 4 mM Dithiothreitol (DTT), reduced for 15 min at 95 °C and finally alkylated by the addition of 55 mM iodoacetamide for 1 h at RT [13]. Proteins were precipitated by the addition of four times the sample volume of cold acetone followed by 1 h centrifugation at −20 °C. The resulting pellet was resuspended in 50 mM phosphate buffer (pH 7.5) and was subjected to chemical acetylation of the free N-terminus amino groups with *N*-acetoxy-[$^2H_3$]-succinimide according to [14]. For detailed description of the sample preparation and N-terminus peptide enrichment, LC-orbitrap MS/MS analysis and protein identification and quantification see [13].

3.2.15. Basic Statistical Analysis

Statistical analysis was performed using Prism 8 (GraphPad software). First, we assessed the normality of groups with a Shapiro-Wilk test. If both groups presented a normal distribution, un unpaired t-test for parametric data was used. In case of non-parametric distribution of the groups, the differences

between both groups were determined conducting a Mann-Whitney test. For the statistical analysis of the proliferation assay, a two-way ANOVA was performed.

3.3. Results

3.3.1. Total inactivation of *Naa20* induces cytoskeleton abnormalities and decreased cell proliferation in MEF cells

NatB has been shown to be a highly conserved enzyme among all multicellular organisms, including plants [15]. In all other eukaryotes, with exception of yeast and *C. elegans*, the biological role of NatB has been always assessed after partial depletion of one of the two subunits, associating the resulting observed defects to a partial NatB-dependent Nt-acetylation reduction [1–7]. Although the NatB biological relevance in MEFs has been assessed when the regulatory subunit Naa25 was totally depleted [10], the role of the catalytic subunit Naa20 was not. Six days after infection with Ad5CMVCre ($Naa20^{-/-}$ MEFs) or AdEmpty (wild type (WT) MEFs), we quantified a 99.6% reduction of *Naa20* WT mRNA expression in $Naa20^{-/-}$ MEFs revealing a near complete inactivation of *Naa20*. We also analysed Naa20 expression and found that this protein was undetectable in $Naa20^{-/-}$ MEFs (Figure 3.1A). Inactivation of *Naa20* was associated to a clear reduction of $Naa20^{-/-}$ MEFs cell proliferation already 4 days after infection (Figure 3.1B). Moreover, six days after AdCre infection, a disorganization of the actin fibers was also visualized in $Naa20^{-/-}$ MEFs in comparison with AdEmpty infected MEFs (Figure 3.1C). As there is a close interaction between actin stress fibers and cellular focal adhesions, we also assessed the integrity of focal adhesions by visualizing vinculin, one of their main components, by immunofluorescence. We found that there was a decrease in the number of focal adhesions in $Naa20^{-/-}$ MEFs, in accordance with actin fibers' disorganization (Figure 3.1C). Taken together, these results confirm that *Naa20* is inactivated in the MEF KO cells, leading to cytoskeleton abnormalities and decreased cell proliferation.

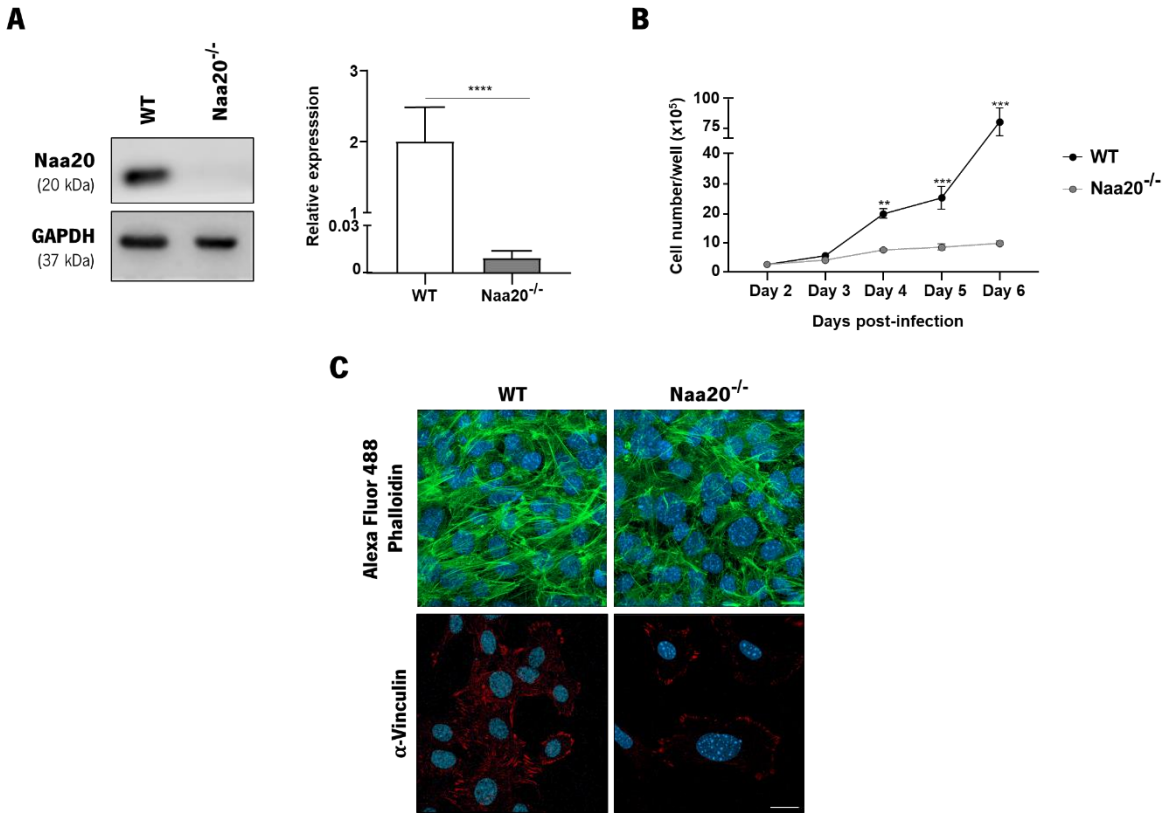

Figure 3.1: In Naa20$^{-/-}$ MEFs cells, lacking the catalytic subunit of NatB, *Naa20* gene and protein are not expressed, and the cell proliferation and the actin cytoskeleton are perturbed. (A) Confirmation of the *Naa20* gene and protein expression in MEF cells 6 days after infection with AdEmpty (WT) and Ad5CMVCre (Naa20$^{-/-}$) cells by RT-PCR and western blot, respectively. GAPDH was used as a loading control. The values display the mean of three independent experiments analysed by t-Student test, where ****p<0.0001. **(B)** Representative plot of the average number of Naa20 AdEmpty (WT) or Naa20 Ad5CMVCre (Naa20$^{-/-}$) infected MEF cells per well along post-infection days. The values display the mean of three independent experiments analysed by two-way ANOVA, where **p<0.01 and ***p<0.001. **(C)** Representative images of actin stained with Alexa Fluor 488-Phalloidin (green) and focal adhesions stained with α-vinculin (red) in MEF cells 6 days after infection with AdEmpty (WT) and Ad5CMVCre (Naa20$^{-/-}$) cells using confocal microscopy. Nuclei are labelled with DAPI (blue). Bar: 25 μM

3.3.2. Quantitative N-terminomics of Naa20$^{-/-}$ MEF cells reveals an unambiguous and specific Nt-acetylation reduction of NatB substrates

To characterize the effects of the complete NatB depletion in MEF cells, we proceeded with an N-terminomics analysis of WT and Naa20$^{-/-}$ MEFs by SILProNAQ [16]. Experimental data were then processed with the EnCOUNTer tool to provide an accurate measurement of the Nt- acetylation pattern and frequency in WT and NatB depleted cells. Analysis of these genotypes together identified 25048 N-termini corresponding to 1988 non-redundant proteoforms (Table 3.1).

Table 3.1: N-terminome analysis of WT and Naa20$^{-/-}$ MEFs. Detailed quantification of the number of N-termini identified, non-redundant proteoforms and quantified NTA values for each condition. The number of N-termini with iMet or without (+NME) the starting methionine and processed N-termini, as well as the acetylation status are also indicated for WT and Naa20$^{-/-}$ MEFs. The values presented are the mean of 8 replicates.

	WT	**Naa20$^{-/-}$**
Identified N-termini	**13149**	**11899**
Non-redundant proteoforms	**1844**	**1675**
Quantified N-termini	**1073**	**945**
Full acetylation (NTA > 95%)	*734*	*586*
Partial acetylation	*90*	*126*
No acetylation (NTA < 5%)	*249*	*233*
iMet (pos. 1)	**244**	**181**
Full acetylation (NTA > 95%)	*194*	*99*
Partial acetylation	*25*	*61*
No acetylation (NTA < 5%)	*25*	*21*
+NME (pos. 2)	**688**	**632**
Full acetylation (NTA > 95%)	*528*	*478*
Partial acetylation	*55*	*56*
No acetylation (NTA < 5%)	*105*	*98*
Processed (pos. > 2)	**141**	**132**
Full acetylation (NTA > 95%)	*12*	*9*
Partial acetylation	*10*	*9*
No acetylation (NTA < 5%)	*119*	*114*

Among all these identified proteoforms, we were able to quantify 1191 unique N-termini (1073 in the WT and 945 in the NatB mutant background) (Table 3.1, Figure 3.2A). Among the quantified N-termini for WT, 688 underwent removal of iMet (Nt-methionine excision, NME) and 244 retained their iMet (Figure 3.2B and C). From the quantified N-termini retaining the iMet, 80% (194/244) were fully acetylated (acetylation yield >95%), while 20% (50/244) were partially or not acetylated (Table 3.1) The fully acetylated proteins are predominantly classical NatB-substrates (N-termini featuring iMet followed by Glu>Asp>>Asn, (124/194). Only 8 NatB-type N-termini were found in the groups of partly or non-acetylated proteins (8/50). The groups of weakly or non-acetylated proteins consisted mostly of NatC- and NatE substrates (Table A2). In MEF cells, when *Naa20* was inactivated, we observed an overall reduction of NTA level in comparison with the WT background (Table 3.1 and 3.2A). This reduction originated only from Met-starting substrates (Figure 3.2B), with a relative decrease in the number of fully acetylated N-termini to only partially acetylated N-termini (Table 3.1, Table A2). In fact, among the quantified N-termini for Naa20$^{-/-}$ MEFs, 632 underwent removal of iMet (NME) and 181 retained the iMet (Table 3.1, Figure 3.2B and C). In this last case, 55% (99/181) were fully acetylated while 34% (61/181) and 12% (21/181) were partially or not acetylated, respectively (Table 3.1). Differently, when we compare

WT and Naa20$^{-/-}$ MEFs, the acetylation level of N-termini devoid of the iMet or N-termini processed downstream were unaffected (Figure 3.2C and D). Remarkably, the majority of N-termini with strong decreased acetylation in the Naa20$^{-/-}$ MEF cells were NatB substrates (Figure 3.2E). Indeed, as shown in the Table 3.2, which comprises a N-terminome analysis containing only the N-termini with an NTA level decrease of at least 20% in the Naa20$^{-/-}$ MEFs, 27 proteins displayed the acidic amino acids Asp and Glu and to a minor extent Gln and Asn at position two (Table 3.2, Figure 3.2E). Moreover, we identified 26 proteins that were acetylated in the WT but displayed significantly less NTA in Naa20$^{-/-}$ MEF cells (Table 3.2). Among them, the 8 most statistically relevant affected proteins are highlighted in green and numbered in the Volcano plot of Figure 3.2F and their characterization reported in Table 3.2, shown in bold. Nonetheless, many NatB substrates were unaffected, which suggests that other unknown NATs can take in charge these NatB substrates.

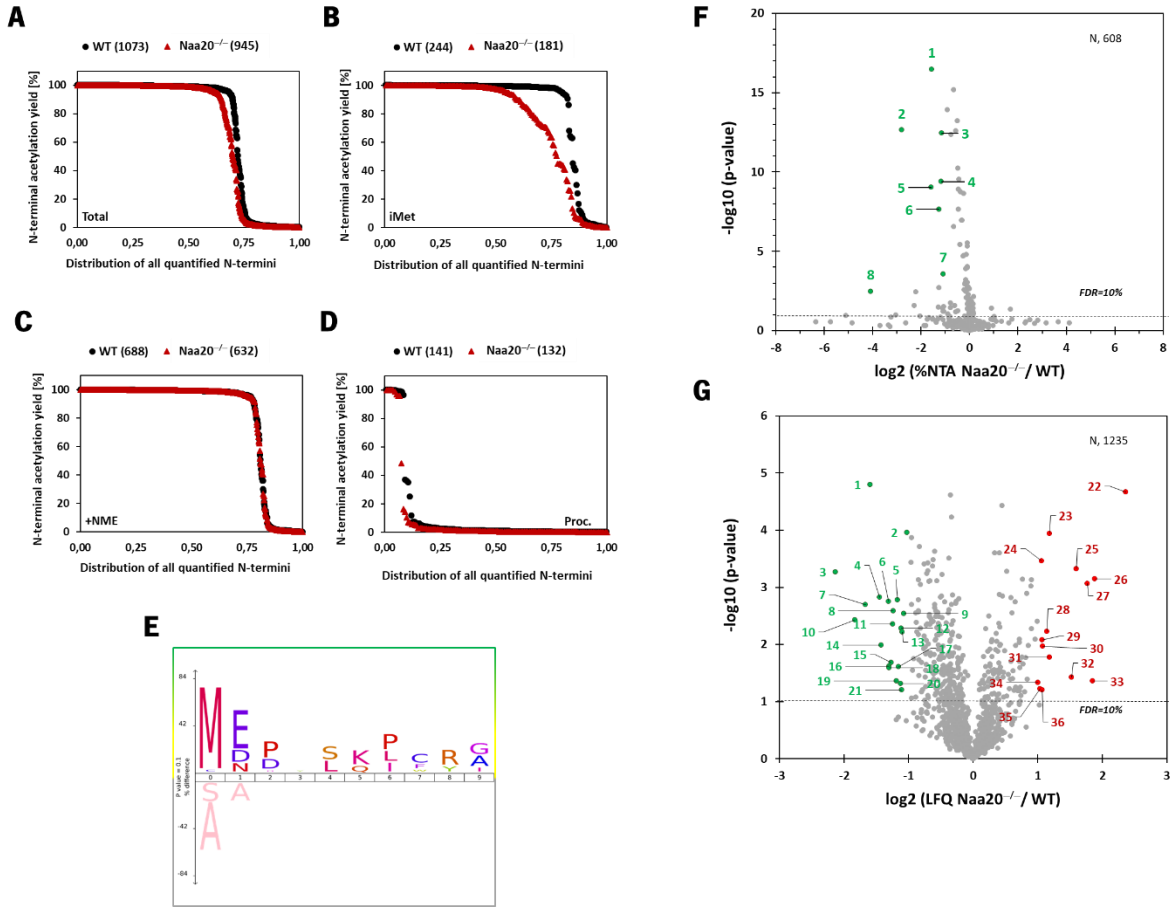

Figure 3.2: N-terminome and proteome analysis of WT and Naa20$^{-/-}$ MEFs show an overall reduction of Nt-acetylation and a deregulation of the expression of a subset of proteins in Naa20$^{-/-}$ MEFs. Distribution plots of the quantified N-termini in relation to the acetylation yield of the **(A)** total identified N-termini, **(B)** N-termini with iMet, **(C)** N-termini undergoing NME and **(D)** processed N-termini. **(E)** IceLogo representation of the N-termini sequences with a 20% minimum decrease of NTA yield to those with less than a 5% variation, when comparing the Naa20$^{-/-}$ MEFs to the WT MEFs. **(F)** Volcano plot of the NTA ratio between Naa20$^{-/-}$ and WT MEFs. The dashed horizontal line shows the p-values cutoff and

the eight points highlighted in green indicate the affected proteins with the highest statistical significance. **(G)** Volcano plot of the LFQ ratio between Naa20$^{-/-}$ and WT MEFs. The dashed horizontal line shows the p-values cutoff and the points highlighted in green and red represent the downregulated and upregulated proteins, respectively. All graphics containing only the N-termini that have been quantified at least once in each condition (WT or Naa20$^{-/-}$). All plots contain only the N-termini that have been quantified at least once in each condition (WT or Naa20$^{-/-}$). FDR - false discovery rate; N – number of samples.

Table 3.2: Most affected Nt-acetylated proteins resulting from *Naa20* inactivation in MEFs. Only the N-termini with an NTA level decrease of at least 20% in the Naa20$^{-/-}$ MEFs were analysed and then correlated with the protein expression level when LFQ was possible in both WT and Naa20$^{-/-}$ MEFs. The values in bold represent the eight most statistically relevant affected proteins. Proteins with a significant decrease in NTA according to a FDR< 5%. *n.i.*: protein not identified in the experiment. The table contains only the N-termini that have been quantified at least once in each condition (WT or Naa20$^{-/-}$).

Uniprot Accession	Entry Name	Protein Description	NTA Position	N-1 Residue	N-terminal Sequence	%NTA (WT)	%NTA (Naa20$^{-/-}$)	%NTA Difference (Naa20$^{-/-}$ - WT)	NTA Ratio (Naa20$^{-/-}$/WT)	LFQ Protein Ratio (Naa20$^{-/-}$/ WT)
P62849	RS24_MOUSE	40S ribosomal protein S24	1	-	MNDTVTIRTR	99.4 ± 0.6	33.9 ± 3.4	-65.5	**0.341**	0.693
P61166	TM258_MOUSE	Transmembrane protein 258	1	-	MELEAMSRYT	93.3 ± 4.2	13.4 ± 2.1	-79.9	**0.144**	-
Q8BIW1	PRUN1_MOUSE	Exopolyphosphatase PRUNE1	1	-	MEDYLQDCRA	99.8 ± 0.3	44.9 ± 1.1	-54.9	**0.450**	2.075
Q9EPL8	IPO7_MOUSE	Importin-7	1	-	MDPNTIIEAL	99.5 ± 0.8	44.3 ± 3.5	-55.1	**0.446**	0.516
Q9CQW9	IFM3_MOUSE	Interferon-induced transmembrane protein 3	1	-	MNHTSQAFIT	97.9 ± 0.6	32.8 ± 1.8	-65.2	**0.335**	-
Q9Z2X8	KEAP1_MOUSE	Kelch-like ECH-associated protein 1	1	-	MQPEPKLSGA	99.1 ± 0.7	41.5 ± 1.4	-57.6	**0.419**	-
Q9R0Q7	TEBP_MOUSE	Prostaglandin E synthase 3	1	-	MQPASAKWYD	86.2 ± 7.3	40.7 ± 0.3	-45.5	**0.472**	0.624
P58742	AAAS_MOUSE	Aladin	2	M	CSLGLFPPPP	99.9 ± 0.0	5.9 ± 5.5	-94.1	0.059	-
Q7TPD0	INT3_MOUSE	Integrator complex subunit 3	1	-	MELQKGKGTV	98.6 ± 0.9	26.1	-72.5	**0.265**	-
Q9Z0H1	WDR46_MOUSE	WD repeat-containing protein 46	1	-	METAPKPGRG	100.0	50.3 ± 0.7	-49.7	0.503	-
Q8R5J9	PRAF3_MOUSE	PRA1 family protein 3	1	-	MDVNLAPLRA	99.7 ± 0.3	52.8 ± 3.8	-46.9	0.529	-
Q8K3W0	BABA2_MOUSE	BRISC and BRCA1-A complex member 2	1	-	MSPEIALNRI	99.2 ± 0.2	57.8	-41.4	0.583	-
Q9CQ71	RFA3_MOUSE	Replication protein A 14 kDa subunit	1	-	MEDIMQLPKA	99.6 ± 0.4	58.5 ± 3.1	-41.1	0.588	-

Table 3.3: Most affected Nt-acetylated proteins resulting from *Naa20* inactivation in MEFs (cont).

Uniprot Accession	Entry Name	Protein Description	NTA Position	N-1 Residue	N-terminal Sequence	%NTA (WT)	%NTA ($Naa20^{-/-}$)	%NTA Difference ($Naa20^{-/-}$ - WT)	NTA Ratio ($Naa20^{-/-}$/WT)	LFQ Protein Ratio ($Naa20^{-/-}$/ WT)
O55222	ILK_MOUSE	Integrin-linked protein kinase	1	-	MDDIFTQCRE	99.9 ± 0.1	63.4 ± 0.9	-36.5	0.635	-
P17809	GTR1_MOUSE	Solute carrier family 2, facilitated glucose transporter member 1	1	-	MDPSSKKVTG	99.3 ± 0.7	63.3 ± 2.3	-36.0	0.638	0.623
Q2TBE6	P4K2A_MOUSE	Phosphatidylinositol 4-kinase type 2-alpha	1	-	MDETSPLVSP	99.0 ± 0.8	66.7	-32.3	0.674	-
Q78JE5	FBX22_MOUSE	F-box only protein 22	1	-	MEPAGGGGGV	99.9 ± 0.0	67.9 ± 2.9	-32.0	0.680	-
Q3UDE2	TTL12_MOUSE	Tubulin–tyrosine ligase-like protein 12	1	-	MEIQSGPQPG	99.9 ± 0.1	70.7	-29.2	0.708	0.748
Q8K274	KT3K_MOUSE	Ketosamine-3-kinase	1	-	METLLKRELG	99.9 ± 0.0	70.9 ± 0.1	-29.1	0.709	-
Q3UFB2	BCD1_MOUSE	Box C/D snoRNA protein 1	1	-	MESAAEKEGT	99.5 ± 0.5	71.9 ± 1.8	-27.5	0.723	-
Q7TMF3	NDUAC_MOUSE	NADH dehydrogenase [ubiquinone] 1 alpha subcomplex subunit 12	1	-	MELVEVLKRG	99.9 ± 0.0	73.3 ± 2.0	-26.7	0.733	-
F8VPU2	FARP1_MOUSE	FERM. ARHGEF and pleckstrin domain-containing protein 1	2	M	GEIEQKPTPA	96.9 ± 2.7	70.4 ± 2.6	-26.6	0.726	0.936
P11983	TCPA_MOUSE	T-complex protein 1 subunit alpha	1	-	MEGPLSVFGD	99.6 ± 0.5	74.0 ± 4.3	-25.5	0.743	0.944
P97822	AN32E_MOUSE	Acidic leucine-rich nuclear phosphoprotein 32 family member E	1	-	MEMKKKINME	99.9 ±0.0	75.8 ± 2.6	-24.2	0.758	0.990
Q8CAY6	THIC_MOUSE	Acetyl-CoA acetyltransferase	1	-	MNAGSDPVVI	99.6 ± 0.3	76.9 ± 4.4	-22.8	0.772	0.921
Q9D0I9	SYRC_MOUSE	Arginine–tRNA ligase	1	-	MDGLVAQCSA	99.5 ± 0.5	79.5 ± 4.7	-20.0	0.799	1.009
P70677	CASP3_MOUSE	Caspase-3	*n.i.*	*n.i.*	MENNKTSVDS	*n.i.*	*n.i.*	*n.i.*	*n.i.*	0.649

Table 3.4: Most affected Nt-acetylated proteins resulting from *Naa20* inactivation in MEFs (cont).

Uniprot Accession	Entry Name	Protein Description	NTA Position	N-1 Residue	N-terminal Sequence	%NTA (WT)	%NTA ($Naa20^{-/-}$)	%NTA Difference ($Naa20^{-/-}$ - WT)	NTA Ratio ($Naa20^{-/-}$/WT)	LFQ Protein Ratio ($Naa20^{-/-}$/ WT)
O89110	CASP8_MOUSE	Caspase-8	*n.i.*	*n.i.*	MDFQSCLYAI	*n.i.*	*n.i.*	*n.i.*	*n.i.*	*n.i.*
Q8C3Q9	CASP9_MOUSE	Caspase-9	*n.i.*	*n.i.*	MDEADRQLLR	*n.i.*	*n.i.*	*n.i.*	*n.i.*	*n.i.*
Q6ZQ89	MARH6_MOUSE	E3 ubiquitin-protein ligase MARCHF6	1	-	MDTAEEDICR	NTA	NTA	-	-	*n.i.*
A2AN08	UBR4_MOUSE	E3 ubiquitin-protein ligase UBR4	*n.i.*	*n.i.*	MATSGGEEAA	*n.i.*	*n.i.*	*n.i.*	*n.i.*	0.699

Regarding label free quantification information (LFQ Protein Ratio), Table 3.3 shows a proteome analysis containing only the proteins with an LFQ ratio either < 0.5 or > 2.0 in the Naa20$^{-/-}$ MEFs. Herein, we found that 36 proteins were deregulated in the Naa20$^{-/-}$ MEF cells, 21 of them being downregulated (LFQ ratio < 0.5) and 15 upregulated (LFQ ratio > 2.0) (Table 3.3 and Figure 3.2G). Interestingly, taking in account the nature of the second amino acid, no NatB substrate was found among the upregulated proteins, while 9 out the 21 downregulated proteins are all most likely NatB substrates, indicated in bold in the Table 3.3. Notably, half of the NTA downregulated proteins are directly associated with apoptosis, and in particular with caspases, such as protein SET [17], protein quaking [18], transgelin [19], general vesicular transport factor p115 [20], spermidine synthase [21], acidic leucine-rich nuclear phosphoprotein 32 family member B [22], cell growth-regulating nucleolar protein [23], lysyl oxidase homolog 1 [24,25], phosphoserine aminotransferase Psat1 [26]. For instance, the acidic leucine-rich nuclear phosphoprotein 32 family member B protein (AN32B - Q9EST5), a multifunction protein is directly cleaved by caspase-3 and a negative regulator of caspase-3-dependent apoptosis (Table 3.3) [22]. Although NTA of procaspase-3, -8 and -9 could not be quantified in the N-terminomics analysis, caspase-3 protein levels were found notably reduced (0.649) in the Naa20$^{-/-}$ MEF cells (Table 3.2). Indeed, searching in the set of the 36 deregulated proteins in which both protein levels and NTA could be quantified we noticed that only 12 respond to this query (Table 3.3). Among them, caveolea associated protein 1 (O54724) is the only protein with a parallel reduction in protein level and significant reduction in the NTA (%). Overall, our results suggest a possible influence of NatB-dependent NTA of specific proteins on their protein half-life and in particular on those involved in apoptosis, including caspases.

Table 3.3: Proteomic analysis of WT and Naa20$^{-/-}$ MEFs reveals differentially expressed proteins when *Naa20* is inactivated in MEFs. Analysis of the proteins with an LFQ ratio either < 0.5 or > 2.0 correspondent to downregulated or upregulated proteins, respectively (separated by the dashed line). The proteins indicated in bold represents the NatB substrates. The NTA difference (%) between the Naa20$^{-/-}$ and WT is presented when applicable. The table contain only the proteins that have been quantified at least in two biological replicates of each condition (WT or Naa20$^{-/-}$).

Uniprot Accession	Entry Name	Protein Description	LFQ Protein Ratio Naa20$^{-/-}$/ WT	% NTA Difference (Naa20$^{-/-}$- WT)
P37804	TAGL_MOUSE	Transgelin	0.331	-1.3 (Ala2)
Q99K85	**SERC_MOUSE**	**Phosphoserine aminotransferase Psat1**	**0.492**	**-0.4 (iMet)**
P28301	LYOX_MOUSE	Protein-lysine 6-oxidase	0.228	-
Q9Z1Z0	**USO1_MOUSE**	**General vesicular transport factor p115**	**0.367**	**-**
Q64674	**SPEE_MOUSE**	**Spermidine synthase**	**0.444**	**-3.3 (iMet)**
Q9EST5	**AN32B_MOUSE**	**Acidic leucine-rich nuclear phosphoprotein 32 family member B**	**0.404**	**-**
Q9EQU5	SET_MOUSE	Protein SET	0.314	-
O54724	**CAVN1_MOUSE**	**Caveolae-associated protein 1**	**0.425**	**-15.9 (iMet)**
Q922J9	FACR1_MOUSE	Fatty acyl-CoA reductase 1	0.474	-
Q00PI9	**HNRL2_MOUSE**	**Heterogeneous nuclear ribonucleoprotein U-like protein 2**	**0.282**	**-**
P97873	LOXL1_MOUSE	Lysyl oxidase homolog 1	0.423	-
Q99P72	**RTN4_MOUSE**	**Reticulon-4**	**0.462**	**-4.0 (iMet)**
P35293	**RAB18_MOUSE**	**Ras-related protein Rab-18**	**0.468**	**-**
P62862	RS30_MOUSE	40S ribosomal protein S30	0.372	0.0 (Lys1)
O35345	**IMA7_MOUSE**	**Importin subunit alpha-7**	**0.416**	**-0.4 (iMet)**
O70251	EF1B_MOUSE	Elongation factor 1-beta	0.405	-
Q9D883	U2AF1_MOUSE	Splicing factor U2AF 35 kDa subunit	0.450	-
P47955	RLA1_MOUSE	60S acidic ribosomal protein P1	0.406	-0.1 (Ala2)

Table 3.3: Proteomic analysis of WT and Naa20$^{-/-}$ MEFs reveals differentially expressed proteins when *Naa20* is inactivated in MEFs (cont).

Uniprot Accession	Entry Name	Protein Description	LFQ Protein Ratio Naa20$^{-/-}$/ WT	% NTA Difference (Naa20$^{-/-}$- WT)
Q91YT7	YTHD2_MOUSE	YTH domain-containing family protein 2	0.438	-0.2 (Ser2)
Q9QYS9	QKI_MOUSE	Protein quaking	0.460	-
Q08288	LYAR_MOUSE	Cell growth-regulating nucleolar protein	0.466	-
Q6WVG3	KCD12_MOUSE	BTB/POZ domain-containing protein KCTD12	5.143	-
P12265	BGLR_MOUSE	Beta-glucuronidase	2.274	-
Q9WV54	ASAH1_MOUSE	Acid ceramidase	2.084	-
Q61391	NEP_MOUSE	Neprilysin	3.020	-
Q9D379	HYEP_MOUSE	Epoxide hydrolase 1	3.681	-
P17710	HXK1_MOUSE	Hexokinase-1	3.404	-
Q9D0K2	SCOT1_MOUSE	Succinyl-CoA:3-ketoacid coenzyme A transferase 1. mitochondrial	2.209	-
O89023	TPP1_MOUSE	Tripeptidyl-peptidase 1	2.099	-
Q0GNC1	INF2_MOUSE	Inverted formin-2	2.108	-0.2 (Ser2)
O88543	CSN3_MOUSE	COP9 signalosome complex subunit 3	2.273	0.0 (Ala2)
P61620	S61A1_MOUSE	Protein transport protein Sec61 subunit alpha isoform 1	2.887	-0.3 (Ala2)
P84228	H32_MOUSE	Histone H3.2	3.601	-
Q62095	DDX3Y_MOUSE	ATP-dependent RNA helicase DDX3Y	2.001	-
P20060	HEXB_MOUSE	Beta-hexosaminidase subunit beta	2.052	-
Q91V12	BACH_MOUSE	Cytosolic acyl coenzyme A thioester hydrolase	2.098	-

3.3.3. *Naa20* inactivation reduces the expression of several apoptosis pathway components

As a significant number of apoptotic proteins are NatB substrates, we performed a kinetics assay after *Naa20* inactivation to analyse the expression of intrinsic and extrinsic apoptosis components, paying special attention to proteins that are NatB substrates. Naa20$^{-/-}$ MEFs 5 and 6 days post-infection showed a significant decrease in the protein level of procaspases-8, -9 and -3, and Bid, without no effects on procaspase-6 and SMAC/DIABLO expression levels, proteins predicted to be Nt-acetylated by NatA based on their second amino acid nature (Figure 3.3A). On the other hand, at 6 days post-infection, no differences were observed in procaspase-8, procaspase-3 and Bid mRNA levels, except on procaspase-9 which showed a decrease not comparable to the strong downregulation of the corresponding protein (Figure 3.3B). In contrast, gene expression of both Bax and Apaf1, also NatB substrates, was markedly upregulated in the absence of the Naa20 subunit, suggesting an increase in their transcriptional activity which was not reflected in protein accumulation (Figure 3.3B). These findings clearly show a strong negative effect of Naa20 knockout in procaspase-3, -8 and -9 protein expression levels as well as in Bid.

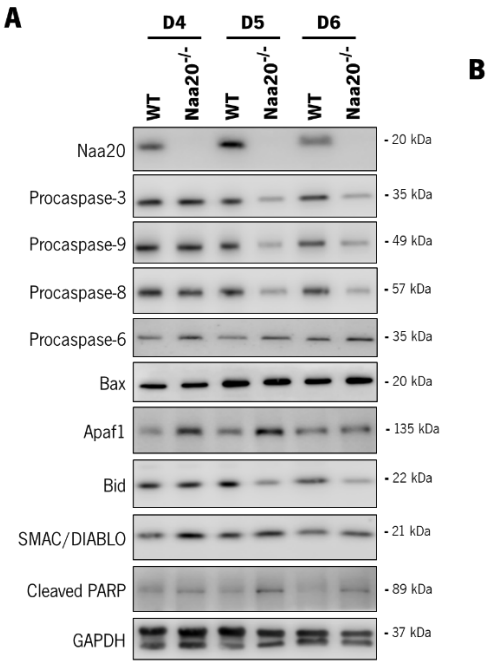

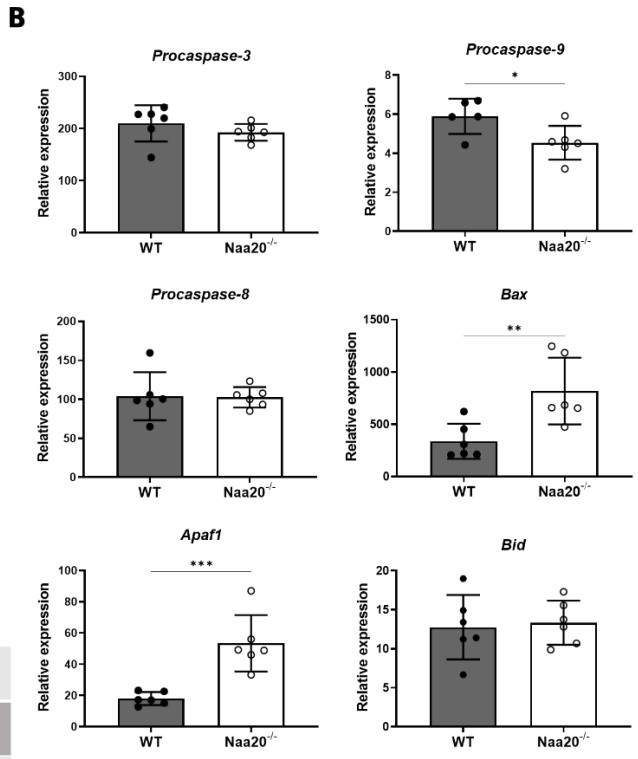

C

	Early Apoptotic cells	Late Apoptotic cells	Necrotic cells
WT	0,097 % ± 0,122	0,227 % ± 0,260	1,080 % ± 0,056
Naa20$^{-/-}$	0,773 % ± 0,758	1,181 % ± 1,229	1,364 % ± 0,801

Figure 3.3: Inactivation of *Naa20* subunit induces a significant decrease in protein expression level of procaspase-3, -9 and -8 and Bid, which is not associated with changes in mRNA expression in the case of *Procaspase-3*, *Procaspase-8* and *Bid*. (A) Representative western blot images of the NatB substrates expression

procaspase-3, -9 and -8, and of Bax, Bid, Apaf1, as well as of the non NatB substrates procaspase-6, SMAC/DIABLO and cleaved PARP. MEF cells were harvested 4, 5 and 6 days after infection with AdEmpty (WT) or Ad5CMVCre ($Naa20^{-/-}$). Procaspase-6 and SMAC/DIABLO were used as controls. GAPDH was used as a loading control. **(B)** Representative plots of mRNA expression of the same NatB substrates as in A, 6 days post-infection. The values display the mean of three independent experiments analysed by t-Student test, where *p<0.05, **p<0.01 and ***p<0.001. **(C)** Average values of early and late apoptotic cells and necrotic cells of MEFs cells 6 days after infection with AdEmpty (WT) or Ad5CMVCre ($Naa20^{-/-}$), assessed by FITC-AV/7-AAD staining with flow cytometry. Values represent the mean values of two independent experiments.

Additionally, the increase of PARP cleavage suggests a slight induction of apoptosis in $Naa20^{-/-}$ MEFs (Figure 3.3A). To further support this interpretation, we assessed the exposure of PS to the outer leaflet of the plasma membrane, and the integrity of the plasma membrane, using the FITC-AV/7-AAD staining assay. Accordingly, $Naa20^{-/-}$ MEFs showed an increase in the percentage of early apoptotic cells in comparison with the WT MEFs, indicating a small subpopulation of apoptotic cells in $Naa20^{-/-}$ MEF cells under basal conditions (Figure 3.3C).

3.3.4. $Naa20^{-/-}$ MEF cells display decreased susceptibility to the apoptotic inducers TNF-alpha plus SMAC mimetic and to etoposide

The observed increment on PARP cleavage in $Naa20^{-/-}$ MEF cells associated with the strong reduction in procaspases protein levels prompted us to assess the susceptibility of $Naa20^{-/-}$ MEFs to different apoptosis inducers like etoposide and to TNF-α plus SMAC mimetic. For both apoptotic stimuli, we found that protein levels of procaspase-8, -9 and -3 decreased in WT cells along the experiment as a result of their proteolytic processing. However, the levels of all these procaspases and of Bid in $Naa20^{-/-}$ MEFs, besides being lower than in the WT MEFs at time 0, were maintained constant until the end of the experiment. Consequently, this decrease was associated with significant lower levels of the cleaved caspases (Figure 3.4). In agreement with these results, we also observed a decrease in PARP cleavage in $Naa20^{-/-}$ MEFs exposed to TNF-α plus SMAC mimetic as well as to etoposide.

Then, we questioned whether the observed blockade of apoptosis induction when *Naa20* is inactivated could be extended to other apoptosis inducers. To this end, we assessed the susceptibility of $Naa20^{-/-}$ MEFs to the ER stress inducer tunicamycin or to the proteasome inhibitor MG132, which induce apoptosis by activating caspase-9 and caspase-8, respectively [27]. Though $Naa20^{-/-}$ MEFs showed initial lower proteins levels of procaspases-8, - 9 and -3 and of their cleaved forms for both treatments in comparison with WT cells, these differences were attenuated at the end of the experiment (Figure A1,

Appendix). Moreover, we found that there was no evident decrease in PARP cleavage in Naa20$^{-/-}$ MEFs for both stimuli, in contrast with TNF-α plus SMAC mimetic and etoposide treatment.

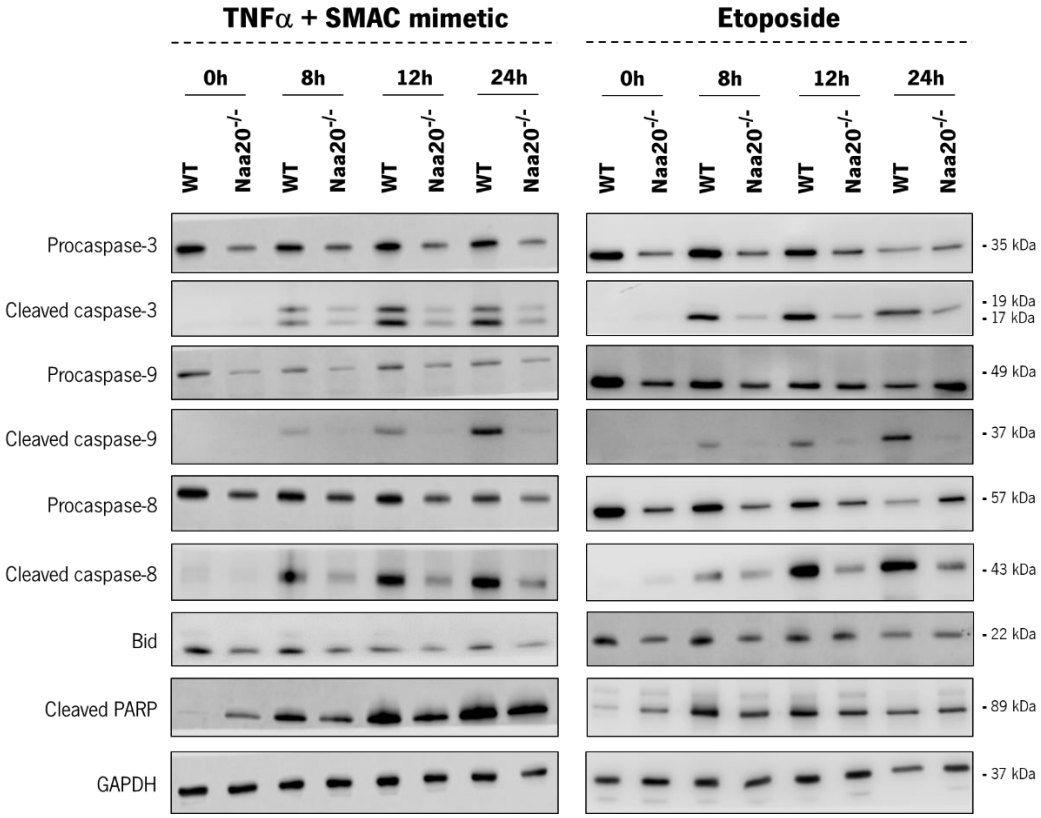

Figure 3.4: Inactivation of *Naa20* causes a decreased susceptibility of MEF cells to the apoptotic inducers TNF-α plus SMAC mimetic and to etoposide. Representative western blot images of procaspases-3, -9 and -8 and of the respective cleaved caspases as well as of Bid and cleaved PARP in MEF cells, 6 days after infection with AdEmpty (WT) or Ad5CMVCre (Naa20$^{-/-}$) and 0, 8, 12 and 24 h after treatment with 100 ng/mL TNF-α plus 500 nM SMAC mimetic or 50 μM etoposide.

3.3.5. Blockage of apoptosis in Naa20$^{-/-}$ MEFs occurs downstream of cytochrome *c* release

As *Naa20* inactivation decreased the susceptibility of Naa20$^{-/-}$ MEFs to intrinsic apoptosis induction by etoposide, we addressed whether blockage of apoptosis could be due to an effect on Bax subcellular localization and/or on Bax activation. A slight increase of mitochondrial Bax was observed in Naa20$^{-/-}$ MEFs under basal conditions comparing with WT MEFs. However, this Bax translocation was not enough to activate Bax and promote a detectable release of cyt *c* and SMAC/DIABLO (Figure 3.5A). Curiously, Naa20$^{-/-}$ and WT MEFs, 12 h after etoposide treatment, showed similar Bax translocation from the cytosol to mitochondria associated with similar release of cyt *c* to the cytosol. Interestingly, we found an evident increase of SMAC/DIABLO in the mitochondria of Naa20$^{-/-}$ MEFs, suggesting a defect in its

release after etoposide addition (Figure 3.5B). The subcellular localization Bax, cyt *c* and SMAC/DIABLO was also assessed when MEFs were treated with MG132 for 8 h. Results showed a similar Bax mitochondrial targeting and cyt *c* and SMAC release from the mitochondria to the cytosol, in both WT and Naa20$^{-/-}$ MEFs (Figure 3.5C). Accordingly, a similar procaspase-9 activation was observed in both WT and Naa20$^{-/-}$ MEF cells, 8h after treatment with MG132 (Figure A1, Appendix).

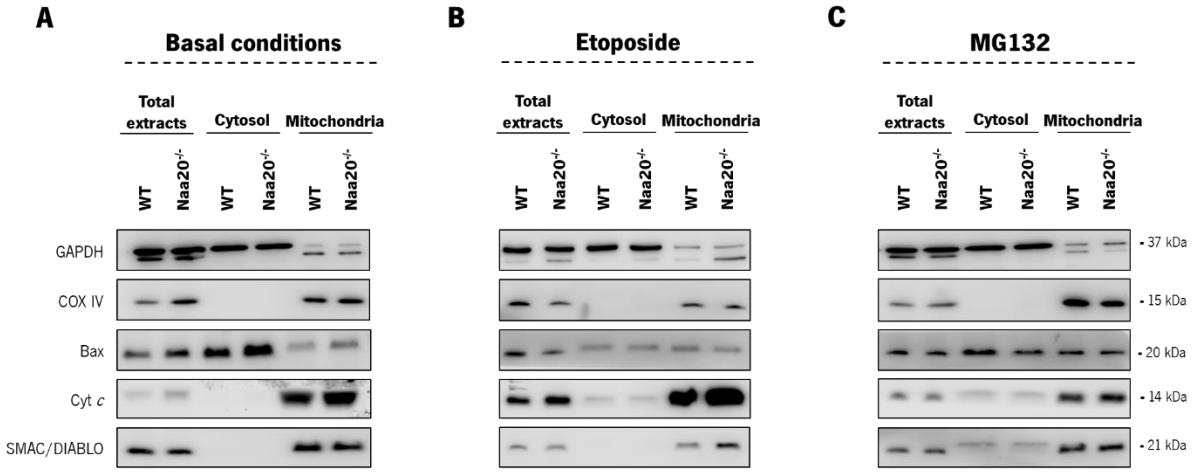

Figure 3. 5: Inactivation of *Naa20* does not impact release of cytochrome *c* in response to etoposide and MG132 but increases the mitochondrial SMAC/DIABLO content in response to etoposide treatment. Representative western blot image of Bax, cyt *c*, Bid and SMAC/DIABLO in total extracts, cytosolic fraction and mitochondrial fraction of MEF cells 6 days after infection with AdEmpty (WT) or Ad5CMVCre (Naa20$^{-/-}$), before (basal conditions) **(A)**, 12 h after 50 μM etoposide treatment **(B)** and 8 h after 5 μM MG132 treatment **(C)**. WT and Naa20$^{-/-}$ MEF cells were fractionated 6 days after virus inoculation. Cytosolic GAPDH and mitochondrial COX IV were used as loading controls of cytosolic and mitochondrial fractions, respectively.

3.3.6. Arg/N-degron pathway is involved in the decrease of procaspase-9 and -8 protein levels in Naa20$^{-/-}$ MEFs and in defects of procaspases activation

As the expression levels of Bid, procaspase-3, -9 and -8 were decreased in the absence of Naa20 (Figure 3.3A), we assessed if the lack of the N-terminal acetyl group in NatB substrates is sensed as an N-degron by the Arg/- or Ac/N-degron pathways, and consequently targeted for degradation. To this end, we used siRNAs to silence the E3 Arg/N-recognins Ubr1, Ubr2 and Ubr4, and the Ac/N-recognins Cnot4 and March6 in both Naa20$^{-/-}$ and WT MEFs, and evaluated the procaspases and Bid protein expression level (Figure 3.6A). While procaspase-3 levels were not affected by silencing any of the ubiquitin ligases tested, silencing of *Ubr4* and *Ubr1* increased the procaspase-8 and -9 levels in Naa20$^{-/-}$ MEFs, respectively (see orange squares in Figure 3.6A). On the other hand, silencing of *Ubr4* or *Ubr1* also increased Bid protein levels. Interestingly, downregulation of *Ubr2* negatively affects procaspase-8 and

procaspase-3 expression in WT MEFs, presenting similar levels to those observed in Naa20$^{-/-}$ MEFs (see red squares in Figure 3.6A).

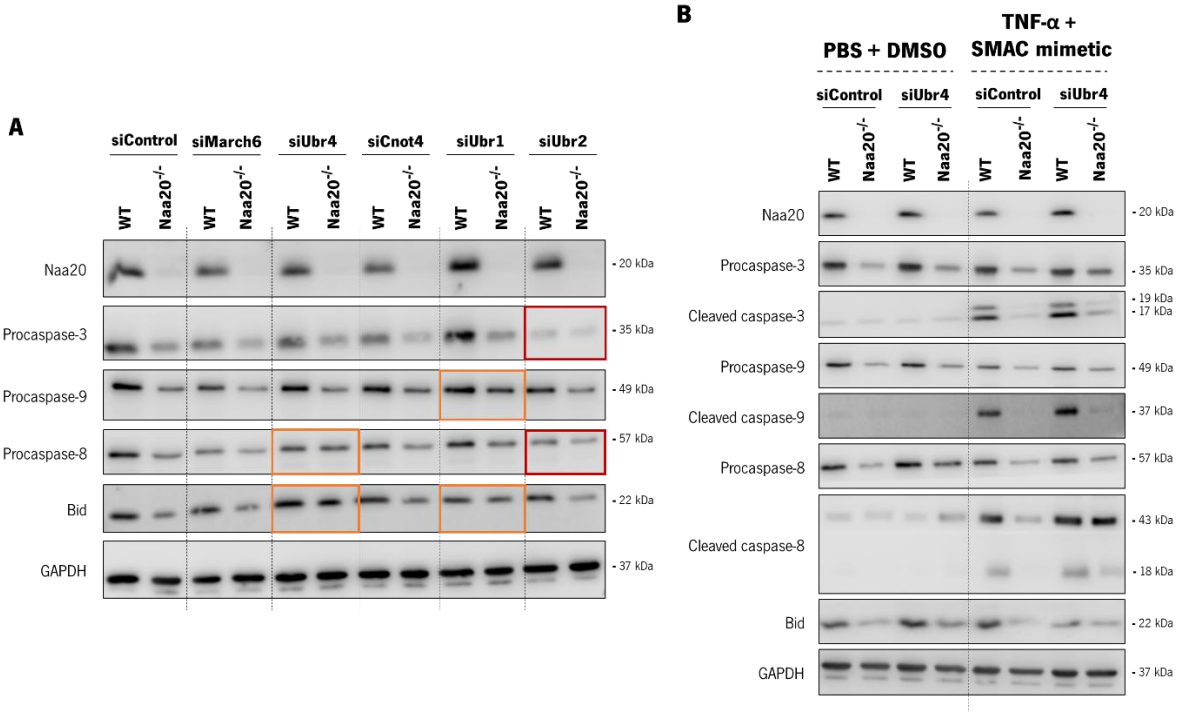

Figure 3.6: Silencing the ubiquitin ligases *Ubr4* and *Ubr1* in Naa20$^{-/-}$ MEFs rescues the decrease in procaspase-8 and -9 protein expression levels, respectively, as well of Bid and promotes the activation of caspase-8 in response to TNF-α plus SMAC mimetic. (A) Representative western blot images of the procaspases-3, -9 and -8 and Bid protein levels after silencing *March6*, *Ubr4*, *Cnot4*, *Ubr1* and *Ubr2* ubiquitin ligases in MEF cells 6 days after infection with AdEmpty (WT) or Ad5CMVCre (Naa20$^{-/-}$). A specific siRNA (siControl) was used as a control. Orange squares indicate the recovery of procaspase-8 and -9 and Bid protein levels in Naa20$^{-/-}$ MEFs; red squares indicate the downregulation of procaspase-3 and -8 proteins levels in WT cells after Ubr2 silencing. **(B)** Representative western blot image of the procaspases and cleaved caspases-3, -9 and -8 and Bid protein levels after silencing the *Ubr4* ubiquitin ligase in MEF cells 6 days after infection with AdEmpty (WT) or Ad5CMVCre (Naa20$^{-/-}$), 12 hours after treatment with 100 ng/mL TNF-α plus 500 nM SMAC mimetic. PBS plus DMSO was used as a negative control of TNF-α plus SMAC mimetic treatment. A specific siRNA (siControl) was used for control.

3.3.7. *Ubr4* silencing partially reverts the Naa20-mediated decrease of procaspase and caspase-8 expression levels in response to TNF-α plus SMAC mimetic

Once we have found that the N-terminal of procaspase-8, -9 and Bid may be recognized as degradation signals when *Naa20* is inactivated, we addressed whether the observed increase after silencing would be able to rescue procaspases activation in Naa20$^{-/-}$ MEFs in response to TNF-α plus SMAC mimetic and to etoposide. Besides restoring procaspase-8 protein levels in Naa20$^{-/-}$ MEFs, silencing of Ubr4 lead to activation of caspases-8 12h after TNF-α plus SMAC treatment, with recovered

caspase-8 p43 polypeptide expression and increased caspase-8 p18 polypeptide expression (Figure 3.6B). *Ubr4* downregulation also promotes a slight caspase-3 and -9 activation in Naa20$^{-/-}$ MEFs. Nonetheless, the activation of caspase-3 and -9 is less pronounced when compared with the activation of caspase-8. Contrarily, although *Ubr1* silencing caused a restoration of procaspase-9 protein levels in Naa20$^{-/-}$ MEFs (Figure 3.6A), it had no effect on caspase-9 activation after etoposide treatment (Figure A2, Appendix). The same phenotype was observed when silencing *Ubr4* in response to etoposide (Figure A2, Appendix). These data indicate that apoptosis blockade in response to TNF-α and SMAC mimetic caused by *Naa20* inactivation can be partially reverted by silencing the UBR4 E3 ubiquitin-protein ligase.

3.4. Discussion

In the last years, owing to the relevance of Nt-acetylation in several biological processes, there has been a growing interest in this protein modification. NatB is the second major contributor to the Nt-acetylome with an important role in different cellular processes [28,29]. Therefore, several studies have been addressing the effect of NatB inactivation in different cell and organism models. When NatB is inactivated in yeast, there is a complete abrogation of initial methionine acetylation when the second residue is a -Glu, -Asp, -Gln or -Asn [3]. Similarly, downregulation of NatB subunits expression in *A. thaliana* to 30% of the WT NatB levels reduces the Nt-acetylation resulting in 63% of NatB substrates being unacetylated or very low Nt-acetylated in the initial methionine, 20% partially acetylated and 17% fully acetylated [2]. On the other hand, inactivation of NatB in *C. elegans* does not lead to a decrease in a high proportion of Nt-acetylation of NatB substrates with a -Glu as second residue [1]. Herein, we extend the study of the effect of NatB inactivation to the MEFs model. We found that though inactivation of NatB catalytic subunit in MEFs reduces the Nt-acetylation of many NatB substrates, this effect is not complete. Indeed, while close to two thirds of NatB identified substrates are not affected by NatB inactivation, the other one third presents a reduction of at least 20% of their Nt-acetylation degree, but none of them being completely unacetylated. A similar behaviour is observed in *A. thaliana* when NatA is inactivated reducing the fully acetylated NatA substrates from 78% in WT cells to 30-34% [30], but just less than 2% of proteins show a significant reduction in their Nt-acetylation degree when NatA is inactivated in MEFs [31] or mutated in human fibroblasts [32]. Interestingly, it was discovered a Naa10 paralog, Naa12, which substitutes Naa10 activity when this subunit is inactivated in MEFs reducing the number of NatA substrates affected [31]. As the inactivation of NatB catalytic subunit is unable to eliminate Nt-acetylation of NatB substrates, it is conceivable that another enzyme or paralog fills the absence of Naa20. Interestingly, it has been recently discovered a new NAT, NatH, which N-terminally acetylates actin, a

protein with an acidic Nt-end. Moreover, NAA80, the catalytic subunit of NatH, can modify *in vitro* initial methionine in peptides that present an aspartic acid as second residue [33] being therefore a candidate to modify NatB substrates when this enzyme is not present. The effect of NatB inactivation in MEFs and *C. elegans* has a lower impact on Nt-acetylation than in yeast and *A. thaliana* while Naa80 is present in mammals and *C. elegans* and absent in yeast and *A. thaliana* [33]. Naa80 is therefore a good candidate to reduce the impact of NatB inactivation on Nt acetylome in mammals and *C. elegans*. Altogether, these evidence support the interpretation that the co-translational and irreversible protein modification mediated by NatB is more complex in mammals than in yeast presenting a higher number of NAT complexes [28,29] with complementary enzymatic activities that warrant optimum maintenance of protein Nt-acetylation.

Nt-acetylation has been shown to impact proteome dynamics modulating the cellular responses to internal and external stimuli with implications in cancer pathogenesis, neurodegenerative diseases and cardiovascular disorders [29,32,34]. Particularly, NatB inactivation or downregulation may affect several cellular processes such as actin cytoskeleton function [3,5–7], stress responses [2,35,36], cell proliferation [4,8,9] and apoptosis [8,10]. Indeed, it was reported that inactivation of both NatB subunits in yeast [6,7] and of Naa25 in *D. melanogaster* [5,9], as well as the silencing of NatB in both HeLa [3,8] and HCC cells [4] perturb cytoskeleton organization and cell proliferation. These effects are explained by the absence of NatB-mediated Nt-acetylation of tropomyosin isoforms and proliferation-related proteins [3,4,7,8]. Accordingly, we found that in the generated Naa20$^{-/-}$ MEFs, *Naa20* inactivation leads to a decreased cell proliferation and perturbations on actin cytoskeleton and focal adhesions.

Apoptosis is a key player in the maintenance of cellular homeostasis whose deregulation is associated with many pathologic processes. Besides affecting cell proliferation and cytoskeleton organization, it has been demonstrated that NatB can regulate apoptosis in MEFs [10] and tumour cells [4]. Indeed, some of the main components of apoptosis have been found Nt-acetylated in human proteomic studies [37,38] being predicted as NatB substrates based on their second amino acid identity [3]. Thus, to further unveil the modulation of apoptosis by NatB-mediated Nt-acetylation, we first explored the effect of *Naa20* inactivation on protein and gene expression levels of several components of the intrinsic and extrinsic apoptotic pathways. We observe a strong and selective decrease in the protein level of the putative NatB substrates, procaspase-3, -9 and -8 and Bid, in contrast with procaspase-6 and SMAC/DIABLO, predicted as NatA substrates. Yet, when Naa20 is inactivated, Bax and Apaf1 mRNAs are upregulated whereas procaspase-3, -9, -8 and Bid gene expression are not affected. Also, in *D. melanogaster, Naa20* knockdown was shown to decrease the protein levels of the NatB substrate Drk,

while the mRNA levels were unaffected [39]. Although apoptotic stimuli lead to proteolytic procaspases activation reducing procaspases presence [40], cleaved caspases-3, -9 and -8 were not detectable in Naa20$^{-/-}$ MEFs, despite presenting an increase of PARP cleavage associated with PS exposure in a small percentage of cells. This suggests that there is an induction of apoptosis in a small cell sub-population, however this effect cannot account for the observed procaspases reduction. All in all, the decrease of procaspase-3, -9 and -8 and Bid proteins in Naa20$^{-/-}$ MEFs is not caused by transcriptional repression of the corresponding genes or by destabilizing the mRNAs, suggesting a selective translational repression or an instability of these proteins.

There is a growing evidence that protein Nt-acetylation plays a role on protein stability acting in some instances as an N-degron [41–43] and in others as a protein stabilizer hiding N-degrons [32,44–46]. Inactivation of *Naa20* affects MEFs proteome showing upregulated and downregulated proteins. Interestingly, a high proportion of downregulated proteins are NatB substrates (43%), similar to the observed in *A. thaliana* when NatA is downregulated where 83% of downregulated proteins are canonical NatA substrates [46]. These data indicate that Nt-acetylation is preventing recognition of N-degrons and plays a role in the maintenance of part of the proteome stability in plants and mammals. On the other hand, among the upregulated proteins in Naa20$^{-/-}$ MEFs, none was found to be NatB substrate indicating that they are not degraded via Ac/N-degron pathway. Several studies assessing the role of Nt-acetylation on specific proteins stability [39,44,46] in addition to a systematic analysis of yeast protein N-terminal sequences effect on proteome stability [45] indicate that Nt-acetylation operates more frequently as protein stabilizer, preventing degradation, than as a N-degron.

Taking this into account, we next addressed whether the reduction in the levels of pro-apoptotic proteins studied could affect the susceptibility of Naa20$^{-/-}$ MEFs to different apoptotic stimuli. Our results point to a partial inhibition of etoposide- and TNF-α plus SMAC mimetic-induced apoptosis in Naa20$^{-/-}$ MEFs in comparison with WT cells. It is well established that the loss of apical initiator caspase-8 and -9 blocks extrinsic or intrinsic apoptosis, respectively [47,48]. This reflects a negative impact of *Naa20* inactivation on both apoptotic pathways. To understand whether this apoptosis blockade could be related to impaired Bax activation, we addressed its subcellular localization and the release of cyt *c* and SMAC/DIABLO. For Naa20$^{-/-}$ MEFs under basal conditions, we found a slight accumulation of mitochondrial Bax which is not associated with an increase of cyt *c* or SMAC/DIABLO release. Though in our previous studies with Naa25$^{-/-}$ MEFs we found a more prominent increase in mitochondrial Bax targeting [10] than in Naa20$^{-/-}$ MEFs, we did also not observe cyt *c* release, as in Naa25$^{-/-}$ MEFs. On the other hand, 12h after etoposide treatment, procaspase-9 protein expression levels as well as Bax

mitochondrial translocation and cyt *c* release were similar in Naa20$^{-/-}$ and WT MEFs. Therefore, the absence of Naa20 causes an apoptotic blockade downstream of cyt *c* release ultimately determining the lower susceptibility of Naa20$^{-/-}$ MEFs to etoposide. Furthermore, as Apaf1 is a putative NatB substrate, the absence of its Nt-acetylation may compromise the apoptosome formation, and also explain the limited procaspase-9 activation. In contrast, apoptosis was not impaired in Naa20$^{-/-}$ MEFs after treatment with other apoptotic inducers, namely with the proteasome inhibitor MG132 and with the ER-stress inducer tunicamycin. One of the first studies investigating the biological function of the hNaa20 showed an increase of HeLa cells sensitivity to MG132 after Naa20 knockdown [8]. In accordance with this result, our previous study with Naa25$^{-/-}$ MEFs revealed an increased susceptibility to MG132 [10]. Also, another study performed in caspase-9$^{-/-}$ MEFs revealed an efficient apoptosis induction by MG132, in contrast with a weak induction of apoptosis by etoposide, which could be restored by synergizing with active cytosolic SMAC/DIABLO [49]. Interestingly, the reduction in procaspases and cleaved caspases protein levels in Naa20$^{-/-}$ MEFs compared with WT cells does not promote a different susceptibility to MG132 neither affect Bax activation nor cyt *c* and SMAC/DIABLO release. Thus, the release of cyt *c* probably allows the apoptosome formation and activation of caspase-9/-3, while the release of SMAC/DIABLO inhibits IAPs activity, ultimately triggering the apoptotic cascade. Similarly, *Naa20* inactivation does not alter susceptibility to tunicamycin. As etoposide is a typical caspase-9 dependent drug [49,50], the reduction of procaspase-9 and of its cleaved form, mediated by *Naa20* inactivation, as well as the reduction of SMAC/DIABLO release, likely affect this drug effectiveness in eliciting apoptosis. On the other hand, TNF-α, a pleiotropic ligand of tumor necrosis factor receptor 1 and 2, is recognized to promote either cell survival by activating NF-kB, or cell death by activating procaspase-8 [51]. The observed defects in the levels of procaspase-8 in the absence of NatB-mediated Nt-acetylation hamper the apoptotic cascade and, consequently, favour TNF-α-induced cell survival. Additionally, as the amount of procaspases determine directly their proteolytic cleavage, and consequent its activation [52], the reduced activation of caspases we observe can be explained by the reduced protein levels of their respective procaspases. Altogether, these data indicate that the effect of *Naa20* inactivation on apoptosis induction, likely due to the reduction in the protein levels of procaspase-3, -9 and -8, and Bid is stimulus-dependent.

As abovementioned, Nt-acetylation is preventing protein degradation and plays a role in the maintenance of part of the proteome stability in MEFs, we sought to identify the N-recognins involved in the degradation of Bid, procaspase-3, -9 and -8 when Naa20 is inactivated. Downregulation of *Ubr1* and *Ubr4* confirmed that the N-terminal of Bid, procaspase-8 and procaspase-9 may be sensed as N-degrons and targeted to degradation. On the other hand, downregulation of *Ubr2* reduces procaspase-8 and

procaspase-3 expression in WT MEFs. This is in accordance with a recent study where it was observed that the Arg/N-degron pathway can also modulate translation of specific mRNAs reducing their expression when UBR2 is not present [53]. Interestingly, *Ubr4* silencing in Naa20$^{-/-}$ MEFs was able to restore procaspase-8 protein levels, and even promoted its activation after TNF-α plus SMAC mimetic treatment. In response to these stimuli, caspase-3 and -9 activation was less pronounced in Naa20$^{-/-}$ MEFs than in WT MEFs when *Ubr4* N-recognin is downregulated, reflecting that the cleavage of Bid by caspase-8 was not enough to activate the intrinsic pathway. Similarly, we show that UBR1 recognizes procaspase-9 as a N-degron as its decreased protein levels in Naa20$^{-/-}$ MEFs were also partially restored after *Ubr1* silencing. However, *Ubr1* downregulation in Naa20$^{-/-}$ MEFs did not promote procaspase-9 activation suggesting that it was not strong enough to restore the activation of the intrinsic pathway in response to etoposide. Given these evidences, the observed defects on cell proliferation in Naa20$^{-/-}$ MEFs may also be associated with low levels of the involved NatB substrates caused by their instability and degradation via Arg/N-degron pathway. However, further studies will be needed to test this possibility.

3.5. Conclusion

Though the relation between apoptosis and Arg/N-degron pathway as well as between apoptosis and Nt-acetylation has been explored, to our knowledge the interplay between Nt-acetylation and N-degron pathways, and its impact on apoptosis regulation, has not been addressed. Our study provides new clues supporting the relevance of protein Nt-acetylation for cellular proteostasis and proper function of relevant biological pathways like apoptosis. Altogether, our findings suggest that UBR1- and UBR4-mediated degradation of procaspases and Bid may determine in a stimulus-dependent way a limited activation of the extrinsic and intrinsic apoptotic pathways when NatB is inhibited, highlighting the impact of NatB and N-degron pathways interdependence on apoptosis modulation.

References

1. Gao J, Barroso C, Zhang P, Kim HM, Li S, Labrador L, et al. N-terminal acetylation promotes synaptonemal complex assembly in *C. Elegans*. Genes Dev. 2016;30: 2404–2416. doi:10.1101/gad.277350.116
2. Huber M, Bienvenut W V., Linster E, Stephan I, Armbruster L, Sticht C, et al. NatB-mediated N-terminal acetylation affects growth and biotic stress responses. Plant Physiol. 2020;182: 792–806. doi:10.1104/pp.19.00792
3. Van Damme P, Lasa M, Polevoda B, Gazquez C, Elosegui-Artola A, Kim DS, et al. N-terminal acetylome analyses and functional insights of the N-terminal acetyltransferase NatB. Proc Natl Acad Sci U S A. 2012;109: 12449–12454. doi:10.1073/pnas.1210303109

4. Neri L, Lasa M, Elosegui-Artola A, D'Avola D, Carte B, Gazquez C, et al. NatB-mediated protein N-α-terminal acetylation is a potential therapeutic target in hepatocellular carcinoma. Oncotarget. 2017;8: 40967–40981. doi:10.18632/oncotarget.17332

5. Kim JH, Cho A, Yin H, Schafer DA, Mouneimne G, Simpson KJ, et al. Psidin, a conserved protein that regulates protrusion dynamics and cell migration. Genes Dev. 2011;25: 730–741. doi:10.1101/gad.2028611

6. Singer JM, Shaw JM. Mdm20 protein functions with Nat3 protein to acetylate Tpm1 protein and regulate tropomyosin-actin interactions in budding yeast. Proc Natl Acad Sci U S A. 2003;100: 7644–7649. doi:10.1073/pnas.1232343100

7. Polevoda B, Cardillo TS, Doyle TC, Bedi GS, Sherman F. Nat3p and Mdm20p are required for function of yeast NatB Nα-terminal acetyltransferase and of actin and tropomyosin. J Biol Chem. 2003;278: 30686–30697. doi:10.1074/jbc.M304690200

8. Ametzazurra A, Larrea E, Civeira MP, Prieto J, Aldabe R. Implication of human *N-α*-acetyltransferase 5 in cellular proliferation and carcinogenesis. Oncogene. 2008;27: 7296–7306. doi:10.1038/onc.2008.332

9. Stephan D, Sánchez-Soriano N, Loschek LF, Gerhards R, Gutmann S, Storchova Z, et al. *Drosophila* Psidin regulates olfactory neuron number and axon targeting through two distinct molecular mechanisms. J Neurosci. 2012;32: 16080–16094. doi:10.1523/JNEUROSCI.3116-12.2012

10. Alves S, Neiri L, Chaves SR, Vieira S, Trindade D, Manon S, et al. N-terminal acetylation modulates Bax targeting to mitochondria. Int J Biochem Cell Biol. 2018;95: 35–42. doi:10.1016/j.biocel.2017.12.004

11. Balasiddaiah A, Moreno D, Guembe L, Prieto J, Aldabe R. Hepatic differentiation of mouse iPS cells and analysis of liver engraftment potential of multistage iPS progeny. J Physiol Biochem. 2013;69: 835–845. doi:10.1007/s13105-013-0260-9

12. Bradford MM. A rapid and sensitive method for the quantitation of microgram quantities of protein utilizing the principle of protein-dye binding. Anal Biochem. 1976;72: 248–254. doi:10.1006/abio.1976.9999

13. Bienvenut W V., Giglione C, Meinnel T. Proteome-wide analysis of the amino terminal status of *Escherichia coli* proteins at the steady-state and upon deformylation inhibition. Proteomics. 2015;15: 2503–2518. doi:10.1002/pmic.201500027

14. Chakraborty A, Regnier FE. Global internal standard technology for comparative proteomics. J Chromatogr A. 2002;949: 173–184. doi:10.1016/S0021-9673(02)00047-X

15. Rathore OS, Faustino A, Prudêncio P, Van Damme P, Cox CJ, Martinho RG. Absence of N-terminal acetyltransferase diversification during evolution of eukaryotic organisms. Sci Rep. 2016;6: 21304(1–13). doi:10.1038/srep21304

16. Bienvenut W V., Giglione C, Meinnel T. SILProNAQ: A Convenient Approach for Proteome-Wide Analysis of Protein N-Termini and N-Terminal Acetylation Quantitation. Protein Terminal Profiling: Methods and Protocols, Methods in Molecular Biology. 2017. pp. 17–34. doi:10.1007/978-1-4939-6850-3

17. Fan Z, Beresford PJ, Oh DY, Zhang D, Lieberman J. Tumor suppressor NM23-H1 is a granzyme A-activated DNase during CTL-mediated apoptosis, and the nucleosome assembly protein SET is its inhibitor. Cell. 2003;112: 659–672. doi:10.1016/s0092-8674(03)00150-8

18. Guo W, Shi X, Liu A, Yang G, Yu F, Zheng Q, et al. RNA binding protein QKI inhibits the ischemia/reperfusion-induced apoptosis in neonatal cardiomyocytes. Cell Physiol Biochem. 2011;28: 593–602. doi:10.1159/000335755

19. Liu J, Zhang Y, Li Q, Wang Y. Transgelins: Cytoskeletal Associated Proteins Implicated in the Metastasis of Colorectal Cancer. Front Cell Dev Biol. 2020;8: 573859. doi:10.3389/fcell.2020.573859

20. Mukherjee S, Shields D. Nuclear import is required for the pro-apoptotic function of the Golgi protein p115. J Biol Chem. 2009;284: 1709–1717. doi:10.1074/jbc.M807263200

21. Noro T, Namekata K, Kimura A, Guo X, Azuchi Y, Harada C, et al. Spermidine promotes retinal ganglion cell survival and optic nerve regeneration in adult mice following optic nerve injury. Cell Death Dis. 2015;6: e1720. doi:10.1038/cddis.2015.93

22. Ohno Y, Koizumi M, Nakayama H, Watanabe T, Hirooka M, Tokumoto Y, et al. Downregulation of ANP32B exerts anti-apoptotic effects in hepatocellular carcinoma. PLoS One. 2017;12: e0177343. doi:10.1371/journal.pone.0177343

23. Qiu S, Liu PY, Liu T. Up-regulation of LYAR blocks Myc-induced cell death. Cell Cycle. 2017;16: 1857–1858. doi:10.1080/15384101.2017.1374682

24. Saatci O, Kaymak A, Raza U, Ersan PG, Akbulut O, Banister CE, et al. Targeting lysyl oxidase (LOX) overcomes chemotherapy resistance in triple negative breast cancer. Nat Commun. 2020;11: 2416. doi:10.1038/s41467-020-16199-4

25. Yu H, Ding J, Zhu H, Jing Y, Zhou H, Tian H, et al. LOXL1 confers antiapoptosis and promotes gliomagenesis through stabilizing BAG2. Cell Death Differ. 2020;27: 3021–3036. doi:10.1038/s41418-020-0558-4

26. Vié N, Copois V, Bascoul-Mollevi C, Denis V, Bec N, Robert B, et al. Overexpression of phosphoserine aminotransferase PSAT1 stimulates cell growth and increases chemoresistance of colon cancer cells. Mol Cancer. 2008;7: 14. doi:10.1186/1476-4598-7-14

27. Iurlaro R, Muñoz-Pinedo C. Cell death induced by endoplasmic reticulum stress. FEBS J. 2016;283: 2640–2652. doi:10.1111/febs.13598

28. Deng S, Marmorstein R. Protein N-Terminal Acetylation: Structural Basis, Mechanism, Versatility, and Regulation. Trends Biochem Sci. 2021;46: 15–27. doi:10.1016/j.tibs.2020.08.005

29. Aksnes H, Ree R, Arnesen T. Co-translational, Post-translational, and Non-catalytic Roles of N-Terminal Acetyltransferases. Mol Cell. 2019;73: 1097–1114. doi:10.1016/j.molcel.2019.02.007

30. Linster E, Stephan I, Bienvenut W V., Maple-Grødem J, Myklebust LM, Huber M, et al. Downregulation of N-terminal acetylation triggers ABA-mediated drought responses in *Arabidopsis*. Nat Commun. 2015;6: 7640(1–13). doi:10.1038/ncomms8640

31. Kweon HY, Lee MN, Dorfel M, Seo S, Gottlieb L, Papazyan T, et al. *Naa12* compensates for *Naa10* in mice in the amino-terminal acetylation pathway. Elife. 2021;10: e65952(1-37). doi:10.7554/eLife.65952

32. Myklebust LM, Van Damme P, Støve SI, Dörfel MJ, Abboud A, Kalvik T V., et al. Biochemical and cellular analysis of Ogden syndrome reveals downstream Nt-acetylation defects. Hum Mol Genet. 2015;24: 1956–1976. doi:10.1093/hmg/ddu611

33. Drazic A, Aksnes H, Marie M, Boczkowska M, Varland S, Timmerman E, et al. NAA80 is actin's N-

terminal acetyltransferase and regulates cytoskeleton assembly and cell motility. Proc Natl Acad Sci U S A. 2018;115: 4399–4404. doi:10.1073/pnas.1718336115

34. Kalvik T V., Arnesen T. Protein N-terminal acetyltransferases in cancer. Oncogene. 2013;32: 269–276. doi:10.1038/onc.2012.82

35. Huber M, Armbruster L, Etherington RD, De La Torre C, Hawkesford MJ, Sticht C, et al. Disruption of the Nα -Acetyltransferase NatB Causes Sensitivity to Reductive Stress in *Arabidopsis thaliana*. Front Plant Sci. 2022;12: 799954. doi:10.3389/fpls.2021.799954

36. Friedrich UA, Zedan M, Hessling B, Fenzl K, Gillet L, Barry J, et al. Nα -terminal acetylation of proteins by NatA and NatB serves distinct physiological roles in *Saccharomyces cerevisiae*. Cell Rep. 2021;34: 108711(1–24). doi:10.1016/j.celrep.2021.108711

37. Gauci S, Helbig AO, Slijper M, Krijgsveld J, Heck AJR, Mohammed S. Lys-N and trypsin cover complementary parts of the phosphoproteome in a refined SCX-based approach. Anal Chem. 2009;81: 4493–4501. doi:10.1021/ac9004309

38. Vaca Jacome AS, Rabilloud T, Schaeffer-Reiss C, Rompais M, Ayoub D, Lane L, et al. N-terminome analysis of the human mitochondrial proteome. Proteomics. 2015;15: 2519–2524. doi:10.1002/pmic.201400617

39. Sheng Z, Du W. NatB regulates Rb mutant cell death and tumor growth by modulating EGFR/MAPK signaling through the N-end rule pathways. PLoS Genet. 2020;16: e1008863(1-25). doi:10.1371/journal.pgen.1008863

40. Tang D, Kang R, Berghe T Vanden, Vandenabeele P, Kroemer G. The molecular machinery of regulated cell death. Cell Res. 2019;29: 347–364. doi:10.1038/s41422-019-0164-5

41. Park SE, Kim J-M, Seok OH, Cho H, Wadas B, Kim S-Y, et al. Control of mammalian G protein signaling by N-terminal acetylation and the N-end rule pathway. Science. 2015;347: 1249–1252. doi:10.1126/science.aaa3844

42. Shemorry A, Hwang CS, Varshavsky A. Control of Protein Quality and Stoichiometries by N-Terminal Acetylation and the N-End Rule Pathway. Mol Cell. 2013;50: 540–551. doi:10.1016/j.molcel.2013.03.018

43. Hwang CS, Shemorroy A, Varshavsky A. N-Terminal Acetylation of Cellular Proteins Creates Specific Degradation Signals. Science. 2010;327: 973–977. doi:10.1126/science.1183147

44. Li Z, Dogra V, Lee KP, Li R, Li M, Li M, et al. N-terminal acetylation stabilizes SIGMA FACTOR BINDING PROTEIN1 involved in salicylic acid-primed cell death. Plant Physiol. 2020;183: 358–370. doi:10.1104/pp.19.01417

45. Kats I, Khmelinskii A, Kschonsak M, Huber F, Knieß RA, Bartosik A, et al. Mapping Degradation Signals and Pathways in a Eukaryotic N-terminome. Mol Cell. 2018;70: 488–501. doi:10.1016/j.molcel.2018.03.033

46. Linster E, Forero Ruiz FL, Miklankova P, Ruppert T, Mueller J, Armbruster L, et al. Cotranslational N-degron masking by acetylation promotes proteome stability in plants. Nat Commun. 2022;13: 810(1–12). doi:10.1038/s41467-022-28414-5

47. McIlwain DR, Berger T, Mak TW. Caspase functions in cell death and disease. Cold Spring Harb Perspect Biol. 2013;5: a008656. doi:10.1101/cshperspect.a008656

48. McComb S, Chan PK, Guinot A, Hartmannsdottir H, Jenni S, Dobay MP, et al. Efficient apoptosis requires feedback amplification of upstream apoptotic signals by effector caspase-3 or -7. Sci Adv.

2019;5: eaau9433(1-11). doi:10.1126/sciadv.aau9433

49. Henderson CJ, Aleo E, Fontanini A, Maestro R, Paroni G, Brancolini C. Caspase activation and apoptosis in response to proteasome inhibitors. Cell Death Differ. 2005;12: 1240–1254. doi:10.1038/sj.cdd.4401729

50. Rodríguez-Enfedaque A, Delmas E, Guillaume A, Gaumer S, Mignotte B, Vayssière JL, et al. ZVAD-fmk upregulates caspase-9 cleavage and activity in etoposide-induced cell death of mouse embryonic fibroblasts. Biochim Biophys Acta. 2012;1823: 1343–1352. doi:10.1016/j.bbamcr.2012.05.013

51. Petersen SL, Wang L, Yalcin-Chin A, Li L, Peyton M, Minna J, et al. Autocrine TNFα Signaling Renders Human Cancer Cells Susceptible to Smac-Mimetic-Induced Apoptosis. Cancer Cell. 2007;12: 445–456. doi:10.1016/j.ccr.2007.08.029

52. Galluzzi L, Vitale I, Aaronson SA, Abrams JM, Adam D, Agostinis P, et al. Molecular mechanisms of cell death: Recommendations of the Nomenclature Committee on Cell Death 2018. Cell Death Differ. 2018;25: 486–541. doi:10.1038/s41418-017-0012-4

53. Vu TTM, Mitchell DC, Gygi SP, Varshavsky A. The Arg/N-degron pathway targets transcription factors and regulates specific genes. Proc Natl Acad Sci U S A. 2020;117: 31094–31104. doi:10.1073/pnas.2020124117

CHAPTER 4

INTERPLAY BETWEEN NT-ACETYLATION AND N-DEGRON PATHWAYS IN THE MODULATION OF APOPTOSIS

This chapter is adapted from the following publication:

Joana P. Guedes, Manuela Côrte-Real **Interplay between Nt-acetylation and N-degron pathways in the modulation of apoptosis.** *Manuscript in preparation*

4.1. Background

In spite of the studies mentioned above (see Chapter 2, section 2.4 and 2.5) showing that protein Nt-acetylation or N-degron pathways can individually affect the apoptotic cell death, the impact of their interaction on apoptosis regulation is far from elucidated. Hence, to fill the gap around these issues, we sought to carry out an *in silico* systematic search for the main components of the apoptotic machinery as potential targets of Nt-acetylation and of degradation by N-degron pathways. This purpose was further supported by the results presented in the previous chapter, which brought new insights on the relevance of NatB-mediated Nt-acetylation and N-degron pathways, namely of the Arg/N-degron pathway, on apoptosis modulation.

4.2. Materials and Methods

The strategy and methodology used throughout this study is depicted in Figure 4.1. Firstly, we selected key components of the apoptotic machinery, in a total of 33 pro-apoptotic proteins and 9 anti-apoptotic proteins. Then, we looked for the N-terminal sequence of each full-length protein using the UNIPROT database. In parallel, taking account the caspase or calpain-mediated proteolytic cleavage of a wide range of apoptotic proteins, a search on the literature for the potential cleavage sites of each full-length protein was carried to access the N-terminal sequence of the generated fragment. Afterwards, we evaluated the potential for each full-length protein (Table 4.1), as well as for the protein fragments (Table 4.2) to be Nt-acetylated, based on NATs´s substrate specificity (see Figure 2.1), or to be degraded by the N-degron pathways, based on the presence of destabilizing Nt-residues (see Figure 2.3). Thus, we assessed if each full-length protein or generated fragment was Nt-acetylated or not, and identified the NAT responsible for this modification. In case the protein was Nt-acetylated, the presence of destabilizing Ac/N-degrons was checked. On the other hand, looking for the N-terminal sequence, the presence of destabilizing residues capable to be degraded via Arg or Gly/N-degron pathway, was also monitored. Since it was recently demonstrated that NME can occur in proteins bearing MN-, MQ- and MD- at their N-terminal creating destabilizing Nt-residues, which are targeted for degradation via Arg/N-degron pathway [1,2], we also evaluated if this could happen with the apoptotic proteins under study. Additionally, Nguyen and colleagues raised the hypothesis that proteins bearing ME- at the N-terminal may also undergo NME. Although this hypothesis has not yet experimentally verified, we also consider it in our analysis (indicated in Table 4.1 with the interrogation point, ?). Importantly, our analysis was performed regarding the information reported in the review by Varshavsky *et al.,* 2019 [3], which considers that although almost all NAT substrates exhibit conditional degrons, they may become prone to degradation by the Ac/N-

degron pathway, as well as reported in Hwang team' papers [1,2] which describe the creation of destabilizing Nt-residues targeted for degradation via the Arg/N-degron pathway after NME. Finally, the outcome of the downregulation of Nt-acetylation or of N-degron pathways on the protein apoptotic function was predicted.

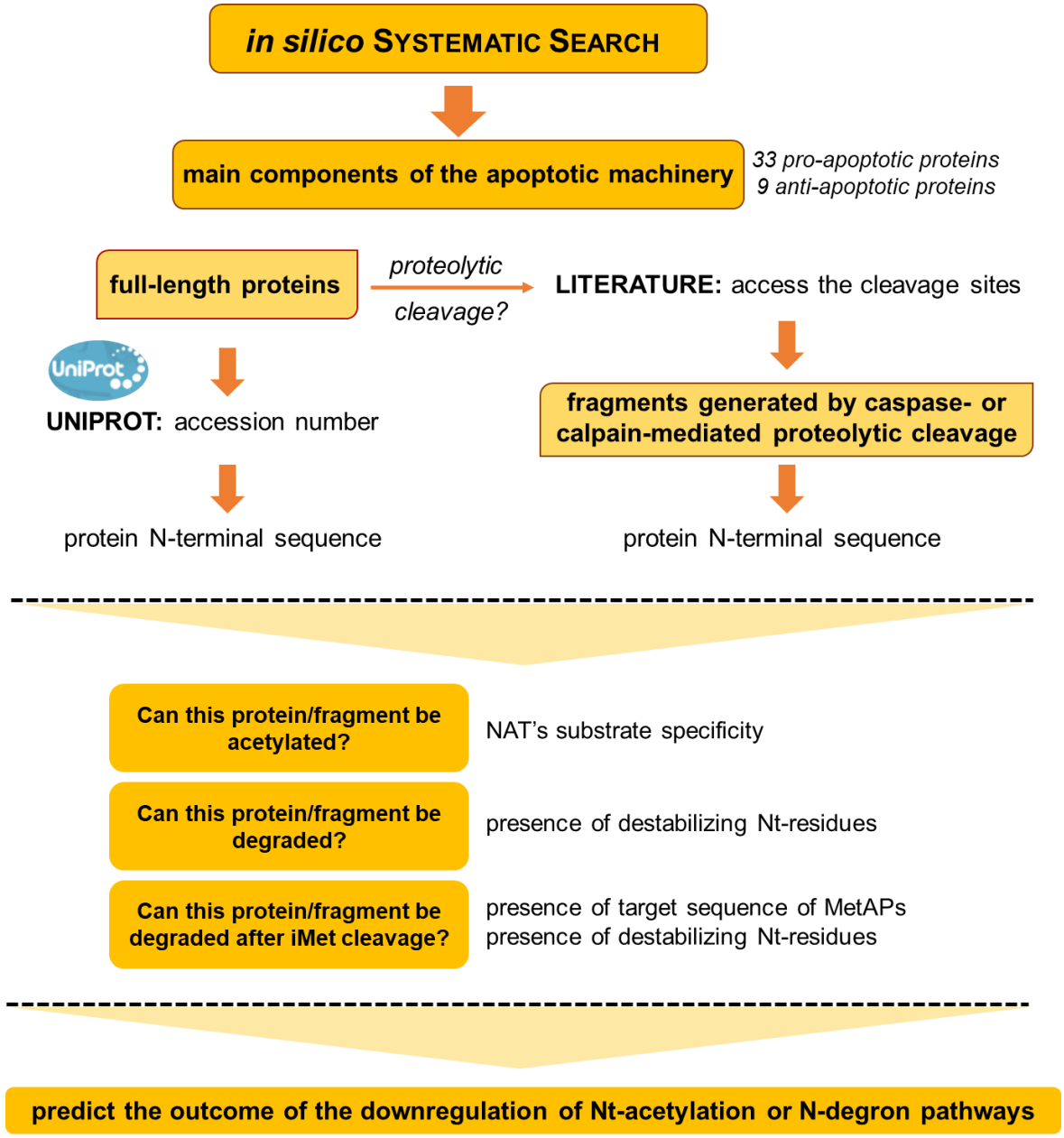

Figure 4.1: Flowchart of the strategy used in the *in silico* search of apoptotic components as NATs and N-recognin substrates.

4.3. Results and Discussion

The analysis covered a total of 42 full-length apoptotic proteins (Table 4.1 and Figure 4.2). Regarding the 33 pro-apoptotic proteins, they are mainly substrates of NatB and NatE with a small percentage of proteins being substrates of NatE, NatC and NatF, and a small percentage of proteins that are not NAT substrates (Figure 4.2). On the other hand, the anti-apoptotic proteins are mainly acetylated by NatE, one acetylated by NatE, NatC and NatF (MCL-1), one acetylated by NatB (c-IAP2), and another not acetylated (c-IAP1) (Figure 4.2). These data indicate a high impact of Nt-acetylation on the function of both pro- and anti-apoptotic proteins. Moreover, besides the known role of NatB [4–6] and NatC [7,8] in apoptosis regulation, our analysis suggests that NatE and NatF may also have a role in apoptosis.

As aforementioned, half-life of pro-apoptotic proteins is also determined by the presence of destabilizing residues at their N-terminus. In particular, it was suggested that degradation of pro-apoptotic N-terminal fragments through the Arg/N-degron pathway restrains the surpassing of the point of no return in response to a weak apoptotic stimulus [3]. Among the 33 pro-apoptotic proteins, we identified 2 (HRK1 and OPA1) exhibiting a N-degron that may be exclusively degraded via the Arg/N-degron pathway (6%) but also 5 proteins (OMA1, PROCASPASE-6 and -10, TNF-α and c-FLIP$_L$) capable of being exclusively degraded via the Ac/N-degron pathway (15%) (Figure 4.2, Table 4.1). If we consider the cleavage of iMet, 23 out of 33 (70%) proteins can be degraded by both pathways. Moreover, CYCS and TNFR1 can be degraded via Gly/N-degron pathway as they bear Gly/N-degrons after cleavage of methionine. NOXA is the only stable protein as it does not exhibit destabilizing Nt-residues.

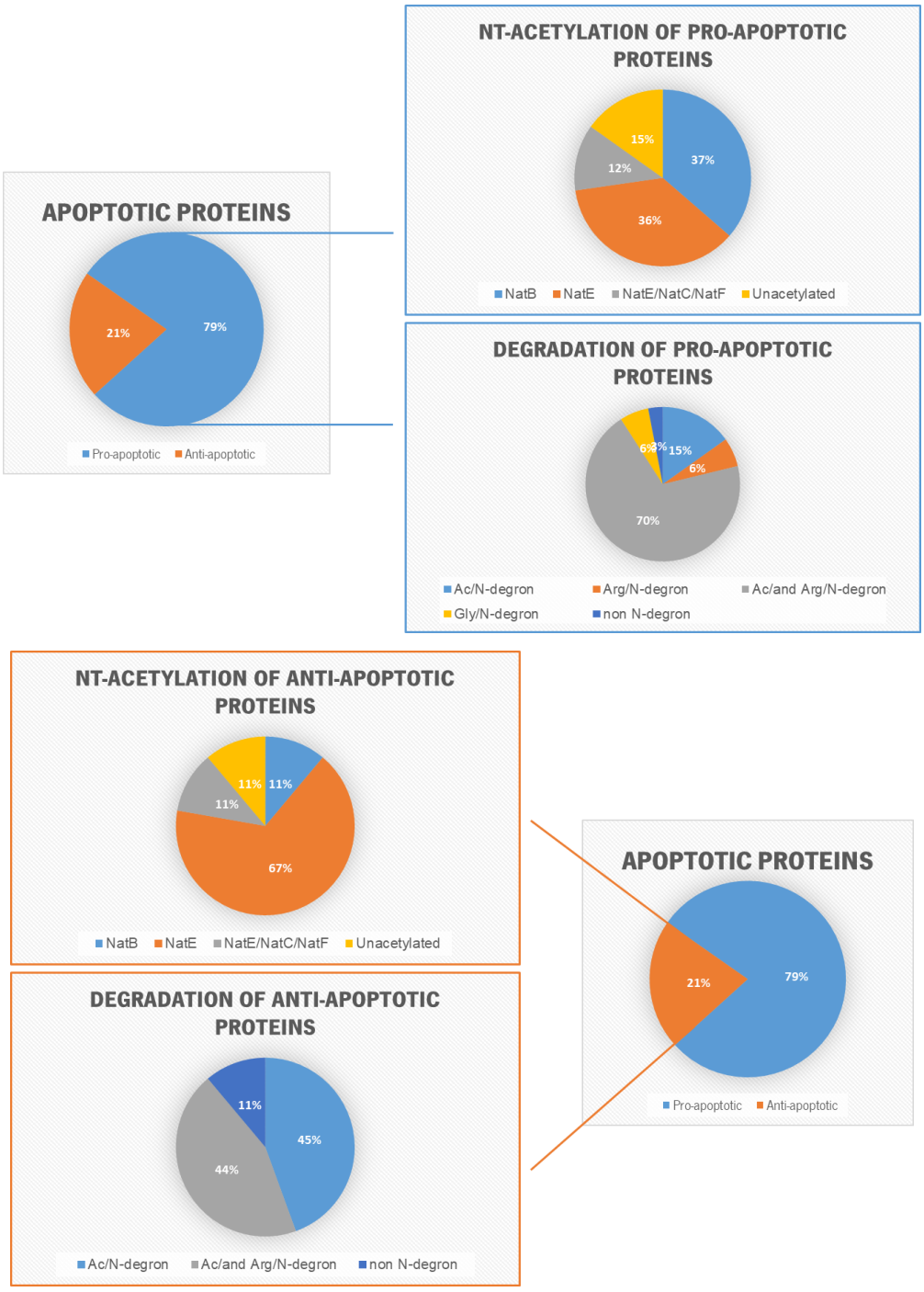

Figure 4.2: The main apoptotic proteins are mostly substrates of the NatB or NatE and of Ac/ or Arg/N-degron pathways. Pie charts exhibiting the percentages of apoptotic proteins undergoing Nt-acetylation and degradation mediated by N-degron pathways. The NATs responsible for the Nt-acetylation as well as the N-degron pathways responsible for the degradation are identified.

Regarding the 9 anti-apoptotic proteins, 4 (BCL-XL, BFL-1, XIAP and c-FLIP$_S$) can be exclusively degraded through Ac/N-degron pathway, 4 (BCL-2, BCL-W, MCL-1 and c-IAP2) display destabilizing Nt-residues capable of being degraded by both Arg/ and Ac/N-degron pathways, and c-IAP1 is the only stable protein.

In sum, 30 of the 33 (≈91%) pro-apoptotic proteins and 8 of the 9 (≈89%) anti-apoptotic proteins display N-degrons and may be mainly degraded via Ac/ and Arg/N-degron pathways (Table 4.1). Taking this into account and given that the degradation of pro- or anti-apoptotic has opposite effects on apoptosis outcome, it appears unrealistic to target N-recognins towards apoptosis modulation. However, as aforementioned, combined treatment of the E3 ubiquitin ligase inhibitor RFC11 with shikonin exhibit antitumor effects by increasing the half-life of RIPK1 and enhancing necroptosis and apoptosis [9]. This study was the first *in vivo* evidence that the inhibition of N-degron pathways may be explored to increase efficiency of chemotherapeutic drugs. Regarding downregulation of NatB, it seems to perturb the proteostasis of 12 pro-apoptotic proteins and of 1 anti-apoptotic protein leading to their degradation and likely to an apoptosis inhibition net outcome, but only when the iMet is removed through the action of MetAPs. Curiously, we have found that inactivation of *NAA20* in MEF cells is associated with a decrease in the levels procaspase-8, -9 and -3 as well as of Bid and to a blockage of apoptosis or not affecting it, depending on the stimulus (Chapter 2). Indeed, Naa20$^{-/-}$ MEFs exhibited decreased susceptibility to TNF-a plus SMAC mimetics as well as to etoposide, while apoptosis triggered by MG132 or by tunicamycin is not affected. It would be interesting to assess whether the stimulus dependent response is related with MetAPs activity. In contrast, downregulation of NatE apparently perturbs the proteostasis of 11 proapoptotic proteins and of 3 anti-apoptotic protein leading to their degradation and likely to apoptosis inhibition net outcome, but only when the iMet is not removed through the action of MetAPs. Whether, like for NatB inactivation, inactivation of NatE perturbs proteostasis of apoptotic proteins and affects the apoptosis outcome in a stimulus-dependent way related with MetAPs activity requires experimental confirmation. In sum, this analysis suggest that apoptosis dysfunction may underlie the pathogenesis of human diseases associated with deregulation of NatB and NatE.

Table 4.1: Nt-acetylation and N-degron pathway impacts the proteostasis of main apoptotic components of the intrinsic and extrinsic pathways. The analysis covers 33 pro-apoptotic proteins and 9 anti-apoptotic proteins regarding their potential to be Nt-acetylated or degraded via N-degron pathways. The N-terminal sequence, the NAT involved in Nt-acetylation and the N-degron pathways responsible for the protein degradation, in the case of non-removal or removal of iMet by methionine aminopeptidases (MetAPs) are identified, as well as the effect the downregulation of the Nt-acetylation or of the N-degron pathways. As the iMet cleavage of proteins bearing ME- at the N-terminal has not yet been experimentally verified, the analysis of these proteins appears with the interrogation point (?). *n.c.*, N-terminal non cleaved by MetAPs, other than MA-, MS-, MT-, MV-, MC-, MD-, MN-, MQ- and ME-.

Accession number	Type	Apoptotic protein	Function	N-terminal	NAT	Ac/N-degron	Arg/N-degron non-associated or associated with MetAPs cleavage	Effect on the protein level caused by Nt-acetylation downregulation non-associated or associated with MetAPs cleavage	Effect on the protein level caused by the N-degron pathways downregulation
Q07812	pro-apoptotic	Bcl-2-associated X **BAX**	apoptotic activator	MD-	NatB	yes	no/yes	**no effect / decrease**	**increase**
Q16611		Bcl-2 homologous killer **BAK**	MOMP	MA-	NatE	yes	yes/no	**decrease / no effect**	**increase**
Q9UMX3		Bcl-2-related ovarian killer protein **BOK**	MOMP; regulation of ER homeostasis	ME-	NatB	yes	no/yes?	**no effect / decrease?**	**increase**
Q9BXH1		p53-upregulated modulator of apoptosis **PUMA**	binding anti-apoptotic proteins; activation of Bax and Bak	MA-	NatE	yes	yes/no	**decrease / no effect**	**increase**
O43521		Bcl-2-interacting mediator of cell death **BIM**	apoptotic activator	MA-	NatE	yes	yes/no	**decrease / no effect**	**increase**
Q13794		phorbol-12-myristate-13-acetate-induced protein 1 **NOXA**	mitochondrial membrane changes; efflux of apoptogenic proteins from the mitochondria; degradation of MCL-1	MP-	-	-	-	-	-
P55957		BH3 interacting domain death agonist **BID**	counter the protective effect of BCL2; caspase activation	MD-	NatB	yes	no/yes	**no effect / decrease**	**increase**

Table 4.1: Nt-acetylation and N-degron pathway impacts the proteostasis of main apoptotic components of the intrinsic and extrinsic pathways (cont).

Accession number	Type	Apoptotic protein	Function	N-terminal	NAT	Ac/N-degron	Arg/N-degron non-associated or associated with MetAPs cleavage	Effect on the protein level caused by Nt-acetylation downregulation non-associated or associated with MetAPs cleavage	Effect on the protein level caused by the N-degron pathways downregulation
Q92934	pro-apoptotic	Bcl2-associated agonist of cell death **BAD**	binding anti-apoptotic proteins; promote MOMP	MF-	NatC, NatE, NatF	yes	yes/n.c.	**decrease / no effect**	**increase**
Q96LC9		Bcl-2-modifying factor **BMF1**	promote MOMP	ME-	NatB	yes	no/yes?	**no effect / decrease?**	**increase**
O00198		Activator of apoptosis harakiri **HRK**	promote MOMP	MC-	-	-	no/yes	**no effect / decrease**	**increase**
P99999		cytochrome *c* somatic **CYCS**	apoptosome formation and activation of procaspase-9	MG-	-	-	-	**decrease via Gly/N-degron pathway after iMet cleavage**	**increase**
Q9NR28		Second mitochondria-derived activator of caspase/Direct IAP-binding protein **SMAC/DIABLO**	IAPs inhibition	MA-	NatE	yes	yes/no	**decrease / no effect**	**increase**
O60313		Mitochondrial dynamin-like 120 kDa protein **OPA1**	release of cyt *c* and SMAC/DIABLO	MW-	-	-	yes/n.c.	**decrease / no effect**	**increase**
Q96E52		Mitochondrial metalloendopeptidase **OMA1**	release of cyt *c* and SMAC/DIABLO	MS-	NatE	yes	no/no	**no effect / no effect**	**increase**
O00429		Dynamin-1-like protein **DRP1**	release of cyt *c* and SMAC/DIABLO	ME-	NatB	yes	no/yes?	**no effect / decrease?**	**increase**
O14727		Apoptotic protease-activating factor 1 **APAF1**	apoptosome formation and activation of procaspase-9	MD-	NatB	yes	no/yes	**no effect / decrease**	**increase**
P55211		**PROCASPASE-9**	apoptosome formation	MD-	NatB	yes	no/yes	**no effect / decrease**	**increase**

Table 4.1: Nt-acetylation and N-degron pathway impacts the proteostasis of main apoptotic components of the intrinsic and extrinsic pathways (cont).

Accession number	Type	Apoptotic protein	Function	N-terminal	NAT	Ac/N-degron	Arg/N-degron non-associated or associated with MetAPs cleavage	Effect on the protein level caused by Nt-acetylation downregulation non-associated or associated with MetAPs cleavage	Effect on the protein level caused by the N-degron pathways downregulation
P42574	pro-apoptotic	**PROCASPASE-3**	executor caspase	ME-	NatB	yes	no/yes?	**no effect / decrease?**	**increase**
P09874		Poly [ADP-ribose] polymerase 1 **PARP1**	apoptosis induction	MA-	NatE	yes	yes/no	**decrease / no effect**	**increase**
P55210		**PROCASPASE-7**	executor caspase	MA-	NatE	yes	yes/no	**decrease / no effect**	**increase**
P55212		**PROCASPASE-6**	executor caspase	MS-	NatE	yes	no/no	**no effect / no effect**	**increase**
Q92851		**PROCASPASE-10**	cleavage and activation of effector caspases	MK-	NatC, NatE, NatF	yes	no/n.c.	**no effect / no effect**	**increase**
Q14790		**PROCASPASE-8**	cleavage and activation of effector caspases	MD-	NatB	yes	no/yes	**no effect / decrease**	**increase**
P25445		Tumor necrosis factor receptor superfamily member 6 **FAS**	receptor for FASL	ML-	NatC, NatE, NatF	yes	yes/n.c.	**decrease / no effect**	**increase**
P48023		Tumor necrosis factor ligand superfamily member 6 **FASL**	cytokine that binds to FAS receptor	MQ-	NatB	yes	no/yes	**no effect / decrease**	**increase**
P19438		Tumor necrosis factor receptor superfamily member 1A **TNFR1**	receptor for TNF-alpha	MG-	-	-	-	**decrease via Gly/N-degron pathway after iMet cleavage**	**increase**
P01375		Tumor necrosis factor ligand superfamily member 2 **TNF-α**	cytokine that binds to TNFR1	MS-	NatE	yes	no/no	**no effect / no effect**	**increase**

Table 4.1: Nt-acetylation and N-degron pathway impacts the proteostasis of main apoptotic components of the intrinsic and extrinsic pathways (cont).

Accession number	Type	Apoptotic protein	Function	N-terminal	NAT	Ac/N-degron	Arg/N-degron non-associated or associated with MetAPs cleavage	Effect on the protein level caused by Nt-acetylation downregulation non-associated or associated with MetAPs cleavage	Effect on the protein level caused by the N-degron pathways downregulation
P50591	pro-apoptotic	Tumor necrosis factor ligand superfamily member 10 **TRAIL**	cytokine that binds to TRAIL receptors	MA-	NatE	yes	yes/no	**decrease / no effect**	**increase**
O00220		Tumor necrosis factor receptor superfamily member 10A **TRAILR1**	receptor for the cytotoxic ligand TRAIL	MA-	NatE	yes	yes/no	**decrease / no effect**	**increase**
O14763		Tumor necrosis factor receptor superfamily member 10B **TRAILR2**	receptor for the cytotoxic ligand TRAIL	ME-	NatB	yes	no/yes?	**no effect / decrease?**	**increase**
Q15628		Tumor necrosis factor receptor type 1-associated death domain protein **TRADD**	TNFR1-FADD interaction	MA-	NatE	yes	yes/no	**decrease / no effect**	**increase**
Q13158		FAS-associated death domain protein **FADD**	death-inducing signaling complex (DISC) assembly	MD-	NatB	yes	no/yes	**no effect / decrease**	**increase**
O15519-1		Cellular FLICE-like inhibitory protein **c-FLIPL**	activation of caspase-8 by death receptors	MS-	NatE	yes	no/no	**no effect / no effect**	**increase**
P10415	anti-apoptotic	B-Cell Lymphoma 2 **BCL-2**	MOMP control; caspase activity inhibitor	MA-	NatE	yes	yes/no	**decrease / no effect**	**increase**
Q07817		B-cell lymphoma-extra-large **BCL-XL**	binding pro-apoptotic members	MS-	NatE	yes	no/no	**no effect / no effect**	**increase**
Q92843		Bcl-2 like protein 2 **BCL-W**	binding pro-apoptotic members; inhibition of Bax	MA-	NatE	yes	yes/no	**decrease / no effect**	**increase**

Table 4.1: Nt-acetylation and N-degron pathway impacts the proteostasis of main apoptotic components of the intrinsic and extrinsic pathways (cont).

Accession number	Type	Apoptotic protein	Function	N-terminal	NAT	Ac/N-degron	Arg/N-degron non-associated or associated with MetAPs cleavage	Effect on the protein level caused by Nt-acetylation downregulation non-associated or associated with MetAPs cleavage	Effect on the protein level caused by the N-degron pathways downregulation
Q16548	anti-apoptotic	Bcl-2 related protein A1 **BFL-1**	binding pro-apoptotic members	MT-	NatE	yes	no/no	**no effect / no effect**	**increase**
Q07820		Bcl-2 like protein 3 **MCL-1**	binding pro-apoptotic members	MF-	NatC, NatE, NatF	yes	yes/n.c.	**decrease / no effect**	**increase**
P98170		X-linked inhibitor of apoptosis **XIAP**	direct caspase inhibitor	MT-	NatE	yes	no/no	**no effect / no effect**	**increase**
Q13490		Cellular inhibitor of apoptosis 1 **c-IAP1**	caspase inactivation; SMAC degradation at mitochondria	MH-	-	-	-	-	-
Q13489		Cellular inhibitor of apoptosis 2 **c-IAP2**	caspase inactivation; SMAC degradation at mitochondria	MN-	NatB	yes	no/yes	**no effect / decrease**	**increase**
O15519-2		Cellular FLICE-like inhibitory protein **c-FLIPs**	inhibition of caspase-8 activation by death receptors	MS-	NatE	yes	no/no	**no effect / no effect**	**increase**

Depending on the number of protein cleavages sites, one or more fragments exhibiting Ac/ or Arg/N-degrons can be generated from each apoptotic protein by caspase- or calpain-mediated proteolytic cleavage (Table 4.2, Figure 4.3 and 4.4).

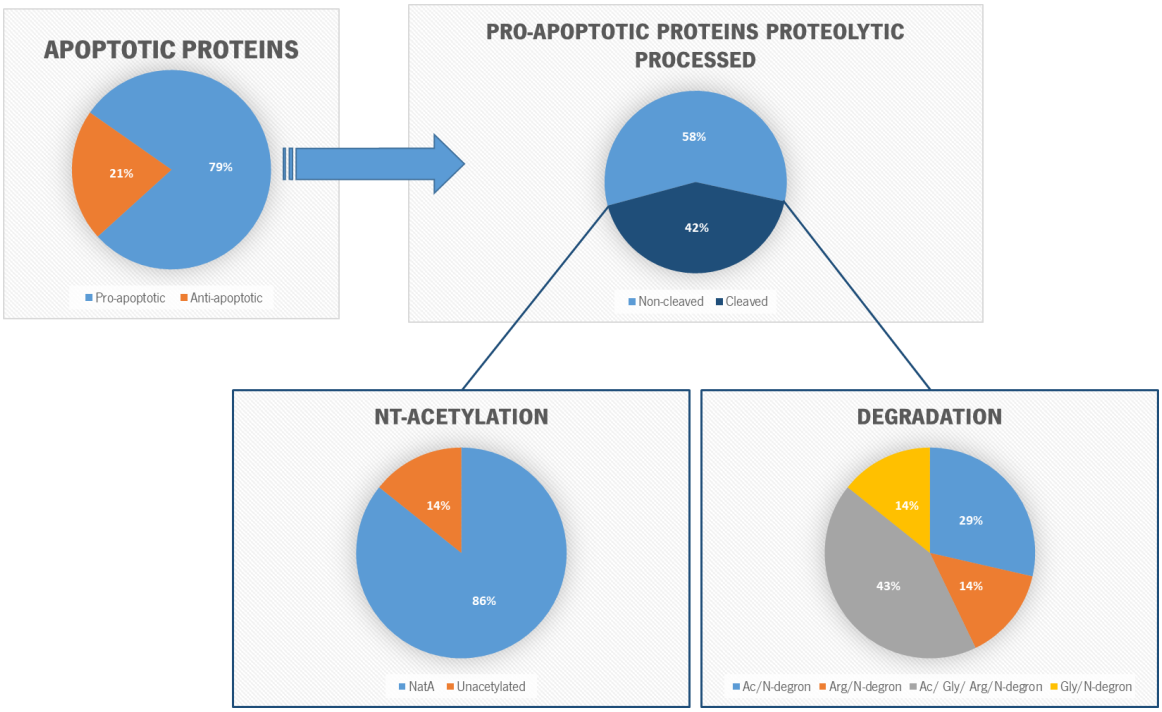

Figure 4.3: NatA acetylates most of the fragments generated by caspase- or calpain-mediated proteolytic cleavage of pro-apoptotic proteins and all N-degron pathways are involved in their degradation. Pie charts exhibiting the percentages of the pro-apoptotic proteins undergoing proteolytic cleavage as well as the percentage of those undergoing Nt-acetylation and degradation mediated by the N-degron pathways. The NATs responsible for the Nt-acetylation as well as the N-degron pathways responsible for the degradation are identified.

Regarding the 33 pro-apoptotic proteins (Figure 4.3, Table 4.2), only 14 may be proteolytic processed generating 31 fragments. We noticed that 12/14 (86%) pro-apoptotic proteins generated fragments that may undergo Nt-acetylation mediated by NatA, while 2 (14%) create fragments that are not substrates of NATs (BAK and BIM). Nonetheless, only 4/12 (AFAF1, PROCASPASE-9, -3 and -10) generate fragments bearing destabilizing Nt-residues capable to be specifically degraded via the Ac/N-degron pathway. 2 out of 14 (BAK and BIM) generate fragments that can be Arg/N-degron exclusive substrates. The cleavage of PARP1 and c-FLIP$_L$ proteins generate fragments exclusively bearing Gly/N-degrons. Regarding the six remaining proteins (BAX, BID, BAD, procaspase-7, procaspase-6 and procaspase-8), they were analyzed separately as they generate fragments bearing Ac/ Arg/ or Gly/N-degrons (43%). The cleavage of BAX or BID results in one fragment bearing a Arg/N-degron and another with a Gly/N-degron. On the other hand, BAD cleavage generates one Ac/N-degron and one Gly/N-

degron. The cleavage of procaspase-7 creates 4 fragments exhibiting Ac/N-degrons and 2 fragments bearing Arg/N-degrons; the cleavage of procaspase-6 creates 2 Ac/N-degron substrates and 1 fragment exhibiting Arg/N-degron; and the cleavage of procaspase-8 generates 2 fragments bearing Ac/N-degrons and 1 Arg/N-degron substrate. Importantly, all protein fragments generated by cleavage of pro-apoptotic proteins retain their pro-apoptotic function, except for APAF1, whose fragment resulting from caspase cleavage exhibits an anti-apoptotic function.

Regarding the anti-apoptotic proteins (Figure 4.4, Table 4.2), 6/9 generate 10 fragments resulting from caspase- or calpain-mediated proteolytic cleavage. Although, we noticed that 4/6 (BCL-2, BCL-XL, MCL-1 and XIAP) generate fragments that undergo Nt-acetylation mediated by NatA, only 2 (BCL-2 and XIAP) generate fragments that can be exclusively degraded via Ac/N-degron pathway. 1 (BFL-1) out of 6 generates a fragment exclusively degraded by Arg/N-degron pathway, and another one (MCL-1) generates two fragments exclusively bearing Gly/N-degrons. The fragment resulting from cleavage of c-IAP1 does not bear destabilizing Nt-residues. Similar to procaspase-7, procaspase-6 and procaspase-8, 2 fragments generated by BCL-XL cleavage display destabilizing Nt-residues capable of being degraded via the Ac/N-degron pathway, and 1 is targeted for degradation via Arg/N-degron pathway. In contrast to the fragments generated from proteolytic cleavage of pro-apoptotic proteins, those generated from proteolytic cleavage of anti-apoptotic proteins lose the function of the original protein, with exception of XIAP.

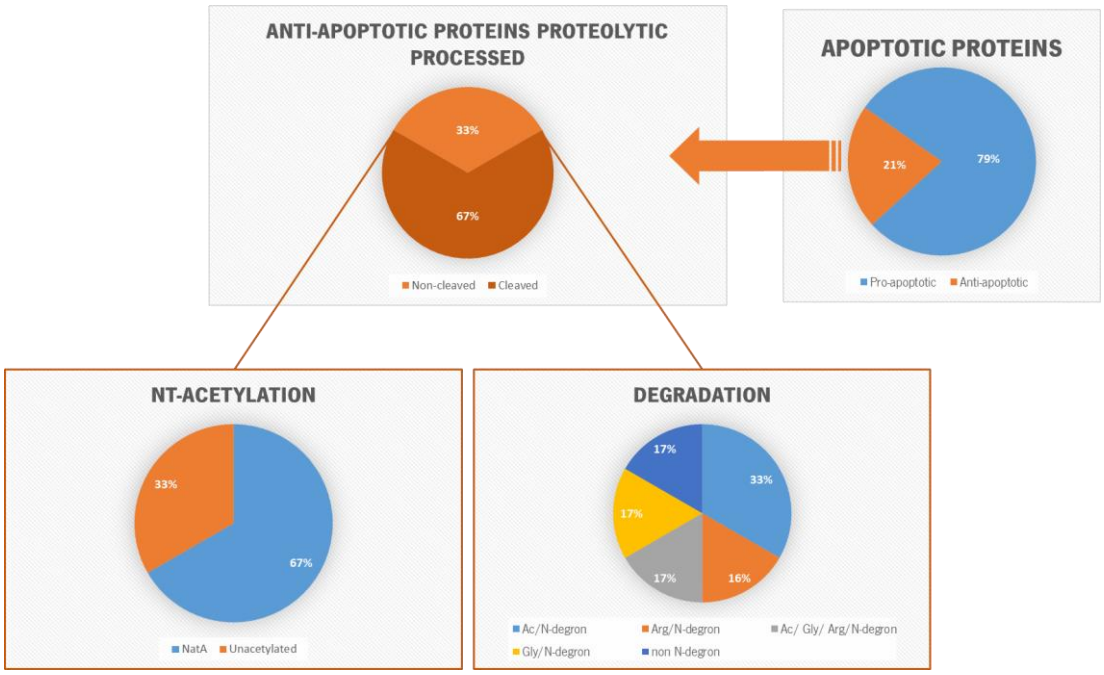

Figure 4.4: NatA acetylates most of the fragments generated by caspase- or calpain-mediated proteolytic cleavage of anti-apoptotic proteins and all N-degron pathways are involved in their degradation. Pie charts exhibiting the percentages of the anti-apoptotic proteins undergoing proteolytic cleavage as well as the percentages of those

undergoing Nt-acetylation and degradation mediated by the N-degron pathways. The NATs responsible for the Nt-acetylation as well as the N-degron pathways responsible for the degradation are identified.

In sum, the cleavage of 20 proteins out of 42 apoptotic proteins, may generate mostly pro-apoptotic fragments (18/20), regardless of the role of the originating protein (Table 4.2). This is consistent with the notion that apoptosis is amplified following caspases and calpain activation. But intriguingly, in contrast to the full-length proteins, 17 out of 18 generate pro-apoptotic fragments bearing destabilizing Nt-residues are recognized by only one of the three N-degron pathways, and can thus be degraded, compromising its pro-apoptotic role. In particular, the pro-apoptotic protein fragments of BID, BIM and BCL-XL were already experimentally confirmed as N-degron substrates [10]. Thus, it can be predicted that reduction of the N-recognins activity will impact not only the level of pro-apoptotic/anti-apoptotic proteins, thus perturbing the apoptosis execution phase (Table 4.1 and 4.2), through changes in the degradation of the pro- and anti-apoptotic fragments generated by caspase and calpain-mediated cleavage of the full-length proteins.

Interestingly, when we compare Table 4.1 and 4.2, we conclude that the cleavage of the apoptotic proteins mediated by caspases or calpains originates a slightly higher percentage of less stable proteins than the original ones. In fact, while around 90% (38/42) full-length apoptotic proteins bear N-degrons (Table 4.1), about 95% (19/20) proteins originate fragments exhibiting destabilizing Nt-residues (Table 4.2). This suggests that the activity of N-recognins must be reduced at some point during the apoptotic process, in order to diminish the degradation of the full-length proteins and fragments (generated by caspase and calpain cleavage) to allow the execution phases of apoptosis.

Table 4.2: The proteolytic cleavage of apoptotic proteins generates fragments prone to Nt-acetylation by NatA and degradation by only one of the three N-degron pathways. The table contains the analysis of the protein fragments generated by caspase- or calpain-mediated cleavage regarding its potential to be Nt-acetylated or degraded by Ac/ or Arg/ or Gly/N-degron pathways. The cleavage site, the NAT involved in Nt-acetylation and the N-degron pathways responsible for the fragment degradation, are identified, as well as the effect on protein level caused by Nt-acetylation and N-degron pathways downregulation. * G residues are considered stable according to the information reported in Fig. 1F from [3].

	Apoptotic protein	Apoptotic fragment generated	Cleaved by	Apoptotic activity	Function	Cleavage site	NAT	Ac/N-degron	Arg/N-degron	Gly/N-degron	Effect on protein level caused by Nt-acetylation downregulation	Effect on protein level caused by N-degron pathways downregulation	Ref
pro-apoptotic proteins	**BAX**	p18 Bax	calpain	pro-apoptotic	accelerates the apoptotic process	D[33]R	-	-	yes	no	-	increase	[11,12]
		$tBax_{29}$	calpain	pro-apoptotic	accelerates the apoptotic process; resistant to Bcl-xL-mediated protection	Q[28]G	NatA	no*	no	yes	**no effect**	increase	[13]
	BAK	BH4 Cl	calpain	pro-apoptotic	ensure robust pore formation and cell death	R[42]H	-	-	yes	no	-	increase	[14]
		BH3 Cl	calpain	pro-apoptotic		R[87]R	-	-	yes	no	-	increase	
	BOK	-	-	-	-	-	-	-	-		-	-	-
	PUMA	-	-	-	-	-	-	-	-		-	-	-
	BIM	$tBim_{EL}$	active caspase-3	pro-apoptotic	more efficient binding to Bcl-2	D[13]R	-	-	yes	no	-	increase	[15]
	NOXA	-	-	-	-	-	-	-	-	-	-	-	-
	BID	t-Bid	active caspase-3/-8	pro-apoptotic	mitochondrial damage, cyt c release, cell shrinkage and nuclear condensation	D[60]G	NatA	no*	no	yes	**no effect**	increase	[16–18]
			calpain	pro-apoptotic		G[70]R	-	-	yes	no	-	increase	
	BAD	$t\text{-}Bad_{14}$	active caspase-3	pro-apoptotic	enhancement of the pro-apoptotic activity	D[14]A	NatA	yes	no	no	increase	increase	[19,20]
		$t\text{-}Bad_{29}$	active caspase-3	pro-apoptotic		D[29]G	NatA	no*	no	yes	**no effect**	increase	

Table 4.2: The proteolytic cleavage of apoptotic proteins generates fragments prone to Nt-acetylation by NatA and degradation by only one of the three N-degron pathways (cont).

	Apoptotic protein	Apoptotic fragment generated	Cleaved by	Apoptotic activity	Function	Cleavage site	NAT	Ac/N-degron	Arg/N-degron	Gly/N-degron	Effect on protein level caused by Nt-acetylation downregulation	Effect on protein level caused by N-degron pathways downregulation	Ref
pro-apoptotic proteins	**BMF1**	-	-	-	-	-	-	-	-	-	-	-	-
	HRK	-	-	-	-	-	-	-	-	-	-	-	-
	CYCS	-	-	-	-	-	-	-	-	-	-	-	-
	SMAC/DIABLO	-	-	-	-	-	-	-	-	-	-	-	-
	OPA1	-	-	-	-	-	-	-	-	-	-	-	-
	OMA1	-	-	-	-	-	-	-	-	-	-	-	-
	DRP1	-	-	-	-	-	-	-	-	-	-	-	-
	APAF1	p30 Apaf-1	active caspase-3	anti-apoptotic	inability to activate effector caspases	$D^{271}S$	NatA	yes	no	no	**increase**	**increase**	[21]
	PROCASPASE-9	-	procaspase -9	pro-apoptotic	activates protease activity	$E^{306}S$	NatA	yes	no	no	**increase**	**increase**	[22]
		p35/p12 cleaved caspase-9	procaspase -9	pro-apoptotic	activates protease activity	$D^{315}A$	NatA	yes	no	no			
		p37/p10 cleaved caspase-9	active caspase-3	pro-apoptotic	activates protease activity	$D^{330}A$	NatA	yes	no	no			
	PROCASPASE-3	-	procaspase -3	pro-apoptotic	activates protease activity	$D^{9}S$	NatA	yes	no	no	**increase**	**increase**	[23–26]
		p17 and p12 subunits	procaspase -3	pro-apoptotic	activates protease activity	$D^{28}S$	NatA	yes	no	no			
			active caspase-8/9/10	pro-apoptotic	activates protease activity	$D^{175}S$	NatA	yes	no	no			

Table 4.2: The proteolytic cleavage of apoptotic proteins generates fragments prone to Nt-acetylation by NatA and degradation by only one of the three N-degron pathways (cont).

	Apoptotic protein	Apoptotic fragment generated	Cleaved by	Apoptotic activity	Function	Cleavage site	NAT	Ac/N-degron	Arg/N-degron	Gly/N-degron	Effect on protein level caused by Nt-acetylation downregulation	Effect on protein level caused by N-degron pathways downregulation	Ref
pro-apoptotic proteins	**PROCASPASE-7**	p20/p12 cleaved caspase-7	active caspase-3/-9	pro-apoptotic	activates protease activity	D[23]A	NatA	yes	no	no	**increase**	**increase**	[27–29]
		p18,5/p12 cleaved caspase-7	calpain	pro-apoptotic	activates protease activity	F[36]S	NatA	yes	no	no			
		p17/p12 cleaved caspase-7	calpain	pro-apoptotic	activates protease activity	M[45]R	-	-	yes	no	-		
		p17/p12 cleaved caspase-7	calpain	pro-apoptotic	activates protease activity	S[47]I	-	-	yes	no	-		
		ΔN caspase-7	active caspase-3/8/9/10	pro-apoptotic	activates protease activity	D[198]S	NatA	yes	no	no	**Increase**		
		NC caspase-7	active caspase-3/8/9/10	pro-apoptotic	activates protease activity	D[206]A	NatA	yes	no	no			
	PROCASPASE-6	Pro/p20 + p10 subunit	procaspase -6; active caspase-3	pro-apoptotic	activates protease activity	D[179]N	-	-	yes	no	-	**increase**	[30,31]
						D[193]A	NatA	yes	no	no	**increase**		
		Pro + p20/p10 subunits	procaspase -6; active caspase-3	pro-apoptotic		D[23]A	NatA	yes	no	no			
	PARP1	-	active caspase-3/7	pro-apoptotic	induction of apoptosis	D[214]G	NatA	no*	no	yes	**no effect**	**increase**	[32]

Table 4.2: The proteolytic cleavage of apoptotic proteins generates fragments prone to Nt-acetylation by NatA and degradation by only one of the three N-degron pathways (cont).

	Apoptotic protein	Apoptotic fragment generated	Cleaved by	Apoptotic activity	Function	Cleavage site	NAT	Ac/N-degron	Arg/N-degron	Gly/N-degron	Effect on protein level caused by Nt-acetylation downregulation	Effect on protein level caused by N-degron pathways downregulation	Ref
pro-apoptotic proteins	**PROCASPASE-10**	p17/p12 cleaved caspase-10	procaspase -10	pro-apoptotic	activates protease activity	$D^{415}A$	NatA	yes	no	no	**increase**	**increase**	[33,34]
	PROCASPASE-8	p43/41 + p12 subunits	procaspase -8	pro-apoptotic	activates protease activity	$D^{374}S$	NatA	yes	no	no	**increase**	**increase**	[35]
		Pro + p18/p10 subunits	procaspase -8; active caspase-9	pro-apoptotic	activates protease activity	$D^{216}S$	NatA	yes	no	no	**increase**		
						$D^{384}L$	-	-	yes	no	-		
	FAS	-	-	-	-	-	-	-	-		-	-	-
	FASL	-	-	-	-	-	-	-	-		-	-	-
	TNFR1	-	-	-	-	-	-	-	-		-	-	-
	TNF-α	-	-	-	-	-	-	-	-		-	-	-
	TRAIL	-	-	-	-	-	-	-	-		-	-	-
	TRAILR1	-	-	-	-	-	-	-	-		-	-	-
	TRAILR2	-	-	-	-	-	-	-	-		-	-	-
	TRADD	-	-	-	-	-	-	-	-		-	-	-
	FADD	-	-	-	-	-	-	-	-		-	-	-
	c-FLIP$_L$	p43c-FLIP	active caspase-8	pro-apoptotic	enhance caspase-8 activity	$D^{376}G$	NatA	no*	no	yes	**no effect**	**increase**	[36]
anti-apoptotic proteins	**BCL-2**	ΔN34 BCL-2 ΔN31 BCL-2	active caspase-3 active caspase-8	pro-apoptotic	release of cyt *c*	$D^{34}V$ $D^{31}A$	NatA	yes	no	no	**increase**	**increase**	[37] [38]
	BCL-W	-	-	-	-	-	-	-	-	-	-	-	-

Table 4.2: The proteolytic cleavage of apoptotic proteins generates fragments prone to Nt-acetylation by NatA and degradation by only one of the three N-degron pathways (cont).

	Apoptotic protein	Apoptotic fragment generated	Cleaved by	Apoptotic activity	Function	Cleavage site	NAT	Ac/N-degron	Arg/N-degron	Gly/N-degron	Effect on protein level caused by Nt-acetylation downregulation	Effect on protein level caused by N-degron pathways downregulation	Ref
anti-apoptotic proteins	**BCL-XL**	ΔN61 BCL-XL	active caspase-3	pro-apoptotic	loss of mitochondrial membrane potential; cyt *c* release	D[61]S	NatA	yes	no	no	increase	increase	[39–41]
		ΔN76 BCL-XL	active caspase-3	pro-apoptotic		D[76]A	NatA	yes	no	no	increase	increase	
		ΔN60 BCL-XL	calpain	pro-apoptotic		A[60]D	-	-	yes	no	-	increase	
	BFL-1	tBfl-1	calpain	pro-apoptotic	MOMP; cyt *c* release	F[71]N	-	-	yes	no	-	increase	[42,43]
	MCL-1	Mcl-1-C1	active caspase-3	pro-apoptotic	increased binding to Bim; physical interaction with t-Bid, Bak and Bax	D[127]G	NatA	no*	no	yes	**no effect**	increase	[44–46]
		Mcl-1-C2	active caspase-3	pro-apoptotic		D[157]G							
	XIAP	BIR1-2;BIR3-Ring	active caspase-3/7	anti-apoptotic	inhibition of caspase-3/7/9	D[242]A	NatA	yes	no	no	increase	increase	[47]
	c-IAP1	-	active caspase-3	pro-apoptotic	limited inhibition of active caspases; suppression of anti-apoptotic activity	D[372]P	-	-	no	no	-	-	[48]
	c-IAP2	-	-	-	-	-	-	-	-	-	-	-	
	c-FLIP$_s$	-	-	-	-	-	-	-	-	-	-	-	-

4.4. Conclusion

With this systematic search, we identified that many apoptotic proteins may bear conditional Ac/N-degrons. As aforementioned, if their protection warranted by proper folding/partner´s interaction is compromised or defective, they can be targeted for degradation via the Ac/N-degron pathway. This evidence supports the idea that, similarly to the Arg/ and Gly/N-degron pathways, the Ac/N-degron pathway may also play a role on apoptosis modulation. Importantly, it must be stressed that our analysis was based on Varshavsky *et al.,* [3], which considers that though almost all NAT substrates exhibit conditional degrons, they may become prone to degradation by the Ac/N-degron pathway, as well as on Nguyen and co-authors' paper [2] where the creation of destabilizing N-degrons of Arg/N-degron pathway after the NME of proteins is described. However, if we consider that NatA and NatB substrates are stable for degradation through the Ac/N-degron pathway, as reported by Kats and co-authors [49], different results would have been obtained.

Taking all this into account, the *in silico* systematic search performed herein offers novel insights into the high complexity of the interplay between the Nt-acetylation and degradation by N-degron pathways, and its impact on the modulation of apoptosis. How cells coordinate these two processes to restrain apoptosis to the levels required for cell homeostasis, and how these two are interconnected when a cell commits into apoptosis or resists to it, is still far from being understood. Experimental validation of our predictions may allow to understand how deregulation of Nt-acetylation and degradation by N-degron pathways may contribute to disease through their impact on apoptosis regulation.

References

1. Kim JM, Seok OH, Ju S, Heo JE, Yeom J, Kim DS, et al. Formyl-methionine as an N-degron of a eukaryotic N-end rule pathway. Science. 2018;362: 1–19. doi:10.1126/science.aat0174
2. Nguyen KT, Kim JM, Park SE, Hwang CS. N-terminal methionine excision of proteins creates tertiary destabilizing N-degrons of the Arg/N-end rule pathway. J Biol Chem. 2019;294: 4464–4476. doi:10.1074/jbc.RA118.006913
3. Varshavsky A. N-degron and C-degron pathways of protein degradation. Proc Natl Acad Sci U S A. 2019;116: 358–366. doi:10.1073/pnas.1816596116
4. Ametzazurra A, Larrea E, Civeira MP, Prieto J, Aldabe R. Implication of human *N*-α-acetyltransferase 5 in cellular proliferation and carcinogenesis. Oncogene. 2008;27: 7296–7306. doi:10.1038/onc.2008.332
5. Ametzazurra A, Larrea E, Civeira MP, Prieto J, Aldabe R. Implication of human N-alpha-acetyltransferase 5 in cellular proliferation and carcinogenesis. Oncogene. 2008;27: 7296–7306. doi:10.1038/onc.2008.332
6. Alves S, Neiri L, Chaves SR, Vieira S, Trindade D, Manon S, et al. N-terminal acetylation modulates

Bax targeting to mitochondria. Int J Biochem Cell Biol. 2018;95: 35–42. doi:10.1016/j.biocel.2017.12.004

7. Starheim KK, Gromyko D, Evjenth R, Ryningen A, Varhaug JE, Lillehaug JR, et al. Knockdown of Human Nα-Terminal Acetyltransferase Complex C Leads to p53-Dependent Apoptosis and Aberrant Human Arl8b Localization. Mol Cell Biol. 2009;29: 3569–3581. doi:10.1128/mcb.01909-08

8. Varland S, Myklebust LM, Goksøyr SØ, Glomnes N, Torsvik J, Varhaug JE, et al. Identification of an alternatively spliced nuclear isoform of human N-terminal acetyltransferase Naa30. Gene. 2018;644: 27–37. doi:10.1016/j.gene.2017.12.019

9. Agarwalla P, Banerjee R. N-end rule pathway inhibition assists colon tumor regression via necroptosis. Mol Ther - Oncolytics. 2016;3: 16020. doi:10.1038/mto.2016.20

10. Piatkov KI, Brower CS, Varshavsky A. The N-end rule pathway counteracts cell death by destroying proapoptotic protein fragments. Proc Natl Acad Sci U S A. 2012;109: E1839–E1847. doi:10.1073/pnas.1207786109

11. Cao X, Deng X, May WS. Cleavage of Bax to p18 Bax accelerates stress-induced apoptosis, and a cathepsin-like protease may rapidly degrade p18 Bax. Blood. 2003;102: 2605–2614. doi:10.1182/blood-2003-01-0211

12. Wood DE, Thomas A, Devi LA, Berman Y, Beavis RC, Reed JC, et al. Bax cleavage is mediated by calpain during drug-induced apoptosis. Oncogene. 1998;17: 1069–1078. doi:10.1038/sj.onc.1202034

13. Toyota H, Yanase N, Yoshimoto T, Moriyama M, Sudo T, Mizuguchi J. Calpain-induced Bax-cleavage product is a more potent inducer of apoptotic cell death than wild-type Bax. Cancer Lett. 2003;189: 221–230. doi:10.1016/S0304-3835(02)00552-9

14. Llambi F, Moldoveanu T, Tait SWG, Bouchier-Hayes L, Temirov J, McCormick LL, et al. A Unified Model of Mammalian BCL-2 Protein Family Interactions at the Mitochondria. Mol Cell. 2011;44: 517–531. doi:10.1016/j.molcel.2011.10.001

15. Chen D, Zhou Q. Caspase cleavage of BimEL triggers a positive feedback amplification of apoptotic signaling. Proc Natl Acad Sci U S A. 2004;101: 1235–1240. doi:10.1073/pnas.0308050100

16. Slee EA, Keogh SA, Martin SJ. Cleavage of BID during cytotoxic drug and UV radiation-induced apoptosis occurs downstream of the point of Bcl-2 action and is catalysed by caspase-3: A potential feedback loop for amplification of apoptosis-associated mitochondrial cytochrome c release. Cell Death Differ. 2000;7: 556–565. doi:10.1038/sj.cdd.4400689

17. Mandic A, Viktorsson K, Strandberg L, Heiden T, Hansson J, Linder S, et al. Calpain-Mediated Bid Cleavage and Calpain-Independent Bak Modulation: Two Separate Pathways in Cisplatin-Induced Apoptosis. Mol Cell Biol. 2002;22: 3003–3013. doi:10.1128/mcb.22.9.3003-3013.2002

18. Li H, Zhu H, Xu CJ, Yuan J. Cleavage of BID by caspase 8 mediates the mitochondrial damage in the Fas pathway of apoptosis. Cell. 1998;94: 491–501. doi:10.1016/s0092-8674(00)81590-1

19. So YS, Chen YB, Ivamovska I, Ranger AM, Hong SJ, Dawson VL, et al. BAD is a pro-survival factor prior to activation of its pro-apoptotic function. J Biol Chem. 2004;279: 42240–42249. doi:10.1074/jbc.M406775200

20. Condorelli F, Salomoni P, Cotteret S, Cesi V, Srinivasula SM, Alnemri ES, et al. Caspase Cleavage Enhances the Apoptosis-Inducing Effects of BAD. Mol Cell Biol. 2001;21: 3025–3036.

doi:10.1128/MCB.21.9.3025–3036.2001

21. Bratton SB, Walker G, Roberts DL, Cain K, Cohen GM. Caspase-3 cleaves Apaf-1 into an ~30 kDa fragment that associates with an inappropriately oligomerized and biologically inactive ~1.4 MDa apoptosome complex. Cell Death Differ. 2001;8: 425–433. doi:10.1038/sj.cdd.4400834

22. Würstle ML, Laussmann MA, Rehm M. The central role of initiator caspase-9 in apoptosis signal transduction and the regulation of its activation and activity on the apoptosome. Exp Cell Res. 2012;318: 1213–1220. doi:10.1016/j.yexcr.2012.02.013

23. Han Z, Hendrickson EA, Bremner TA, Wyche JH. A sequential two-step mechanism for the production of the mature p17:p12 form of caspase-3 *in vitro*. J Biol Chem. 1997;272: 13432–13436. doi:10.1074/jbc.272.20.13432

24. Li P, Nijhawan D, Budihardjo I, Srinivasula SM, Ahmad M, Alnemri ES, et al. Cytochrome c and dATP-dependent formation of Apaf-1/caspase-9 complex initiates an apoptotic protease cascade. Cell. 1997;91: 479–489. doi:10.1016/S0092-8674(00)80434-1

25. Ponder KG, Boise LH. The prodomain of caspase-3 regulates its own removal and caspase activation. Cell Death Discov. 2019;5: 56(1–10). doi:10.1038/s41420-019-0142-1

26. Stennicke HR, Jürgensmeier JM, Shin H, Deveraux Q, Wolf BB, Yang X, et al. Pro-caspase-3 is a major physiologic target of caspase-8. J Biol Chem. 1998;273: 27084–27090. doi:10.1074/jbc.273.42.27084

27. Srinivasula SM, Ahmad M, Fernandes-Alnemri T, Alnemri ES. Autoactivation of procaspase-9 by Apaf-1-mediated oligomerization. Mol Cell. 1998;1: 949–957. doi:10.1016/S1097-2765(00)80095-7

28. Gafni J, Cong X, Chen SF, Gibson BW, Ellerby LM. Calpain-1 cleaves and activates caspase-7. J Biol Chem. 2009;284: 25441–25449. doi:10.1074/jbc.M109.038174

29. Denault JB, Salvesen GS. Human Caspase-7 Activity and Regulation by Its N-terminal Peptide. J Biol Chem. 2003;278: 34042–34050. doi:10.1074/jbc.M305110200

30. Inoue S, Browne G, Melino G, Cohen GM. Ordering of caspases in cells undergoing apoptosis by the intrinsic pathway. Cell Death Differ. 2009;16: 1053–1061. doi:10.1038/cdd.2009.29

31. Klaiman G, Champagne N, LeBlanc AC. Self-activation of Caspase-6 *in vitro* and *in vivo*: Caspase-6 activation does not induce cell death in HEK293T cells. Biochim Biophys Acta. 2009;1793: 592–601. doi:10.1016/j.bbamcr.2008.12.004

32. Boulares AH, Yakovlev AG, Ivanova V, Stoica BA, Wang G, Iyer S, et al. Role of poly(ADP-ribose) polymerase (PARP) cleavage in apoptosis. J Biol Chem. 1999;274: 22932–22940. doi:10.1074/jbc.274.33.22932

33. Shin MS, Kim HS, Kang CS, Park WS, Kim SY, Lee SN, et al. Inactivating mutations of *CASP10* gene in non-Hodgkin lymphomas. Blood. 2002;99: 4094–4099. doi:10.1182/blood.V99.11.4094

34. Zhu S, Hsu AP, Vacek MM, Zheng L, Schäffer AA, Dale JK, et al. Genetic alterations in caspase-10 may be causative or protective in autoimmune lymphoproliferative syndrome. Hum Genet. 2006;119: 284–294. doi:10.1007/s00439-006-0138-9

35. Hoffmann JC, Pappa A, Krammer PH, Lavrik IN. A New C-Terminal Cleavage Product of Procaspase-8, p30, Defines an Alternative Pathway of Procaspase-8 Activation. Mol Cell Biol. 2009;29: 4431–4440. doi:10.1128/mcb.02261-07

36. Koenig A, Buskiewicz IA, Fortner KA, Russell JQ, Asaoka T, He YW, et al. The c-FLIPL cleavage product p43FLIP promotes activation of Extracellular Signal-regulated Kinase (ERK), nuclear factor κ b (NF-κ B), and caspase-8 and T cell survival. J Biol Chem. 2014;289: 1183–1191. doi:10.1074/jbc.M113.506428

37. Cheng EH-Y, Kirsch DG, Clem RJ, Ravi R, Kastan MB, Bedi A, et al. Conversion of Bcl-2 to a Bax-like Death Effector by Caspases. Science. 1997;278: 1966–1968. doi:10.1126/science.278.5345.1966

38. Zhu J, Yang Y, Wu J. Bcl-2 cleavages at two adjacent sites by different caspases promote cisplatin-induced apoptosis. Cell Res. 2007;17: 441–448. doi:10.1038/cr.2007.36

39. Basañez G, Zhang J, Chau BN, Maksaev GI, Frolov VA, Brandt TA, et al. Pro-apoptotic Cleavage Products of Bcl-xL Form Cytochrome *c*-conducting Pores in Pure Lipid Membranes. J Biol Chem. 2001;276: 31083–31091. doi:10.1074/jbc.M103879200

40. Fujita N, Nagahashi A, Nagashima K, Rokudai S, Tsuruo T. Acceleration of apoptotic cell death after the cleavage of Bcl-XL protein by caspase-3-like proteases. Oncogene. 1998;17: 1295–1304. doi:10.1038/sj.onc.1202065

41. Nakagawa T, Yuan J. Cross-talk between two cysteine protease families: Activation of caspase-12 by calpain in apoptosis. J Cell Biol. 2000;150: 887–894. doi:10.1083/jcb.150.4.887

42. Kucharczak JF, Simmons MJ, Duckett CS, Gélinas C. Constitutive proteasome-mediated turnover of Bfl-1/A1 and its processing in response to TNF receptor activation in FL5.12 pro-B cells convert it into prodeath factor. Cell Death Differ. 2005;12: 1225–1239. doi:10.1038/sj.cdd.4401684

43. Valero JG, Cornut-Thibaut A, Jugé R, Debaud AL, Giménez D, Gillet G, et al. μ-calpain conversion of antiapoptotic Bfl-1 (BCL2A1) into a prodeath factor reveals two distinct alpha-helices inducing mitochondria-mediated apoptosis. PLoS One. 2012;7: e28620(1-12). doi:10.1371/journal.pone.0038620

44. Ménoret E, Gomez-Bougie P, Surget S, Trichet V, Oliver L, Pellat-Deceunynck C, et al. Mcl-1128-350 fragment induces apoptosis through direct interaction with Bax. FEBS Lett. 2010;584: 487–492. doi:10.1016/j.febslet.2009.11.094

45. Weng C, Li Y, Xu D, Shi Y, Tang H. Specific cleavage of Mcl-1 by caspase-3 in tumor necrosis factor-related apoptosis-inducing ligand (TRAIL)-induced apoptosis in Jurkat leukemia T cells. J Biol Chem. 2005;280: 10491–10500. doi:10.1074/jbc.M412819200

46. Herrant M, Jacquel A, Marchetti S, Belhacène N, Colosetti P, Luciano F, et al. Cleavage of Mcl-1 by caspases impaired its ability to counteract Bim-induced apoptosis. Oncogene. 2004;23: 7863–7873. doi:10.1038/sj.onc.1208069

47. Deveraux QL, Leo E, Stennicke HR, Welsh K, Salvesen GS, Reed JC. Cleavage of human inhibitor of apoptosis protein XIAP results in fragments with distinct specificities for caspases. EMBO J. 1999;18: 5242–5251. doi:10.1093/emboj/18.19.5242

48. Clem RJ, Sheu TT, Richter BWM, He WW, Thornberry NA, Duckett CS, et al. c-IAP1 Is Cleaved by Caspases to Produce a Proapoptotic C-terminal Fragment. J Biol Chem. 2001;276: 7602–7608. doi:10.1074/jbc.M010259200

49. Kats I, Khmelinskii A, Kschonsak M, Huber F, Knieß RA, Bartosik A, et al. Mapping Degradation Signals and Pathways in a Eukaryotic N-terminome. Mol Cell. 2018;70: 488–501. doi:10.1016/j.molcel.2018.03.033

CHAPTER 5

ACETIC ACID TRIGGERS CYTOCHROME *C* RELEASE IN YEAST HETEROLOGOUSLY EXPRESSING HUMAN BAX

This chapter is adapted from the following publication:

Joana P. Guedes*, Vitória Baptista*, Cátia Santos-Pereira, Maria João Sousa, Stéphen Manon, Susana R. Chaves, Manuela Côrte-Real (2022) **Acetic acid triggers cytochrome *c* release in yeast heterologously expressing human Bax**. *Apoptosis.* doi: 10.1007/s10495-022-01717-0

*Both authors contributed equally

5.1. Background

Proteins of the Bcl-2 protein family, including pro-apoptotic Bax and anti-apoptotic Bcl-xL, are critical for the regulation of mitochondrial-mediated apoptosis [1,2]. Due to their biological relevance and potential as therapeutic targets, these proteins have thus been studied extensively. Briefly, Bax is a critical player in apoptosis progression, since it is involved in the formation of mitochondrial pores, causing MOMP [3–5]. However, when in its inactive form, Bax is largely cytosolic or weakly bound to mitochondria. As Bax plays a key role in the decision of cell fate, its regulation must be a well-coordinated process. Indeed, it is known that Bax can be regulated by interactions with other proteins, namely by Bcl-2 family members or by post-translational modifications (see Chapter 2, section 2.3 for detailed information).

Since yeasts lacks obvious orthologs of Bcl-2 family members [6–10], their heterologous expression in *S. cerevisiae* has been providing new insights into their structure, function, regulation and interactions, without interference from the remaining apoptotic network. In particular, yeast has already contributed to the elucidation of several aspects concerning Bax regulation and mechanism of action, and to the identification of key residues for its function [11]. However, many questions remain to be answered, and thus further understanding of Bax regulation is vital towards its exploitation as a therapeutic target. So far, studies taking advantage of heterologous expression of human Bax in yeast to unveil regulation of Bax activation have relied on the use of artificial mutated or mitochondrial tagged Bax for its activation, rather than the WT Bax (Bax α, which is naturally inactive). Thus, in the present study, we aimed to exploit yeast heterologously expressing human Bax α to further study its regulation under conditions closely resembling the natural Bax function in the cellular context. Previous studies from our lab have determined 16 h after addition of galactose 1% as the optimal conditions for the expression of Bax α in yeast. Under these conditions, human Bax α decreases the specific growth rate of yeast cells, but neither affected cell viability nor metabolic activity, assessed by colony forming units (CFUs) counts and by staining with FUN-1 (Figure 5.1).

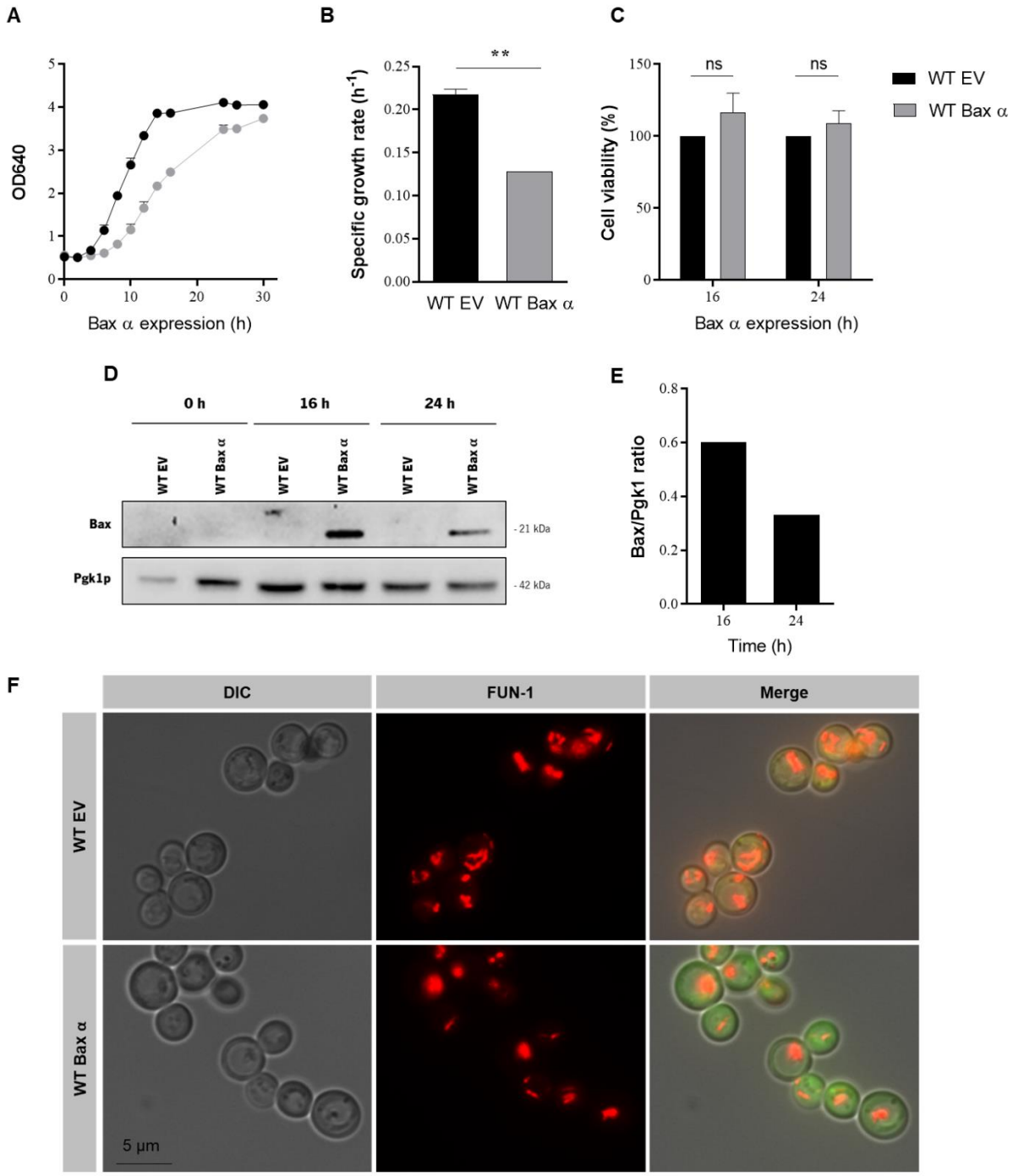

Figure 5.1: Expression of human Bax α in yeast decreases cell growth rate without compromising cell viability. (A) Growth curves of WT control cells (empty vector - EV) and WT Bax α. **(B)** Specific growth rate (h-1) of both strains calculated using the formula μ = ln Xt–ln $Xt0$ / t–$t0$ and using OD640 values corresponding to exponential phase. Values represent the mean ± SEM of three independent experiments and significant differences were analysed by an unpaired Student's t-test, where **p≤0.01. **(C)** Percentage of cell viability evaluated by CFUs normalized to OD640. Cell viability of Bax α-expressing cells is normalized to time zero of expression induction (T0) and to EV. Values represent the mean ± SEM of three independent experiments. ns – non-significant. **(D)** Immunodetection of Bax in control (WT EV) and Bax α-expressing cells (WT Bax α) along 24 h of expression. Pgk1p was used as the loading control. **(E)** Quantification of the levels of Bax

expression in control cells (WT EV) and Bax α-expressing cells (WT Bax α) in relation to Pgk1p. (F) Fluorescence microscopy images of cells 16 h after Bax or EV expression and stained with 4 μM FUN-1 for 30 min at 30 °C, in the dark. The photomicrographs shown are representative of several microscope fields. Bar, 5 μm [12,13].

As Bax α did not induced cell death of *S. cerevisiae* expressing this pro-apoptotic protein, it recapitulated what happens in mammalian cells under non-apoptotic inducing conditions. Nonetheless, as in mammalian cells, we found that Bax α induces loss of yeast cell survival in response to an exogenous trigger [12–14]. Indeed, sub-lethal concentrations of acetic acid triggered loss of viability of yeast cells expressing human Bax α without compromising plasma membrane integrity (Figure 5.2).

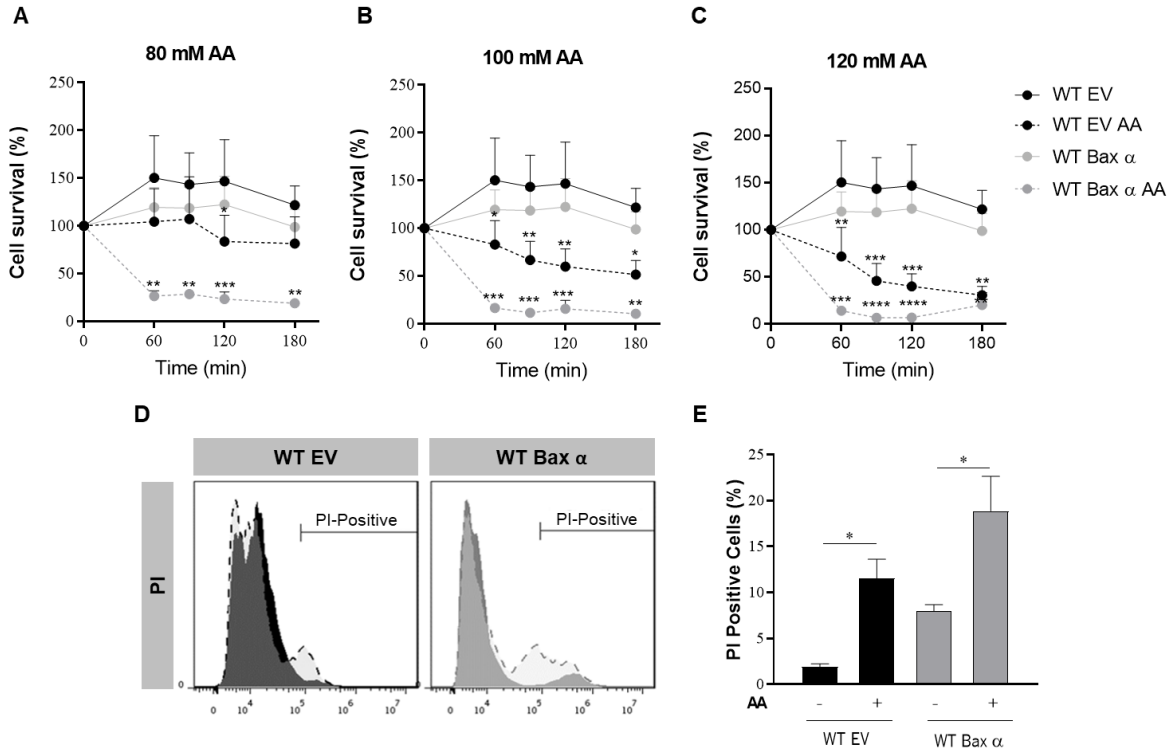

Figure 5.2: Sub-lethal concentrations of acetic acid trigger loss of viability of yeast cells expressing human Bax α without compromising plasma membrane integrity. The percentage of cell survival of yeast cells expressing human Bax α was analysed along 180 min of treatment with **(A)** 80 mM, **(B)** 100 mM or **(C)** 120 mM of acetic acid (AA), at pH 3.0. For each concentration, non-treated control cells (WT EV) were also subjected to the same growth conditions. Cell survival of Bax α-expressing cells was normalized to T0 and the values are the mean of three independent experiments analysed by two-way ANOVA, where *p<0.05, **p<0.01, ***p<0.001, ****p<0.0001. **(D)** Representative monoparametric histograms of the red fluorescence of PI-stained cells 60 min after treatment with acetic acid. Full line histograms correspond to non-treated cells (0 mM AA) and punctuate line histograms correspond to cells treated with 80 mM acetic acid. (E) Percentage of cells exhibiting loss of plasma membrane integrity determined by PI staining of the indicated yeast strains treated or not with 80 mM acetic acid, pH 3.0, for 60 min. The values display the mean of three independent experiments analysed by one-way ANOVA, where *p<0.05 [12,13].

In the present study, we then sought to search whether cell death induced by exposing Bax α-expressing cells to sub-lethal concentrations of acetic acid was associated with altered Bax localization and cyt *c* release. Additionally, in order to validate this experimental setup as tool to screen for Bax regulators yet unidentified, we assessed whether co-expression of Bcl-2 family members, namely of Bcl-xL or of its truncated form Bcl-xLΔC, could revert the acetic acid-induced death of cells expressing human Bax α. In this line, the dependence of acetic acid-induced cell death of yeast cells expressing Bax α on Rim11p, the yeast ortholog of the human GSK3β and a well-established Bax regulator, was also assessed.

5.2. Materials and Methods

5.2.1. Yeast strains and plasmids

All *S. cerevisiae* strains used in this study are listed in Table 5.1. The yeast *S. cerevisiae* haploid strain W303-1A (*mat a*; *ade2-1*; *his3-11*,*15*; *leu2-3*,*112*; *trp1-1*; *ura3-1*), provided by Stéphen Manon [15] was used throughout this study as the WT strain. The W303-1A *rim11*Δ (W303-1A *rim11*Δ::KanMX4) strain was constructed by homologous recombination of the WT strain with a disruption cassette amplified by PCR from genomic DNA of the respective Euroscarf mutant strain. Correct integration was confirmed by colony PCR. All strains were transformed with pYES3/CT Empty Vector (EV) (Invitrogen) and pYES3/CT plasmid expressing human WT Bax α, under the control of a GAL1/10 promoter [16]. For some experiments, these strains were also transformed with pYES2/CT EV (Invitrogen), pYES2/CT plasmid expressing human Bcl-xL and pYES2/CT plasmid expressing human Bcl-xLΔC, under the control of a GAL1/10 promoter [17]. All transformations were performed by the lithium acetate method [18] and the resulting transformants were grown in selective media lacking the appropriate amino acids.

Table 5.1: List of *S. cerevisiae* strains used in this study.

Strain	Genotype
W303-1A (WT)	*mat a*; *ade2-1*; *his3-11,15*; *leu2-3,112*; *trp1-1*; *ura3-1*
WT EV	W303-1A harbouring pYES3 EV
WT Bax α	W303-1A harbouring pYES3 Bax α
WT EV + EV	W303-1A harbouring pYES3 EV and pYES2 EV
WT EV + Bcl-xL	W303-1A harbouring pYES3 EV and pYES2 Bcl-xL
WT EV + Bcl-xLΔC	W303-1A harbouring pYES3 EV and pYES2 Bcl-xLΔC
WT Bax α + EV	W303-1A harbouring pYES3 Bax α and pYES2 EV
WT Bax α + Bcl-xL	W303-1A harbouring pYES3 Bax α and pYES2 Bcl-xL
WT Bax α + Bcl-xLΔC	W303-1A harbouring pYES3 Bax α and pYES2 Bcl-xLΔC
*rim11*Δ	W303-1A r*im11*Δ::*KanMX4*
*rim11*Δ EV	W303-1A *rim11*Δ harbouring pYES3 EV
*rim11*Δ Bax α	W303-1A *nat3*Δ harbouring pYES3 Bax α

5.2.2. Growth conditions and acetic acid treatment

Cells were grown overnight aerobically in synthetic complete medium [SC; 0.175% (w/v) Yeast nitrogen base without amino acids and ammonium sulphate, 0.5% ammonium sulphate, 0.1% potassium phosphate, 0.2% (w/v) Drop-out mixture, and 0.01% auxotrophic requirements; pH 5.5] supplemented with 2% (w/v) glucose starting at an OD640 = 0.05. Cells were then diluted in SC medium lacking the appropriate amino acids and supplemented with 2% lactate (v/v) as a carbon source at pH 5.5, to provide a full differentiation of mitochondria, at an OD640 = 0.2. After approximately 24 h, the cultures were diluted to OD640 = 0.5 in fresh SC lactate medium. Afterwards, 1% galactose (w/v) was added to trigger the expression of Bax, and the cultures were grown for 16 h. Regarding acetic acid treatment, upon 16 h of Bax expression, cells were harvested to an OD640 = 0.5 in SC medium supplemented with 2% lactate (v/v) and 1% galactose (w/v) at pH 3.0. Cells were then treated with 50, 80, 100 or 120 mM of acetic acid, followed by 180 min of incubation. Cells without acetic acid treatment were used as a negative control. All incubations were performed at 30 °C in an orbital shaker at 200 rpm, with a ratio of flask volume/medium of 5:1.

5.2.3. Viability assays

Cells were grown in SC medium as described above and samples were taken at the indicated times. Yeast cell viability was then evaluated by CFUs counts of five drops of 40 μL of the 10^{-4} dilution

plated on YPD (1% of yeast extract, 2% of peptone and 2% of glucose) after 2-3 days incubation at 30 °C. The number of colonies counted was corrected for changes in OD640, and viability was calculated as the percentage of colonies at the indicated times normalized to time 0 (T0), and in some assays normalized to the control cells.

5.2.4. Yeast cell fractionation

Yeast cells were grown and treated under the conditions described above. Cells were harvested, washed twice with dH_2O and resuspended in suspension buffer (1.2 M Sorbitol, 60 mM Sodium Phosphate and 1 mM EDTA). Cells were then digested with zymolyase 20 T (ImmunO, MP Biomedicals) and β-mercaptoethanol for 1 h at 32 °C. Afterwards, spheroplasts were washed twice with ice-cold 1.2 M Sorbitol and re-suspended in lysis buffer (0.5 M sorbitol, 20 mM Tris pH 7.5, 1 mM EDTA). The suspension was then transferred to an ice-cold hand-potter and carefully homogenized. Cell debris along with whole cells were pelleted by centrifuging two times at 1110 ×*g* and one time at 2770 ×*g*, for 10 min. Finally, the supernatant was recovered and centrifuged at 16602 ×*g* for 15 min in order to separate fractions. The resulting pellet corresponded to mitochondria and the supernatant held the cytosol. Subsequently, mitochondrial fractions were washed to be contaminant-free by multiple 15 min 16602 ×*g* centrifugations and, at the end, resuspended in lysis buffer and stored at -80 °C.

5.2.5. Co-immunoprecipitation assay

Yeast cell cultures were washed and then resuspended in resuspension buffer containing 10 mM Tris/Maleate pH 6.8, 0.2 M Mannitol, 0.1 M NaCl and 2 mM EGTA supplemented with antiproteases (Complete™, Roche). After, cells were broken mechanically by shaking with glass beads for 4 min at 25 Hz in a Mixer Mill (Retsch MM400). A 10 min 900 ×*g* centrifugation eliminated unbroken cells and nuclei. Supernatants were added with 1/9 volume of 10 × IP buffer (Sigma) supplemented with 0.1 M NaCl, and gently shaken at 4 °C during 30 min. After incubation with IP buffer, 2 μg of mouse monoclonal anti-Bax antibodies (2D2 or 6A7, Santa Cruz) were added and incubated overnight at 4 °C. Then, 50 μL Protein G-agarose beads (Sigma or GE Healthcare) were added for 4 h. Washing on IP column (Sigma) was performed with 4 × 500 μL of IP buffer 1 × and twice with 500 μL of IP buffer 0.1 ×. Agarose beads were added with 25 μL of Laemmli buffer (without 2-mercaptoethanol) and heated at 65 °C for 30 min. After centrifugation, samples were loaded on SDS-PAGE.

5.2.6. Preparation of total extracts, protein determination and western blot analysis

Preparation of total cell extracts was performed as previously described [19]. Briefly, 1 ml of exponentially growing cells at OD640=1 was harvested by centrifugation at 5000 ×*g* for 3 min and washed once with dH_2O. Cells were then resuspended in 500 µl water containing 50 µl lysis buffer 3.5% (v/v) β-mercaptoethanol in 2 M NaOH, and incubated for 15 min on ice. Next, 50 µl of 3 M trichloroacetic acid were added and incubated for 30 min to precipitate the proteins. The extracts were centrifuged at 12000 ×*g* 10 min 4 °C, washed with 100 µl acetone and centrifuged again at 12000 ×*g* 5 min, 4 °C. Finally, protein extracts were resuspended in 12.5 µl Laemmli buffer (2% (v/v) β-mercaptoethanol, 0.1 M Tris pH 8.8, 20% (v/v) glycerol, 0.02% (v/v) bromophenol blue) and 37.5 µl 1 M NaOH with 2% SDS). Samples were heated at 70 °C for 15 min and stored at −20 °C, or 15 µl were used immediately for Western blot. The protein concentration of the mitochondrial fraction was determined by the Lowry method [20], using a calibration curve obtained with increasing concentrations of BSA – 5 to 100 µg/µL. Depending on the experiments, the volume corresponding to 400 µg of protein was completed with dH_2O to a final volume of 100 µl. Protein precipitation and sample processing was carried out as for the total extracts. In the final step, mitochondrial protein extracts were resuspended in 3.75 µl of Laemmli buffer and 11.25 µl 1 M NaOH with 2% SDS. Samples were heated at 70 °C for 15 min and loaded in the gel. Samples were then separated electrophoretically on a 12.5% sodium dodecyl sulphate-polyacrylamide gel and transferred to Polyvinylidene Difluoride (PVDF, GE Healthcare) membranes at 60 mA per membrane for 1 h and 30 min. The membranes were blocked PBS with 0.1% Tween® 20 detergent (PBST) 0.1% containing 5% (w/v) non-fat milk. Then, membranes were incubated with primary antibodies mouse monoclonal anti-yeast phosphoglycerate kinase (Pgk1) antibody (1:5000, Molecular Probes), mouse monoclonal anti-yeast porin (Por1) antibody (1:10000, Invitrogen), rabbit cyt *c* antibody (1:2500, DavidsBio), mouse monoclonal anti-human Bax antibody (1:2500, Santa Cruz Biotechnology), and rabbit polyclonal anti-human Bcl-xL antibody (1:1000, Cell Signaling), followed by incubation with secondary antibodies against mouse and rabbit igG peroxidase (1:5000, Sigma-Aldrich). Immunodetection of bands was revealed by chemiluminescence using the ECL detection system (Millipore-Merck) in a ChemiDoc XRS image system with the Quantity One software (BioRad) or with X-ray films.

5.2.7. Statistical analysis

GraphPad Prism 6.0 (Graph-Pad Software, Inc., La Jolla, CA, USA) was used to perform statistical analysis. The analyses were made between groups and the corresponding used test is referred in figure

legends. The results are exhibited in form of mean ± S.E.M of at least three independent experiments, and significance was recognized for P≤0.05.

5.3. Results

5.3.1. Sub-lethal concentrations of acetic acid induce human Bax α mitochondrial translocation and cytochrome *c* release in yeast cells

In mammalian cells, in response to an apoptotic stimulus, Bax α changes from a globular cytosolic conformation to an extended membrane-embedded protein and then may oligomerize forming pores that lead to MOMP and, consequently, to cyt *c* release [17,21–23]. As we previously found that yeast cells expressing Bax α displayed increased sensitivity to acetic acid [14], we aimed to assess if this acid could affect Bax α cellular distribution and trigger cyt *c* release. For that purpose, mitochondrial fractions from control (WT EV) and Bax α-expressing untreated or acetic acid-treated cells were isolated, and the localization of Bax and cyt *c* was assessed. No differences in mitochondrial cyt *c* levels were observed for control cells, whether treated with acetic acid or not (Figure A3, Appendix). However, a pronounced decrease of cyt *c* in the mitochondrial fraction of acetic acid-treated cells expressing Bax α was found, indicating that it is released to the cytosol. This phenotype was associated with Bax translocation to the mitochondria (Figure 5.3A). However, Bax translocation and cyt *c* release were not associated with the standard Bax active conformation. Indeed, the average amount of Bax immunoprecipitated from control and acetic acid-treated Bax α-expressing cells with the anti-Bax antibody 6A7, which detects active Bax, was not significantly different and, in some experiments, was lower than that immunoprecipitated from untreated cells (Figure 5.3B, C). Taken together, these results suggest that the higher sensitivity of Bax α-expressing cells to acetic acid is a reflection of increased ability to release cyt *c*, resulting in cell death through the yeast endogenous mitochondrial pathway of apoptosis.

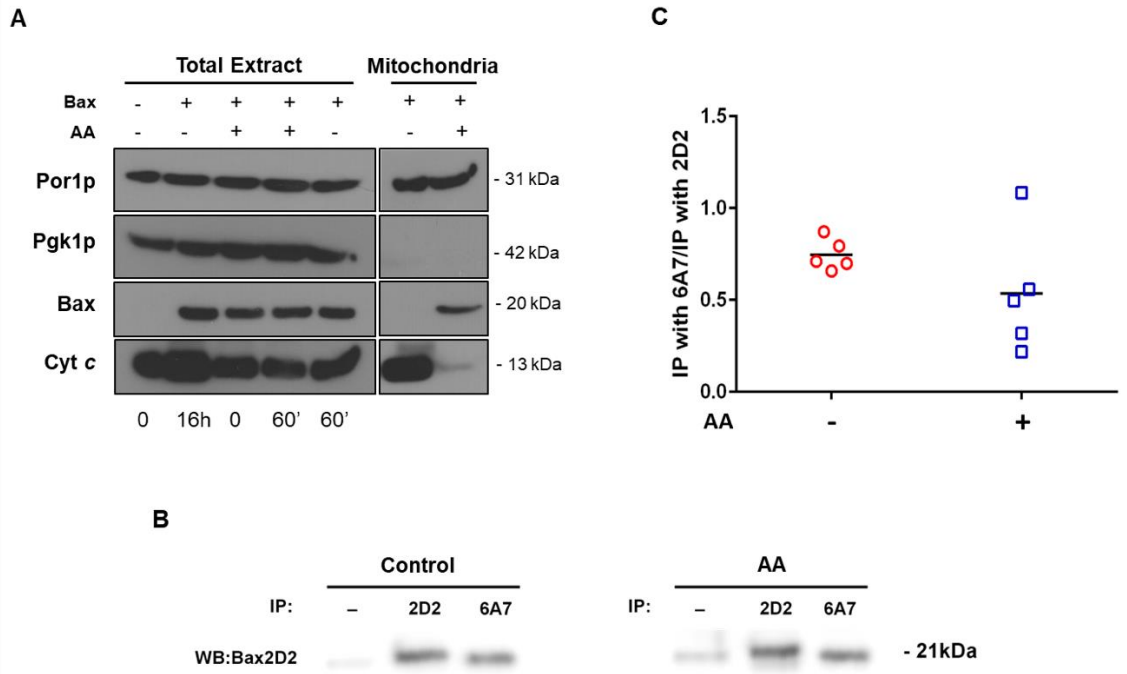

Figure 5.3: A sub-lethal concentration of acetic acid promotes human Bax mitochondrial translocation and cytochrome *c* release but not 6A7 active Bax detection in yeast cells expressing Bax α. (A) Representative immunodetection of Bax and cyt *c* in total extracts of yeast cells expressing Bax α 0 and 16 h after expression, and 0 and 60 min after incubation without (-) or with (+) acetic acid; and in mitochondrial fractions 60 min after incubation without (-) and with (+) 80 mM acetic acid, pH 3.0. Pgk1p and Por1p were used as loading controls for cytosol and mitochondrial fractions, respectively. **(B)** Bax was immunoprecipitated from cell extracts with 2D2 or 6A7 monoclonal antibodies in both untreated and acetic-treated cells expressing Bax α. Western blots were revealed with the monoclonal anti-Bax N20. **(C)** Bax activation status assessed by anti-Bax antibody 6A7 in untreated and acetic acid-treated cells expressing Bax α. Representative graphic of the ratio of the 6A7-immunoprecipitate signal over the one of 2D2-immunoprecipitate, in yeast cells expressing Bax α 16 h after expression and 60 min treatment without (-) and with (+) 80 mM acetic acid, pH 3.0. Quantification of band intensities was performed with Image J. For each sample, the ratio of the signal of 6A7-immunoprecipitate over the one of 2D2-immunoprecipitate was calculated. AA – acetic acid.

5.3.2. Bcl-xL rescues yeast cells expressing human Bax α from acetic acid-induced cell death

We next aimed to find if, in our experimental setup, well-known Bax partners from the Bcl-2 family could revert acetic acid-induced cell death of yeast cells expressing Bax α. It has been demonstrated that Bax interacts with Bcl-xL in both mammalian and yeast cells [17]. Bcl-xL counteracts Bax activation by forming inhibitory complexes in mitochondria, but the interaction with Bcl-xL also appears to regulate Bax localization, as co-expression with Bax favours Bax translocation to mitochondria as well as its retrotranslocation to the cytosol [17,24]. Preliminary results from our lab [12,13] have shown that acetic

acid-induced cell death of Bax α-expressing cells was abrogated by the co-expression of Bcl-xL but not by Bcl-xLΔC, under the control of a GAL1/10 promoter. Bcl-xLΔC does not contain the C-terminal transmembrane domain and is unable to promote Bax retrotranslocation [17]. As at that time we could not confirm the expression levels of Bax and of both forms of Bcl-xL, we prepared new transformants and confirmed by western blot that the expression levels of Bax and Bcl-xL were similar among the different strains (Figure 5.4A). Since cells were grown in lactate medium, glucose was not present to repress the protein expression, and thus, a basal expression of Bcl-xL was observed at 0 h of expression, though lower than at 16 h of expression as expected. After 16 h of Bax expression, no significant differences in cell viability were found (Figure 5.4B). On the other hand, after exposure to acetic acid, cell viability decreased in cells expressing Bax α alone (Figure 5.4C). However, co-expression of Bax α with full-length Bcl-xL significantly increased cell survival in comparison with the strain expressing Bax α alone, suggesting that Bcl-xL protects Bax expressing cells from cell death induced by acetic acid. In contrast, death of cells co-expressing Bcl-xLΔC and Bax α was not significantly different from that of the strain expressing only Bax α.

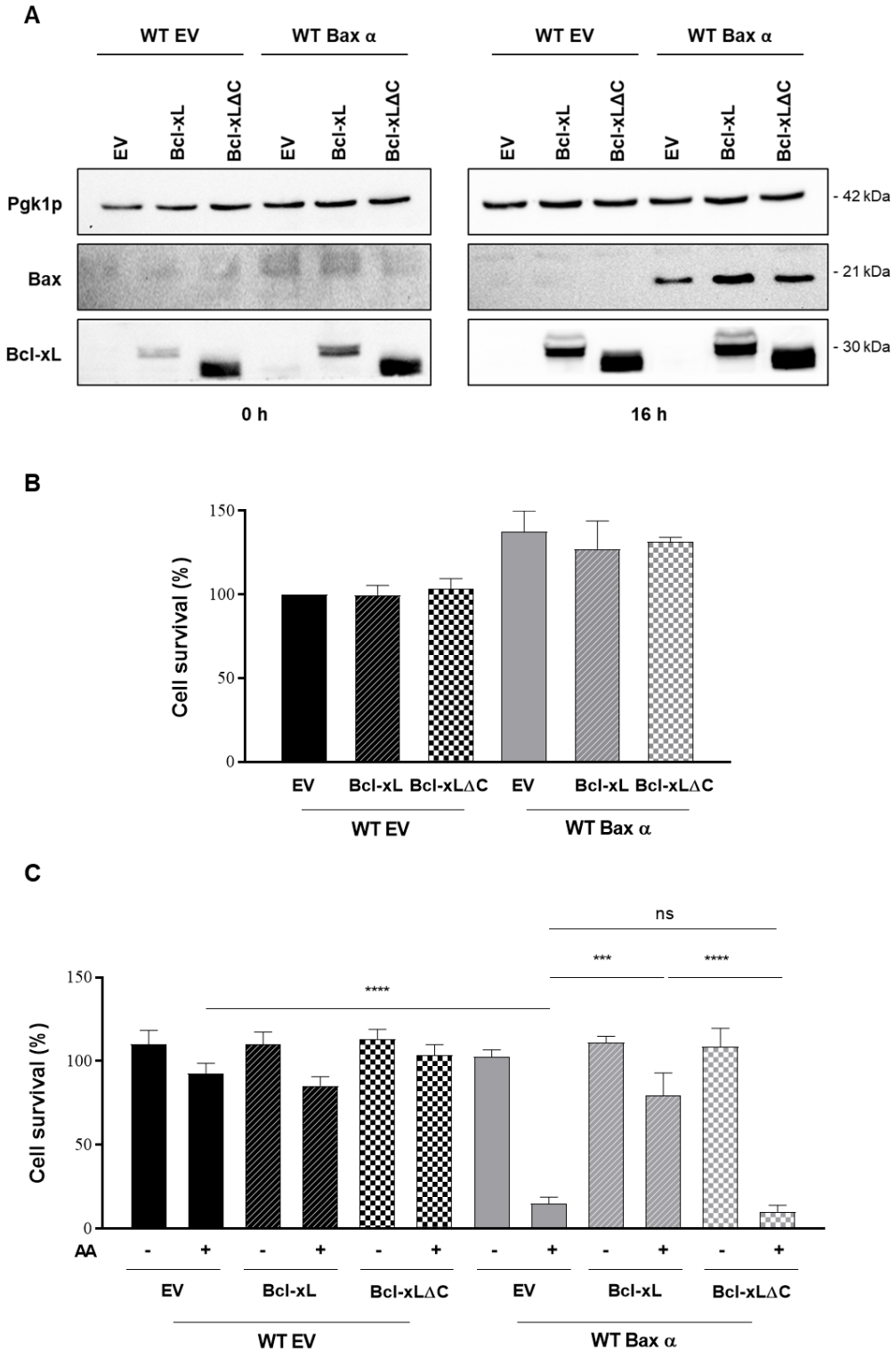

Figure 5.4: Expression of Bcl-xL, but not of its truncated form Bcl-xLΔC, protects human Bax α-expressing cells from acetic acid-induced death. (A) Representative western blot image of Bax and Bcl-xL protein expression in yeast cells not expressing (WT EV) and expressing Bax α (WT Bax α) at 0 h and 16 h. Pgk1p was used as loading control. **(B)** Cell viability assessed by CFU counting of yeast cells co-expressing Bax α and Bcl-xL or Bcl-xLΔC, 16 h after induction of expression. The values displayed are normalized to T0 of expression induction and to control cells (transformed with both EVs). **(C)** Cell

viability of yeast cells co-expressing Bax α and Bcl-xL or Bcl-xLΔC 16 h after Bax expression, and 60 min after incubation without (-) and with (+) 80 mM acetic acid, pH 3.0. Data are normalized to T0 of acetic acid treatment and are the mean of three independent experiments analysed by one-way ANOVA, where ***p<0.001, **** p<0.0001 and ns – non-significant. AA – acetic acid.

5.3.3. The yeast orthologue of GSK3β is required for acetic acid-induced cell death in yeast cells expressing human Bax α

Linseman and co-authors found that Bax phosphorylation at residue S163 by GSK3β is required for apoptosis induction [25]. In fact, inhibition of GSK3β in mammalian cells suppresses Bax activity and its associated translocation to the mitochondria. We have also previously found [12,13] that the absence of Rim11p, the yeast orthologue of GSK3β, does not affect Bax α viability in yeast cells (Figure 5.5A). Herein, after confirming that Bax expression levels were similar in *rim11*Δ and WT strains (Figure 5.5B) we next assessed whether Rim11p, the yeast orthologue of the human GSK3β, could also regulate acetic acid-induced cell death of yeast cells expressing Bax α. Although deletion of *RIM11* did not affect the viability of Bax α-expressing cells (Figure 5.5B), it reverted the loss of cell viability of acetic acid-treated Bax α-expressing cells (Figure 5.5C). These results raise the hypothesis that Rim11p is also required for acetic acid-induced cell death in yeast cells expressing Bax α.

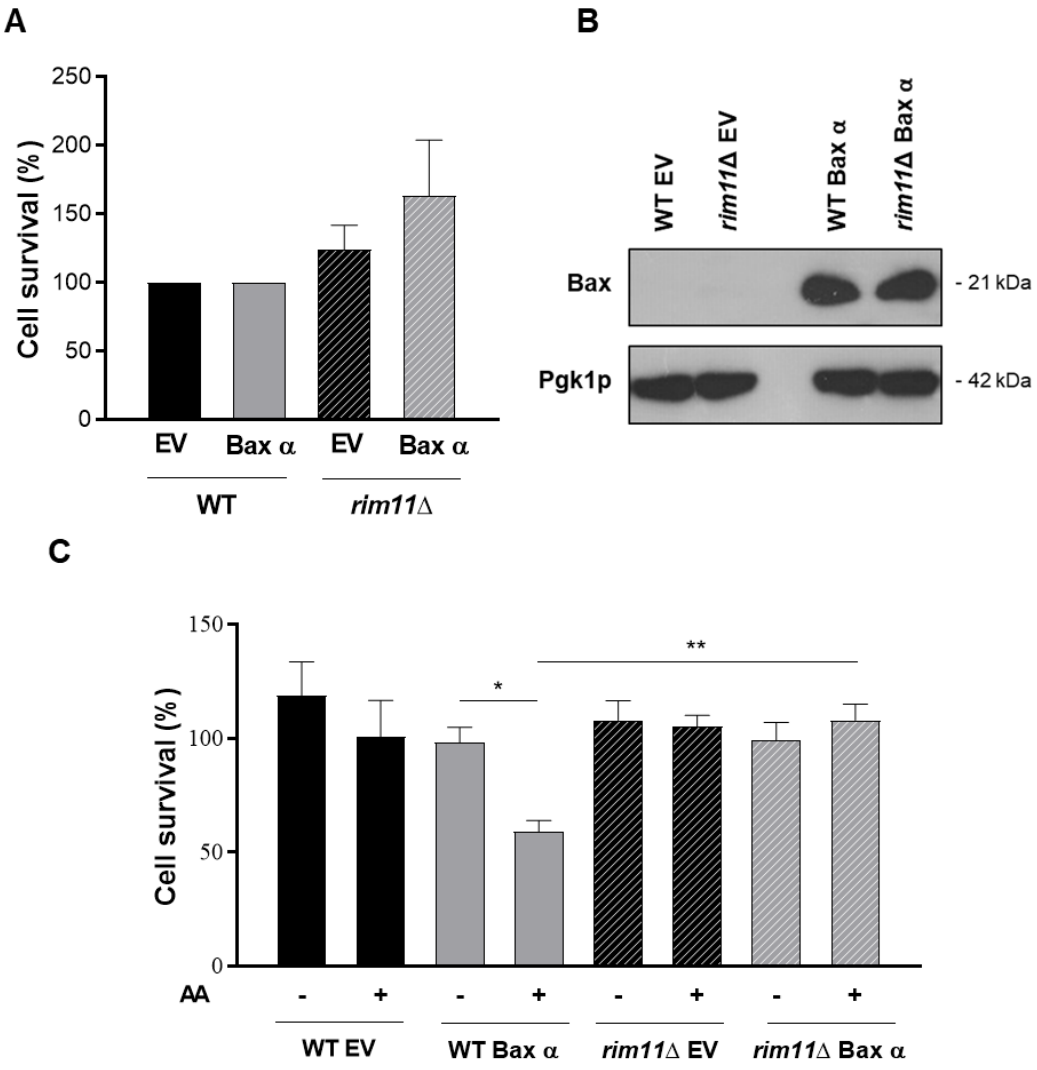

Figure 5.5: Absence of the yeast ortholog of GSK3β rescues human Bax α-expressing yeast cells from acetic acid-induced cell death. (A) Assessment of cell survival by CFUs counting of *rim11*Δ cells after 16h Bax α expression and respective control cells (transformed with the EV), (results obtained by [12,13]). Cell survival of Bax α-expressing cells is normalized to T0 and to control cells and values are the mean of three independent experiments analysed by one-way ANOVA. **(B)** Representative western blot image of Bax expression levels after 16 h expression in both WT and *rim11*Δ strains. Pgk1p was used as loading control. **(C)** Cell viability of yeast cells expressing EV and Bax α, 16 h after Bax expression, and 60 min after incubation without (-) and with (+) 80 mM acetic acid, pH 3.0. Data are normalized to T0 of acetic acid treatment and are the mean of three independent experiments analysed by one-way ANOVA, where *p<0.05 and **p<0.01. AA – acetic acid.

5.4. Discussion

Given the important role of the pro-apoptotic protein Bax in cell death, its potential as a therapeutic target in diseases associated with misregulated cell death arose quickly. In fact, its mode of action and regulation have been extensively studied, but multiple aspects remain elusive, as the model systems used are complex. Here, we took advantage of the genetically tractable yeast *S. cerevisiae*, whose

genome lacks genes coding obvious homologues of the human Bcl-2 family, to study Bax independently of the intricate mammalian apoptotic network. In particular, this yeast has been used to unveil human Bax activation through the expression of artificial mutated or tagged active forms, as Bax α is inactive under the expression conditions usually employed [17,26,27]. We previously found that sub-lethal concentrations of acetic acid triggered loss of viability of yeast cells expressing human Bax α [14] without compromising plasma membrane integrity [12,13]. Taking this into account, herein, we sought to further characterize the response of Bax α-expressing cells to acetic acid treatment by addressing whether a sub-lethal concentration of acetic acid was associated with altered Bax localization and cyt *c* release. To achieve this goal, we heterologously expressed human native Bax α in *S. cerevisiae* under the control of a GAL1/10 promoter, an already well-characterized system [17,26,27]. As the highest Bax α expression level was achieved 16 h after induction with 1% galactose, these conditions were used in all assays. We observed that acetic acid reduces the levels of cyt *c* in mitochondria of Bax-expressing cells treated with acetic acid, in accordance with the significantly decrease in the viability of cells expressing Bax in response to acetic acid. However, unexpectedly, we found that acetic acid does not increase the amount of Bax in its standard active conformation, detected by anti-Bax 6A7. One hypothesis is that Bax shifts to an "active" conformation that is not detected by this antibody. A second explanation is that the increased cyt *c* release observed is not due to increased levels of active Bax but a result of increased levels of Bax at mitochondria. This increased accumulation of Bax, either inactive or in a not already characterized active conformation, leads to mitochondrial membrane permeabilization and subsequent cyt *c* release. A similar scenario has been described for the S184V and S184A mutations on the C-terminal domain of Bax; these mutations lead to an increased Bax mitochondrial localization and cyt *c* release, but not associated with increased Bax activation detected with anti-Bax 6A7 [27]. It is known that at a pH below its pKa (pKa=4.76), acetic acid is mainly present in its undissociated form (CH_3COOH), so it can enter the cell, where it dissociates into protons (H^+) and acetate (CH_3COO) and, depending on the pH gradient across the plasma membrane, it can lead to intracellular acidification and acetate accumulation, affecting metabolic activity [28,29]. Moreover, in previous works, short-chain fatty acids (SCFA), including acetic acid and propionic acid, have been explored in the therapy and prevention against some diseases, and have been shown to induce differentiation, growth arrest and apoptotic cell death in colorectal cancer cells [30–32]. Considering these previous works and our study, we can predict that formic and propionic acids could render the same Bax phenotype, but this remains to be tested further.

We further sought to explore if known inhibitors of Bax function revert death of yeast cells expressing Bax α induced by acetic acid. We first analyzed Bcl-xL, an anti-apoptotic protein known as one

of the main partners of Bax, playing a protective role in cell survival [24,33]. In the presence of lethal doses of acetic acid, expression of Bcl-xL in yeast cells increases cell survival, according to its pro-survival role [34]. In this work, we used sub-lethal concentrations, thus acetic acid does not lead to any detrimental effect in cell survival of control cells, contrary to what was detected for Bax α -expressing or co-expressing strains. Acetic acid-induced cell death of Bax α expressing cells was partly reverted by co-expressing Bcl-xL, but not Bcl-xLΔC. While full-length Bcl-xL was shown to modulate Bax translocation to mitochondria and its retrotranslocation to the cytosol [15,24,35], Bcl-xLΔC is able to modulate Bax localization, but owing to its inability to promote Bax retrotranslocation, it induces Bax mitochondrial localization to a higher extent than the unmodified protein. As a result, this truncated protein is therefore not able to impair the Bax cytotoxic effect like Bcl-xL does [17,36], which we also observed here.

Another mechanism described to suppress Bax activation and translocation to mitochondria in mammalian cells undergoing apoptosis is inhibition of GSK3β [25,37]. Indeed, this kinase targets Bax residue S163 and is needed for induction of apoptosis [25]. Thus, we sought to determine if the abrogation of Rim11p, the yeast orthologue of GSK3β, would impair acetic acid-induced cell death of Bax α-expressing cells. In fact, under conditions of Bax α translocation through the use of sub-lethal doses of acetic acid, the knockout of Rim11p expressing Bax α was able to restore cell viability, in agreement with Bax α inactivation. The absence of Bax α-dependent acetic acid cytotoxicity in such conditions is in agreement with the suppression of Bax activation and translocation to mitochondria by inhibition of GSK3β in mammalian cells undergoing apoptosis [25,37].

5.5. Conclusion

In this study, we developed a novel simple and time- and cost-effective tool to increase Bax-mediated cyt *c* release that relies on the use of sub-lethal doses of acetic acid. This was accompanied by Bax-mediated cell death, which was reverted by co-expression with Bcl-xL, but not with its truncated form, as well as by deletion of Rim11p. Therefore, we recapitulated in yeast the partial activation of Bax α by an exogenous stimulus and the interaction with its regulators, mimicking what occurs in apoptotic mammalian cells. The use of this model is an excellent alternative to the non-natural phosphomimetics or non-phosphorylatable mutants or of mitochondrial tagged versions of Bax. We believe this yeast-based tool will be valuable to screen for novel Bax regulators, to provide new clues about its function and to develop novel therapeutic strategies targeting Bax.

References

1. Rouchidane Eyitayo A, Gonin M, Arokium H, Manon S. Contribution of yeast studies to the understanding of BCL-2 family intracellular trafficking. Int J Mol Sci. 2021;22: 4086. doi:10.3390/ijms22084086
2. Lalier L, Vallette F, Manon S. Bcl-2 Family Members and the Mitochondrial Import Machineries: The Roads to Death. Biomolecules. 2022;12: 162(1–19). doi:10.3390/biom12020162
3. Adams JM, Cory S. The Bcl-2 protein family: Arbiters of cell survival. gScience (New York, NY). 1998;281: 1322–1326. doi:10.1126/science.281.5381.1322
4. Kale J, Osterlund EJ, Andrews DW. BCL-2 family proteins: Changing partners in the dance towards death. Cell Death Differ. 2018;25: 65–80. doi:10.1038/cdd.2017.186
5. Peña-Blanco A, García-Sáez AJ. Bax, Bak and beyond - mitochondrial performance in apoptosis. FEBS J. 2018;285: 416–431. doi:10.1111/febs.14186
6. Carmona-Gutierrez D, Eisenberg T, Büttner S, Meisinger C, Kroemer G, Madeo F. Apoptosis in yeast: Triggers, pathways, subroutines. Cell Death Differ. 2010;17: 763–773. doi:10.1038/cdd.2009.219
7. Polčic P, Jaká P, Mentel M. Yeast as a tool for studying proteins of the Bcl-2 family. Microb Cell. 2015;2: 74–87. doi:10.15698/mic2015.03.193
8. Priault M, Camougrand N, Kinnally KW, Vallette FM, Manon S. Yeast as a tool to study Bax/mitochondrial interactions in cell death. FEMS Yeast Res. 2003;4: 15–27. doi:10.1016/S1567-1356(03)00143-0
9. Pereira C, Silva RD, Saraiva L, Johansson B, Sousa MJ, Côrte-Real M. Mitochondria-dependent apoptosis in yeast. Biochim Biophys Acta - Mol Cell Res. 2008;1783: 1286–1302. doi:10.1016/j.bbamcr.2008.03.010
10. Carmona-Gutierrez D, Bauer MA, Zimmermann A, Aguilera A, Austriaco N, Ayscough K, et al. Guidelines and recommendations on yeast cell death nomenclature. Microb Cell. 2018;5: 4–31. doi:10.15698/mic2018.01.607
11. Renault TT, Manon S. Bax: Addressed to kill. Biochimie. 2011;93: 1379–1391. doi:10.1016/j.biochi.2011.05.013
12. Baptista V. Exploring yeast as a tool to study the regulation of the human pro-apoptotic protein Bax. 2018 (Master thesis).
13. Guedes JP, Baptista V, Santos-Pereira C, Sousa MJ, Manon S, Chaves SR, et al. Acetic acid triggers cytochrome *c* release in yeast heterologously expressing human Bax. Apoptosis. 2022;27: 368–381. doi:10.1007/s10495-022-01717-0
14. Pereira H, Oliveira CSF, Castro L, Preto A, Chaves SR, Côrte-Real M. Yeast as a tool to explore cathepsin D function. Microb Cell. 2015;2: 225–234. doi:10.15698/mic2015.07.212
15. Garenne D, Renault TT, Manon S. Bax mitochondrial relocation is linked to its phosphorylation and its interaction with Bcl-xL. Microb Cell. 2016;3: 597–605. doi:10.15698/mic2016.12.547
16. Arokium H, Ouerfelli H, Velours G, Camougrand N, Vallette FM, Manon S. Substitutions of potentially phosphorylatable serine residues of bax reveal how they may regulate its interaction with mitochondria. J Biol Chem. 2007;282: 35104–35112. doi:10.1074/jbc.M704891200
17. Renault TT, Teijido O, Missire F, Ganesan YT, Velours G, Arokium H, et al. Bcl-xL stimulates Bax

relocation to mitochondria and primes cells to ABT-737. Int J Biochem Cell Biol. 2015;64: 136–146. doi:10.1016/j.biocel.2015.03.020

18. Gietz RD, Akio S. New yeast-*Escherichia coli* shuttle vectors constructed with *in vitro* mutagenized yeast genes lacking six-base pair restriction sites. Gene. 1988;74: 527–534. doi:10.1016/0378-1119(88)90185-0

19. Camougrand N, Grelaud-Coq A, Marza E, Priault M, Bessoule JJ, Manon S. The product of the *UTH1* gene, required for Bax-induced cell death in yeast, is involved in the response to rapamycin. Mol Microbiol. 2003;47: 495–506. doi:10.1046/j.1365-2958.2003.03311.x

20. Lowry OH, Rosebrough NJ, Farr AL, Randall RJ. Protein measurement with the Folin phenol reagent. J Biol Chem. 1951;193: 265–275.

21. Schellenberg B, Wang P, Keeble JA, Rodriguez-enriquez R, Walker S, Owens TW, et al. Bax Exists in a Dynamic Equilibrium between the Cytosol and Mitochondria to Control Apoptotic Priming. Mol Cell. 2013;49: 959–971. doi:10.1016/j.molcel.2012.12.022

22. Westphal D, Kluck RM, Dewson G. Building blocks of the apoptotic pore: how Bax and Bak are activated and oligomerize during apoptosis. Cell Death Differ. 2014;21: 196–205. doi:10.1038/cdd.2013.139

23. Lalier L, Cartron PF, Juin P, Nedelkina S, Manon S, Bechinger B, et al. Bax activation and mitochondrial insertion during apoptosis. Apoptosis. 200712: 887–896. doi:10.1007/s10495-007-0749-1

24. Renault TT, Dejean LM, Manon S. A brewing understanding of the regulation of Bax function by Bcl-xL and Bcl-2. Mech Ageing Dev. 2017;161: 201–210. doi:10.1016/j.mad.2016.04.007

25. Linseman DA, Butts BD, Precht TA, Phelps RA, Le SS, Laessig TA, et al. Glycogen synthase kinase-3β phosphorylates bax and promotes its mitochondrial localization during neuronal apoptosis. J Neurosci. 2004;24: 9993–10002. doi:10.1523/JNEUROSCI.2057-04.2004

26. Alves S, Neiri L, Chaves SR, Vieira S, Trindade D, Manon S, et al. N-terminal acetylation modulates Bax targeting to mitochondria. Int J Biochem Cell Biol. 2018;95: 35–42. doi:10.1016/j.biocel.2017.12.004

27. Simonyan L, Renault TT, Da Costa Novais MJ, Sousa MJ, Côrte-Real M, Camougrand N, et al. Regulation of Bax/mitochondria interaction by AKT. FEBS Lett. 2016;590: 13–21. doi:10.1002/1873-3468.12030

28. Casal M, Cardoso H, Leão C. Mechanisms regulating the transport of acetic acid in *Saccharomyces cerevisiae*. Microbiology. 1996;142: 1385–1390. doi:10.1099/13500872-142-6-1385

29. Casey E, Sedlak M, Ho NWY, Mosier NS. Effect of acetic acid and pH on the cofermentation of glucose and xylose to ethanol by a genetically engineered strain of *Saccharomyces cerevisiae*. FEMS Yeast Res. 2010;10: 385–393. doi:10.1111/j.1567-1364.2010.00623.x

30. Lan A, Lagadic-Gossmann D, Lemaire C, Brenner C, Jan G. Acidic extracellular pH shifts colorectal cancer cell death from apoptosis to necrosis upon exposure to propionate and acetate, major end-products of the human probiotic propionibacteria. Apoptosis. 2007;12: 573–591. doi:10.1007/s10495-006-0010-3

31. Jan G, Belzacq AS, Haouzi D, Rouault A, Métivier D, Kroemer G, et al. Propionibacteria induce apoptosis of colorectal carcinoma cells via short-chain fatty acids acting on mitochondria. Cell

Death Differ. 2002;9: 179–188. doi:10.1038/sj.cdd.4400935

32. Marques C, Oliveira CSF, Alves S, Chaves SR, Coutinho OP, Côrte-Real M, et al. Acetate-induced apoptosis in colorectal carcinoma cells involves lysosomal membrane permeabilization and cathepsin D release. Cell Death Dis. 2013;4: e507–e507. doi:10.1038/cddis.2013.29

33. Manon S, Chaudhuri B, Guérin M. Release of cytochrome c and decrease of cytochrome c oxidase in Bax-expressing yeast cells, and prevention of these effects by coexpression of Bcl-xL. FEBS Lett. 1997;415: 29–32. doi:10.1016/S0014-5793(97)01087-9

34. Saraiva L, Silva RD, Pereira G, Gonçalves J, Côrte-Real M. Specific modulation of apoptosis and Bcl-xL phosphorylation in yeast by distinct mammalian protein kinase C isoforms. J Cell Sci. 2006;119: 3171–3181. doi:10.1242/jcs.03033

35. Edlich F, Banerjee S, Suzuki M, Cleland MM, Arnoult D, Wang C, et al. Bcl-xL retrotranslocates Bax from the mitochondria into the cytosol. Cell. 2011;145: 104–116. doi:10.1016/j.cell.2011.02.034

36. Todt F, Cakir Z, Reichenbach F, Youle RJ, Edlich F. The C-terminal helix of Bcl-xL mediates Bax retrotranslocation from the mitochondria. Cell Death Differ. 2013;20: 333–342. doi:10.1038/cdd.2012.131

37. Zhang L, Zhang Y, Xing DA. LPLI inhibits apoptosis upstream of bax translocation via a GSK-3β -inactivation mechanism. J Cell Physiol. 2010;224: 218–228. doi:10.1002/jcp.22123

CHAPTER 6

Role of NatB-mediated Bax Nt-acetylation on its interaction with Bcl-xL and in acetic acid-induced cell death

6.1. Background

The yeast model has been successfully used to study Nt-acetylation, namely in the identification of new Nt-acetylated proteins, by comparing the level of Nt-acetylation of a putative NAT substrate between a normal control strain and a yeast NAT (yNAT)-deleted mutant using proteomics methods, as already shown in Chapter 2 and by Alves and colleagues [1]. Besides the identification of new NAT substrates and the degree of Nt-acetylation, yeast NAT-deleted mutants have been a powerful tool for characterizing NAT phenotypes. Examples of this are the well-studied *ard1*(hNAA10)- and *nat3*(hNAA20)-deleted mutants. For a long time, several studies have shown that yeast *nat3*Δ cells display the most prominent phenotypes, including temperature sensitivity, increased sensitivity to osmotic agents and DNA damaging chemicals, defects on mating, cell polarity, morphology and cytoskeleton function, as well as in mitochondrial and vacuolar inheritance [2–6]. Some of the Nt-acetylated substrates that contribute to these phenotypic alterations have been identified. For instance, the incapacity of *nat3*Δ cells to form stable actin cables is due to the loss of Nt-acetylation of actin and tropomyosin. Indeed, Mdm20p, the regulatory subunit of yNatB and ortholog of hNAA25, was initially identified as an essential protein for tropomyosin-F-actin interaction and therefore stabilization of actin cables [3]. After, Mdm20p was associated with Nat3p for the proper acetylation of Tpm1p [4,6]. Later, it was unveiled that restoration of the actin filaments is not enough to rescue the *nat3*Δ phenotype, suggesting that additional Nat3 substrates are required for proper actin assembly [2–4,6]. The loss of actin Nt-acetylation in *nat3*Δ cells is also the reason for the abnormal budding and the decreased growth rate. Caeser and colleagues showed that although *nat3*Δ and *mdm20*Δ cells share some features, the proteins may have individual functions since depletion of Mdm20p does not have the same impact on cell growth and morphology as deletion of *NAT3*. Notably, *mdm20*Δ cells do not exhibit defects on cell growth and also differ from *nat3*Δ cells in stress tolerance [2]. Moreover, the increased temperature sensitivity of *nat3*Δ cells may be related to the heat shock protein Hsp104p, a NatB target associated with thermo tolerance and stress response [7,8], while the defects in mitochondrial inheritance could be due to loss of Ugo1p Nt-acetylation, a protein required for mitochondrial fusion [9,10]. A recent study by Friedrich and colleagues revealed that the lack of NatB activity causes a stronger impact on protein homeostasis than the lack of NatA activity, resulting in misfolding and aggregation of several proteins, and affecting expression of genes involved in stress responses, amino acid biosynthesis, and translation [11]. The authors further showed that the loss of NatB-mediated Nt-acetylation compromises the structural integrity of NatB substrates, resulting in increased protein aggregation. Besides these cellular processes, yeast cells have also been used to study the involvement of Nt-acetylation on cell cycle progression [9], protein sorting [12], protein stability and

degradation [13–18], and in apoptosis [1]. Indeed, as referred in previous chapters, our group recently identified the pro-apoptotic Bax protein as a new NatB substrate, taking advantage of the yeast cell model. For this purpose, the In-gel Stable-Isotope Labelling approach, that allows quantifying the degree of protein acetylation, was used to compare the Nt-acetylation levels of human Bax α in WT yeast cells and in a mutant strain lacking the NatB catalytic subunit hNAA20 (*nat3*Δ) cells. Bax was found to be fully Nt-acetylated in WT W303 but not in W303 *nat3*Δ cells, which indicates that ectopically expressed human Bax is Nt-acetylated by yeast Naa20p. This is in accordance with the Met-Asp amino-acid sequence at the Bax N-terminus. In addition, our group demonstrated that the Nt-acetylation of Bax is essential to maintain Bax in an inactive conformation in the cytosol of both yeast (*nat3*Δ) and Naa25$^{-/-}$ MEF cells. Since Bax is a therapeutic target in diseases with apoptotic dysfunctions, the use of the yeast as cellular model demonstrated for the first time that the Nt-acetylation of Bax by NatB is involved in Bax mitochondrial targeting, suggesting that by manipulating the Nt-acetylation of Bax it is possible to regulate its cellular localization, which may be an attractive therapeutic target.

In short, these and other studies using yeast as a cell model highlight how yeast cell-based systems have fostered advances in the identification of Nat substrates, as well as some of their roles in the regulation of key cellular processes, while unveiling the functional complexity and diversity of NATs, which has only begun to be discerned. As yeast and human NatB enzymatic activity is partially redundant [19], and taking into account the yeast genetic tractability and simple cultivation to perform different assays, in this chapter, we took advantage of the yeast cell model to further unravel the molecular mechanisms underlying the regulation of Bax by Nt-acetylation. Specifically, we aimed to determine the consequences of Nt-acetylation on the interaction of Bax with other members of the Bcl-2 family, as well as on the acetic acid-induced cell death of yeast cells heterologously expressing human Bax.

6.2. Material and methods

6.2.1. Yeast strains and plasmids

All *S. cerevisiae* strains used in this study are listed in Table 6.1. The yeast *S. cerevisiae* haploid strain W303-1B (*mat a*, *ade2*, *his3*, *leu2*, *trp1*, *ura3*), provided by Stéphen Manon, was used throughout this study as the WT strain. The W303 *nat3*Δ strain was generated in our previous study [1]. The W303 *mdm20*Δ strain was generated by transformation of parental strain W303–1B with a disruption cassette amplified by PCR from genomic DNA of the BY4741 *mdm20*Δ strain (Euroscarf). Correct integration of the cassette was confirmed by PCR. All strains were transformed with pYES3/CT E) (Invitrogen) and pYES3/CT plasmid expressing human WT Bax α, under the control of a GAL1/10 promoter [20]. For

some experiments, the strains were also transformed with pYES2/CT EV (Invitrogen) and pYES2/CT plasmid expressing human Bcl-xL, under the control of a GAL1/10 promoter [21]. All transformations were performed by the lithium acetate method [22] and the resulting transformants were grown in selective media lacking the appropriate amino acids.

Table 6.1: List of *S. cerevisiae* strains used in this study.

Strain	Genotype
W303-1B (WT)	*mat a*, *ade2*, *his3*, *leu2*, *trp1*, *ura3*
WT EV	W303-1B harbouring pYES3 EV
WT Bax α	W303-1B harbouring pYES3 Bax α
WT EV + EV	W303-1B harbouring pYES3 EV and pYES2 EV
WT EV + Bcl-xL	W303-1B harbouring pYES3 EV and pYES2 Bcl-xL
WT Bax α + EV	W303-1B harbouring pYES3 Bax α and pYES2 EV
WT Bax α + Bcl-xL	W303-1B harbouring pYES3 Bax α and pYES2 Bcl-xL
*nat3*Δ	W303-1B *nat3*Δ::KanMX4
*nat3*Δ EV	W303-1B *nat3*Δ harbouring pYES3 EV
*nat3*Δ Bax α	W303-1B *nat3*Δ harbouring pYES3 Bax α
*nat3*Δ EV + EV	W303-1B *nat3*Δ harbouring pYES3 EV + pYES2 EV
*nat3*Δ EV + Bcl-xL	W303-1B *nat3*Δ harbouring pYES3 EV + pYES2 Bcl-xL
*nat3*Δ Bax α + EV	W303-1B *nat3*Δ harbouring pYES3 Bax α + pYES2 EV
*nat3*Δ Bax α + Bcl-xL	W303-1B *nat3*Δ harbouring pYES3 Bax α + pYES2 Bcl-xL
*mdm20*Δ	W303-1B *mdm20*Δ::KanMX4
*mdm20*Δ EV	W303-1B *mdm20*Δ harbouring pYES3 EV
*mdm20*Δ Bax α	W303-1B *mdm20*Δ harbouring pYES3 Bax α

6.2.2. Growth conditions

S. cerevisiae strains were grown overnight aerobically in synthetic complete (SC) glucose medium [SC; 0.175% (w/v) Yeast nitrogen base without amino acids and ammonium sulphate, 0.5% ammonium sulphate, 0.2% (w/v) Drop-out mixture and 0.01% auxotrophic requirements] supplemented with 2% (w/v) glucose. The cultures were transferred to the SC medium lacking the appropriate amino acids and supplemented with 0.5% (w/v) of the non-fermentable carbon source lactate/ethanol instead of glucose, to an OD640=0.05 for WT cells and an OD640=0.1 for mutant cells. After approximately 26 h, the WT cells were diluted to an OD640=0.25 and mutant cells to an OD640=0.45 in fresh SC lactate/ethanol medium. 5 h later, cultures reached the OD640=0.5 and 2% of galactose (w/v) was added to trigger the

expression of Bax and, in some cases, of Bcl-xL, and the cultures were grown for 14 h. All culture incubations were performed at 30 °C in an orbital shaker at 200 rpm, with a ratio of flask volume/medium of 5:1.

6.2.3. Stability assay

Yeast cells were grown as described in previous section. After 14 h of Bax expression, cells were washed with dH_20 and resuspended in SC Glucose medium to repress the galactose promoter and then repress Bax expression. Cells were grown during 0, 4, 6, 8 and 24 h. At each time point, samples were collected to prepare 1 mL of cell suspensions at OD640=1 for protein extracts.

6.2.4. Acetic acid treatment

For acetic treatment, cells were grown as described in 6.2.2. After 14 h of induction of Bax expression, cells were harvested to an OD640= 0.5 in SC lactate/ethanol medium and supplemented with 2% galactose (w/v) at pH 3.0, so that added acetic acid (160 mM) could enter the cells in its undissociated form (CH_3COOH), by simple diffusion [23]. Samples were then harvested after 90 and 180 min of incubation. Cells without acetic acid treatment were used as a negative control. All incubations were performed at 30 °C in an orbital shaker at 200 rpm, with a ratio of flask volume/medium of 5:1.

6.2.5. Protein extraction and western blot analysis

To prepare protein extracts, 1 mL of exponentially growing cells at OD640=1 was collected by centrifugation at 5000 ×g for 3 min and washed once with dH_2O. Cells were then resuspended in 500 µl water and 50 µl lysis buffer [3.5% (v/v) β-mercaptoethanol in 2 M NaOH], and incubated for 15 min on ice. Next, 50 µl of 3 M trichloroacetic acid were added and incubated for 30 min on ice to precipitate the proteins. The extracts were centrifuged at 12000 ×g 10 min 4 °C, washed with 100 µl acetone and centrifuged again at 12000 ×g 5 min, 4 °C. Finally, protein extracts were resuspended in 12.5 µl Laemmli buffer (2% (v/v) β-mercaptoethanol, 0.1 M Tris pH 8.8, 20% (v/v) glycerol, 0.02% (v/v) bromophenol blue) and 37.5 µl 0.1 M NaOH with 2% SDS. Samples were heated at 70 °C for 15 min and stored at -20 °C, or 15 µl were used immediately for Western blot. Protein extracts were then separated electrophoretically on a 12.5% sodium dodecyl sulphate-polyacrylamide gel (SDS-PAGE) at 20 mA per gel, and transferred to PVDF (GE Healthcare) membranes at 60 mA per membrane for 1 h and 30 min. To prevent non-specific binding, the membranes were blocked in 5% (w/v) non-fat milk containing 0.1% PBST, for 1 h at RT with agitation. Afterwards, membranes were incubated overnight with agitation at 4

°C with primary antibodies listed in Table 6.2. After washing with 1× PBST during 15 min, membranes were incubated with the corresponding secondary antibodies (Table 6.2) for 1 h at RT with agitation. Finally, membranes were washed with 1× PBST during 15 min. Immunodetection of bands was revealed by chemiluminescence using the ECL detection system (Millipore-Merck) in a ChemiDoc XRS image system with the Quantity One software (BioRad) or with X-ray films.

Table 6.2: List of primary and secondary antibodies used in this study.

Antibody	Size (kDa)	Dilution	Temperature (°C)	Incubation time	Manufacturer
Monoclonal anti-yeast phosphoglycerate kinase **(Pgk1)** (mouse)	42	1:5000	4 °C	Overnight	Molecular Probes
Monoclonal anti-human **Bax** (mouse)	21	1:1000	4 °C	Overnight	Santa Cruz Biotechnology
Polyclonal anti-human **Bcl-xL** (rabbit)	30	1:1000	4 °C	Overnight	Cell Signalling
Secondary anti-**mouse** (Goat)	-	1:5000	RT	1 h	Jackson ImmunoResearch
Secondary anti-**rabbit** (Goat)	-	1:5000	RT	1 h	Jackson ImmunoResearch

6.2.6. Assessment of plasma membrane integrity by PI staining

Propidium Iodide (PI) was used to assess plasma membrane integrity. This fluorescent nucleic acid intercalating agent is not able to enter the cell unless its plasma membrane is compromised. WT and *nat3*Δ cells expressing Bax α and, in some cases, co-expressing Bcl-xL were grown and treated as described above. Depending on the analysis, by flow cytometry or fluorescence microscopy, PI staining was performed differently, as described below.

6.2.7. Flow cytometry analysis

Cells were harvested (1 mL at DO640=0.1) and resuspended in 500 µL of PBS 1× with 2 µL of PI (stock solution of 1 mg/mL, Sigma-Aldrich) and incubated for 10 min at RT in the dark. As *nat3*Δ cells form aggregates, after PI staining, cells were washed twice with 1× PBS, resuspended in 500 µL of 1× PBS and then sonicated for 1 min. After confirming the absence of aggregates, the samples were then analysed by flow cytometry. The detection of the fluorescence was achieved by collecting red fluorescence through a band-pass filter corresponding to the ECD channel. For each sample, about 10 000 events were collected and analysed using CytExpert program.

6.2.8. Fluorescence microscopy

Cells were harvested (1 mL at DO640=0.1) and resuspended in 500 μL of 1× PBS with 2 μL of PI (stock solution of 1 mg/mL, Sigma-Aldrich) and incubated for 10 min at RT in the dark. The fluorescence was detected by a Leica Microsystems DM-5000B epifluorescence microscope using the 100x oil-immersion objective with the appropriate filter settings for differential phase contrast (DIC) and red fluorescence (N21).

6.3. Results and discussion

6.3.1. Does Nt-acetylation affect the stability of the pro-apoptotic Bax protein in yeast *S. cerevisiae* cells?

In the previous chapters, we showed that Nt-acetylation displays an important role on the stability of apoptotic proteins. Some studies claim a protective role against protein degradation [3,18,24–26], while others point Nt-acetylated protein residues as degradation signals [13–15]. Herein, we aimed to evaluate the stability of the NatB substrate Bax in W303 *nat3*Δ and W303 *mdm20*Δ yeast cells expressing human Bax under the control of a GAL1/10 promoter [20]. To achieve this goal, we performed a stability assay in which Bax α expression was first induced by the addition of 2% galactose for 14 h, and then repressed by transfer to a medium with glucose up to 24 h. We found a decrease in Bax protein levels after 6h of galactose deprivation in the three strains, though more pronounced in *nat3*Δ and *mdm20*Δ cells (Figure 6.1A). Moreover, at 24 h, while Bax protein was observed in WT cells, no expression of Bax was observed in *nat3*Δ and *mdm20*Δ cells. These results suggest that the absence of Nat3p or Mdm20p in yeast cells affects the stability of Bax, supporting a role of Nt-acetylation in conferring stability to this protein. Accordingly, even under normal growth conditions (after 14 h of induction of Bax expression with galactose), the expression of Bax in *nat3*Δ cells was significantly lower when compared with WT cells (Figure 6.1B).

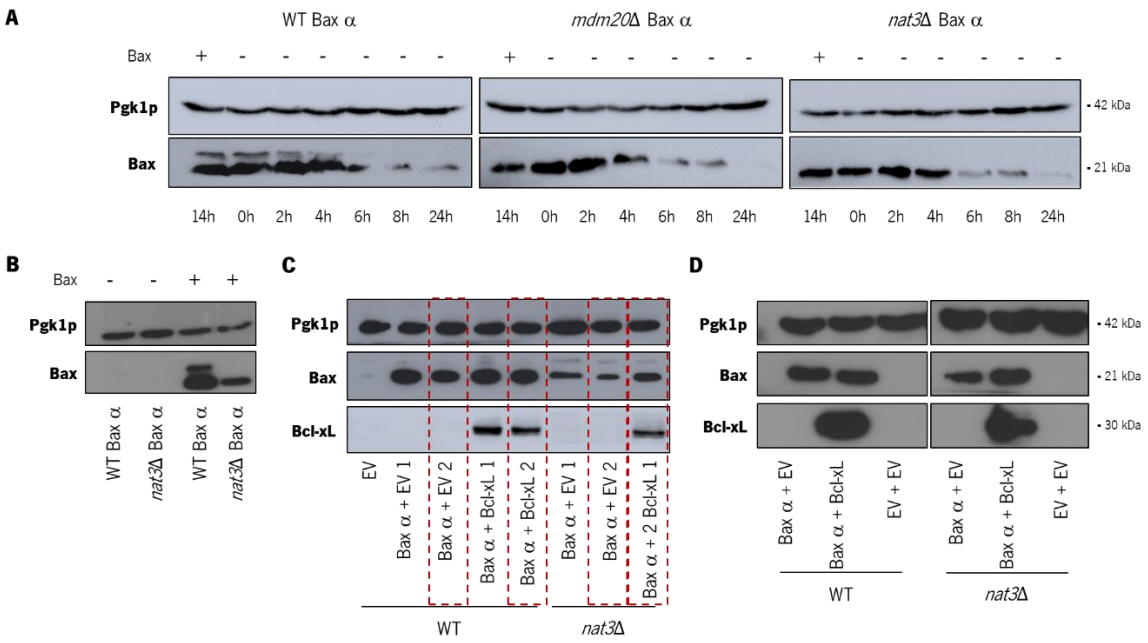

Figure 6.1: Absence of Nat3p and Mdm20p in yeast cells compromises the stability of Bax, which is partially recovered by Bcl-xL. Immunodetection of Bax **(A)** in WT, *nat3*Δ and *mdm20*Δ yeast cells expressing Bax α 14 h after expression, and 0, 2, 4, 6, 8 and 24 h after repression of Bax expression with glucose; **(B)** in WT and *nat3*Δ yeast cells expressing Bax α 0 and 14 h after induction of Bax expression with galactose; **(C)** in WT and *nat3*Δ yeast cells expressing Bax α and co-expressing Bcl-xL 14 h after induction of Bax expression with galactose. 1 and 2 represents the different transformants resulting from co-expression of Bax and Bcl-xL or the respective empty vector (EV); **(D)** in WT and *nat3*Δ yeast cells expressing Bax α and Bcl-xL or the respective EV (selected from C, red dashed squares) and expressing both EVs 14 h after induction of Bax expression with galactose. Pgk1p was used as loading control.

Interestingly, when we heterologously co-expressed Bax α and Bcl-xL in *nat3*Δ cells, also under the control of the GAL1/10 promoter [21], the expression levels of Bax increased in comparison with the mutant cells expressing Bax alone, approaching the WT protein levels. This suggests that Bcl-xL confers stability to Bax in the absence of Nat3p (Figure 6.1C and D). Curiously, Bcl-xL was found stable in the mutant cells (Figure 6.1C and D), probably due to the fact that it is not a NatB substrate as it does not display any of NatB's Nt-target sequence. Of note, although the results must be reproduced, the independent experiments follow the same pattern and, therefore, Bax is most likely unstable in the absence of NatB-mediated Nt-acetylation. Although Bax in Naa20$^{-/-}$ MEFs seems to be stable when *Naa20* is inactivated, we noticed that other NatB substrates such as procaspase-8, -9, -3 and Bid are unstable (Chapter 3). As *S. cerevisiae* lacks obvious orthologs of Bcl-2 family members, the expression of human proteins like Bax in the absence of the interaction with Bcl-xL or with other Bcl-2 family members, likely facilitated the detection of decreased Bax protein levels. Therefore, the observed protein degradation caused by the absence of Nt-acetylation pointed as the consequence of instability of the

procaspases in Naa20$^{-/-}$ MEFs, can also be pointed to explain the instability of Bax in *nat3*Δ cells expressing human Bax. In fact, considering the idea that Nt-acetylation hides the N-degrons of proteins [18,24–26], the absence of this Nt-modification can expose the N-terminal of Bax and trigger its degradation. Indeed, as human Bax displays the N-terminal Met-Asp (MD-) amino-acid sequence [1] and Nt-acetylation hampers the cleavage of iMet [27,28], it is likely that the absence of Nt-acetylation can promote NME and, then, create a secondary destabilizing residue of the Arg/N-degron pathway [28,29]. Thus, we can hypothesize that, after cleavage of the iMet, non-acetylated human Bax (DGSGE-) can be targeted for degradation in two steps: first, the N-terminal undergoes arginylation mediated by the R-transferase *ATE1*, followed by degradation carried out by the *S. cerevisiae* RING-type Ubr1 and HECT-type Ufd4 E3 ubiquitin ligases [30]. A set of different yeast mutants namely a double mutant lacking Nat3p or Mdm20p and Ate1p, as well as a double mutant lacking Nat3p or Mdm20p and Ubr1p, could be constructed and tested to validate this hypothesis. As the Arg/N-degron pathway is widely studied in *S. cerevisiae*, focusing on studies in this pathway will be a step forward to understand the effect of Nt-acetylation on Bax stability.

6.3.2. Deletion of *NAT3* increases the susceptibility of yeast cells expressing human Bax α to acetic acid

We sought to evaluate whether Nt-acetylation affects the sensitivity of yeast cells expressing human Bax α to an apoptotic stimulus, as observed in MEFs. Acetic acid was used as an exogenous trigger to activate Bax α, as described in Chapter 5 in both WT and *nat3*Δ cells expressing human Bax α. As *nat3*Δ cells cannot be used for standard CFU assays due to aggregation [2,4], we monitored loss of plasma membrane integrity of the WT and *nat3*Δ cells expressing Bax α by PI staining, upon treatment with 160 mM acetic acid for 90 and 180 min. Samples were sonicated before flow cytometer acquisition to avoid clogging caused by the presence of cell aggregates. Flow cytometry analysis showed that, 14 h after induction of Bax expression with galactose but before acetic acid treatment, there was a residual percentage of WT and *nat3*Δ cells transformed with the EV or with the Bax expressing-plasmid PI-positive stained, indicative of a negligible sub-population of dead cells (Figure 6.2A-C and Figure A4, Appendix). After 90 min of exposure to 160 mM acetic acid, both WT and *nat3*Δ cells expressing Bax α displayed an increase in the percentage of PI-positive cells (6% and 35 %, respectively) when compared with non-treated cells, which was statistically significant in the case of *nat3*Δ cells. These percentages slightly increased to 8% and 49%, respectively, after 180 min of acetic acid treatment. When we directly compared WT and *nat3*Δ cells expressing human Bax, it was clear that the mutant cells exhibit a much higher

susceptibility to acetic acid. Importantly, no toxicity was observed for either WT or *nat3*Δ cells transformed with the EV untreated or treated with acetic acid. These results were confirmed by fluorescence microscopy (Figure 6.2D). In fact, although PI staining (red fluorescence) was mainly observed in the strains expressing Bax α after acetic acid exposure, *nat3*Δ cells revealed a much higher number of cells stained with PI than WT cells. Almost no red fluorescent cells were visualized for WT and *nat3*Δ EV cells in the presence of acetic acid, which was indicative of no toxicity in the absence of Bax α. Altogether, flow cytometry and fluorescence microscopy analysis showed that the absence of Nat3 mediated Nt-acetylation renders cells more sensitive to acetic acid as assessed by the loss of plasma membrane integrity. These results are in agreement with a study in HeLa cells showing that inhibition of *Naa20* sensitizes cells to apoptosis induced by the proteasome inhibitor MG132 [31]. Also, our previous study showed that Naa25$^{-/-}$ MEFs are more sensitive to MG132 [1]. Accordingly, a recent study found that NatB plays an important role in stress prevention [11]. Interestingly, when we exposed Naa20$^{-/-}$ MEFs to different apoptotic stimuli, we found a stimulus-dependent effect of *Naa20* inactivation (Chapter 3).

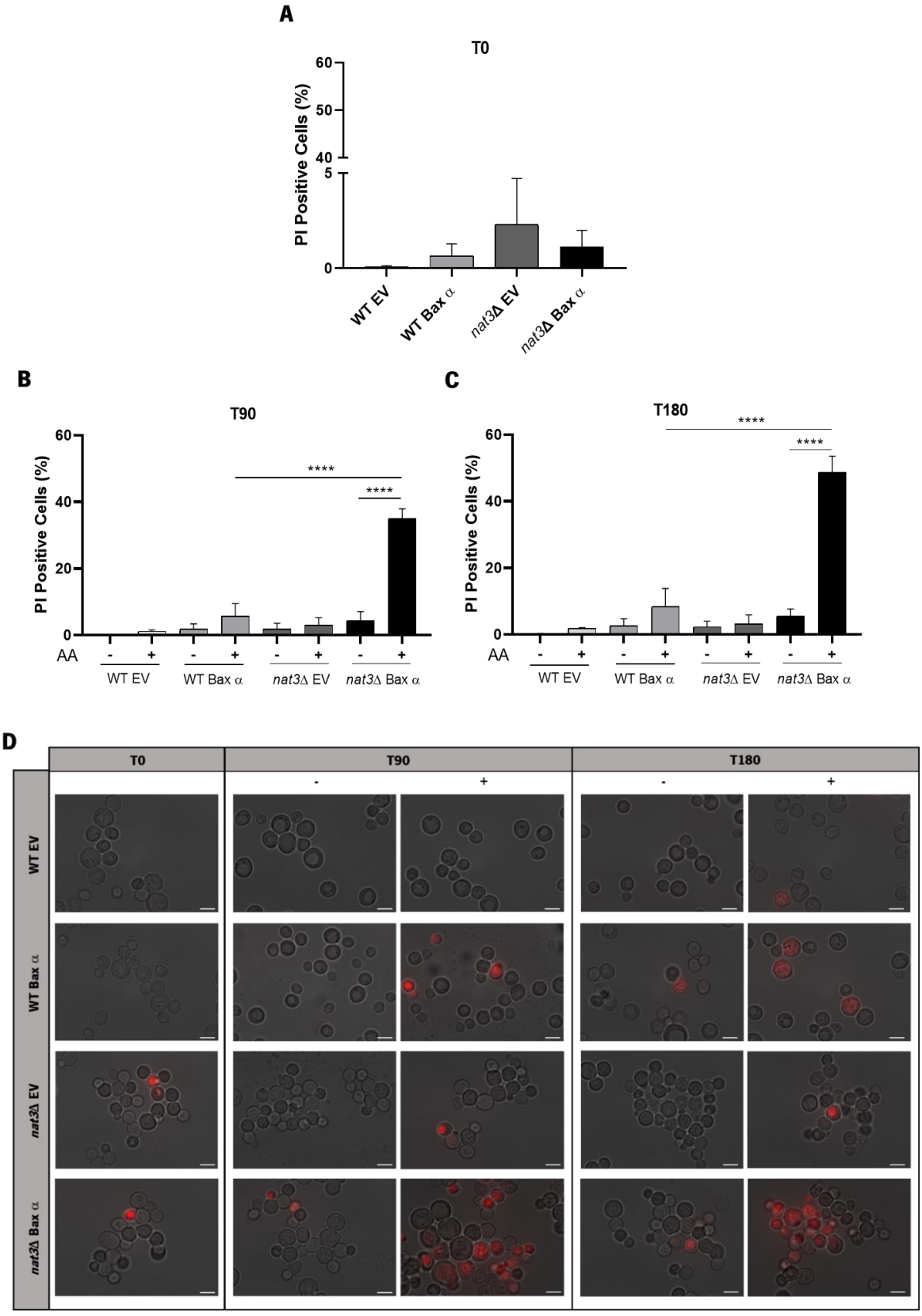

Figure 6.2: Acetic acid induces loss of plasma membrane integrity in *nat3*Δ yeast cells expressing human Bax α. Percentage of WT and *nat3*Δ yeast cells expressing EV or human Bax α exhibiting loss of plasma membrane integrity assessed by PI staining at flow cytometry **(A-C)** or fluorescence microscopy **(D)**. Representative plots of the quantification of the percentage of PI-positive cells **(A)** 14 h after Bax expression without treatment, **(B)** 90 min and **(C)** 180 min after treatment

without (-) or with (+) 160 mM acetic acid, pH 3.0. The percentage of PI positive cells were adjusted to autofluorescence. The values display the mean of three independent experiments analysed by one-way ANOVA, where ****p<0.0001. **(D)** Fluorescence microscopy images of the indicated yeast strains treated (+) or not (-) with 160 mM acetic acid, pH 3.0, for 0, 90 and 180 min and stained with 4 mg/mL of PI for 10 min at RT in the dark. The images shown are representative of several microscope fields. Bar: 5 μm. AA – acetic acid.

6.3.3. Bcl-xL does not rescue *nat3*Δ yeast cells expressing human Bax α from acetic acid-induced cell death

As Bcl-xL rescued WT yeast cells expressing Bax α from acetic acid-induced cell death in (Chapter 5), we sought to address whether Bcl-xL was also able to revert the susceptibility of *nat3*Δ cells to acetic acid in the absence of NatB-mediated Bax Nt-acetylation. To this end, plasma membrane integrity of *nat3*Δ cells heterologously co-expressing Bax α and Bcl-xL or the respective EV was monitored 90 and 180 min after exposure to 160 mM of acetic acid. Flow cytometry analysis revealed a residual percentage of PI-positive cells 14 h after Bax α and Bcl-xL expression (Figure 6.3A and Figure A5, Appendix). Although the percentage of PI-positive cells was slightly lower in *nat3*Δ cells co-expressing Bax α and Bcl-xL than in *nat3*Δ expressing Bax α and the EV 90 min (25% and 28%, respectively) and 180 min (37% and 46%, respectively) after acetic acid treatment, it was still much higher than in non-treated cells, and statistically significant after 180 min (Figure 6.3B, C). Fluorescence microscopy confirmed that *nat3*Δ cells co-expressing Bax α and EV, and co-expressing Bax α and Bcl-xL exhibit higher but similar percentages of PI-positive stained cells after acetic acid treatment (Figure 6.3D) in comparison with non-treated cells. Altogether, flow cytometry and fluorescence microscopy analysis showed that, contrarily to what was observed with WT cells expressing Bax α (Chapter 5), Bcl-xL does not seem to exhibit a protective role in *nat3*Δ cells. This suggests that the absence of Nt-acetylation not only reduces the levels of pro-apoptotic Bax but may also interfere with in the interaction between Bax and Bcl-xL, compromising the anti-apoptotic role of Bcl-xL.

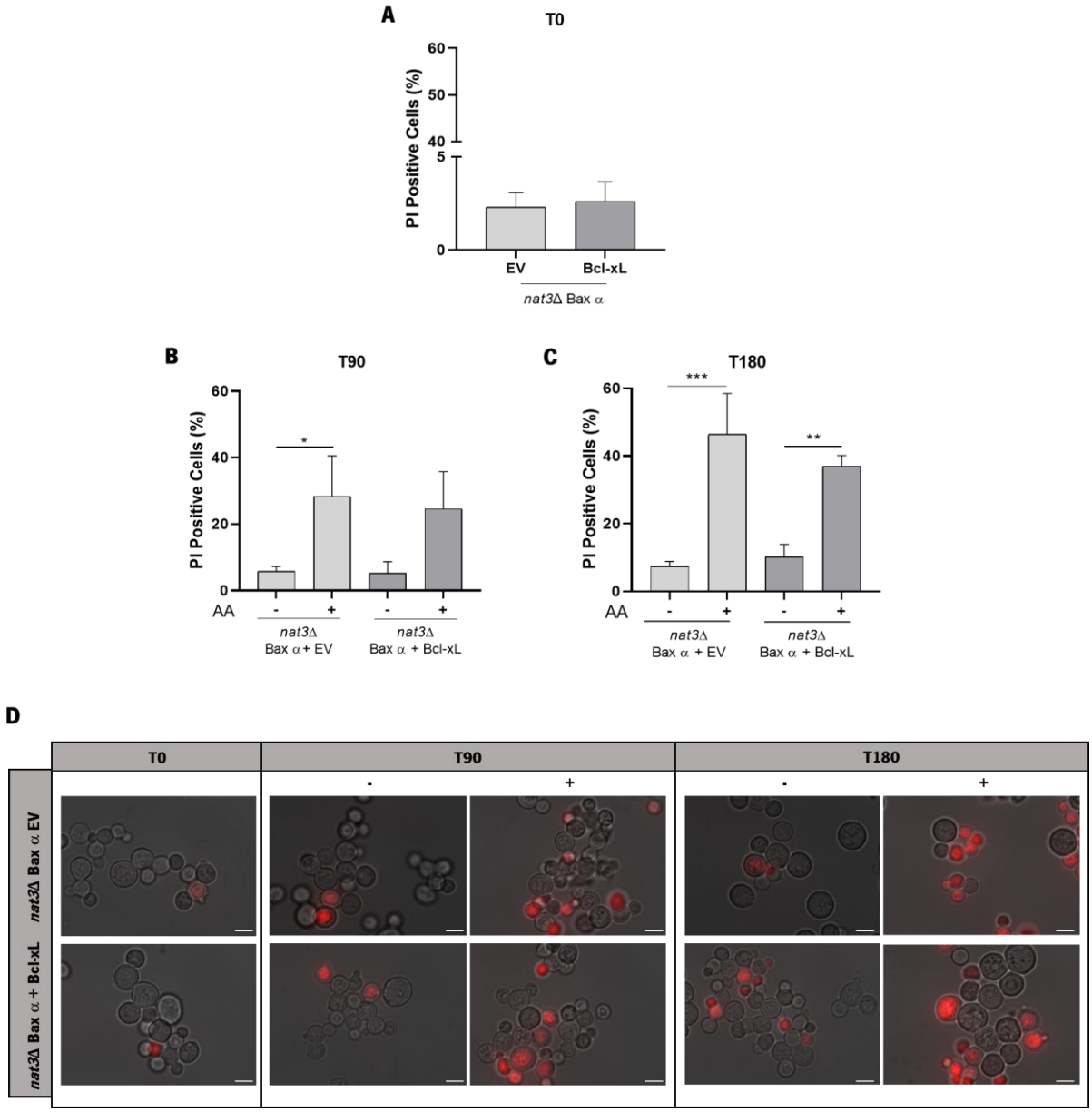

Figure 6.3: Absence of Nat3p abrogates Bcl-xL protection of human Bax α-expressing yeast cells from acetic acid-induced loss of plasma membrane integrity. Plasma membrane integrity was assessed by PI staining of *nat3*Δ yeast cells co-expressing human Bax α and Bcl-xL or the respective empty vector (EV). Representative plots of PI-positive stained cells **(A)** 14 h after Bax and Bcl-xL expression without treatment, **(B)** 90 min and **(C)** 180 min after treatment without (-) or with (+) 160 mM acetic acid, pH 3.0. The percentage of PI-positive positive cells were adjusted to autofluorescence. The values display the mean of three independent experiments analysed by one-way ANOVA, where *p<0.05, **p<0.01 and ***p<0.001. **(D)** Fluorescence microscopy images of the indicated yeast strains treated (+) or not (-) with 160 mM acetic acid, pH 3.0, for 0, 90 and 180 min and stained with 4 mg/mL PI for 10 min at RT in the dark. The images shown are representative of several microscope fields. Bar: 5 μm. AA – acetic acid.

6.4. Conclusion

The results gathered in this study demonstrated that Nt-acetylation may have a crucial role in Bax regulation namely on its stability and interaction with the anti-apoptotic protein Bcl-xL, and consequently on death of yeast cells heterologously expressing Bax and co-expressing Bax and Bcl-xL in response to acetic acid. Indeed, the absence of Nat3-mediated Bax Nt-acetylation decreases the stability of Bax, suggesting that Nt-acetylation confers protection from degradation to the pro-apoptotic protein Bax. Interestingly, reduction of Bax expression levels in *nat3*Δ cells was rescued by Bcl-xL co-expression but the susceptibility to acetic acid was not, suggesting that Nt-acetylation also impacts the anti-apoptotic role of Bcl-xL in Bax expressing cells committed to cell death in response to acetic acid.

References

1. Alves S, Neiri L, Chaves SR, Vieira S, Trindade D, Manon S, et al. N-terminal acetylation modulates Bax targeting to mitochondria. Int J Biochem Cell Biol. 2018;95: 35–42. doi:10.1016/j.biocel.2017.12.004
2. Caesar R, Warringer J, Blomberg A. Physiological importance and identification of novel targets for the N-terminal acetyltransferase NatB. Eukaryot Cell. 2006;5: 368–378. doi:10.1128/EC.5.2.368-378.2006
3. Hermann GJ, King EJ, Shaw JM. The yeast gene, *MDM20*, is necessary for mitochondrial inheritance and organization of the actin cytoskeleton. J Cell Biol. 1997;137: 141–153. doi:10.1083/jcb.137.1.141
4. Polevoda B, Cardillo TS, Doyle TC, Bedi GS, Sherman F. Nat3p and Mdm20p are required for function of yeast NatB Nα-terminal acetyltransferase and of actin and tropomyosin. J Biol Chem. 2003;278: 30686–30697. doi:10.1074/jbc.M304690200
5. Polevoda B, Norbeck J, Takakura H, Blomberg A, Sherman F. Identification and specificities of N-terminal acetyltransferases from *Saccharomyces cerevisiae*. EMBO J. 1999;18: 6155–6168. doi:10.1093/emboj/18.21.6155
6. Singer JM, Shaw JM. Mdm20 protein functions with Nat3 protein to acetylate Tpm1 protein and regulate tropomyosin-actin interactions in budding yeast. Proc Natl Acad Sci U S A. 2003;24: 7644–7649. doi:10.1073/pnas.1232343100
7. Auesukaree C, Damnernsawad A, Kruatrachue M, Pokethitiyook P, Boonchird C, Kaneko Y, et al. Genome-wide identification of genes involved in tolerance to various environmental stresses in *Saccharomyces cerevisiae*. J Appl Genet. 2009;50: 301–310. doi:10.1007/BF03195688
8. Bösl B, Grimminger V, Walter S. The molecular chaperone Hsp104-A molecular machine for protein disaggregation. J Struct Biol. 2006;156: 139–148. doi:10.1016/j.jsb.2006.02.004
9. Helbig AO, Rosati S, Pijnappel PWWM, van Breukelen B, Timmers MHTH, Mohammed S, et al. Perturbation of the yeast N-acetyltransferase NatB induces elevation of protein phosphorylation levels. BMC Genomics. 2010;11: 685(1–15). doi:10.1186/1471-2164-11-685
10. Sesaki H, Jensen RE. Ugo1p links the Fzo1p and Mgm1p GTPases for mitochondrial fusion. J Biol

Chem. 2004;279: 28298–28303. doi:10.1074/jbc.M401363200

11. Friedrich UA, Zedan M, Hessling B, Fenzl K, Gillet L, Barry J, et al. Nα-terminal acetylation of proteins by NatA and NatB serves distinct physiological roles in *Saccharomyces cerevisiae*. Cell Rep. 2021;34: 108711. doi:10.1016/j.celrep.2021.108711

12. Forte GMA, Pool MR, Stirling CJ. N-terminal acetylation inhibits protein targeting to the endoplasmic reticulum. PLoS Biol. 2011;9: e1001073. doi:10.1371/journal.pbio.1001073

13. Park SE, Kim J-M, Seok OH, Cho H, Wadas B, Kim S-Y, et al. Control of mammalian G protein signaling by N-terminal acetylation and the N-end rule pathway. Science. 2015;347: 1249–1252. doi:10.1126/science.aaa3844

14. Shemorry A, Hwang CS, Varshavsky A. Control of Protein Quality and Stoichiometries by N-Terminal Acetylation and the N-End Rule Pathway. Mol Cell. 2013;50: 540–551. doi:10.1016/j.molcel.2013.03.018

15. Hwang CS, Shemorroy A, Varshavsky A. N-Terminal Acetylation of Cellular Proteins Creates Specific Degradation Signals. Bone. 2010;327: 973–977. doi:doi:10.1126/science.1183147

16. Oh JH, Hyun JY, Varshavsky A. Control of Hsp90 chaperone and its clients by N-terminal acetylation and the N-end rule pathway. Proc Natl Acad Sci U S A. 2017;114: E4370–E4379. doi:10.1073/pnas.1705898114

17. Zattas D, Adle DJ, Rubenstein EM, Hochstrasser M. N-terminal acetylation of the yeast Derlin Der1 is essential for Hrd1 ubiquitin-ligase activity toward luminal ER substrates. Mol Biol Cell. 2013;24: 890–900. doi:10.1091/mbc.E12-11-0838

18. Kats I, Khmelinskii A, Kschonsak M, Huber F, Knieß RA, Bartosik A, et al. Mapping Degradation Signals and Pathways in a Eukaryotic N-terminome. Mol Cell. 2018;70: 488–501. doi:10.1016/j.molcel.2018.03.033

19. Van Damme P, Lasa M, Polevoda B, Gazquez C, Elosegui-Artola A, Kim DS, et al. N-terminal acetylome analyses and functional insights of the N-terminal acetyltransferase NatB. Proc Natl Acad Sci U S A. 2012;109: 12449–12454. doi:10.1073/pnas.1210303109

20. Arokium H, Ouerfelli H, Velours G, Camougrand N, Vallette FM, Manon S. Substitutions of potentially phosphorylatable serine residues of bax reveal how they may regulate its interaction with mitochondria. J Biol Chem. 2007;282: 35104–35112. doi:10.1074/jbc.M704891200

21. Renault TT, Teijido O, Missire F, Ganesan YT, Velours G, Arokium H, et al. Bcl-xL stimulates Bax relocation to mitochondria and primes cells to ABT-737. Int J Biochem Cell Biol. 2015;64: 136–146. doi:10.1016/j.biocel.2015.03.020

22. Gietz RD, Woods RA. Yeast transformation by the LiAc/SS Carrier DNA/PEG method. Methods Mol Biol. 2006;313: 107–120. doi:10.1385/1-59259-958-3:107

23. Casal M, Cardoso H, Leão C. Mechanisms regulating the transport of acetic acid in *Saccharomyces cerevisiae*. Microbiology. 1996;142: 1385–1390. doi:10.1099/13500872-142-6-1385

24. Linster E, Forero Ruiz FL, Miklankova P, Ruppert T, Mueller J, Armbruster L, et al. Cotranslational N-degron masking by acetylation promotes proteome stability in plants. Nat Commun. 2022;13: 810(1–12). doi:10.1038/s41467-022-28414-5

25. Li Z, Dogra V, Lee KP, Li R, Li M, Li M, et al. N-terminal acetylation stabilizes SIGMA FACTOR BINDING PROTEIN1 involved in salicylic acid-primed cell death. Plant Physiol. 2020;183: 358–

370. doi:10.1104/pp.19.01417

26. Myklebust LM, Van Damme P, Støve SI, Dörfel MJ, Abboud A, Kalvik T V., et al. Biochemical and cellular analysis of Ogden syndrome reveals downstream Nt-acetylation defects. Hum Mol Genet. 2015;24: 1956–1976. doi:10.1093/hmg/ddu611

27. Van Damme P, Hole K, Gevaert K, Arnesen T. N-terminal acetylome analysis reveals the specificity of Naa50 (Nat5) and suggests a kinetic competition between N-terminal acetyltransferases and methionine aminopeptidases. Proteomics. 2015;15: 2436–2446. doi:10.1002/pmic.201400575

28. Nguyen KT, Kim JM, Park SE, Hwang CS. N-terminal methionine excision of proteins creates tertiary destabilizing N-degrons of the Arg/N-end rule pathway. J Biol Chem. 2019;294: 4464–4476. doi:10.1074/jbc.RA118.006913

29. Kim JM, Seok OH, Ju S, Heo JE, Yeom J, Kim DS, et al. Formyl-methionine as an N-degron of a eukaryotic N-end rule pathway. Science. 2018;362: 1–19. doi:10.1126/science.aat0174

30. Hwang CS, Shemorry A, Auerbach D, Varshavsky A. The N-end rule pathway is mediated by a complex of the RING-type Ubr1 and HECT-type Ufd4 ubiquitin ligases. Nat Cell Biol. 2010;12: 1177–1185. doi:10.1038/ncb2121

31. Ametzazurra A, Larrea E, Civeira MP, Prieto J, Aldabe R. Implication of human N-alpha-acetyltransferase 5 in cellular proliferation and carcinogenesis. Oncogene. 2008;27: 7296–7306. doi:10.1038/onc.2008.332

CHAPTER 7

CONCLUDING REMARKS AND FUTURE PERSPECTIVES

7.1. Conclusions and final remarks

Taking into account that in our previous work we identified a link between Nt-acetylation and apoptosis through the pro-apoptotic Bax protein [1], and the fact that the main apoptotic proteins are putative NatB substrates, the main goal of this thesis was to further understand the role of Nt-acetylation on apoptosis regulation. Additionally, given the emerging studies on Nt-acetylation and protein degradation via N-degron pathways [2–8], we also focused our work on predicting how the interplay between these two processes may modulate apoptosis. Taking advantage of the conservation of many cellular processes between yeast and mammals, both MEFs and yeast cells were used as complementary models to achieve our goals. Our results are presented in four different chapters: Chapter 3 and 4 dedicated to explore the relation between Nt-acetylation and protein degradation via N-degron pathways on apoptosis regulation, with Chapter 3 focused specifically on the experimental results obtained with MEF cells. Chapter 5 develops a yeast model system to screen for new Bax regulators, and chapter 6 includes the studies to assess the role of Nat3-mediated Nt-acetylation on Bax stability, on its interaction with Bcl-xL as well as on the susceptibility of Bax expressing cells to a sub-lethal concentration of acetic acid.

Regarding the effect of Nt-acetylation on apoptosis regulation, we have previously found that the NatB regulatory subunit Naa25 is involved in mitochondrial targeting of the pro-apoptotic Bax protein and affects the sensitivity of MEF cells to an apoptotic stimulus [1]. Interestingly, this previous study is the only achieving a total depletion of Naa25 in the MEF model. Indeed, all studies have assessed the biological significance of NatB through partial depletion of one of the two NatB subunits in eukaryotes other than MEF cells [9–15]. Taking this into account, we decided to study the impact of Nt-acetylation on apoptosis regulation in MEFs where the catalytic subunit Naa20 was completely inactivated. Before proceeding with other experiments, we confirmed and validated the efficiency of Naa20 inactivation by western blot and Real-Time PCR. Our results confirm not only that *Naa20* is totally inactivated in the MEF KO cells, but also that this inactivation leads to cytoskeleton abnormalities and decreased cell proliferation. After that, to better characterize the effects of complete NatB depletion in MEF cells, we performed a N-terminomics analysis of WT and Naa20$^{-/-}$ MEFs. We mainly found an overall reduction of Nt-acetylation levels in Naa20$^{-/-}$ MEFs in comparison with WT MEFs, with a relative decrease in the number of fully acetylated N-termini to only partially acetylated N-termini. Notably, the majority of N-termini with strong decreased acetylation in the Naa20$^{-/-}$ MEF cells are NatB substrates. Interestingly, we also found that half of the NTA downregulated proteins are directly associated with apoptosis, and in particular with caspases, which suggests a possible influence of NatB-dependent NTA of specific proteins

on their protein half-life and in particular of those involved in apoptosis. Indeed, we confirmed by western blot that Naa20$^{-/-}$ MEFs exhibit a significant reduction in protein levels of procaspase-3, -9, -8 and Bid, associated with a decreased susceptibility to etoposide and TNF-α plus SMAC/DIABLO mimetic. This reduced expression levels were restored by silencing Arg/N-recognins E3 ubiquitin protein ligases Ubr4 and Ubr1. Moreover, we discovered that Ubr4 silencing partially reverts the decreased susceptibility to TNF-α plus SMAC/DIABLO mimetic. Altogether, our findings highlight the impact of NatB-mediated Nt-acetylation and Arg/N-degron pathway on apoptosis regulation. Following these findings, we sought to perform an *in silico* systematic search to identify among the major components of the apoptotic machinery, and of the respective fragments generated by caspase- and calpain-mediated proteolytic cleavage, those which are substrates of Nt-acetylation, as well as those which are substrates of N-recognins. Based on this search, we found that the majority of the full-length apoptotic proteins analysed are mostly putative substrates of NATs. In addition, we found that the majority of apoptotic proteins analysed are most likely substrates of the N-degron pathways. Altogether these findings suggest a high impact of Nt-acetylation and N-degron pathways on the proteostasis, and in some cases on the function, of both pro- and anti-apoptotic proteins. Of note, NatB, NatE, and to a lesser extend NatC and NatF, are the most prominent NATs acetylating these apoptotic proteins. Regarding the protein fragments, our analysis showed that NatA may acetylate the majority and, in contrast to the full-length proteins, they can be recognized by only one of the three N-degron pathways. Curiously, we found that cleavage of the apoptotic proteins may generate mostly pro-apoptotic fragments, regardless the original function of the protein. Moreover, we noticed that the proteolytic cleavage originates a slightly higher percentage of less stable proteins than the original ones, which may indicate that N-recognins activity must be reduced at some point during the apoptotic process, thereby favoring the execution phases of apoptosis. In general, we conclude that, besides the NatA, NatB and NatC well-known roles in apoptosis, NatE and NatF may also have a role in apoptosis. Likewise, the Ac/N-degron pathway may also be crucial during the apoptotic process, similarly to the Arg/ and Gly/N-degron pathways, as many apoptotic proteins bear conditional Ac/N-degrons leading to its degradation by Ac/N-degron pathway, when they are not under protection by proper folding/partner´s interaction, as a consequence of cell´s commitment to apoptosis.

Among the main apoptotic proteins, Bax is a key player in the apoptotic-cell death process, governing the cell fate decision [16]. Although several reports address the mechanisms of human Bax activation, how this protein remains inactive and becomes activated is still unclear. Therefore, to shed light on how Bax function can be regulated, we used WT human Bax α heterologously expressed in *S. cerevisiae*. As our previous results showed that sub-lethal concentrations of acetic acid induced loss of

viability of Bax α-expressing yeast cells without compromising plasma membrane integrity [17,18], we sought to investigate if this could be associated with an altered Bax localization and cyt *c* release. We found a significant decrease in mitochondrial cyt *c* together with Bax translocation to the mitochondria, even though it is not related with the standard Bax active conformation. In fact, no differences were detected for active Bax between non-treated and treated cells. Furthermore, using yeast cells co-expressing Bax α with Bcl-xL and Bcl-xLΔC, we showed that Bcl-xL, but not Bcl-xLΔC, protects yeast cells from cell death induced by acetic acid. Since the inhibition of GSK3β in mammalian cells abrogates Bax activation [19,20], using a yeast strain deleted for its yeast orthologue Rim11p, we found that the absence of this protein reverted the loss of cell viability of Bax α-expressing cells after acetic acid exposure. Taken together, our findings point to acetic acid as an exogenous trigger of Bax α-mediated cell death, which triggers Bax mitochondrial translocation and cyt *c* release, closely resembling the natural Bax function in the cellular context. Importantly, this regulated cell death process was reverted by the co-expression with Bcl-xL, but not with Bcl-xLΔC, as well as in the absence of Rim11p. This novel system mimics human Bax α regulation by Bcl-xL and GSK3β, and can therefore be used as a platform to uncover novel Bax regulators and explore its therapeutic modulation.

Given the known role of Nt-acetylation of Bax previously established in Naa25$^{-/-}$ MEFs [1] together with the previous evidences showing that yeast cells expressing Bax α are susceptible to acetic acid-induced cell death, which in turn, is recovered by the interaction with Bcl-xL, we decided to use the yeast model to dissect the role of Bax Nt-acetylation mediated by the yeast NatB catalytic subunit Nat3p on Bax regulation. Although our results must be reproduced, we found a reduction in Bax expression levels in the absence of Nat3-mediated Nt-acetylation, which is rescued in the presence of Bcl-xL. Moreover, our flow cytometry and fluorescence microscopy analysis showed that the absence of Nat3p greatly increases the sensitivity of yeast cells expressing Bax α to acetic acid treatment. Most likely due to the absence of Bax Nt-acetylation, we noticed that Bcl-xL, in spite of protecting Bax from degradation, loses its anti-apoptotic role, as the absence of Nat3p abrogates its protection of human Bax α-expressing yeast cells from acetic acid-induced loss of plasma membrane integrity. It is known that Bcl-xL can counteract Bax activation either by forming inhibitory complexes in the mitochondria or by promoting the retrotranslocation of Bax to the cytosol. The absence of Bax Nt-acetylation may compromise one or both of these Bcl-xL protective functions. Indeed, unacetylated Bax may inhibit the formation of inhibitory complexes or may inhibit Bax retrotranslocation leading to its mitochondrial accumulation, explaining the higher sensitivity of *nat3*Δ cells to acetic acid than WT cells. Altogether, our results highlight the importance of Nt-acetylation in

conferring stability to proteins, in this case to Bax, and likely in warranting protection by Bcl-xL from loss of plasma membrane integrity of Bax-expressing cells induced by acetic acid.

Our findings also offer novel insights on the high complexity of the interplay between the Nt-acetylation and degradation by N-degron pathways, and its impact on the modulation of apoptosis. Indeed, our data from MEFs and yeast cells suggest that the absence of NatB-mediated Nt-acetylation significantly impacts the stability of key apoptotic proteins, as they are mainly NatB substrates. As a consequence, in the absence of NatB, the unacetylated proteins became prone to degradation through the Arg/N-degron pathway. Indeed, an anti-apoptotic role has been pointed for this N-degron pathway [21–23]. Interestingly, our study raises the idea that apoptosis can also be regulated by the Ac/N-degron pathway, if the acetylated proteins are not quickly protected by proper folding or by their interacting partners just after synthesis. Additionally, our study stresses the importance of using two different complementary cell models. In fact, yeast showed to be a powerful model system to tackle the processes occurring in MEFs. Since the genome of the yeast *S. cerevisiae* is devoid of genes encoding orthologues of the human Bcl-2 family, it was possible to unravel the effect of Nt-acetylation on the members of the Bcl-2 family, namely Bax and Bcl-xL, without interference of the mammalian apoptotic network. For instance, while in Naa20$^{-/-}$ MEFs Bax was found stable likely due to the presence of Bcl-xL, in yeast cells expressing human Bax alone, this protein was seemingly less stable in the absence of Nt-acetylation. Bax expression levels were recovered by co-expression of Bcl-xL, which likely displays a protective role against Arg/N-degron-mediated Bax degradation when Bax is unacetylated, though it is unable to protect *nat3*Δ cells expressing Bax from loss of plasma membrane integrity in response to acetic acid. Therefore, taking into account the short generation time, easy handling and tractability and easy genetic manipulation of yeast cells, together with the high level of conservation of cellular processes, they emerge as a versatile and robust model system to further understand the role of Nt-acetylation on cellular proteostasis and apoptosis regulation.

7.2. Future perspectives

Although this study answered to several biological questions, it also raises many others. Below, we suggest several experimental approaches that can be performed in the future in order to deepen our knowledge about the regulation of apoptosis mediated by Nt-acetylation and N-degron pathways.

Regarding the cell response of MEF and yeast cells to the induction of apoptosis in the absence of Nt-acetylation, our results showed a stimulus-dependent effect for Naa20$^{-/-}$ MEFs and a higher sensitivity to acetic acid for yeast cells expressing human Bax. To directly compare the effect of *Naa20*

inactivation on apoptosis induction in MEFs and yeast cells, a further treatment with acetate could be performed with the MEF cells model. In turn, it would be interesting to assess the sensitivity of yeast *nat3*Δ cells to etoposide. As etoposide is unable to induce apoptosis in yeast cells carrying WT topoisomerase II [24,25], mutant strains with the etoposide hypersensitive *top2S740W* allele instead of the WT allele, or strains overexpressing topoisomerase II should be used, in order to increase cell sensitivity to etoposide. Moreover, since *nat3*Δ cells exhibit growth defects, clonogenic assays to evaluate the cell survival of the strains were not performed and are in practice difficult to implement due to the presence of cell aggregates. Although sonication after labelling with fluorescent probes allows monitoring different cellular parameters, this sample processing cannot be applied to CFUs assays, as it is not possible to discard whether sonication before plating can affect the cell viability. To further characterise cell death of *nat3*Δ cells in response to acetic acid, other apoptotic (e.g. exposure of PS, endonucleosomal DNA degradation, ROS accumulation and mitochondrial membrane potential) or non-apoptotic markers (e.g. early loss of plasma membrane integrity and nuclear-cytosolic translocation of the yeast ortholog of the mammalian high-mobility group box 1 protein (HMGB1) Nhp6Ap) should be monitored. Additionally, we noticed that the absence of Nt-acetylation, besides reducing the level of pro-apoptotic Bax levels, also interferes with the anti-apoptotic role of Bcl-xL when co-expressed with Bax. Importantly, in WT cells, the effect of Bcl-xL on acetic acid-induced death of cells expressing Bax α was assessed by monitoring cell viability by CFU assay, while in the experiments with *nat3*Δ cells, death was monitored by PI staining. As loss of plasma membrane integrity may reflect a secondary necrosis following apoptosis, or a non-apoptotic regulated or non-regulated cell death, other cell death markers, should be assessed to better understand the impact of Nat3-mediated Nt-acetylation in the death of yeasts co-expressing Bax and Bcl-xL in response to acetic acid. It was reported that, in yeast cells, the expression of c-*myc*-tagged Bax, an active form of Bax, induces loss of plating efficiency, which is not associated with the loss of plasma membrane integrity or with typical apoptotic markers but instead displayed autophagic features [26]. However, inhibition of autophagy did not prevent Bax-induced loss of plating efficiency and, curiously, accelerated it. In order to understand whether the high susceptibility of acetic acid observed in *nat3*Δ cells expressing Bax α is due to inhibition of autophagy, expression of the autophagy-related Atg8p protein could be assessed by western blot in *nat3*Δ cells expressing Bax after treatment with acetic acid. Furthermore, we could also assess Bax α localization and cyt *c* release by immunodetection in mitochondrial and cytosolic fractions of WT and *nat3*Δ cells co-expressing Bax and Bcl-xL in response to acetic acid. This experiment will allow comparing the mitochondrial levels of Bax between both strains

and thus understand if Bcl-xL has lost its anti-apoptotic role due to its inability to retrotranslocate Bax to the cytosol or to form inhibitory complexes with unacetylated Bax.

Regarding the role of Nt-acetylation and N-degron pathways in regulating apoptosis, the main open questions are how these two processes are interconnected to maintain cellular homeostasis and to induce/inhibit apoptosis in response to a stimulus. Although the apoptotic proteins identified as putative target substrates of Nt-acetylation and of proteolytic pathways must be experimentally validated, our study only starts to lift the veil on cell fate regulation by these processes, and may help to understand how the Nt-acetylation and N-degron pathways can be modulated to fight diseases in which apoptosis is deregulated. Exploring whether E3 ubiquitin ligases of the Ac/ and Arg/N-degron pathways display distinct affinity/specificity to pro- and antiapoptotic proteins could allow their selective inhibition as a strategy to enhance or inhibit apoptosis, respectively. Although this kind of strategies may impact on several other cellular processes, it was recently shown for the first time that the *in vivo* inhibition of N-degron pathways can be explored to increase efficiency of chemotherapeutic drugs [27]. Therefore, even seemingly non druggable targets, studies on apoptosis in cell models with deregulation of NATs and E3 ubiquitin ligases will help to further understand whether apoptosis is involved in pathogenesis and if its modulation may be used as a therapeutic strategy.

Another remaining issue of this study regards the stability of Bax in the absence of Nt-acetylation. Although our results appear to indicate that Nt-acetylation may have a protective role against Bax degradation in yeast cells and likely in MEFs, by conferring stability to this protein, the experiments performed in yeast should be reproduced. Furthermore, as the Arg/N-degron pathway is widely studied in *S. cerevisiae*, focusing on studies on this pathway might thus be a good step to better understand the effect of Nt-acetylation on the stability of Bax. Indeed, as performed in MEFs, a set of different yeast mutant constructions can help further elucidate the possible involvement of the Arg/N-degron pathway on Bax degradation. In particular, it would be interesting to assess the expression levels of Bax in a double mutant deleted for Nat3p or Mdm20p and Ubr1p, as well as in a mutant deleted for Nat3p or Mdm20p and Ate1p. It is expected that the loss of Ate1p or Ubr1p will rescue the protein levels of Bax through inhibition of its degradation. Another complementary approach could be monitoring the interaction between Bax and Bcl-xL by immunoprecipitation to confirm whether these proteins still interact even in the absence of Bax Nt-acetylation, and whether this interaction may protect unacetylated Bax from degradation. Additionally, it would be interesting to assess Bax stability in Naa20$^{-/-}$ MEFs silenced for Bcl-xL, although the presence of other Bax interactors can take over the role of Bcl-xL in its absence.

Furthermore, when attempting to understand the outcome of silencing the Arg/ and Ac N-recognins in Naa20$^{-/-}$ MEFs after an apoptotic stimulus, we found that the decreased susceptibility to TNF-α plus SMAC mimetic was partially reverted by Ubr4 silencing. However, as caspase-3 and caspase-9 activation was still limited, Bax, cyt *c* and SMAC/DIABLO localization can be assessed to ascertain if this stimulus also mediates the intrinsic apoptotic pathway.

Another interesting feature regards the changes at the protein level observed in the apoptotic proteins in Naa20$^{-/-}$ MEFs that were not reflected in the proteomic study. Indeed, while caspase-3, -8 and -9 as well as Bid levels were decreased, as detected by western blot, caspase-3 was the only protein downregulated that was identified in the proteomic analysis of Naa20$^{-/-}$ MEFs. Moreover, the Nt-acetylation degree was not determined for any of the four referred proteins. These can be explained by technical limitations of the proteomic and N-terminomics approach. However, the instability of the proteins caused by the absence of Nt-acetylation, or less often by its presence, may target them for degradation through the Arg/ and Ac/N-degron pathway, respectively, and explain their non-detection in the proteomic studies [28]. Also, though some natural Ac/N-degrons are generally mainly conditional, they can become prone to degradation if the protection conferred by proper protein folding, interaction with partners or by integration in a protein complex is compromised, which most often occur under stress conditions associated with apoptosis induction [29]. Therefore, proteomic studies performed with cells inactivated for *Naa20* after exposure to apoptotic stimuli as well as with silencing of N-recognins, enzymes involved in Nt-deamidation, arginylation, or even in NME, may thus provide a clearer picture of the impact of Nt-acetylation and degradation via the N-degrons pathways on apoptosis regulation. In another approach, the *in silico* systematic search carried out can drive the experimental validation of the apoptotic components identified as putative substrates of NATs and N-recognins, and bring new clues to the understanding of apoptosis modulation by Nt-acetylation and through degradation via the N-degrons pathways.

References

1. Alves S, Neiri L, Chaves SR, Vieira S, Trindade D, Manon S, et al. N-terminal acetylation modulates Bax targeting to mitochondria. Int J Biochem Cell Biol. 2018;95: 35–42. doi:10.1016/j.biocel.2017.12.004
2. Myklebust LM, Van Damme P, Støve SI, Dörfel MJ, Abboud A, Kalvik T V., et al. Biochemical and cellular analysis of Ogden syndrome reveals downstream Nt-acetylation defects. Hum Mol Genet. 2015;24: 1956–1976. doi:10.1093/hmg/ddu611
3. Shemorry A, Hwang CS, Varshavsky A. Control of Protein Quality and Stoichiometries by N-Terminal Acetylation and the N-End Rule Pathway. Mol Cell. 2013;50: 540–551.

doi:10.1016/j.molcel.2013.03.018

4. Hwang CS, Shemorroy A, Varshavsky A. N-Terminal Acetylation of Cellular Proteins Creates Specific Degradation Signals. Bone. 2010;327: 973–977. doi:doi:10.1126/science.1183147

5. Park SE, Kim J-M, Seok OH, Cho H, Wadas B, Kim S-Y, et al. Control of mammalian G protein signaling by N-terminal acetylation and the N-end rule pathway. Science. 2015;347: 1249–1252. doi:10.1126/science.aaa3844

6. Kats I, Khmelinskii A, Kschonsak M, Huber F, Knieß RA, Bartosik A, et al. Mapping Degradation Signals and Pathways in a Eukaryotic N-terminome. Mol Cell. 2018;70: 488–501. doi:10.1016/j.molcel.2018.03.033

7. Li Z, Dogra V, Lee KP, Li R, Li M, Li M, et al. N-terminal acetylation stabilizes SIGMA FACTOR BINDING PROTEIN1 involved in salicylic acid-primed cell death. Plant Physiol. 2020;183: 358–370. doi:10.1104/pp.19.01417

8. Linster E, Forero Ruiz FL, Miklankova P, Ruppert T, Mueller J, Armbruster L, et al. Cotranslational N-degron masking by acetylation promotes proteome stability in plants. Nat Commun. 2022;13: 810(1–12). doi:10.1038/s41467-022-28414-5

9. Singer JM, Shaw JM. Mdm20 protein functions with Nat3 protein to acetylate Tpm1 protein and regulate tropomyosin-actin interactions in budding yeast. Proc Natl Acad Sci U S A. 2003;100: 7644–7649. doi:10.1073/pnas.1232343100

10. Polevoda B, Cardillo TS, Doyle TC, Bedi GS, Sherman F. Nat3p and Mdm20p are required for function of yeast NatB Nα-terminal acetyltransferase and of actin and tropomyosin. J Biol Chem. 2003;278: 30686–30697. doi:10.1074/jbc.M304690200

11. Kim JH, Cho A, Yin H, Schafer DA, Mouneimne G, Simpson KJ, et al. Psidin, a conserved protein that regulates protrusion dynamics and cell migration. Genes Dev. 2011;25: 730–741. doi:10.1101/gad.2028611

12. Van Damme P, Lasa M, Polevoda B, Gazquez C, Elosegui-Artola A, Kim DS, et al. N-terminal acetylome analyses and functional insights of the N-terminal acetyltransferase NatB. Proc Natl Acad Sci U S A. 2012;109: 12449–12454. doi:10.1073/pnas.1210303109

13. Gao J, Barroso C, Zhang P, Kim HM, Li S, Labrador L, et al. N-terminal acetylation promotes synaptonemal complex assembly in *C. Elegans*. Genes Dev. 2016;30: 2404–2416. doi:10.1101/gad.277350.116

14. Neri L, Lasa M, Elosegui-Artola A, D'Avola D, Carte B, Gazquez C, et al. NatB-mediated protein N-α-terminal acetylation is a potential therapeutic target in hepatocellular carcinoma. Oncotarget. 2017;8: 40967–40981. doi:10.18632/oncotarget.17332

15. Huber M, Bienvenut W V., Linster E, Stephan I, Armbruster L, Sticht C, et al. NatB-mediated N-terminal acetylation affects growth and biotic stress responses. Plant Physiol. 2020;182: 792–806. doi:10.1104/pp.19.00792

16. Renault TT, Manon S. Bax: Addressed to kill. Biochimie. 2011;93: 1379–1391. doi:10.1016/j.biochi.2011.05.013

17. Guedes JP, Baptista V, Santos-Pereira C, Sousa MJ, Manon S, Chaves SR, et al. Acetic acid triggers cytochrome *c* release in yeast heterologously expressing human Bax. Apoptosis. 2022;27: 368–381. doi:10.1007/s10495-022-01717-0

18. Pereira H, Oliveira CSF, Castro L, Preto A, Chaves SR, Côrte-Real M. Yeast as a tool to explore

cathepsin D function. Microb Cell. 2015;2: 225–234. doi:10.15698/mic2015.07.212

19. Zhang L, Zhang Y, Xing DA. LPLI inhibits apoptosis upstream of bax translocation via a GSK-3β-inactivation mechanism. J Cell Physiol. 2010;224: 218–228. doi:10.1002/jcp.22123

20. Linseman DA, Butts BD, Precht TA, Phelps RA, Le SS, Laessig TA, et al. Glycogen synthase kinase-3βphosphorylates bax and promotes its mitochondrial localization during neuronal apoptosis. J Neurosci. 2004;24: 9993–10002. doi:10.1523/JNEUROSCI.2057-04.2004

21. Ditzel M, Wilson R, Tenev T, Zachariou A, Paul A, Deas E, et al. Degradation of DIAP1 by the N-end rule pathway is essential for regulating apoptosis. Nat Cell Biol. 2003;5: 467–473. doi:10.1038/ncb984

22. Xu Z, Payoe R, Fahlman RP. The C-terminal proteolytic fragment of the breast cancer susceptibility type 1 protein (BRCA1) is degraded by the N-end rule pathway. J Biol Chem. 2012;287: 7495–7502. doi:10.1074/jbc.M111.301002

23. Piatkov KI, Brower CS, Varshavsky A. The N-end rule pathway counteracts cell death by destroying proapoptotic protein fragments. Proc Natl Acad Sci U S A. 2012;109: E1839–E1847. doi:10.1073/pnas.1207786109

24. Baldwin EL, Berger AC, Corbett AH, Osheroff N. Mms22p protects *Saccharomyces cerevisiae* from DNA damage induced by topoisomerase II. Nucleic Acids Res. 2005;33: 1021–1030. doi:10.1093/nar/gki246

25. Sabourin M, Nitiss JL, Nitiss KC, Tatebayashi K, Ikeda H, Osheroff N. Yeast recombination pathways triggered by topoisomerase II-mediated DNA breaks. Nucleic Acids Res. 2003;31: 4373–4384. doi:10.1093/nar/gkg497

26. Kiššova I, Plamondon LT, Brisson L, Priault M, Renouf V, Schaeffer J, et al. Evaluation of the roles of apoptosis, autophagy, and mitophagy in the loss of plating efficiency induced by Bax expression in yeast. J Biol Chem. 2006;281: 36187–36197. doi:10.1074/jbc.M607444200

27. Agarwalla P, Banerjee R. N-end rule pathway inhibition assists colon tumor regression via necroptosis. Mol Ther - Oncolytics. 2016;3: 16020. doi:10.1038/mto.2016.20

28. Varshavsky A. N-degron and C-degron pathways of protein degradation. Proc Natl Acad Sci U S A. 2019;116: 358–366. doi:10.1073/pnas.1816596116

29. Hwang CS, Shemorry A, Auerbach D, Varshavsky A. The N-end rule pathway is mediated by a complex of the RING-type Ubr1 and HECT-type Ufd4 ubiquitin ligases. Nat Cell Biol. 2010;12: 1177–1185. doi:10.1038/ncb2121

APPENDIX

Appendix Figures

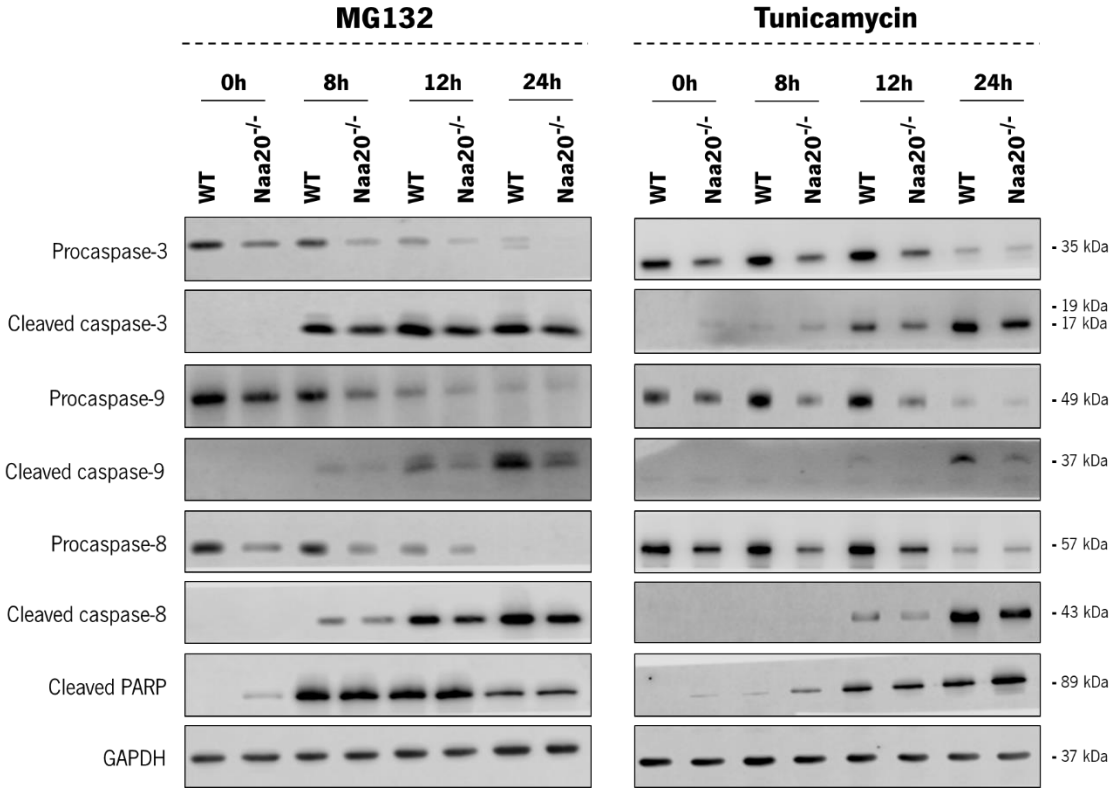

Figure A1: Inactivation of *Naa20* causes a reduction in the expression levels of procaspases and cleaved caspases-8, -9 and -3 but does not alter the susceptibility to the apoptotic inducers MG132 and tunicamycin. Representative western blot images of procaspases -3, -9 and -8 and of respective cleaved caspases as well as cleaved PARP in MEF cells, 6 days after infection with AdEmpty (WT) or Ad5CMVCre ($Naa20^{-/-}$) and 0, 8, 12 and 24 h after treatment with 5 μM of MG132 and 5 ng/μl of tunicamycin.

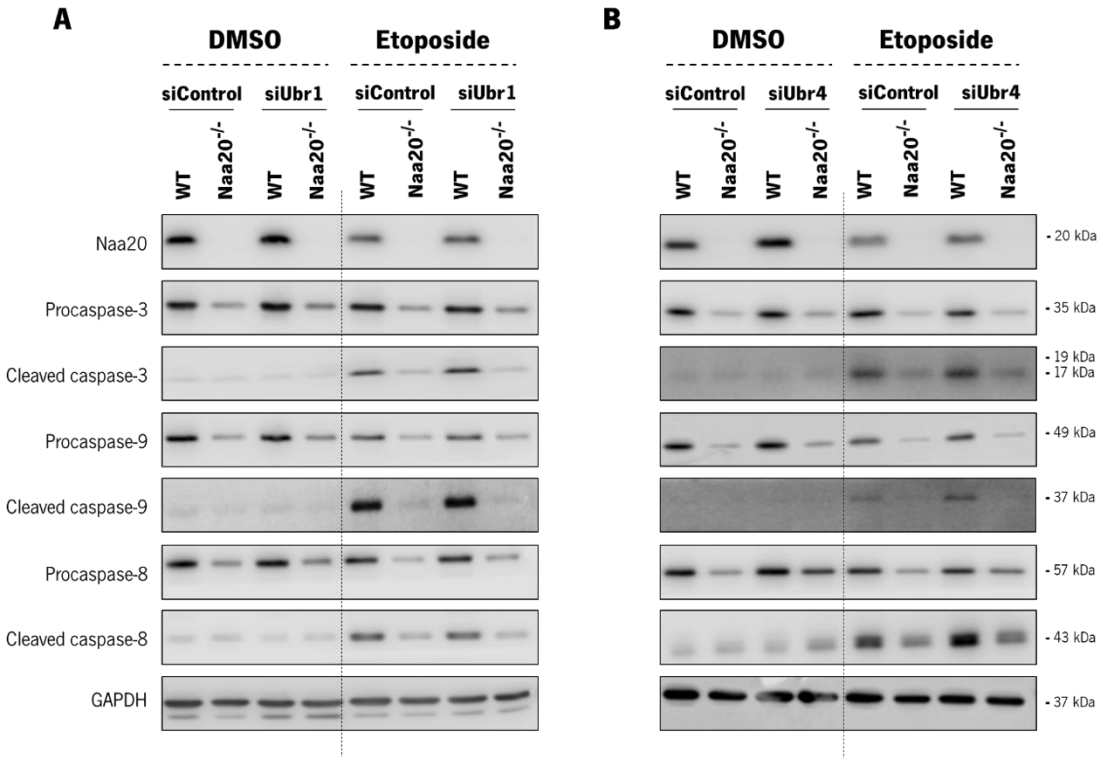

Figure A2: Silencing of *Ubr1* and *Ubr4* is unable to restore the procaspase-9 expression levels in response to etoposide in Naa20$^{-/-}$MEF cells. Representative western blot images of the procaspases and cleaved caspases-3, -9 and -8 protein levels after silencing the *Ubr1* **(A)** and Ubr4 **(B)** ubiquitin ligase in MEF cells 6 days after infection with AdEmpty (WT) or Ad5CMVCre (Naa20$^{-/-}$), 12 h after 50 μM etoposide treatment. Vehicle (DMSO) was used as a negative control of etoposide treatment. A specific siRNA (siControl) was used for control.

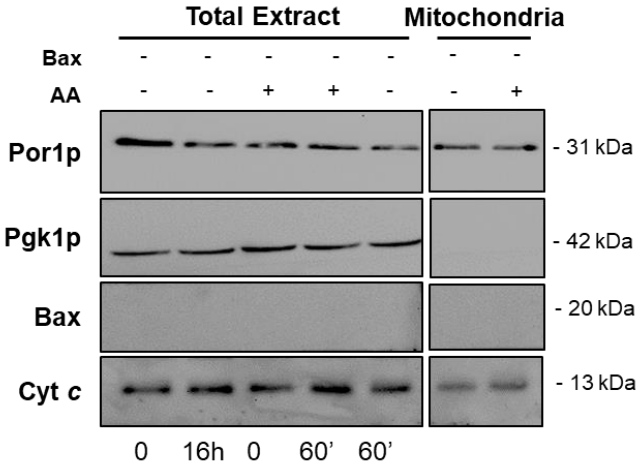

Figure A3: Sub-lethal concentrations of acetic acid do not affect cytochrome *c* mitochondrial content in yeast cells expressing the empty vector. Representative immunodetection of Bax and cyt *c* in total extracts of control (EV) yeast cells 0 and 16 after galactose induction, and 0 and 60 min after incubation with acetic acid (+) and after 60 min without acetic acid (-); and in mitochondrial fractions 60 min after incubation without (-) and with (+) 80 mM acetic acid, pH 3.0. Pgk1p and Por1p were used as loading controls for cytosol and mitochondrial fractions, respectively.

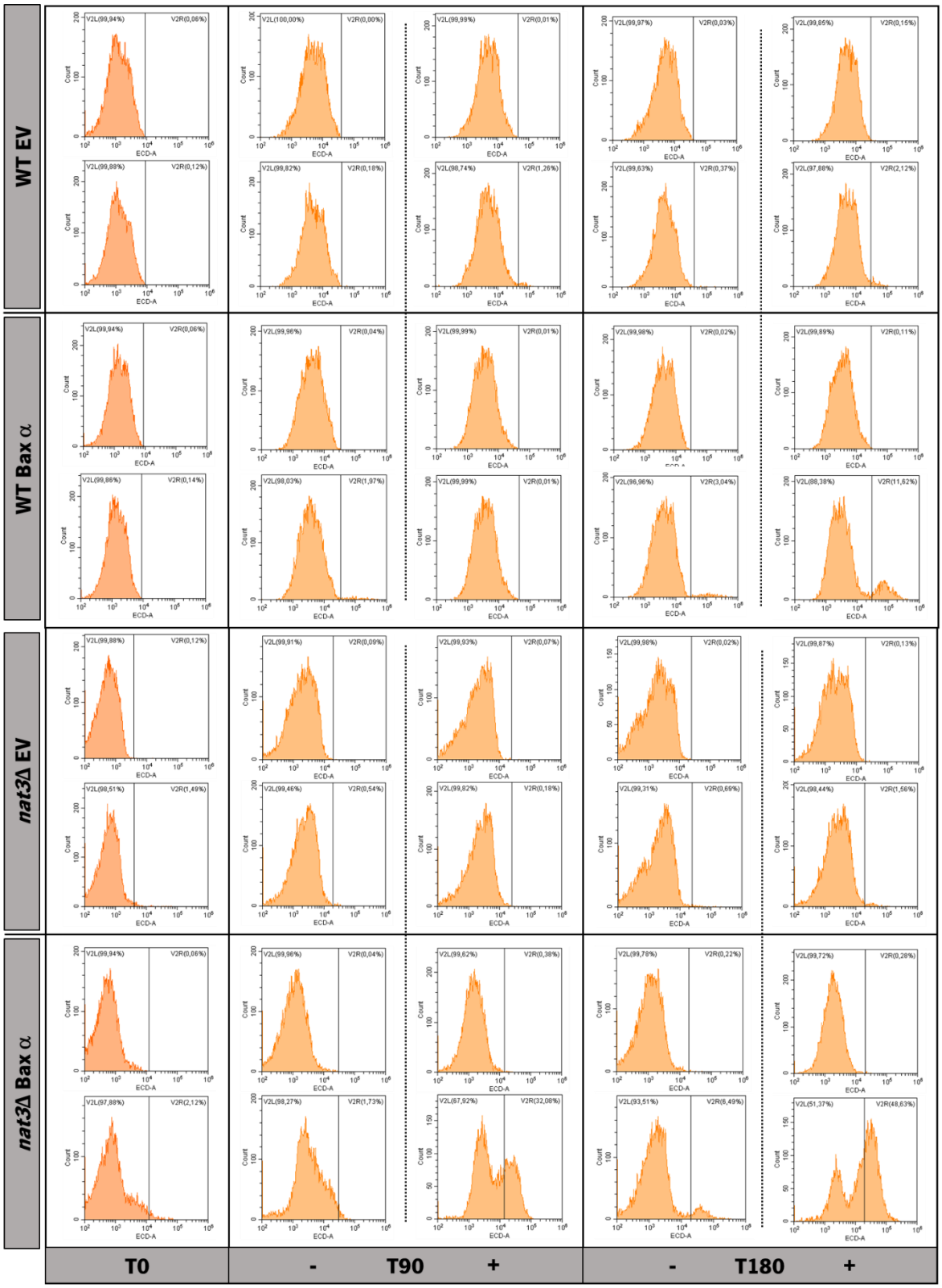

Figure A4: *nat3*Δ yeast cells expressing human Bax α exhibit enhanced loss of plasma membrane integrity in response to acetic acid. Representative monoparametric histograms of the red fluorescence of PI-stained WT and *nat3*Δ yeast cells expressing EV or human Bax α. Cells were treated (+) or not (-) with 160 mM of acetic acid, pH 3.0 for 0, 90 and 180 min and stained with 4 mg/mL of PI for 10 min at RT, in the dark. Cursors were positioned to the right side of

autofluorescence and the values presented in the right side of the histogram were considered PI positive. The histograms shown are representative of three independent experiments.

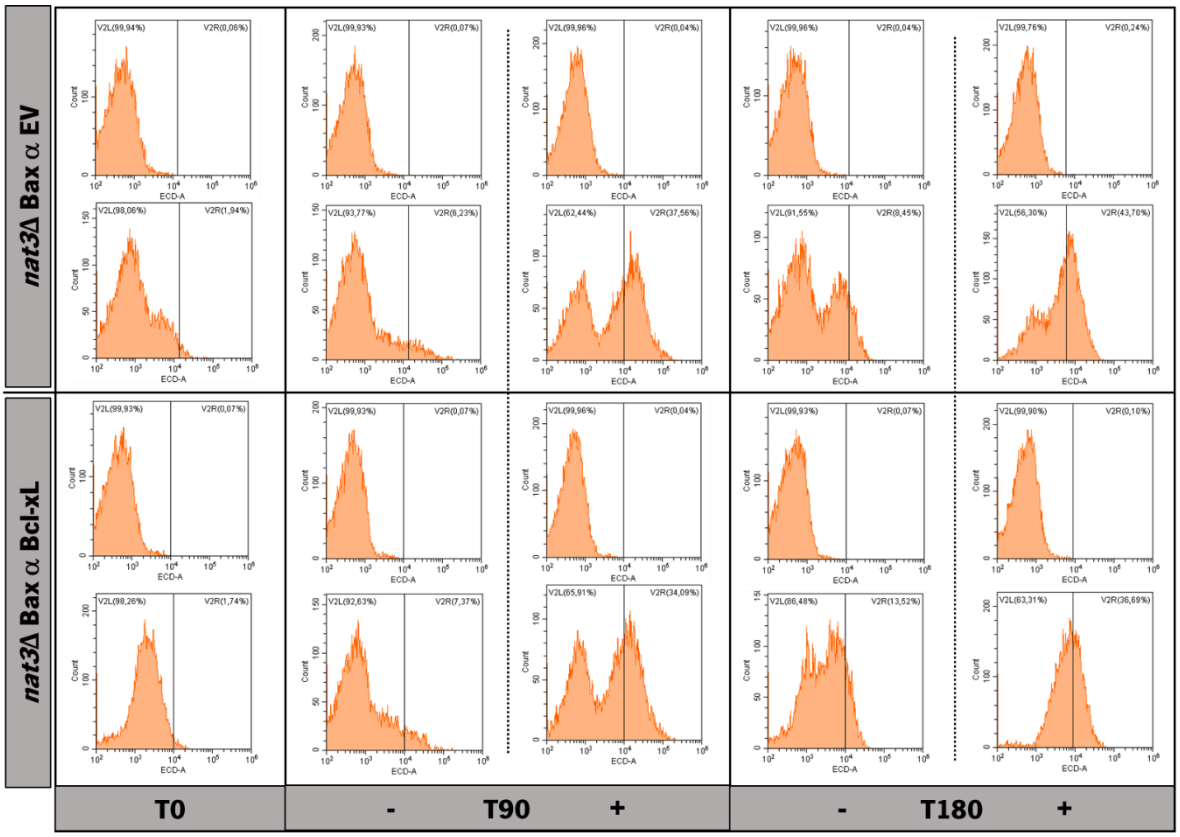

Figure A5: Absence of Nat3p abrogates Bcl-xL protection of human Bax α-expressing yeast cells from acetic acid-induced loss of plasma membrane integrity. Representative monoparametric histograms of the red fluorescence of PI-stained *nat3*Δ yeast cells co-expressing human Bax α and Bcl-xL or the respective empty vector (EV). Cells were treated (+) or not (-) with 160 mM of acetic acid, pH 3.0 for 0, 90 and 180 min and stained with 4 mg/mL PI for 10 min at RT, in the dark. Cursors were positioned to the right side of autofluorescence and the values presented in the right side of the histogram are considered PI positive. The histograms shown are representative of three independent experiments.

Appendix Tables

Table A1: Amino acid single and three letter codes.

Amino acid	Three letter symbol	One letter symbol
ALANINE	Ala	A
ARGININE	Arg	R
ASPARAGINE	Asn	N
ASPARTIC ACID	Asp	D
CYSTEINE	Cys	C
GLUTAMIC ACID	Glu	E
GLUTAMINE	Gln	Q
GLYCINE	Gly	G
HISTIDINE	His	H
ISOLEUCINE	Ile	I
LEUCINE	Leu	L
LYSINE	Lys	K
METHIONINE	Met	M
PHENYLALANINE	Phe	F
PROLINE	Pro	P
SERINE	Ser	S
THREONINE	Thr	T
TRYPTOPHAN	Trp	W
TYROSINE	Tyr	Y
VALINE	Val	V

Table A2: N-terminome analysis of WT and Naa20$^{-/-}$ MEF cells. Analysis of the N-termini quantified at least once condition for which it has been possible to calculate a p-value (2 sided distributions, for 2 samples with equal variance). The theoretical and observed N-termini sequences are presented. The NAT type is predicted for the observed N-termini sequences. NTA percentage of WT and Naa20$^{-/-}$ MEFs as well as NTA difference (%) and ratio between the Naa20$^{-/-}$ and WT are also presented.

UniProt Accession	Entry Name	Protein Description	Theoretical N-ter Sequence	Observed N-ter Sequence	NAT type (observed)	WT %NTA	Naa20$^{-/-}$ %NTA	%NTA Difference (Naa20$^{-/-}$-WT)	Ratio %NTA (Naa20$^{-/-}$/WT)
P62849	RS24_MOUSE	40S ribosomal protein S24	MNDTVTIRTR	MNDTVTIRTR	B	99.4 ± 0.6	33.9 ± 3.4	-65.5	0.341
P17809	GTR1_MOUSE	Solute carrier family 2	MDPSSKKVTG	MDPSSKKVTG	B	99.3 ± 0.7	63.3 ± 2.3	-36.0	0.638
Q8R5J9	PRAF3_MOUSE	PRA1 family protein 3	MDVNLAPLRA	MDVNLAPLRA	B	99.7 ± 0.3	52.8 ± 3.8	-46.9	0.529
Q8K274	KT3K_MOUSE	Ketosamine-3-kinase	METLLKRELG	METLLKRELG	B	100 ± 0	70.9 ± 0.1	-29.1	0.709
P61166	TM258_MOUSE	Transmembrane protein 258	MELEAMSRYT	MELEAMSRYT	B	93.3 ± 4.2	13.4 ± 2.1	-79.9	0.144
Q78JE5	FBX22_MOUSE	F-box only protein 22	MEPAGGGGGV	MEPAGGGGGV	B	100 ± 0	68 ± 2.9	-32.0	0.680
Q8BIW1	PRUN1_MOUSE	Exopolyphosphatase PRUNE1	MEDYLQDCRA	MEDYLQDCRA	B	99.8 ± 0.3	44.9 ± 1.1	-54.9	0.450
Q9CQ71	RFA3_MOUSE	Replication protein A 14 kDa subunit	MEDIMQLPKA	MEDIMQLPKA	B	99.6 ± 0.4	58.5 ± 3.1	-41.1	0.588
Q3UFB2	BCD1_MOUSE	Box C/D snoRNA protein 1	MESAAEKEGT	MESAAEKEGT	B	99.5 ± 0.5	72 ± 1.8	-27.5	0.723
P11983	TCPA_MOUSE	T-complex protein 1 subunit alpha	MEGPLSVFGD	MEGPLSVFGD	B	99.6 ± 0.5	74 ± 4.3	-25.5	0.743
Q9EPL8	IPO7_MOUSE	Importin-7	MDPNTIIEAL	MDPNTIIEAL	B	99.5 ± 0.8	44.3 ± 3.5	-55.1	0.446
Q9CQW9	IFM3_MOUSE	Interferon-induced transmembrane protein 3	MNHTSQAFIT	MNHTSQAFIT	B	98 ± 0.6	32.8 ± 1.8	-65.2	0.335
Q7TMF3	NDUAC_MOUSE	NADH dehydrogenase [ubiquinone] 1 alpha subcomplex subunit 12	MELVEVLKRG	MELVEVLKRG	B	100 ± 0	73.3 ± 2	-26.7	0.733
Q8CAY6	THIC_MOUSE	Acetyl-CoA acetyltransferase	MNAGSDPVVI	MNAGSDPVVI	B	99.6 ± 0.3	76.9 ± 4.4	-22.8	0.772
P63101	1433Z_MOUSE	14-3-3 protein zeta/delta	MDKNELVQKA	MDKNELVQKA	B	99.9 ± 0.1	85.3 ± 1.1	-14.6	0.854
Q9Z2X8	KEAP1_MOUSE	Kelch-like ECH-associated protein 1	MQPEPKLSGA	MQPEPKLSGA	B	99.1 ± 0.7	41.5 ± 1.4	-57.6	0.419
F8VPU2	FARP1_MOUSE	FERM. ARHGEF and pleckstrin domain-containing protein 1	MGEIEQKPTP	GEIEQKPTPA	A	97 ± 2.7	70.4 ± 2.6	-26.6	0.726
P68254	1433T_MOUSE	14-3-3 protein theta	MEKTELIQKA	MEKTELIQKA	B	99.8 ± 0.1	80.7 ± 1.1	-19.0	0.809
Q9D0I9	SYRC_MOUSE	Arginine–tRNA ligase	MDGLVAQCSA	MDGLVAQCSA	B	99.5 ± 0.5	79.5 ± 4.7	-20.0	0.799
O55222	ILK_MOUSE	Integrin-linked protein kinase	MDDIFTQCRE	MDDIFTQCRE	B	99.9 ± 0.1	63.4 ± 0.9	-36.5	0.635

Table A2: N-terminome analysis of WT and Naa20$^{-/-}$ MEF cells (cont).

UniProt Accession	Entry Name	Protein Description	Theoretical N-ter Sequence	Observed N-ter Sequence	NAT type (observed)	WT %NTA	Naa20$^{-/-}$ %NTA	%NTA Difference (Naa20$^{-/-}$-WT)	Ratio %NTA (Naa20$^{-/-}$/WT)
Q8C854	MYEF2_MOUSE	Myelin expression factor 2	MADADKSEAA	ADADKSEAAA	A	99.7 ± 0.2	94 ± 2	-5.7	0.943
P97822	AN32E_MOUSE	Acidic leucine-rich nuclear phosphoprotein 32 family member E	MEMKKKINME	MEMKKKINME	B	100 ± 0	75.8 ± 2.6	-24.2	0.758
Q922Q8	LRC59_MOUSE	Leucine-rich repeat-containing protein 59	MTKAGSKGGN	TKAGSKGGNL	A	50.6 ± 0.5	47.9 ± 0.8	-2.7	0.947
Q9CQU3	RER1_MOUSE	Protein RER1	MSEGDSVGDS	SEGDSVGDSV	A	73.1 ± 0.8	66.7 ± 0.8	-6.4	0.913
Q9ES00	UBE4B_MOUSE	Ubiquitin conjugation factor E4 B	MEELSADEIR	MEELSADEIR	B	99.6 ± 0.5	84.7 ± 3.1	-15.0	0.850
O54724	CAVN1_MOUSE	Caveolae-associated protein 1	MEDVTLHIVE	MEDVTLHIVE	B	99.4 ± 0.8	83.5 ± 1.3	-15.9	0.840
P10922	H10_MOUSE	Histone H1.0	MTENSTSAPA	TENSTSAPAA	A	44.1 ± 0.9	41.6 ± 0.6	-2.6	0.941
P40142	TKT_MOUSE	Transketolase	MEGYHKPDQQ	MEGYHKPDQQ	B	98.9 ± 0.6	93.3 ± 2.1	-5.6	0.944
Q9CQV8	1433B_MOUSE	14-3-3 protein beta/alpha	MTMDKSELVQ	MTMDKSELVQ	C	99.1 ± 0.4	89.5 ± 0.1	-9.6	0.903
Q9R0Q7	TEBP_MOUSE	Prostaglandin E synthase 3	MQPASAKWYD	MQPASAKWYD	B	86.2 ± 7.3	40.7 ± 0.3	-45.5	0.472
D3Z5L6	S18B1_MOUSE	MFS-type transporter SLC18B1	MDEAGSPAPA	MDEAGSPAPA	B	100 ± 0.1	90.2 ± 2.9	-9.8	0.902
Q9D554	SF3A3_MOUSE	Splicing factor 3A subunit 3	METILEQQRR	METILEQQRR	B	99.6 ± 0.5	93.5 ± 3.4	-6.1	0.939
Q9WTV7	RNF12_MOUSE	E3 ubiquitin-protein ligase RLIM	MENSDSNDKG	MENSDSNDKG	B	99.7 ± 0.2	88.6 ± 1.1	-11.1	0.889
Q9CQC6	BZW1_MOUSE	Basic leucine zipper and W2 domain-containing protein 1	MNNQKQQKPT	MNNQKQQKPT	B	99.3 ± 0.7	86.7 ± 6.7	-12.6	0.873
Q9QZ73	DCNL1_MOUSE	DCN1-like protein 1	MNKLKSSQKD	MNKLKSSQKD	B	100 ± 0	96.8 ± 0.4	-3.2	0.968
P97311	MCM6_MOUSE	DNA replication licensing factor MCM6	MDLAAAAEPG	MDLAAAAEPG	B	99.1 ± 0.7	94.2 ± 2.3	-4.9	0.950
Q05CL8	LARP7_MOUSE	La-related protein 7	METENQKTME	METENQKTME	B	99.9 ± 0.1	97.6 ± 1.4	-2.3	0.977
P26041	MOES_MOUSE	Moesin	MPKTISVRVT	PKTISVRVTT	?	1.2 ± 0.4	0.5 ± 0.2	-0.7	0.416
Q9JLR9	HIG1A_MOUSE	HIG1 domain family member 1A	MSTNTDLSLS	STNTDLSLSS	A	99 ± 0.2	99.7 ± 0.1	0.7	1.007
Q99K48	NONO_MOUSE	Non-POU domain-containing octamer-binding protein	MQSNKAFNLE	MQSNKAFNLE	B	98.7 ± 1	94.8 ± 0.6	-3.9	0.960
Q9CYR6	AGM1_MOUSE	Phosphoacetylglucosamine mutase	MDLEAVCKRS	MDLEAVCKRS	B	99.4 ± 0.2	85.8 ± 5.4	-13.7	0.863

Table A2: N-terminome analysis of WT and Naa20$^{-/-}$ MEF cells (cont).

UniProt Accession	Entry Name	Protein Description	Theoretical N-ter Sequence	Observed N-ter Sequence	NAT type (observed)	WT %NTA	Naa20$^{-/-}$ %NTA	%NTA Difference (Naa20$^{-/-}$-WT)	Ratio %NTA (Naa20$^{-/-}$/WT)
P58742	AAAS_MOUSE	Aladin	MCSLGLFPPP	CSLGLFPPPP	?	100 ± 0	5.9 ± 5.5	-94.1	0.059
P60060	SC61G_MOUSE	Protein transport protein Sec61 subunit gamma	MDQVMQFVEP	MDQVMQFVEP	B	99.5 ± 0.5	89.7 ± 6.1	-9.7	0.902
Q9DBR7	MYPT1_MOUSE	Protein phosphatase 1 regulatory subunit 12A	MKMADAKQKR	MKMADAKQKR	C	10.3 ± 0.4	2.2 ± 2.3	-8.1	0.215
Q9DC50	OCTC_MOUSE	Peroxisomal carnitine O-octanoyltransferase	MENQLTKSVE	MENQLTKSVE	B	99.6 ± 0.5	97 ± 1.2	-2.6	0.974
P16858	G3P_MOUSE	Glyceraldehyde-3-phosphate dehydrogenase	MVKVGVNGFG	MVKVGVNGFG	C	64.3 ± 2.6	72.7 ± 1.4	8.4	1.131
Q99P72	RTN4_MOUSE	Reticulon-4	MEDIDQSSLV	MEDIDQSSLV	B	99 ± 0.5	95.1 ± 1.1	-4.0	0.960
Q9Z0P4	PALM_MOUSE	Paralemmin-1	MEVLATDTAS	MEVLATDTAS	B	99.4 ± 0.4	90.8 ± 5.4	-8.6	0.914
P62137	PP1A_MOUSE	Serine/threonine-protein phosphatase PP1-alpha catalytic subunit	MSDSEKLNLD	SDSEKLNLDS	A	99.1 ± 0.3	99.7 ± 0.2	0.6	1.006
Q9CQV8	1433B_MOUSE	14-3-3 protein beta/alpha	MTMDKSELVQ	TMDKSELVQK	A	99.3 ± 0.2	97 ± 0.8	-2.3	0.977
Q9WV03	FA50A_MOUSE	Protein FAM50A	MAQYKGAASE	AQYKGAASEA	A	97.9 ± 0.7	99.4 ± 0.1	1.5	1.015
Q9D3B1	HACD2_MOUSE	Very-long-chain (3R)-3-hydroxyacyl-CoA dehydratase 2	MAAAAATAAT	AAAAATAATK	A	54.1 ± 1.8	57.2 ± 2.1	3.1	1.057
P61327	MGN_MOUSE	Protein mago nashi homolog	MESDFYLRYY	MESDFYLRYY	B	99.2 ± 1.2	96.8 ± 1.4	-2.4	0.976
Q9D2M8	UB2V2_MOUSE	Ubiquitin-conjugating enzyme E2 variant 2	MAVSTGVKVP	AVSTGVKVPR	A	99.8 ± 0.2	99.2 ± 0.4	-0.6	0.994
P62717	RL18A_MOUSE	60S ribosomal protein L18a	MKASGTLREY	MKASGTLREY	C	2.6 ± 0.7	1.5 ± 0.7	-1.1	0.583
P97429	ANXA4_MOUSE	Annexin A4	MEAKGGTVKA	MEAKGGTVKA	B	99.3 ± 0.2	97.4 ± 1	-1.9	0.981
Q9JIW9	RALB_MOUSE	Ras-related protein Ral-B	MAANKGKSQG	AANKGKSQGS	A	95.6 ± 0.6	100 ± 0	4.4	1.046
O88569	ROA2_MOUSE	Heterogeneous nuclear ribonucleoproteins A2/B1	MEKTLETVPL	MEKTLETVPL	B	99.3 ± 0.7	93.9 ± 5.1	-5.4	0.946
P24288	BCAT1_MOUSE	Branched-chain-amino-acid aminotransferase	MKDCSNGCSA	MKDCSNGCSA	C	40.2 ± 0.8	44.9 ± 2.8	4.7	1.116

Table A2: N-terminome analysis of WT and Naa2$^{-/-}$ MEF cells (cont).

UniProt Accession	Entry Name	Protein Description	Theoretical N-ter Sequence	Observed N-ter Sequence	NAT type (observed)	WT %NTA	Naa20$^{-/-}$ %NTA	%NTA Difference (Naa20$^{-/-}$-WT)	Ratio %NTA (Naa20$^{-/-}$/WT)
Q9Z1Q2	ABHGA_MOUSE	Phosphatidylserine lipase ABHD16A	MAKLLSCVLG	AKLLSCVLGP	A	96.3 ± 2.1	93.3 ± 1.1	-3.0	0.969
Q3UPL0	SC31A_MOUSE	Protein transport protein Sec31A	MKLKEIDRTA	MKLKEIDRTA	C	12.2 ± 3.5	8 ± 1.9	-4.1	0.660
Q9EQ61	PESC_MOUSE	Pescadillo homolog	MGGLEKKKYE	GGLEKKKYER	A	1.5 ± 0.4	0.3 ± 0.2	-1.2	0.205
P63038	CH60_MOUSE	60 kDa heat shock protein	MLRLPTVLRQ	AKDVKFGADA	A?	0.7 ± 0.2	0.4 ± 0.2	-0.4	0.481
Q8C4J7	TBL3_MOUSE	Transducin beta-like protein 3	MAETAAGLCR	AETAAGLCRF	A	98.1 ± 0.5	99.6 ± 0	1.5	1.015
Q03265	ATPA_MOUSE	ATP synthase subunit alpha	MLSVRVAAAV	QKTGTAEMSS	?	2.7 ± 1.2	1.1 ± 0.9	-1.6	0.411
Q8QZY9	SF3B4_MOUSE	Splicing factor 3B subunit 4	MAAGPISERN	AAGPISERNQ	A	98.8 ± 0.8	100 ± 0	1.1	1.011
P56480	ATPB_MOUSE	ATP synthase subunit beta	MLSLVGRVAS	QASAAPKAGT	?	0.2 ± 0	0.1 ± 0	-0.1	0.581
Q64674	SPEE_MOUSE	Spermidine synthase	MEPGPDGPAA	MEPGPDGPAA	B	99.5 ± 0.5	96.3 ± 3.5	-3.3	0.967
P62754	RS6_MOUSE	40S ribosomal protein S6	MKLNISFPAT	MKLNISFPAT	C	1.2 ± 0.4	2.2 ± 0.5	1.0	1.877
P26040	EZRI_MOUSE	Ezrin	MPKPINVRVT	PKPINVRVTT	?	1.2 ± 0.2	0.6 ± 0.2	-0.7	0.463
P62843	RS15_MOUSE	40S ribosomal protein S15	MAEVEQKKKR	AEVEQKKKRT	A	99.3 ± 0.6	96.9 ± 2.7	-2.4	0.976
P14685	PSMD3_MOUSE	26S proteasome non-ATPase regulatory subunit 3	MKQEGSARRR	MKQEGSARRR	C	23.8 ± 0.8	26.4 ± 0.9	2.6	1.108
Q80UU9	PGRC2_MOUSE	Membrane-associated progesterone receptor component 2	MAAGDGDVKL	AAGDGDVKLS	A	97.4 ± 0.6	95.8 ± 0.8	-1.7	0.983
E9PVA8	GCN1_MOUSE	eIF-2-alpha kinase activator GCN1	MAADTQVSET	AADTQVSETL	A	76.3 ± 3.1	72.3 ± 3.2	-4.0	0.948
B7ZMP1	XPP3_MOUSE	Xaa-Pro aminopeptidase 3	MPSLLSTPKL	SLQPAPVKKI	A?	0.3 ± 0.2	0.9 ± 0.1	0.6	3.262
O09110	MP2K3_MOUSE	Dual specificity mitogen-activated protein kinase kinase 3	MESPAASPPA	MESPAASPPA	B	99 ± 0.4	99.8 ± 0.2	0.7	1.007
P63087	PP1G_MOUSE	Serine/threonine-protein phosphatase PP1-gamma catalytic subunit	MADIDKLNID	ADIDKLNIDS	A	99.9 ± 0.1	99.5 ± 0.3	-0.4	0.996
Q9ESZ8	GTF2I_MOUSE	General transcription factor II-I	MAQVVMSALP	AQVVMSALPA	A	99.2 ± 0.6	99.8 ± 0.1	0.6	1.006
Q62084	PP14B_MOUSE	Protein phosphatase 1 regulatory subunit 14B	MADSGPAGGA	ADSGPAGGAA	A	99.2 ± 0.6	100 ± 0	0.8	1.008

Table A2: N-terminome analysis of WT and Naa20$^{-/-}$ MEF cells (cont).

UniProt Accession	Entry Name	Protein Description	Theoretical N-ter Sequence	Observed N-ter Sequence	NAT type (observed)	WT %NTA	Naa20$^{-/-}$ %NTA	%NTA Difference (Naa20$^{-/-}$-WT)	Ratio %NTA (Naa20$^{-/-}$/WT)
P63325	RS10_MOUSE	40S ribosomal protein S10	MLMPKKNRIA	MLMPKKNRIA	C	2 ± 0.4	1.4 ± 0.2	-0.5	0.721
P80314	TCPB_MOUSE	T-complex protein 1 subunit beta	MASLSLAPVN	ASLSLAPVNI	A	99.5 ± 0.4	99.9 ± 0.1	0.4	1.004
P17095	HMGA1_MOUSE	High mobility group protein HMG-I/HMG-Y	MSESGSKSSQ	SESGSKSSQP	A	98.8 ± 0.9	99.6 ± 0.3	0.7	1.007
P27773	PDIA3_MOUSE	Protein disulfide-isomerase A3	MRFSCLALLP	SDVLELTDEN	A?	0.6 ± 0.3	0.3 ± 0.2	-0.3	0.471
Q9Z266	SNAPN_MOUSE	SNARE-associated protein Snapin	MAAAGSAAVS	AAAGSAAVSG	A	98.8 ± 0.5	99.8 ± 0.3	1.0	1.010
Q9D6N5	NC2A_MOUSE	Dr1-associated corepressor	MPSKKKKYNA	PSKKKKYNAR	?	0.6 ± 0.2	0.3 ± 0.2	-0.3	0.478
Q9CZ69	CKLF6_MOUSE	CKLF-like MARVEL transmembrane domain-containing protein 6	MENGAVYSPT	MENGAVYSPT	B	98.8 ± 0.7	99.8 ± 0.2	1.0	1.010
P07607	TYSY_MOUSE	Thymidylate synthase	MLVVGSELQS	MLVVGSELQS	C	62.8 ± 1.9	70.2 ± 2.4	7.4	1.118
O35887	CALU_MOUSE	Calumenin	MDLRQFLMCL	KPTEKKDRVH	?	1.4 ± 0.2	0.9 ± 0	-0.5	0.672
P52482	UB2E1_MOUSE	Ubiquitin-conjugating enzyme E2 E1	MSDDDSRAST	SKNSKLLSTS	A?	99.1 ± 0.1	99.7 ± 0.4	0.7	1.007
Q3TSG4	ALKB5_MOUSE	RNA demethylase ALKBH5	MAAASGYTDL	AAASGYTDLR	A	99.7 ± 0.2	100 ± 0	0.3	1.003
Q9DBJ1	PGAM1_MOUSE	Phosphoglycerate mutase 1	MAAYKLVLIR	AAYKLVLIRH	A	99.7 ± 0.3	100 ± 0	0.2	1.002
Q9JKV1	ADRM1_MOUSE	Proteasomal ubiquitin receptor ADRM1	MTTSGALFPS	TTSGALFPSL	A	99.2 ± 0.6	99.8 ± 0.3	0.6	1.006
Q9JJX7	TYDP2_MOUSE	Tyrosyl-DNA phosphodiesterase 2	MASGSSSDAA	ASGSSSDAAE	A	99.7 ± 0.4	99.9 ± 0.1	0.3	1.003
Q60973	RBBP7_MOUSE	Histone-binding protein RBBP7	MASKEMFEDT	ASKEMFEDTV	A	99.3 ± 0.6	99.8 ± 0.3	0.6	1.006
Q8BP71	RFOX2_MOUSE	RNA binding protein fox-1 homolog 2	MAEGGQAQQQ	AEGGQAQQQP	A	99.9 ± 0.2	99.6 ± 0.2	-0.2	0.998
Q64152	BTF3_MOUSE	Transcription factor BTF3	MRRTGAPTQA	MKETIMNQEK	?	6.2 ± 0.2	6.9 ± 0.4	0.8	1.129
Q99KK7	DPP3_MOUSE	Dipeptidyl peptidase 3	MADTQYILPN	ADTQYILPND	A	98.7 ± 0.3	99.2 ± 0.4	0.5	1.005
P49817	CAV1_MOUSE	Caveolin-1	MSGGKYVDSE	SGGKYVDSEG	A	98.2 ± 1.5	99.9 ± 0.1	1.7	1.017
Q61576	FKB10_MOUSE	Peptidyl-prolyl cis-trans isomerase FKBP10	MFLVGSSSHT	SPAGAPLEDV	A?	0.6 ± 0.3	0.3 ± 0.2	-0.3	0.539

Table A2: N-terminome analysis of WT and Naa20$^{-/-}$ MEF cells (cont).

UniProt Accession	Entry Name	Protein Description	Theoretical N-ter Sequence	Observed N-ter Sequence	NAT type (observed)	WT %NTA	Naa20$^{-/-}$ %NTA	%NTA Difference (Naa20$^{-/-}$-WT)	Ratio %NTA (Naa20$^{-/-}$/WT)
Q9D8U8	SNX5_MOUSE	Sorting nexin-5	MAAVPELLEQ	AAVPELLEQQ	A	99.7 ± 0.3	99 ± 0.6	-0.7	0.993
P62270	RS18_MOUSE	40S ribosomal protein S18	MSLVIPEKFQ	SLVIPEKFQH	A	99.5 ± 0.4	100 ± 0	0.4	1.004
Q8CDN6	TXNL1_MOUSE	Thioredoxin-like protein 1	MVGVKPVGSD	MVGVKPVGSD	C	40.5 ± 0.8	45 ± 2.3	4.5	1.111
Q99JX4	EIF3M_MOUSE	Eukaryotic translation initiation factor 3 subunit M	MSVPAFIDIS	SVPAFIDISE	A	99.6 ± 0.4	99.1 ± 0.3	-0.5	0.995
Q8BUY5	TIDC1_MOUSE	Complex I assembly factor TIMMDC1	MGAPPPAPRS	AVAADSPGFV	A?	0.7 ± 0.3	0.1 ± 0.1	-0.6	0.122
Q8BHL3	TB10B_MOUSE	TBC1 domain family member 10B	METGPAPLVA	METGPAPLVA	B	100 ± 0	98.4 ± 1.2	-1.6	0.984
P57776	EF1D_MOUSE	Elongation factor 1-delta	MATNFLAHEK	ATNFLAHEKI	A	99.7 ± 0.3	100 ± 0	0.3	1.003
P25206	MCM3_MOUSE	DNA replication licensing factor MCM3	MAGTVVLDDV	AGTVVLDDVE	A	99.4 ± 0.6	99.9 ± 0.3	0.5	1.005
Q3THK3	T2FA_MOUSE	General transcription factor IIF subunit 1	MAALGSSSQN	AALGSSSQNV	A	98.7 ± 1.5	99.9 ± 0.1	1.2	1.012
O35143	ATIF1_MOUSE	ATPase inhibitor	MAGSALAVRA	SDSSDSMDTG	A?	25 ± 37.5	0.7 ± 0.8	-24.3	0.029
P50516	VATA_MOUSE	V-type proton ATPase catalytic subunit A	MDFSKLPKIR	MDFSKLPKIR	B	99.7 ± 0.3	98.5 ± 1	-1.2	0.988
Q7TSG2	CTDP1_MOUSE	RNA polymerase II subunit A C-terminal domain phosphatase	MEAPPAAGVP	MEAPPAAGVP	B	99.3 ± 0.2	99.7 ± 0.1	0.5	1.005
Q8CIN4	PAK2_MOUSE	Serine/threonine-protein kinase PAK 2	MSDNGELEDK	SDNGELEDKP	A	99.4 ± 0.6	99.8 ± 0.2	0.5	1.005
P37804	TAGL_MOUSE	Transgelin	MANKGPSYGM	ANKGPSYGMS	A	98.6 ± 0.8	97.3 ± 0.9	-1.3	0.987
Q8C878	UBA3_MOUSE	NEDD8-activating enzyme E1 catalytic subunit	MADGEEPEKK	ADGEEPEKKR	A	98.6 ± 0.6	99.8 ± 0.2	1.1	1.012
P46471	PRS7_MOUSE	26S proteasome regulatory subunit 7	MPDYLGADQR	PDYLGADQRK	?	0.3 ± 0.3	0.1 ± 0.1	-0.2	0.244
P97351	RS3A_MOUSE	40S ribosomal protein S3a	MAVGKNKRLT	AVGKNKRLTK	A	0.3 ± 0	0.3 ± 0	0.0	0.879
P61979	HNRPK_MOUSE	Heterogeneous nuclear ribonucleoprotein K	METEQPEETF	METEQPEETF	B	97.9 ± 0.6	99.1 ± 0.2	1.2	1.013
Q9DBH5	LMAN2_MOUSE	Vesicular integral-membrane protein VIP36	MAAEAWLWRW	DITDGNSEHL	?	4.2 ± 2	2.4 ± 1.6	-1.8	0.578

Table A2: N-terminome analysis of WT and Naa20$^{-/-}$ MEF cells (cont).

UniProt Accession	Entry Name	Protein Description	Theoretical N-ter Sequence	Observed N-ter Sequence	NAT type (observed)	WT %NTA	Naa20$^{-/-}$ %NTA	%NTA Difference (Naa20$^{-/-}$-WT)	Ratio %NTA (Naa20$^{-/-}$/WT)
Q99MN1	SYK_MOUSE	Lysine–tRNA ligase	MATLQESEVK	ATLQESEVKV	A	99.3 ± 0.2	99.7 ± 0.2	0.4	1.004
Q02053	UBA1_MOUSE	Ubiquitin-like modifier-activating enzyme 1	MSSSPLSKKR	AKNGSEADID	A?	99.3 ± 0.7	99.8 ± 0.4	0.5	1.005
Q3V3R1	C1TM_MOUSE	Monofunctional C1-tetrahydrofolate synthase	MSVRLPLLLR	SSSGGGDPEG	A?	1.4 ± 0.7	2.8 ± 1.5	1.4	2.021
P31786	ACBP_MOUSE	Acyl-CoA-binding protein	MSQAEFDKAA	SQAEFDKAAE	A	99.8 ± 0.1	99.6 ± 0.3	-0.2	0.998
Q61249	IGBP1_MOUSE	Immunoglobulin-binding protein 1	MAASEDELLL	AASEDELLLP	A	99.3 ± 0.3	99.7 ± 0.4	0.5	1.005
Q7TND5	RPF1_MOUSE	Ribosome production factor 1	MAKAGEKSVG	AKAGEKSVGG	A	28.4 ± 1.3	25.7 ± 3.1	-2.7	0.904
Q9DBE9	SPB1_MOUSE	pre-rRNA 2'-O-ribose RNA methyltransferase FTSJ3	MGKKGKVGKS	GKKGKVGKSR	A	1.2 ± 0.7	0.5 ± 0.3	-0.7	0.436
Q9D1G2	PMVK_MOUSE	Phosphomevalonate kinase	MAPLGASPRL	APLGASPRLV	A	0.4 ± 0.3	0 ± 0	-0.3	0.107
Q9Z0Y1	DCTN3_MOUSE	Dynactin subunit 3	MAALTDVQRL	AALTDVQRLQ	A	99.9 ± 0	100 ± 0	0.1	1.001
Q9ERE7	MESD_MOUSE	LRP chaperone MESD	MAASRWLRAV	ADTPGEATPP	A?	1.1 ± 0.8	0.3 ± 0.3	-0.7	0.313
Q99M08	CD003_MOUSE	Uncharacterized protein C4orf3 homolog	MEVSQAASGT	MEVSQAASGT	B	99.1 ± 0.6	97.7 ± 2.3	-1.5	0.985
Q99KJ8	DCTN2_MOUSE	Dynactin subunit 2	MADPKYADLP	ADPKYADLPG	A	100 ± 0	99.8 ± 0.1	-0.2	0.998
Q8CB77	ELOA1_MOUSE	Elongin-A	MAAESALQVV	AAESALQVVE	A	96 ± 1.4	92.3 ± 3	-3.7	0.961
O35887	CALU_MOUSE	Calumenin	MDLRQFLMCL	LSKPTEKKDR	?	0.9 ± 0.1	0.5 ± 0.3	-0.4	0.555
Q9CVB6	ARPC2_MOUSE	Actin-related protein 2/3 complex subunit 2	MILLEVNNRI	MILLEVNNRI	C	0.3 ± 0.2	0.6 ± 0.5	0.3	2.042
Q8VBW6	ULA1_MOUSE	NEDD8-activating enzyme E1 regulatory subunit	MAQPGKILKE	AQPGKILKEQ	A	99.6 ± 0.4	100 ± 0	0.3	1.003
P35279	RAB6A_MOUSE	Ras-related protein Rab-6A	MSAGGDFGNP	SAGGDFGNPL	A	99.2 ± 0.7	97.9 ± 1.5	-1.3	0.987
Q3UVL4	VPS51_MOUSE	Vacuolar protein sorting-associated protein 51 homolog	MAAAAAVGPG	AAAAAVGPGL	A	87 ± 11.8	98.8 ± 0.6	11.8	1.136
Q01730	RSU1_MOUSE	Ras suppressor protein 1	MSKSLKKLVE	SKSLKKLVEE	A	98.9 ± 0.6	99.7 ± 0.3	0.8	1.008

Table A2: N-terminome analysis of WT and Naa20$^{-/-}$ MEF cells (cont).

UniProt Accession	Entry Name	Protein Description	Theoretical N-ter Sequence	Observed N-ter Sequence	NAT type (observed)	WT %NTA	Naa20$^{-/-}$ %NTA	%NTA Difference (Naa20$^{-/-}$-WT)	Ratio %NTA (Naa20$^{-/-}$/WT)
Q9CPT5	NOP16_MOUSE	Nucleolar protein 16	MPKAKGKTRR	PKAKGKTRRQ	?	0.4 ± 0	0.4 ± 0	0.0	1.085
P13020	GELS_MOUSE	Gelsolin	MAPYRSSLLC	VVEHPEFLKA	A?	3.1 ± 2.5	0.9 ± 0.3	-2.2	0.300
P63037	DNJA1_MOUSE	DnaJ homolog subfamily A member 1	MVKETTYYDV	VKETTYYDVL	A	1.5 ± 0.5	0.5 ± 0.2	-0.9	0.355
Q6PB66	LPPRC_MOUSE	Leucine-rich PPR motif-containing protein	MAALLRPARW	AIVAEKRDLQ	A?	0.3 ± 0.3	0.1 ± 0.1	-0.2	0.408
O89050	MKLN1_MOUSE	Muskelin	MAAGGAVAVA	AAGGAVAVAP	A	98.2 ± 1.7	99.3 ± 0.6	1.2	1.012
P97825	JUPI1_MOUSE	Jupiter microtubule associated homolog 1	MTTTTTFKGV	TTTTTFKGVD	A	99.4 ± 0.2	99.8 ± 0.3	0.4	1.004
Q9QZD9	EIF3I_MOUSE	Eukaryotic translation initiation factor 3 subunit I	MKPILLQGHE	MKPILLQGHE	C	3.4 ± 2.7	1.2 ± 0.4	-2.2	0.350
Q5XJY5	COPD_MOUSE	Coatomer subunit delta	MVLLAAAVCT	VLLAAAVCTK	A	0.5 ± 0.2	1.6 ± 0.9	1.1	3.376
P10922	H10_MOUSE	Histone H1.0	MTENSTSAPA	MTENSTSAPA	C	98.1 ± 2.2	99.4 ± 0.6	1.3	1.014
P10107	ANXA1_MOUSE	Annexin A1	MAMVSEFLKQ	AMVSEFLKQA	A	99.6 ± 0.4	99.8 ± 0.3	0.3	1.003
Q64310	SURF4_MOUSE	Surfeit locus protein 4	MGQNDLMGTA	GQNDLMGTAE	A	3.2 ± 0.9	2.4 ± 0.1	-0.8	0.746
P22935	RABP2_MOUSE	Cellular retinoic acid-binding protein 2	MPNFSGNWKI	PNFSGNWKII	?	0.8 ± 0.5	1.5 ± 0.9	0.7	1.852
Q9CQW0	EMC6_MOUSE	ER membrane protein complex subunit 6	MAAVVAKREG	AAVVAKREGP	A	100 ± 0	99.9 ± 0.1	-0.1	0.999
P19157	GSTP1_MOUSE	Glutathione S-transferase P 1	MPPYTIVYFP	PPYTIVYFPV	?	0.6 ± 0.5	1.1 ± 0.7	0.6	2.034
Q03265	ATPA_MOUSE	ATP synthase subunit alpha. mitochondrial	MLSVRVAAAV	KTGTAEMSSI	?	0.1 ± 0.1	0.5 ± 0.4	0.4	5.668
Q9JK23	PSMG1_MOUSE	Proteasome assembly chaperone 1	MAATFFGEVV	AATFFGEVVK	A	99.7 ± 0.4	100 ± 0	0.3	1.003
O35215	DOPD_MOUSE	D-dopachrome decarboxylase	MPFVELETNL	PFVELETNLP	?	5.6 ± 4.8	10.8 ± 2.6	5.3	1.946

Table A2: N-terminome analysis of WT and Naa20$^{-/-}$ MEF cells (cont).

UniProt Accession	Entry Name	Protein Description	Theoretical N-ter Sequence	Observed N-ter Sequence	NAT type (observed)	WT %NTA	Naa20$^{-/-}$ %NTA	%NTA Difference (Naa20$^{-/-}$-WT)	Ratio %NTA (Naa20$^{-/-}$/WT)
Q91VJ5	PQBP1_MOUSE	Polyglutamine-binding protein 1	MPLPVALQTR	PLPVALQTRL	?	0.4 ± 0.3	0.3 ± 0.2	-0.2	0.572
E9Q5G3	KIF23_MOUSE	Kinesin-like protein KIF23	MKSAKAKTVR	MKSAKAKTVR	C	96.4 ± 2.6	98.9 ± 1.6	2.4	1.025
P16546	SPTN1_MOUSE	Spectrin alpha chain. non-erythrocytic 1	MDPSGVKVLE	MDPSGVKVLE	B	98.9 ± 0.8	99.6 ± 0.4	0.7	1.007
Q61206	PA1B2_MOUSE	Platelet-activating factor acetylhydrolase IB subunit alpha2	MSQGDSNPAA	SQGDSNPAAI	A	98.7 ± 0.3	99.4 ± 0.6	0.7	1.007
Q9CPT4	MYDGF_MOUSE	Myeloid-derived growth factor	MAAPSGGFWT	VSEPTTVPFD	A?	0.1 ± 0	0 ± 0	0.0	0.469
Q9DBC7	KAP0_MOUSE	cAMP-dependent protein kinase type I-alpha regulatory subunit	MASGSMATSE	ASGSMATSEE	A	99.5 ± 0.8	99.9 ± 0.1	0.4	1.004
Q9CQS8	SC61B_MOUSE	Protein transport protein Sec61 subunit beta	MPGPTPSGTN	PGPTPSGTNV	?	0.9 ± 0.3	0.7 ± 0.3	-0.2	0.774
Q6PD26	PIGS_MOUSE	GPI transamidase component PIG-S	MAAAGAAATD	AAAGAAATDL	A	19.6 ± 1.9	11 ± 11	-8.6	0.562
P48678	LMNA_MOUSE	Prelamin-A/C	METPSQRRAT	METPSQRRAT	B	99.8 ± 0.2	99.1 ± 0.9	-0.7	0.993
Q8VEK0	CC50A_MOUSE	Cell cycle control protein 50A	MAMNYSAKDE	AMNYSAKDEV	A	98.7 ± 0.3	97.9 ± 0.7	-0.8	0.992
P60710	ACTB_MOUSE	Actin. cytoplasmic 1	MDDDIAALVV	DDDIAALVVD	?	99.6 ± 0.5	99.8 ± 0.2	0.2	1.002
P16045	LEG1_MOUSE	Galectin-1	MACGLVASNL	ACGLVASNLN	A	99.6 ± 0.4	99.9 ± 0.2	0.3	1.003
P07356	ANXA2_MOUSE	Annexin A2	MSTVHEILCK	STVHEILCKL	A	98.2 ± 0.6	99.5 ± 0.4	1.3	1.013
Q62203	SF3A2_MOUSE	Splicing factor 3A subunit 2	MDFQHRPGGK	MDFQHRPGGK	B	99.1 ± 0.6	97.1 ± 2.8	-2.0	0.980
Q6P8I4	PCNP_MOUSE	PEST proteolytic signal-containing nuclear protein	MADGKAGEEK	ADGKAGEEKP	A	96.4 ± 2.5	94.7 ± 0.2	-1.8	0.982
Q9D753	EXOS8_MOUSE	Exosome complex component RRP43	MAAGFKTVEP	AAGFKTVEPL	A	98.3 ± 0.9	95.2 ± 4.7	-3.1	0.968
Q60876	4EBP1_MOUSE	Eukaryotic translation initiation factor 4E-binding protein 1	MSAGSSCSQT	SAGSSCSQTP	A	100 ± 0	100 ± 0	0.0	1.000
Q8BMA6	SRP68_MOUSE	Signal recognition particle subunit SRP68	MAAEKQIPGG	AAEKQIPGGG	A	54.2 ± 1.4	51.6 ± 0.6	-2.6	0.952

Table A2: N-terminome analysis of WT and Naa20$^{-/-}$ MEF cells (cont).

UniProt Accession	Entry Name	Protein Description	Theoretical N-ter Sequence	Observed N-ter Sequence	NAT type (observed)	WT %NTA	Naa20$^{-/-}$ %NTA	%NTA Difference (Naa20$^{-/-}$-WT)	Ratio %NTA (Naa20$^{-/-}$/WT)
Q4VAA2	CDV3_MOUSE	Protein CDV3	MAETEERSLD	AASGAGGSSA	A?	0.1 ± 0.1	0.4 ± 0.3	0.3	7.061
P49586	PCY1A_MOUSE	Choline-phosphate cytidylyltransferase A	MDAQSSAKVN	MDAQSSAKVN	B	99.9 ± 0.3	100 ± 0	0.1	1.001
Q9CZU6	CISY_MOUSE	Citrate synthase. mitochondrial	MALLTAATRL	ASASSTNLKD	A?	0.7 ± 0.2	0.4 ± 0.1	-0.3	0.636
P97379	G3BP2_MOUSE	Ras GTPase-activating protein-binding protein 2	MVMEKPSPLL	VMEKPSPLLV	A	2.8 ± 1.4	1.9 ± 0.9	-0.9	0.687
Q60972	RBBP4_MOUSE	Histone-binding protein RBBP4	MADKEAAFDD	ADKEAAFDDA	A	99.2 ± 0.7	99.6 ± 0.5	0.4	1.004
Q6DVA0	LEMD2_MOUSE	LEM domain-containing protein 2	MAGLSDLELR	AGLSDLELRR	A	99.3 ± 0.8	100 ± 0	0.7	1.007
Q6ZWU9	RS27_MOUSE	40S ribosomal protein S27	MPLAKDLLHP	PLAKDLLHPS	?	0.9 ± 0.2	1.1 ± 0.3	0.2	1.190
Q9CQA5	MED4_MOUSE	Mediator of RNA polymerase II transcription subunit 4	MAASSSGEKE	AASSSGEKEK	A	99.4 ± 0.8	99.8 ± 0.3	0.4	1.004
P0C0S6	H2AZ_MOUSE	Histone H2A.Z	MAGGKAGKDS	AGGKAGKDSG	A	3.5 ± 1.3	4.3 ± 0.5	0.8	1.226
P61620	S61A1_MOUSE	Protein transport protein Sec61 subunit alpha isoform 1	MAIKFLEVIK	AIKFLEVIKP	A	2.7 ± 0.1	2.4 ± 0.2	-0.3	0.879
Q3UHJ0	AAK1_MOUSE	AP2-associated protein kinase 1	MKKFFDSRRE	MKKFFDSRRE	C	99.1 ± 0.8	100 ± 0	0.9	1.009
P31230	AIMP1_MOUSE	Aminoacyl tRNA synthase complex-interacting multifunctional protein 1	MATNDAVLKR	ATNDAVLKRL	A	79.5 ± 35.7	99 ± 0.6	19.5	1.245
P17426	AP2A1_MOUSE	AP-2 complex subunit alpha-1	MPAVSKGDGM	PAVSKGDGMR	?	0.6 ± 0.3	0.4 ± 0.2	-0.2	0.698
P63154	CRNL1_MOUSE	Crooked neck-like protein 1	MAASTAAGKQ	AASTAAGKQR	A	100 ± 0	99.7 ± 0.2	-0.3	0.997
Q9DCM4	DNAL4_MOUSE	Dynein axonemal light chain 4	MGETEGKKEE	GETEGKKEEA	A	98.9 ± 1.1	97.6 ± 0.5	-1.3	0.987
Q9WUD1	CHIP_MOUSE	E3 ubiquitin-protein ligase CHIP	MKGKEEKEGG	MKGKEEKEGG	C	16.7 ± 8.4	21.9 ± 2	5.2	1.313
Q9QX47	SON_MOUSE	Protein SON	MAADIEQVFR	AADIEQVFRS	A	99.2 ± 0.9	99.8 ± 0.2	0.6	1.006
Q9D824	FIP1_MOUSE	Pre-mRNA 3'-end-processing factor FIP1	MSAGEVERLV	SAGEVERLVE	A	100 ± 0	99.6 ± 0.4	-0.4	0.996

Table A2: N-terminome analysis of WT and Naa20$^{-/-}$ MEF cells (cont).

UniProt Accession	Entry Name	Protein Description	Theoretical N-ter Sequence	Observed N-ter Sequence	NAT type (observed)	WT %NTA	Naa20$^{-/-}$ %NTA	%NTA Difference (Naa20$^{-/-}$-WT)	Ratio %NTA (Naa20$^{-/-}$/WT)
P62077	TIM8B_MOUSE	Mitochondrial import inner membrane translocase subunit Tim8 B	MAELGEADEA	AELGEADEAE	A	98.7 ± 1.2	99.7 ± 0.4	1.0	1.010
P62196	PRS8_MOUSE	26S proteasome regulatory subunit 8	MALDGPEQME	ALDGPEQMEL	A	99.2 ± 0.9	99.8 ± 0.2	0.5	1.006
Q9CWJ9	PUR9_MOUSE	Bifunctional purine biosynthesis protein ATIC	MAPSQLALFS	APSQLALFSV	A	1.2 ± 0.4	0.8 ± 0.3	-0.5	0.626
Q8CIV8	TBCE_MOUSE	Tubulin-specific chaperone E	MSDILPLDVI	SDILPLDVIG	A	100 ± 0	97.8 ± 1.4	-2.2	0.978
Q9WVL3	S12A7_MOUSE	Solute carrier family 12 member 7	MPTNFTVVPV	PTNFTVVPVE	?	0.1 ± 0.1	0.2 ± 0.1	0.1	2.147
P56480	ATPB_MOUSE	ATP synthase subunit beta	MLSLVGRVAS	AAQASAAPKA	A?	0.4 ± 0.2	0.5 ± 0.2	0.1	1.358
Q9R0P6	SC11A_MOUSE	Signal peptidase complex catalytic subunit SEC11A	MLSLDFLDDV	MLSLDFLDDV	C	2.6 ± 2.6	6.5 ± 0.4	3.9	2.516
O70493	SNX12_MOUSE	Sorting nexin-12	MSDTAVADTR	SDTAVADTRR	A	99.9 ± 0	99.3 ± 1.3	-0.7	0.993
Q9DBS1	TMM43_MOUSE	Transmembrane protein 43	MAANYSSTSS	AANYSSTSSR	A	99.6 ± 0.3	97.6 ± 2.4	-1.9	0.980
Q91YE3	EGLN1_MOUSE	Egl nine homolog 1	MASDSGGPGV	ASDSGGPGVL	A	99.9 ± 0.1	100 ± 0	0.1	1.001
Q9D2U5	LSMD1_MOUSE	N-alpha-acetyltransferase 38. NatC auxiliary subunit	MAGAGPTMLL	AGAGPTMLLR	A	100 ± 0	100 ± 0	0.0	1.000
Q80YR4	ZN598_MOUSE	E3 ubiquitin-protein ligase ZNF598	MAAAAGAEGR	AAAAGAEGRR	A	99.8 ± 0.1	100 ± 0	0.2	1.002
Q8BKC5	IPO5_MOUSE	Importin-5	MAAAAAEQQQ	AAAAAEQQQF	A	99.6 ± 0.1	99.8 ± 0.2	0.2	1.002
Q9QYJ0	DNJA2_MOUSE	DnaJ homolog subfamily A member 2	MANVADTKLY	ANVADTKLYD	A	98.8 ± 0.6	99.6 ± 0.1	0.8	1.009
Q9CSN1	SNW1_MOUSE	SNW domain-containing protein 1	MALTSFLPAP	ALTSFLPAPT	A	98.5 ± 0.6	99.1 ± 0.3	0.6	1.006
P61759	PFD3_MOUSE	Prefoldin subunit 3	MAAAKDGCGL	AAAKDGCGLE	A	98.1 ± 0.3	97.5 ± 0.7	-0.6	0.994
Q91X20	ASH2L_MOUSE	Set1/Ash2 histone methyltransferase complex subunit ASH2	MAAAGAGPGP	AAAGAGPGPG	A	98.7 ± 0.7	99.1 ± 0.6	0.4	1.004
P17742	PPIA_MOUSE	Peptidyl-prolyl cis-trans isomerase A	MVNPTVFFDI	VNPTVFFDIT	A	37.2 ± 15.9	48.2 ± 2.7	11.1	1.298
P19253	RL13A_MOUSE	60S ribosomal protein L13a	MAEGQVLVLD	AEGQVLVLDG	A	77.6 ± 3	75.4 ± 4.3	-2.2	0.971

Table A2: N-terminome analysis of WT and Naa20$^{-/-}$ MEF cells (cont).

UniProt Accession	Entry Name	Protein Description	Theoretical N-ter Sequence	Observed N-ter Sequence	NAT type (observed)	WT %NTA	Naa20$^{-/-}$ %NTA	%NTA Difference (Naa20$^{-/-}$-WT)	Ratio %NTA (Naa20$^{-/-}$/WT)
Q99JY0	ECHB_MOUSE	Trifunctional enzyme subunit beta	MTTILTSTFR	SAPAVQTKSK	A?	2.3 ± 0.3	1.8 ± 0.4	-0.5	0.770
P19783	COX41_MOUSE	Cytochrome c oxidase subunit 4 isoform 1	MLASRALSLI	AHGSVVKSED	A?	1.1 ± 0.6	14.5 ± 13.7	13.4	12.697
Q6ZWM4	LSM8_MOUSE	U6 snRNA-associated Sm-like protein LSm8	MTSALENYIN	TSALENYINR	A	97.9 ± 1.7	98.9 ± 1.4	1.1	1.011
Q9JLI8	SART3_MOUSE	Squamous cell carcinoma antigen recognized by T-cells 3	MATTAASSAS	ATTAASSASE	A	98.6 ± 0.4	99.3 ± 0.1	0.7	1.007
Q9DCM0	ETHE1_MOUSE	Persulfide dioxygenase ETHE1	MASAVVRVAG	SQQSASGAPV	A?	3.2 ± 2.7	0 ± 0	-3.2	0.012
Q923D2	BLVRB_MOUSE	Flavin reductase	MTVKKIAIFG	TVKKIAIFGA	A	0.3 ± 0.1	1.4 ± 1.1	1.1	5.022
Q8CIE6	COPA_MOUSE	Coatomer subunit alpha	MLTKFETKSA	MLTKFETKSA	C	6.9 ± 1.1	5.7 ± 2.3	-1.2	0.829
Q9D823	RL37_MOUSE	60S ribosomal protein L37	MTKGTSSFGK	TKGTSSFGKR	A	14.7 ± 34.8	0.3 ± 0.1	-14.5	0.019
P10605	CATB_MOUSE	Cathepsin B	MWWSLILLSC	IDLPETFDAR	?	0.6 ± 0.4	0.4 ± 0.3	-0.2	0.659
Q01405	SC23A_MOUSE	Protein transport protein Sec23A	MTTYLEFIQQ	TTYLEFIQQN	A	92.4 ± 8	98 ± 0.6	5.6	1.060
P70295	AUP1_MOUSE	Lipid droplet-regulating VLDL assembly factor AUP1	MEPPPAPGPE	MEPPPAPGPE	B	99.8 ± 0.1	99.6 ± 0.1	-0.2	0.998
Q922Q8	LRC59_MOUSE	Leucine-rich repeat-containing protein 59	MTKAGSKGGN	MTKAGSKGGN	C	98.2 ± 1.9	99.8 ± 0.3	1.6	1.016
O08547	SC22B_MOUSE	Vesicle-trafficking protein SEC22b	MVLLTMIARV	VLLTMIARVA	A	0.6 ± 0.3	0.9 ± 0.5	0.3	1.502
Q99K85	SERC_MOUSE	Phosphoserine aminotransferase	MEATKQVVNF	MEATKQVVNF	B	99.7 ± 0.3	99.3 ± 0.6	-0.4	0.996
O70435	PSA3_MOUSE	Proteasome subunit alpha type-3	MSSIGTGYDL	SSIGTGYDLS	A	99.2 ± 0.5	99.5 ± 0.3	0.3	1.003
O54774	AP3D1_MOUSE	AP-3 complex subunit delta-1	MALKMVKGSI	ALKMVKGSID	A	99.6 ± 0.4	99.9 ± 0.3	0.3	1.003
Q7TSV4	PGM2_MOUSE	Phosphoglucomutase-2	MAAATPTETP	AAATPTETPA	A	99.7 ± 0.6	100 ± 0	0.3	1.003
Q91WQ3	SYYC_MOUSE	Tyrosine–tRNA ligase	MGDAPSPEEK	GDAPSPEEKL	A	93.1 ± 0.7	92.2 ± 0.8	-0.9	0.990
P54818	GALC_MOUSE	Galactocerebrosidase	MANSQPKASQ	YVLDDSDGLG	?	0.2 ± 0.2	0.1 ± 0.1	-0.1	0.387
Q9DAS9	GBG12_MOUSE	Guanine nucleotide-binding protein G(I)/G(S)/G(O) subunit gamma-12	MSSKTASTNS	SSKTASTNSI	A	97.8 ± 1.7	99 ± 1	1.3	1.013

Table A2: N-terminome analysis of WT and Naa20$^{-/-}$ MEF cells (cont).

UniProt Accession	Entry Name	Protein Description	Theoretical N-ter Sequence	Observed N-ter Sequence	NAT type (observed)	WT %NTA	Naa20$^{-/-}$ %NTA	%NTA Difference (Naa20$^{-/-}$-WT)	Ratio %NTA (Naa20$^{-/-}$/WT)
P61087	UBE2K_MOUSE	Ubiquitin-conjugating enzyme E2 K	MANIAVQRIK	ANIAVQRIKR	A	99.8 ± 0.1	99.9 ± 0	0.2	1.002
Q9D8S3	ARFG3_MOUSE	ADP-ribosylation factor GTPase-activating protein 3	MGDPSKQDIL	GDPSKQDILA	A	99.8 ± 0.2	99.6 ± 0.3	-0.2	0.998
O70439	STX7_MOUSE	Syntaxin-7	MSYTPGIGGD	SYTPGIGGDS	A	99.4 ± 0.5	98.9 ± 1.2	-0.5	0.995
P51655	GPC4_MOUSE	Glypican-4	MARLGLLALL	AELKSKSCSE	A?	0.3 ± 0.1	0.2 ± 0.1	-0.1	0.546
P39749	FEN1_MOUSE	Flap endonuclease 1	MGIHGLAKLI	GIHGLAKLIA	A	0.5 ± 0.3	0.3 ± 0.2	-0.2	0.617
Q61508	ECM1_MOUSE	Extracellular matrix protein 1	MGTVSRAALI	ASEGAFKASD	A?	1 ± 1.3	0.2 ± 0.2	-0.8	0.162
P39098	MA1A2_MOUSE	Mannosyl-oligosaccharide 1,2-alpha-mannosidase IB	MTTPALLPLS	TTPALLPLSG	A	64.9 ± 1.2	64 ± 0.4	-0.9	0.986
P67778	PHB_MOUSE	Prohibitin	MAAKVFESIG	AAKVFESIGK	A	100 ± 0	99.7 ± 0.3	-0.3	0.997
P27048	RSMB_MOUSE	Small nuclear ribonucleoprotein-associated protein B	MTVGKSSKML	TVGKSSKMLQ	A	4.5 ± 2.3	22.4 ± 34.7	17.8	4.920
P62311	LSM3_MOUSE	U6 snRNA-associated Sm-like protein LSm3	MADDVDQQQT	ADDVDQQQTT	A	99.2 ± 1.4	98.1 ± 0.6	-1.1	0.989
Q8C4B4	U119B_MOUSE	Protein unc-119 homolog B	MSGSNPKAAT	SGSNPKAATA	A	96.7 ± 1.8	99.2 ± 0.7	2.5	1.025
P61358	RL27_MOUSE	60S ribosomal protein L27	MGKFMKPGKV	GKFMKPGKVV	A	5.9 ± 0.2	5.6 ± 0.5	-0.3	0.948
Q8CIG8	ANM5_MOUSE	Protein arginine N-methyltransferase 5	MAAMAVGGAG	AAMAVGGAGG	A	97.2 ± 3.3	98.8 ± 1.6	1.6	1.016
Q9D0R2	SYTC_MOUSE	Threonine–tRNA ligase 1	MSQEKASSPS	SQEKASSPSG	A	99.5 ± 0.5	99.8 ± 0.1	0.3	1.003
P30681	HMGB2_MOUSE	High mobility group protein B2	MGKGDPNKPR	GKGDPNKPRG	A	0.8 ± 0.3	13.2 ± 32.8	12.5	17.475
Q9EPV8	UBL5_MOUSE	Ubiquitin-like protein 5	MIEVVCNDRL	MIEVVCNDRL	C	0 ± 0	0.2 ± 0.2	0.2	9.050
Q8VEJ4	NLE1_MOUSE	Notchless protein homolog 1	MAAAVVEEAA	AAAVVEEAAA	A	98.7 ± 0.8	98 ± 1.2	-0.7	0.993
P63242	IF5A1_MOUSE	Eukaryotic translation initiation factor 5A-1	MADDLDFETG	ADDLDFETGD	A	99.7 ± 0.1	99.5 ± 0.2	-0.2	0.998
Q62432	SMAD2_MOUSE	Mothers against decapentaplegic homolog 2	MSSILPFTPP	SSILPFTPPV	A	99.8 ± 0.1	99.4 ± 0.3	-0.4	0.996
P10605	CATB_MOUSE	Cathepsin B	MWWSLILLSC	LPETFDAREQ	?	0 ± 0	0.1 ± 0	0.1	3.076

Table A2: N-terminome analysis of WT and Naa20$^{-/-}$ MEF cells (cont).

UniProt Accession	Entry Name	Protein Description	Theoretical N-ter Sequence	Observed N-ter Sequence	NAT type (observed)	WT %NTA	Naa20$^{-/-}$ %NTA	%NTA Difference (Naa20$^{-/-}$-WT)	Ratio %NTA (Naa20$^{-/-}$/WT)
Q9D0G0	RT30_MOUSE	28S ribosomal protein S30	MAAARYWKLV	LSQNAAAKAS	?	0.6 ± 0.1	0.5 ± 0	-0.1	0.762
Q91YQ5	RPN1_MOUSE	Dolichyl-diphosphooligosaccharide–protein glycosyltransferase subunit 1	MESPVALLLL	SSEAPPLVNE	A?	1.1 ± 0.5	0.8 ± 0.2	-0.3	0.763
Q9QXX4	CMC2_MOUSE	Calcium-binding mitochondrial carrier protein Aralar2	MAAAKVALTK	AAAKVALTKR	A	99.8 ± 0.2	99.9 ± 0.2	0.1	1.001
P17225	PTBP1_MOUSE	Polypyrimidine tract-binding protein 1	MDGIVPDIAV	GNDSKKFKGD	A?	11.4 ± 11.8	0.4 ± 0.2	-11.0	0.035
Q8BGQ7	SYAC_MOUSE	Alanine–tRNA ligase	MDATLTAREI	MDATLTAREI	B	99.4 ± 0.5	99.7 ± 0.5	0.3	1.003
P58771	TPM1_MOUSE	Tropomyosin alpha-1 chain	MDAIKKKMQM	MDAIKKKMQM	B	100 ± 0	100 ± 0	0.0	1.000
Q569Z6	TR150_MOUSE	Thyroid hormone receptor-associated protein 3	MSKTNKSKSG	SKTNKSKSGS	A	96 ± 0.8	97.1 ± 1.8	1.2	1.012
Q9QZ08	NAGK_MOUSE	N-acetyl-D-glucosamine kinase	MAALYGGVEG	AALYGGVEGG	A	99.2 ± 0.1	99.4 ± 0.3	0.2	1.002
Q9ESX5	DKC1_MOUSE	H/ACA ribonucleoprotein complex subunit DKC1	MADAEVITFP	ADAEVITFPK	A	99.4 ± 0.4	99.7 ± 0.3	0.3	1.003
Q925J9	MED1_MOUSE	Mediator of RNA polymerase II transcription subunit 1	MKAQGETEDS	MKAQGETEDS	C	44.9 ± 1.3	43.7 ± 1.8	-1.2	0.974
Q9R045	ANGL2_MOUSE	Angiopoietin-related protein 2	MRPLCMTYWW	ATGPEADVEG	A?	0.2 ± 0.1	1.4 ± 1.9	1.2	6.507
Q9WVG6	CARM1_MOUSE	Histone-arginine methyltransferase CARM1	MAAAAATAVG	AAAAATAVGP	A	99.4 ± 0.2	99.2 ± 0.1	-0.2	0.998
Q9Z2X1	HNRPF_MOUSE	Heterogeneous nuclear ribonucleoprotein F	MMLGPEGGEG	MLGPEGGEGY	?	99.7 ± 0.4	99.9 ± 0.2	0.2	1.002
Q01279	EGFR_MOUSE	Epidermal growth factor receptor	MRPSGTARTT	GALEEKKVCQ	A?	0.2 ± 0	0.2 ± 0.1	-0.1	0.705
P05064	ALDOA_MOUSE	Fructose-bisphosphate aldolase A	MPHPYPALTP	PHPYPALTPE	?	4.1 ± 1.5	3.2 ± 1.5	-0.8	0.796
Q6VN19	RBP10_MOUSE	Ran-binding protein 10	MAAATADPGA	AAATADPGAG	A	99.4 ± 0.1	98.7 ± 0.8	-0.7	0.993
Q6P7W2	SHKB1_MOUSE	SH3KBP1-binding protein 1	MAVATTAVEG	AVATTAVEGV	A	99.5 ± 0.8	100 ± 0	0.5	1.005
Q9WV32	ARC1B_MOUSE	Actin-related protein 2/3 complex subunit 1B	MAYHSFLVEP	AYHSFLVEPI	A	99.6 ± 0.4	99.9 ± 0	0.3	1.003

Table A2: N-terminome analysis of WT and Naa20$^{-/-}$ MEF cells (cont).

UniProt Accession	Entry Name	Protein Description	Theoretical N-ter Sequence	Observed N-ter Sequence	NAT type (observed)	WT %NTA	Naa20$^{-/-}$ %NTA	%NTA Difference (Naa20$^{-/-}$-WT)	Ratio %NTA (Naa20$^{-/-}$/WT)
Q6P5D8	SMHD1_MOUSE	Structural maintenance of chromosomes flexible hinge domain-containing protein 1	MAAEGASDPA	AAEGASDPAG	A	99.6 ± 0.5	99.8 ± 0.2	0.2	1.002
Q9CZB3	THUM2_MOUSE	THUMP domain-containing protein 2	MAVAQADPGS	AVAQADPGSD	A	99.1 ± 0.4	99.5 ± 0.4	0.4	1.004
Q08943	SSRP1_MOUSE	FACT complex subunit SSRP1	MAETLEFNDI	AETLEFNDIF	A	99.5 ± 0.2	84.1 ± 21.7	-15.4	0.845
Q9D1H7	GET4_MOUSE	Golgi to ER traffic protein 4 homolog	MAAAAAMAEQ	AAAAAMAEQE	A	99.3 ± 0.7	99.6 ± 0.4	0.3	1.003
O08586	PTEN_MOUSE	Phosphatidylinositol 3.4.5-trisphosphate 3-phosphatase and dual-specificity protein phosphatase PTEN	MTAIIKEIVS	TAIIKEIVSR	A	99.5 ± 1.1	99.9 ± 0.2	0.4	1.004
Q80U93	NU214_MOUSE	Nuclear pore complex protein Nup214	MGDEMDAMIP	GDEMDAMIPE	A	99.4 ± 1.2	99.9 ± 0.3	0.5	1.005
Q91VC3	IF4A3_MOUSE	Eukaryotic initiation factor 4A-III	MAANATMATS	AANATMATSG	A	99.7 ± 0.3	99.8 ± 0.3	0.1	1.001
O35387	HAX1_MOUSE	HCLS1-associated protein X-1	MSVFDLFRGF	SVFDLFRGFF	A	99.8 ± 0.3	100 ± 0	0.2	1.002
O55091	IMPCT_MOUSE	Protein IMPACT	MAEEEVGNSQ	AEEEVGNSQR	A	98.1 ± 1.3	98.9 ± 0.6	0.8	1.008
Q9WTP6	KAD2_MOUSE	Adenylate kinase 2. mitochondrial	MAPNVLASEP	APNVLASEPE	A	0.4 ± 0.3	0.6 ± 0	0.2	1.524
Q61937	NPM_MOUSE	Nucleophosmin	MEDSMDMDMS	MEDSMDMDMS	B	99.7 ± 0.5	99.9 ± 0	0.3	1.003
Q9DAW9	CNN3_MOUSE	Calponin-3	MTHFNKGPSY	THFNKGPSYG	A	93.2 ± 8.1	98.4 ± 0.5	5.2	1.056
Q9WTM5	RUVB2_MOUSE	RuvB-like 2	MATVAATTKV	ATVAATTKVP	A	99.5 ± 0.4	99.7 ± 0.4	0.2	1.002
Q6A0A2	LAR4B_MOUSE	La-related protein 4B	MTSDQDAKVV	MTSDQDAKVV	C	99.6 ± 0.6	99.9 ± 0.1	0.3	1.003
P35700	PRDX1_MOUSE	Peroxiredoxin-1	MSSGNAKIGY	SSGNAKIGYP	A	99.9 ± 0.1	100 ± 0.1	0.1	1.001
Q9D1M7	FKB11_MOUSE	Peptidyl-prolyl cis-trans isomerase FKBP11	MTLSPLLLPL	EAGPETESPV	?	0.1 ± 0.1	0.1 ± 0	-0.1	0.491
P62878	RBX1_MOUSE	E3 ubiquitin-protein ligase RBX1	MAAAMDVDTP	AAAMDVDTPS	A	99.3 ± 0.7	99.6 ± 0.5	0.3	1.003
P70296	PEBP1_MOUSE	Phosphatidylethanolamine-binding protein 1	MAADISQWAG	AADISQWAGP	A	99.3 ± 0.4	98.5 ± 1	-0.7	0.993

Table A2: N-terminome analysis of WT and Naa20$^{-/-}$ MEF cells (cont).

UniProt Accession	Entry Name	Protein Description	Theoretical N-ter Sequence	Observed N-ter Sequence	NAT type (observed)	WT %NTA	Naa20$^{-/-}$ %NTA	%NTA Difference (Naa20$^{-/-}$-WT)	Ratio %NTA (Naa20$^{-/-}$/WT)
Q8K310	MATR3_MOUSE	Matrin-3	MSKSFQQSSL	SKSFQQSSLG	A	98.7 ± 0.1	99 ± 0.4	0.2	1.002
P08207	S10AA_MOUSE	Protein S100-A10	MPSQMEHAME	PSQMEHAMET	?	0.4 ± 0.2	0.6 ± 0.4	0.2	1.372
Q91XI1	DUS3L_MOUSE	tRNA-dihydrouridine(47) synthase	MAETAAESGG	AETAAESGGG	A	99.3 ± 0.6	99.6 ± 0.5	0.3	1.003
O35309	NMI_MOUSE	N-myc-interactor	MDADKDNIKQ	MDADKDNIKQ	B	99.3 ± 0.7	99.9 ± 0.1	0.6	1.006
O35345	IMA7_MOUSE	Importin subunit alpha-7	METMASPGKD	METMASPGKD	B	99.6 ± 0.4	99.2 ± 0	-0.4	0.996
Q7TQK5	CCD93_MOUSE	Coiled-coil domain-containing protein 93	MGLPKGPEGQ	GLPKGPEGQG	A	12.7 ± 1.1	11.2 ± 1	-1.5	0.880
Q9D1J3	SARNP_MOUSE	SAP domain-containing ribonucleoprotein	MAAETVELHK	AAETVELHKL	A	99.9 ± 0.1	99.9 ± 0.1	0.1	1.001
Q9DCD5	TJAP1_MOUSE	Tight junction-associated protein 1	MSSAAPAKKP	SSAAPAKKPY	A	97.1 ± 2.7	99.5 ± 0.4	2.4	1.025
Q9R059	FHL3_MOUSE	Four and a half LIM domains protein 3	MSEAFDCAKC	SEAFDCAKCN	A	99.7 ± 0.5	100 ± 0	0.2	1.002
Q64213	SF01_MOUSE	Splicing factor 1	MATGANATPL	ATGANATPLD	A	99.2 ± 0.8	99.6 ± 0.5	0.4	1.004
P52293	IMA1_MOUSE	Importin subunit alpha-1	MSTNENANLP	STNENANLPA	A	98.3 ± 2.1	96.9 ± 2.7	-1.4	0.986
P34022	RANG_MOUSE	Ran-specific GTPase-activating protein	MAAAKDSHED	AAAKDSHEDH	A	98.7 ± 0.3	98.2 ± 0.3	-0.5	0.995
P68040	RACK1_MOUSE	Receptor of activated protein C kinase 1	MTEQMTLRGT	TEQMTLRGTL	A	98.4 ± 3	99.9 ± 0.1	1.5	1.015
Q9DBG5	PLIN3_MOUSE	Perilipin-3	MSSNGTDAPA	SSNGTDAPAE	A	99.2 ± 0.6	98.6 ± 1	-0.6	0.994
B9EJ86	OSBL8_MOUSE	Oxysterol-binding protein-related protein 8	MEAALADGEP	MEAALADGEP	B	100 ± 0	99.9 ± 0.1	-0.1	0.999
Q8CDN6	TXNL1_MOUSE	Thioredoxin-like protein 1	MVGVKPVGSD	VGVKPVGSDP	A	0.7 ± 0.7	1.1 ± 0.4	0.4	1.629
Q8VC31	CCDC9_MOUSE	Coiled-coil domain-containing protein 9	MATTLDLKSK	ATTLDLKSKE	A	99.8 ± 0.2	98.9 ± 1.1	-0.9	0.991
Q99N96	RM01_MOUSE	39S ribosomal protein L1. mitochondrial	MAAAVRCLRR	AAAAAAATKP	A?	0.3 ± 0.2	0.2 ± 0.2	-0.1	0.708
Q9CR16	PPID_MOUSE	Peptidyl-prolyl cis-trans isomerase D	MSHASPAAKP	SHASPAAKPS	A	98.9 ± 1.1	99.3 ± 0.5	0.4	1.004

Table A2: N-terminome analysis of WT and Naa20$^{-/-}$ MEF cells (cont).

UniProt Accession	Entry Name	Protein Description	Theoretical N-ter Sequence	Observed N-ter Sequence	NAT type (observed)	WT %NTA	Naa20$^{-/-}$ %NTA	%NTA Difference (Naa20$^{-/-}$-WT)	Ratio %NTA (Naa20$^{-/-}$/WT)
Q08093	CNN2_MOUSE	Calponin-2	MSSTQFNKGP	SSTQFNKGPS	A	99.3 ± 0.7	98.4 ± 2.3	-0.9	0.991
Q9JMA2	TGT_MOUSE	Queuine tRNA-ribosyltransferase catalytic subunit 1	MAAVGSPGSL	AAVGSPGSLE	A	98.8 ± 0.9	99.3 ± 0.3	0.6	1.006
P83882	RL36A_MOUSE	60S ribosomal protein L36a	MVNVPKTRRT	VNVPKTRRTF	A	0.1 ± 0.1	0.2 ± 0.2	0.1	1.712
P97496	SMRC1_MOUSE	SWI/SNF complex subunit SMARCC1	MAATAGGGPG	AATAGGGPGA	A	91.3 ± 16.3	98.1 ± 1	6.8	1.075
P19536	COX5B_MOUSE	Cytochrome c oxidase subunit 5B	MASRLLRGVG	ASGGGVPTDE	A?	2.1 ± 2.8	1.2 ± 1.3	-1.0	0.538
Q5U3K5	RABL6_MOUSE	Rab-like protein 6	MFSALKKLVG	MFSALKKLVG	C	100 ± 0	99.4 ± 0.7	-0.5	0.995
P56959	FUS_MOUSE	RNA-binding protein FUS	MASNDYTQQA	ASNDYTQQAT	A	99.6 ± 0.5	99.9 ± 0.1	0.3	1.003
P21981	TGM2_MOUSE	Protein-glutamine gamma-glutamyltransferase 2	MAEELLLERC	AEELLLERCD	A	100 ± 0	98.7 ± 1.3	-1.3	0.987
Q8BVF2	PDCL3_MOUSE	Phosducin-like protein 3	MQDPNADTEW	MQDPNADTEW	B	99.9 ± 0.1	100 ± 0	0.1	1.001
O08539	BIN1_MOUSE	Myc box-dependent-interacting protein 1	MAEMGSKGVT	AEMGSKGVTA	A	99.6 ± 0.3	99.8 ± 0	0.2	1.002
P63328	PP2BA_MOUSE	Serine/threonine-protein phosphatase 2B catalytic subunit alpha isoform	MSEPKAIDPK	SEPKAIDPKL	A	99 ± 0.8	99.6 ± 0.4	0.6	1.007
Q9D710	TMX2_MOUSE	Thioredoxin-related transmembrane protein 2	MAVLAPLIAL	AVLAPLIALV	A	2.8 ± 0.8	2 ± 0.1	-0.8	0.704
Q99MR3	S12A9_MOUSE	Solute carrier family 12 member 9	MASESSPLLA	ASESSPLLAY	A	100 ± 0	99.8 ± 0.2	-0.1	0.999
Q64525	H2B2B_MOUSE	Histone H2B type 2-B	MPDPAKSAPA	KVQKKDGKKR	?	3.8 ± 1.9	4.9 ± 1.4	1.1	1.277
Q61191	HCFC1_MOUSE	Host cell factor 1	MASAVSPANL	ASAVSPANLP	A	99.5 ± 0.3	99.7 ± 0.4	0.2	1.002
Q9CQR6	PPP6_MOUSE	Serine/threonine-protein phosphatase 6 catalytic subunit	MAPLDLDKYV	APLDLDKYVE	A	1 ± 0.8	0.6 ± 0.1	-0.4	0.603
P54822	PUR8_MOUSE	Adenylosuccinate lyase	MAASGDPGSA	AASGDPGSAE	A	99.1 ± 0.8	99.4 ± 0.6	0.3	1.003
P51881	ADT2_MOUSE	ADP/ATP translocase 2	MTDAAVSFAK	TDAAVSFAKD	A	98 ± 1.8	99.8 ± 0	1.8	1.018

Table A2: N-terminome analysis of WT and Naa20$^{-/-}$ MEF cells (cont).

UniProt Accession	Entry Name	Protein Description	Theoretical N-ter Sequence	Observed N-ter Sequence	NAT type (observed)	WT %NTA	Naa20$^{-/-}$ %NTA	%NTA Difference (Naa20$^{-/-}$-WT)	Ratio %NTA (Naa20$^{-/-}$/WT)
P11087	CO1A1_MOUSE	Collagen alpha-1(I) chain	MFSFVDLRLL	QEDIPEVSCI	?	4.8 ± 2.1	6.6 ± 3.8	1.9	1.393
Q99KU0	VMP1_MOUSE	Vacuole membrane protein 1	MAENGKNCDQ	AENGKNCDQR	A	100 ± 0.1	100 ± 0	0.0	1.000
Q9Z0R9	FADS2_MOUSE	Acyl-CoA 6-desaturase	MGKGGNQGEG	GKGGNQGEGS	A	1.9 ± 0.6	1.3 ± 0.5	-0.6	0.684
Q9DBS9	OSBL3_MOUSE	Oxysterol-binding protein-related protein 3	MSDEKNLGVS	SDEKNLGVSQ	A	98.5 ± 1.6	99.6 ± 0.3	1.1	1.011
Q9CQ18	RNH2C_MOUSE	Ribonuclease H2 subunit C	MKNPEEAADG	MKNPEEAADG	C	93.3 ± 4.2	95.3 ± 2.7	2.0	1.022
Q9Z0N1	IF2G_MOUSE	Eukaryotic translation initiation factor 2 subunit 3. X-linked	MAGGEGGVTL	AGGEGGVTLG	A	79 ± 2.1	77.3 ± 4.1	-1.7	0.979
Q8VDD5	MYH9_MOUSE	Myosin-9	MAQQAADKYL	AQQAADKYLY	A	99.6 ± 0.5	99.9 ± 0.1	0.3	1.003
P51125	ICAL_MOUSE	Calpastatin	MSQPGPKPAA	SQPGPKPAAS	A	99.4 ± 0.4	99.7 ± 0.3	0.3	1.003
P49718	MCM5_MOUSE	DNA replication licensing factor MCM5	MSGFDDPGIF	SGFDDPGIFY	A	99.1 ± 0.6	99.4 ± 0.1	0.3	1.003
Q8BHS3	RBM22_MOUSE	Pre-mRNA-splicing factor RBM22	MATSLGSNTY	ATSLGSNTYN	A	97.9 ± 0.3	98.1 ± 0.2	0.2	1.002
Q61183	PAPOA_MOUSE	Poly(A) polymerase alpha	MPFPVTTQGS	PFPVTTQGSQ	?	1.5 ± 2.2	0.2 ± 0.1	-1.4	0.098
Q64525	H2B2B_MOUSE	Histone H2B type 2-B	MPDPAKSAPA	AVTKVQKKDG	A?	4 ± 3	5.3 ± 2.1	1.3	1.336
P43883	PLIN2_MOUSE	Perilipin-2	MAAAVVDPQQ	AAAVVDPQQS	A	99.4 ± 0.7	99.6 ± 0.5	0.3	1.003
Q68FD5	CLH1_MOUSE	Clathrin heavy chain 1	MAQILPIRFQ	AQILPIRFQE	A	99.9 ± 0.3	100 ± 0	0.1	1.001
Q9EQQ9	OGA_MOUSE	Protein O-GlcNAcase	MVQKESQAAL	VQKESQAALE	A	1.2 ± 1	0.9 ± 0.8	-0.4	0.693
P62737	ACTA_MOUSE	Actin. aortic smooth muscle	MCEEEDSTAL	CEEEDSTALV	?	96.1 ± 2.3	94.3 ± 0.5	-1.7	0.982
Q0GNC1	INF2_MOUSE	Inverted formin-2	MSVKEGAQRK	SVKEGAQRKW	A	100 ± 0	99.8 ± 0.3	-0.2	0.998
Q8BGC0	HTSF1_MOUSE	HIV Tat-specific factor 1 homolog	MSGNNLSGND	SGNNLSGNDE	A	99.3 ± 0.6	99.1 ± 0.3	-0.2	0.998
P63260	ACTG_MOUSE	Actin. cytoplasmic 2	MEEEIAALVI	MEEEIAALVI	B	98.4 ± 0.4	98.9 ± 0.6	0.5	1.005
Q8BLR9	HIF1N_MOUSE	Hypoxia-inducible factor 1-alpha inhibitor	MAATAAEVAA	AATAAEVAAS	A	99.6 ± 0.3	99.8 ± 0.3	0.2	1.002
P52432	RPAC1_MOUSE	DNA-directed RNA polymerases I and III subunit RPAC1	MAAAQAVEEM	AAAQAVEEMR	A	96.9 ± 6.1	100 ± 0	3.1	1.032

Table A2: N-terminome analysis of WT and Naa20$^{-/-}$ MEF cells (cont).

UniProt Accession	Entry Name	Protein Description	Theoretical N-ter Sequence	Observed N-ter Sequence	NAT type (observed)	WT %NTA	Naa20$^{-/-}$ %NTA	%NTA Difference (Naa20$^{-/-}$-WT)	Ratio %NTA (Naa20$^{-/-}$/WT)
Q9ER73	ELP4_MOUSE	Elongator complex protein 4	MAAADTCGAG	AAADTCGAGT	A	99.4 ± 0.4	99.7 ± 0.3	0.3	1.003
P02468	LAMC1_MOUSE	Laminin subunit gamma-1	MTGGGRAALA	AMDECADEGG	A?	1 ± 0.8	0.3 ± 0.1	-0.7	0.276
Q921I9	EXOS4_MOUSE	Exosome complex component RRP41	MAGLELLSDQ	AGLELLSDQG	A	99.3 ± 0.3	99.5 ± 0.3	0.2	1.002
Q3U0V1	FUBP2_MOUSE	Far upstream element-binding protein 2	MSDYNTGGPP	SDYNTGGPPP	A	99 ± 0.6	98.7 ± 0.4	-0.3	0.997
Q6P5F9	XPO1_MOUSE	Exportin-1	MPAIMTMLAD	PAIMTMLADH	?	0.3 ± 0.2	0.7 ± 0.8	0.3	1.985
Q8QZT1	THIL_MOUSE	Acetyl-CoA acetyltransferase	MAALVALHGV	ASKPTLNEVV	A?	0.7 ± 0.3	0.5 ± 0.1	-0.2	0.762
Q9CQR2	RS21_MOUSE	40S ribosomal protein S21	MQNDAGEFVD	MQNDAGEFVD	B	98.8 ± 1.2	99.3 ± 0.6	0.4	1.004
Q8BKG3	PTK7_MOUSE	Inactive tyrosine-protein kinase 7	MGARPLTLLR	AIVFIKEPSS	A?	1.1 ± 1.2	0.6 ± 0.4	-0.5	0.568
Q8CGY8	OGT1_MOUSE	UDP-N-acetylglucosamine-peptide N-acetylglucosaminyltransferase 110 kDa subunit	MASSVGNVAD	ASSVGNVADS	A	99.4 ± 0.5	99.1 ± 0.7	-0.3	0.997
P40124	CAP1_MOUSE	Adenylyl cyclase-associated protein 1	MADMQNLVER	ADMQNLVERL	A	99.7 ± 0.3	99.5 ± 0.5	-0.1	0.999
Q3V1V3	ESF1_MOUSE	ESF1 homolog	MSSKQEIMDD	SSKQEIMDDQ	A	99.8 ± 0.2	100 ± 0	0.1	1.001
Q6P1B1	XPP1_MOUSE	Xaa-Pro aminopeptidase 1	MAPKVTSELL	APKVTSELLR	A	0.9 ± 0.5	0.7 ± 0.7	-0.3	0.720
P47754	CAZA2_MOUSE	F-actin-capping protein subunit alpha-2	MADLEEQLSD	ADLEEQLSDE	A	99.1 ± 0.9	99.5 ± 0.6	0.4	1.004
Q8BFQ4	WDR82_MOUSE	WD repeat-containing protein 82	MKLTDSVLRS	MKLTDSVLRS	C	8.8 ± 2.5	6.6 ± 3.4	-2.3	0.742
P47962	RL5_MOUSE	60S ribosomal protein L5	MGFVKVVKNK	GFVKVVKNKA	A	14.7 ± 34.5	1.1 ± 0.1	-13.6	0.077
P53811	PIPNB_MOUSE	Phosphatidylinositol transfer protein beta isoform	MVLIKEFRVV	VLIKEFRVVL	A	0.2 ± 0.1	0.3 ± 0.3	0.1	1.523
Q99JI4	PSMD6_MOUSE	26S proteasome non-ATPase regulatory subunit 6	MPLENLEEEG	PLENLEEEGL	?	1.6 ± 1.1	2.1 ± 0.4	0.6	1.366
Q99N92	RM27_MOUSE	39S ribosomal protein L27	MAAAALTLRT	ASKKTGGSSK	A?	0.9 ± 1.3	0.3 ± 0.1	-0.6	0.286
Q9ESW4	AGK_MOUSE	Acylglycerol kinase	MTAFFKTLRN	TAFFKTLRNH	A	99.9 ± 0.1	100 ± 0	0.1	1.001

Table A2: N-terminome analysis of WT and Naa20$^{-/-}$ MEF cells (cont).

UniProt Accession	Entry Name	Protein Description	Theoretical N-ter Sequence	Observed N-ter Sequence	NAT type (observed)	WT %NTA	Naa20$^{-/-}$ %NTA	%NTA Difference (Naa20$^{-/-}$-WT)	Ratio %NTA (Naa20$^{-/-}$/WT)
Q61733	RT31_MOUSE	28S ribosomal protein S31	MLHRIPAFLR	SKKVDQSVPA	A?	1.8 ± 0.2	1.4 ± 0.5	-0.4	0.758
Q99KN2	CIAO1_MOUSE	Probable cytosolic iron-sulfur protein assembly protein CIAO1	MKDSLVLQSR	MKDSLVLQSR	C	1 ± 0.8	0.7 ± 0.9	-0.4	0.657
Q9D0B6	PBDC1_MOUSE	Protein PBDC1	MDAAGESEEP	MDAAGESEEP	B	99.9 ± 0.1	99.8 ± 0.3	-0.1	0.999
Q91VY9	ZN622_MOUSE	Zinc finger protein 622	MAALTCITCR	AALTCITCRV	A	97.4 ± 0.1	98.1 ± 1.7	0.7	1.007
Q9CPW7	ZMAT2_MOUSE	Zinc finger matrin-type protein 2	MASGSGTKNL	ASGSGTKNLD	A	95.5 ± 5.7	98 ± 2	2.5	1.026
P56480	ATPB_MOUSE	ATP synthase subunit beta	MLSLVGRVAS	ASAAPKAGTA	A?	0.2 ± 0.1	0.2 ± 0.1	0.0	1.222
Q8K124	PKHO2_MOUSE	Pleckstrin homology domain-containing family O member 2	MEEESIKEGS	MEEESIKEGS	B	99.6 ± 0.6	99.8 ± 0.4	0.2	1.002
P62281	RS11_MOUSE	40S ribosomal protein S11	MADIQTERAY	ADIQTERAYQ	A	99.6 ± 0.7	99.9 ± 0.1	0.3	1.003
P24527	LKHA4_MOUSE	Leukotriene A-4 hydrolase	MPEVADTCSL	PEVADTCSLA	?	1.3 ± 1.4	2 ± 2.3	0.7	1.584
P42932	TCPQ_MOUSE	T-complex protein 1 subunit theta	MALHVPKAPG	ALHVPKAPGF	A	98.3 ± 1.7	99.1 ± 0.5	0.8	1.008
Q9QWF0	CAF1A_MOUSE	Chromatin assembly factor 1 subunit A	MLEEPEAATR	MLEEPEAATR	C	97.6 ± 2.2	98.8 ± 0.9	1.2	1.012
Q9R0P5	DEST_MOUSE	Destrin	MASGVQVADE	ASGVQVADEV	A	99.4 ± 0.7	99.6 ± 0.6	0.2	1.002
Q8R3E3	WIPI1_MOUSE	WD repeat domain phosphoinositide-interacting protein 1	MEAEAADAPP	MEAEAADAPP	B	100 ± 0	100 ± 0	0.0	1.000
Q9JJ28	FLII_MOUSE	Protein flightless-1 homolog	MEATGVLPFV	MEATGVLPFV	B	98.4 ± 3.8	100 ± 0	1.6	1.017
P26638	SYSC_MOUSE	Serine–tRNA ligase	MVLDLDLFRV	VLDLDLFRVD	A	0.1 ± 0.1	0.2 ± 0.1	0.1	1.430
Q6PDI5	ECM29_MOUSE	Proteasome adapter and scaffold protein ECM29	METGSDSDQL	METGSDSDQL	B	98.6 ± 2.6	99.3 ± 0.6	0.7	1.007
O09167	RL21_MOUSE	60S ribosomal protein L21	MTNTKGKRRG	MTNTKGKRRG	C	3.3 ± 1.7	2.9 ± 0.5	-0.5	0.860
P60670	NPL4_MOUSE	Nuclear protein localization protein 4 homolog	MAESIIIRVQ	AESIIIRVQS	A	99.9 ± 0.2	100 ± 0	0.1	1.001
Q3TZZ7	ESYT2_MOUSE	Extended synaptotagmin-2	MSSAGGEGPE	SSAGGEGPEA	A	99 ± 0.4	99.3 ± 0.8	0.2	1.003

Table A2: N-terminome analysis of WT and Naa20$^{-/-}$ MEF cells (cont).

UniProt Accession	Entry Name	Protein Description	Theoretical N-ter Sequence	Observed N-ter Sequence	NAT type (observed)	WT %NTA	Naa20$^{-/-}$ %NTA	%NTA Difference (Naa20$^{-/-}$-WT)	Ratio %NTA (Naa20$^{-/-}$/WT)
Q9D8X2	CC124_MOUSE	Coiled-coil domain-containing protein 124	MPKKFQGENS	PKKFQGENSK	?	0.5 ± 0.2	0.6 ± 0.3	0.2	1.330
P54227	STMN1_MOUSE	Stathmin	MASSDIQVKE	ASSDIQVKEL	A	99 ± 0.9	99.4 ± 0.8	0.3	1.003
Q9D0F3	LMAN1_MOUSE	Protein ERGIC-53	MAVSRRRVPQ	TGGDAAAPGA	A?	2.2 ± 0.9	1.8 ± 0.9	-0.3	0.844
P12382	PFKAL_MOUSE	ATP-dependent 6-phosphofructokinase	MATVDLEKLR	ATVDLEKLRM	A	99.4 ± 0.6	99.6 ± 0.5	0.2	1.002
Q6NV83	SR140_MOUSE	U2 snRNP-associated SURP motif-containing protein	MADKTPGGSQ	ADKTPGGSQK	A	99.5 ± 0.5	99.7 ± 0.3	0.1	1.001
Q61166	MARE1_MOUSE	Microtubule-associated protein RP/EB family member 1	MAVNVYSTSV	AVNVYSTSVT	A	98.3 ± 1.6	98.9 ± 1	0.6	1.006
Q8BMJ3	IF1AX_MOUSE	Eukaryotic translation initiation factor 1A. X-chromosomal	MPKNKGKGGK	PKNKGKGGKN	?	1 ± 0.3	0.9 ± 0.1	-0.1	0.933
Q9CZX8	RS19_MOUSE	40S ribosomal protein S19	MPGVTVKDVN	PGVTVKDVNQ	?	0.2 ± 0.2	0.3 ± 0.2	0.1	1.313
P19324	SERPH_MOUSE	Serpin H1	MRSLLLGTLC	LSSKATTLAE	?	0.2 ± 0.1	0.1 ± 0.1	-0.1	0.531
Q61768	KINH_MOUSE	Kinesin-1 heavy chain	MADPAECNIK	ADPAECNIKV	A	99.3 ± 0.7	99.5 ± 0.6	0.2	1.002
Q64311	NTAN1_MOUSE	Protein N-terminal asparagine amidohydrolase	MPLLVDGQRV	PLLVDGQRVR	?	0.5 ± 0.8	0.1 ± 0	-0.5	0.103
Q9CY16	RT28_MOUSE	28S ribosomal protein S28	MAALCRSHAG	ASTESGSESA	A?	0.7 ± 0.4	0.5 ± 0.4	-0.2	0.682
Q9ER72	SYCC_MOUSE	Cysteine–tRNA ligase. cytoplasmic	MAGSSAEQAA	AGSSAEQAAD	A	98.2 ± 2.5	99.4 ± 0.4	1.2	1.012
Q9DBG9	TX1B3_MOUSE	Tax1-binding protein 3	MSYTPGQPVT	SYTPGQPVTA	A	99.2 ± 0.6	99.4 ± 0.6	0.2	1.002
Q922D8	C1TC_MOUSE	C-1-tetrahydrofolate synthase	MAPAGILNGK	APAGILNGKL	A	0.2 ± 0.2	0.3 ± 0.2	0.1	1.272
P62996	TRA2B_MOUSE	Transformer-2 protein homolog beta	MSDSGEQNYG	SDSGEQNYGE	A	98.8 ± 0.6	99.3 ± 0.5	0.5	1.005
Q8BWY3	ERF1_MOUSE	Eukaryotic peptide chain release factor subunit 1	MADDPSAADR	ADDPSAADRN	A	100 ± 0	100 ± 0.1	0.0	1.000
Q922H9	ZN330_MOUSE	Zinc finger protein 330	MPKKKTGARK	PKKKTGARKK	?	0.4 ± 0	0.3 ± 0.1	-0.1	0.839
Q920B9		SP16H_MOUSE	MAVTLDKDAY	AVTLDKDAYY	A	99.6 ± 0.6	99.8 ± 0.3	0.2	1.002

Table A2: N-terminome analysis of WT and Naa20$^{-/-}$ MEF cells (cont).

UniProt Accession	Entry Name	Protein Description	Theoretical N-ter Sequence	Observed N-ter Sequence	NAT type (observed)	WT %NTA	Naa20$^{-/-}$ %NTA	%NTA Difference (Naa20$^{-/-}$-WT)	Ratio %NTA (Naa20$^{-/-}$/WT)
Q9CR62	M2OM_MOUSE	Mitochondrial 2-oxoglutarate/malate carrier protein	MAATASPGAG	AATASPGAGR	A	95 ± 3.4	96.7 ± 2.1	1.7	1.018
O88796	RPP30_MOUSE	Ribonuclease P protein subunit p30	MAAFADLDLR	AAFADLDLRA	A	99.9 ± 0.2	99.8 ± 0.2	-0.1	0.999
Q61205	PA1B3_MOUSE	Platelet-activating factor acetylhydrolase IB subunit alpha1	MSGEGENPAS	SGEGENPASK	A	99.2 ± 0.6	99.4 ± 0.4	0.2	1.002
B2RQC6	PYR1_MOUSE	CAD protein [Includes: Glutamine-dependent carbamoyl-phosphate synthase	MAALVLEDGS	AALVLEDGSV	A	99.3 ± 0.5	99.5 ± 0.3	0.2	1.002
Q9WTN0	GGPPS_MOUSE	Geranylgeranyl pyrophosphate synthase	MEKTKEKAER	MEKTKEKAER	B	99.9 ± 0.1	99.8 ± 0.2	-0.1	0.999
Q9DBG6	RPN2_MOUSE	Dolichyl-diphosphooligosaccharide–protein glycosyltransferase subunit 2	MAPPGSSAVF	LTPTHYLTKQ	?	2.1 ± 2.3	1.4 ± 1	-0.6	0.697
Q4VBD2	TAPT1_MOUSE	Transmembrane anterior posterior transformation protein 1	MAGVCDAAAP	AGVCDAAAPG	A	97.5 ± 1.1	97 ± 1.7	-0.5	0.995
P14131	RS16_MOUSE	40S ribosomal protein S16	MPSKGPLQSV	PSKGPLQSVQ	?	0.3 ± 0.2	0.4 ± 0.2	0.1	1.202
P16675	PPGB_MOUSE	Lysosomal protective protein	MPGTALSPLL	APDQDEIDCL	A?	0.9 ± 0.3	1 ± 0.1	0.2	1.176
Q60930	VDAC2_MOUSE	Voltage-dependent anion-selective channel protein 2	MAECCVPVCP	AECCVPVCPR	A	99.6 ± 0.5	99.7 ± 0.3	0.1	1.001
P63260	ACTG_MOUSE	Actin. cytoplasmic 2	MEEEIAALVI	EEEIAALVID	?	99.7 ± 0.3	99.8 ± 0.1	0.1	1.001
Q71FD7	FBLI1_MOUSE	Filamin-binding LIM protein 1	MASKPEKRVA	ASKPEKRVAS	A	99.8 ± 0.2	99.5 ± 0.7	-0.3	0.997
Q9D0F9	PGM1_MOUSE	Phosphoglucomutase-1	MVKIVTVKTQ	VKIVTVKTQA	A	0.7 ± 0.2	0.9 ± 0.4	0.2	1.255
Q9D8T7	SLIRP_MOUSE	SRA stem-loop-interacting RNA-binding protein	MAASAIKGLS	AASAIKGLSA	A	98.4 ± 1.9	99 ± 1.3	0.6	1.006
O35639	ANXA3_MOUSE	Annexin A3	MASIWVGPRG	ASIWVGPRGT	A	99.6 ± 0.3	99.5 ± 0.3	-0.1	0.999
P62889	RL30_MOUSE	60S ribosomal protein L30	MVAAKKTKKS	VAAKKTKKSL	A	1.2 ± 0.4	1.1 ± 0.1	-0.1	0.914
Q8R2T8	TF3C5_MOUSE	General transcription factor 3C polypeptide 5	MAAAEPDADP	AAAEPDADPK	A	98.4 ± 0.8	99.1 ± 0.9	0.7	1.007
P14824	ANXA6_MOUSE	Annexin A6	MAKIAQGAMY	AKIAQGAMYR	A	99.6 ± 0.4	99.7 ± 0.3	0.1	1.001
Q2NL51	GSK3A_MOUSE	Glycogen synthase kinase-3 alpha	MSGGGPSGGG	SGGGPSGGGP	A	99.7 ± 0.3	99.5 ± 0.3	-0.2	0.998

Table A2: N-terminome analysis of WT and Naa20$^{-/-}$ MEF cells (cont).

UniProt Accession	Entry Name	Protein Description	Theoretical N-ter Sequence	Observed N-ter Sequence	NAT type (observed)	WT %NTA	Naa20$^{-/-}$ %NTA	%NTA Difference (Naa20$^{-/-}$-WT)	Ratio %NTA (Naa20$^{-/-}$/WT)
Q9DAR7	DCPS_MOUSE	m7GpppX diphosphatase	MADTAPQLKR	ADTAPQLKRK	A	99.4 ± 0.8	99.6 ± 0.4	0.2	1.002
Q9CPP0	NPM3_MOUSE	Nucleoplasmin-3	MAAGAAAALA	AAGAAAALAF	A	99.6 ± 0.4	99.8 ± 0.1	0.1	1.001
Q9D662	SC23B_MOUSE	Protein transport protein Sec23B	MATYLEFIQQ	ATYLEFIQQN	A	99.7 ± 0.4	99.8 ± 0.2	0.1	1.001
P26369	U2AF2_MOUSE	Splicing factor U2AF 65 kDa subunit	MSDFDEFERQ	SDFDEFERQL	A	99.9 ± 0.1	99.8 ± 0.1	-0.1	0.999
Q6P9P6	KIF11_MOUSE	Kinesin-like protein KIF11	MASQPSSLKK	ASQPSSLKKK	A	99.8 ± 0.2	99.7 ± 0.2	-0.1	0.999
Q8BG32	PSD11_MOUSE	26S proteasome non-ATPase regulatory subunit 11	MAAAAVVEFQ	AAAAVVEFQR	A	98.4 ± 2.2	99 ± 1.5	0.5	1.005
P10605	CATB_MOUSE	Cathepsin B	MWWSLILLSC	DIDLPETFDA	?	0.3 ± 0.4	0.2 ± 0.2	-0.1	0.693
P63017	HSP7C_MOUSE	Heat shock cognate 71 kDa protein	MSKGPAVGID	SKGPAVGIDL	A	99.7 ± 0.2	99.6 ± 0.5	-0.1	0.999
Q9D1M0	SEC13_MOUSE	Protein SEC13 homolog	MVSVMNTVDT	VSVMNTVDTS	A	99.5 ± 0.7	99.8 ± 0.1	0.3	1.003
P80316	TCPE_MOUSE	T-complex protein 1 subunit epsilon	MASVGTLAFD	ASVGTLAFDE	A	99 ± 1.5	99.5 ± 0.4	0.5	1.005
Q91V01	MBOA5_MOUSE	Lysophospholipid acyltransferase 5	MASTADGDMG	ASTADGDMGE	A	99.6 ± 0.4	99.7 ± 0.4	0.1	1.001
P70441	NHRF1_MOUSE	Na(+)/H(+) exchange regulatory cofactor NHE-RF1	MSADAAAGEP	SADAAAGEPL	A	99.6 ± 0.5	99.5 ± 0.3	-0.2	0.998
Q8CCS6	PABP2_MOUSE	Polyadenylate-binding protein 2	MAAAAAAAAA	AAAAAAAAAA	A	99 ± 0.4	99.1 ± 0.1	0.1	1.001
Q9DBD5	PELP1_MOUSE	Proline-. glutamic acid- and leucine-rich protein 1	MAAAVLSGAS	AAAVLSGASA	A	99.4 ± 0.5	99.3 ± 0.4	-0.2	0.998
Q9DCF9	SSRG_MOUSE	Translocon-associated protein subunit gamma	MAPKGGSKQQ	APKGGSKQQS	A	1.5 ± 0.5	2 ± 1.4	0.5	1.340
Q9D6Y9	GLGB_MOUSE	1.4-alpha-glucan-branching enzyme	MAAPAAPAAG	AAPAAPAAGE	A	99.7 ± 0.3	99.6 ± 0.4	-0.1	0.999
Q3UJB9	EDC4_MOUSE	Enhancer of mRNA-decapping protein 4	MASCASIDIE	ASCASIDIED	A	98.9 ± 0.4	98.8 ± 0.3	-0.1	0.998
Q8R0H9	GGA1_MOUSE	ADP-ribosylation factor-binding protein GGA1	MEPAMEPETL	MEPAMEPETL	B	99.6 ± 0.3	99 ± 1	-0.6	0.994
P63024	VAMP3_MOUSE	Vesicle-associated membrane protein 3	MSTGVPSGSS	STGVPSGSSA	A	99.6 ± 0.4	99.5 ± 0.3	-0.1	0.999
Q8BJY1	PSMD5_MOUSE	26S proteasome non-ATPase regulatory subunit 5	MAAQAVSLLR	AAQAVSLLRE	A	99.8 ± 0.3	99.7 ± 0.4	-0.1	0.999

Table A2: N-terminome analysis of WT and Naa20$^{-/-}$ MEF cells (cont).

UniProt Accession	Entry Name	Protein Description	Theoretical N-ter Sequence	Observed N-ter Sequence	NAT type (observed)	WT %NTA	Naa20$^{-/-}$ %NTA	%NTA Difference (Naa20$^{-/-}$-WT)	Ratio %NTA (Naa20$^{-/-}$/WT)
Q7TQI3	OTUB1_MOUSE	Ubiquitin thioesterase OTUB1	MAAEEPQQQK	AAEEPQQQKQ	A	98.5 ± 0.1	98.2 ± 0.8	-0.3	0.997
Q80WB5	NTAQ1_MOUSE	Protein N-terminal glutamine amidohydrolase	MEGDGPAATA	MEGDGPAATA	B	90.7 ± 12.5	81.9 ± 17.5	-8.8	0.903
Q9CW46	RAVR1_MOUSE	Ribonucleoprotein PTB-binding 1	MAADVSVTHR	AADVSVTHRP	A	98.2 ± 1.5	97.3 ± 1.2	-0.8	0.992
Q99NB9	SF3B1_MOUSE	Splicing factor 3B subunit 1	MAKIAKTHED	AKIAKTHEDI	A	96.3 ± 1.8	95.7 ± 0.6	-0.6	0.994
Q9Z204	HNRPC_MOUSE	Heterogeneous nuclear ribonucleoproteins C1/C2	MASNVTNKTD	ASNVTNKTDP	A	96.2 ± 2.2	95.4 ± 3.9	-0.8	0.992
Q8BML9	SYQ_MOUSE	Glutamine–tRNA ligase	MATPDSLALF	ATPDSLALFT	A	99.4 ± 0.3	99.3 ± 0.3	-0.2	0.998
Q9CQX2	CYB5B_MOUSE	Cytochrome b5 type B	MATPEASGSG	ATPEASGSGE	A	99.1 ± 1.2	98.8 ± 0.6	-0.3	0.997
O35874	SATT_MOUSE	Neutral amino acid transporter A	MEKSGETNGY	MEKSGETNGY	B	99.7 ± 0.3	99.5 ± 0.8	-0.2	0.998
Q9CZB0	C560_MOUSE	Succinate dehydrogenase cytochrome b560 subunit	MAAFLLRHVS	LGTTAKEEME	?	2.5 ± 1.8	2.1 ± 1	-0.4	0.848
Q9CZ13	QCR1_MOUSE	Cytochrome b-c1 complex subunit 1	MAASAVCRAA	TATFAQALQS	A?	1.1 ± 0.4	0.9 ± 0.3	-0.1	0.864
Q6IRU2	TPM4_MOUSE	Tropomyosin alpha-4 chain	MAGLNSLEAV	AGLNSLEAVK	A	99.5 ± 0.5	99.4 ± 0.6	-0.1	0.999
P62627	DLRB1_MOUSE	Dynein light chain roadblock-type 1	MAEVEETLKR	AEVEETLKRL	A	99.6 ± 0.4	99.7 ± 0.4	0.1	1.001
Q91ZX7	LRP1_MOUSE	Prolow-density lipoprotein receptor-related protein 1	MLTPPLLLLL	ATMDAPKTCS	A?	1.5 ± 0.8	1.9 ± 0.6	0.4	1.248
Q9CXK9	RBM33_MOUSE	RNA-binding protein 33	MAAALGAGGG	AAALGAGGGA	A	99.2 ± 0.4	98.8 ± 1	-0.4	0.996
Q8VCB1	NDC1_MOUSE	Nucleoporin NDC1	MATAASGPCA	ATAASGPCAG	A	38.9 ± 3	40.3 ± 2.8	1.4	1.036
Q9ES97	RTN3_MOUSE	Reticulon-3	MAESSAATQS	AESSAATQSP	A	98.7 ± 0.8	99.1 ± 0.8	0.4	1.004
Q99L04	DHRS1_MOUSE	Dehydrogenase/reductase SDR family member 1	MVAPMKGQVC	VAPMKGQVCV	A	2.6 ± 1.2	2.9 ± 0.6	0.3	1.134
Q9CZE3	RAB32_MOUSE	Ras-related protein Rab-32	MAGEGLGQQG	AGEGLGQQGA	A	35.7 ± 35.3	48.1 ± 34	12.4	1.348
A2AJQ3	D19L4_MOUSE	Probable C-mannosyltransferase DPY19L4	MAKEEGTSVE	AKEEGTSVEP	A	95.5 ± 2.5	96.2 ± 1.4	0.7	1.008
P20152	VIME_MOUSE	Vimentin	MSTRSVSSSS	SLYSSSPGGA	A?	1.2 ± 1.8	2.1 ± 2	0.9	1.717

Table A2: N-terminome analysis of WT and Naa20$^{-/-}$ MEF cells (cont).

UniProt Accession	Entry Name	Protein Description	Theoretical N-ter Sequence	Observed N-ter Sequence	NAT type (observed)	WT %NTA	Naa20$^{-/-}$ %NTA	%NTA Difference (Naa20$^{-/-}$-WT)	Ratio %NTA (Naa20$^{-/-}$/WT)
Q62422	OSTF1_MOUSE	Osteoclast-stimulating factor 1	MSKPPPKPVK	SKPPPKPVKP	A	98.9 ± 0.7	99.2 ± 0.3	0.3	1.003
P80315	TCPD_MOUSE	T-complex protein 1 subunit delta	MPENVASRSG	PENVASRSGA	?	40.3 ± 48.8	25.2 ± 43.2	-15.1	0.626
Q8BVG4	DPP9_MOUSE	Dipeptidyl peptidase 9	MCSGVSPVEQ	CSGVSPVEQV	?	99.9 ± 0.1	100 ± 0	0.0	1.000
P34884	MIF_MOUSE	Macrophage migration inhibitory factor	MPMFIVNTNV	PMFIVNTNVP	?	1.1 ± 0.8	0.9 ± 0.6	-0.2	0.798
O35143	ATIF1_MOUSE	ATPase inhibitor	MAGSALAVRA	SSDSMDTGAG	A?	0.2 ± 0.1	0.2 ± 0.1	0.0	1.318
P43274	H14_MOUSE	Histone H1.4	MSETAPAAPA	SETAPAAPAA	A	96.7 ± 0.4	97 ± 0.7	0.3	1.003
Q9ERR7	SEP15_MOUSE	Selenoprotein F	MAAGQGGWLR	AEFASEACRE	A?	0.3 ± 0.1	0.2 ± 0.1	0.0	0.850
Q64012	RALY_MOUSE	RNA-binding protein Raly	MSLKIQTSNV	SLKIQTSNVT	A	99.1 ± 0.9	99.4 ± 0.6	0.2	1.002
Q8CH25	SLTM_MOUSE	SAFB-like transcription modulator	MAAAAGAVVA	AAAAGAVVAS	A	99.1 ± 0.4	98.8 ± 0.9	-0.3	0.997
Q9D8Y0	EFHD2_MOUSE	EF-hand domain-containing protein D2	MATDELASKL	ATDELASKLS	A	99.8 ± 0.3	99.7 ± 0.4	-0.1	0.999
P80318	TCPG_MOUSE	T-complex protein 1 subunit gamma	MMGHRPVLVL	MMGHRPVLVL	C	99.5 ± 0.5	99.3 ± 0.7	-0.2	0.998
Q922R8	PDIA6_MOUSE	Protein disulfide-isomerase A6	MARLVLGLVS	LYSSSDDVIE	?	6.2 ± 0.9	5.6 ± 1.8	-0.7	0.893
P56480	ATPB_MOUSE	ATP synthase subunit beta	MLSLVGRVAS	AQASAAPKAG	A?	0.4 ± 0.2	0.4 ± 0.3	0.0	1.136
P47955	RLA1_MOUSE	60S acidic ribosomal protein P1	MASVSELACI	ASVSELACIY	A	99.9 ± 0.1	99.8 ± 0.3	-0.1	0.999
P60122	RUVB1_MOUSE	RuvB-like 1	MKIEEVKSTT	MKIEEVKSTT	C	2.1 ± 1.2	1.9 ± 0.8	-0.2	0.892
Q9CPW4	ARPC5_MOUSE	Actin-related protein 2/3 complex subunit 5	MSKNTVSSAR	SKNTVSSARF	A	98.6 ± 0.8	98.9 ± 0.1	0.3	1.003
Q9CT10	RANB3_MOUSE	Ran-binding protein 3	MADLANEEKP	ADLANEEKPA	A	99 ± 0.3	98.8 ± 0.3	-0.2	0.998
Q8BIJ6	SYIM_MOUSE	Isoleucine–tRNA ligase	MHWGLCPRGP	VAGADSPQSS	A?	0.2 ± 0.1	0.2 ± 0.2	0.0	0.805
Q8JZM7	CDC73_MOUSE	Parafibromin	MADVLSVLRQ	ADVLSVLRQY	A	99.5 ± 0.6	99.3 ± 1.4	-0.2	0.998
Q9EP71	RAI14_MOUSE	Ankycorbin	MKSLKAKFRK	MKSLKAKFRK	C	100 ± 0	100 ± 0	0.0	1.000
P10605	CATB_MOUSE	Cathepsin B	MWWSLILLSC	EDIDLPETFD	?	0.3 ± 0.2	0.3 ± 0.1	0.0	1.148
Q9CQJ6	DENR_MOUSE	Density-regulated protein	MATDISESSG	ATDISESSGA	A	99 ± 0.2	98.8 ± 0.6	-0.2	0.998

Table A2: N-terminome analysis of WT and Naa20$^{-/-}$ MEF cells (cont).

UniProt Accession	Entry Name	Protein Description	Theoretical N-ter Sequence	Observed N-ter Sequence	NAT type (observed)	WT %NTA	Naa20$^{-/-}$ %NTA	%NTA Difference (Naa20$^{-/-}$-WT)	Ratio %NTA (Naa20$^{-/-}$/WT)
Q8JZQ9	EIF3B_MOUSE	Eukaryotic translation initiation factor 3 subunit B	MQDAENVAVP	MQDAENVAVP	B	98.5 ± 1.5	98.2 ± 2.1	-0.4	0.996
Q9CXW4	RL11_MOUSE	60S ribosomal protein L11	MAQDQGEKEN	AQDQGEKENP	A	99.4 ± 0.6	99.3 ± 0.7	-0.1	0.999
P53810	PIPNA_MOUSE	Phosphatidylinositol transfer protein alpha isoform	MVLLKEYRVI	VLLKEYRVIL	A	0.6 ± 0.2	0.7 ± 0.5	0.1	1.121
P70349	HINT1_MOUSE	Histidine triad nucleotide-binding protein 1	MADEIAKAQV	ADEIAKAQVA	A	99.6 ± 0.3	99.6 ± 0.1	-0.1	0.999
Q8BK64	AHSA1_MOUSE	Activator of 90 kDa heat shock protein ATPase homolog 1	MAKWGEGDPR	AKWGEGDPRW	A	99.8 ± 0.2	99.6 ± 0.5	-0.2	0.998
Q8BJW6	EIF2A_MOUSE	Eukaryotic translation initiation factor 2A	MAPSTPLLTV	APSTPLLTVR	A	0.2 ± 0.2	0.3 ± 0.2	0.0	1.210
Q8CFE6	S38A2_MOUSE	Sodium-coupled neutral amino acid transporter 2	MKKTEMGRFN	MKKTEMGRFN	C	99.3 ± 1.3	99.6 ± 0.6	0.3	1.003
Q8C1B7	SEP11_MOUSE	Septin-11	MAVAVGRPSN	AVAVGRPSNE	A	98.7 ± 1	98.4 ± 1	-0.3	0.997
Q9QXS1	PLEC_MOUSE	Plectin	MVAGMLMPLD	VAGMLMPLDR	A	0.7 ± 0.4	0.6 ± 0.2	-0.1	0.824
P58069	RASA2_MOUSE	Ras GTPase-activating protein 2	MAAAAPAAAA	AAAAPAAAAS	A	99.4 ± 0.8	99.6 ± 0.3	0.2	1.002
P60867	RS20_MOUSE	40S ribosomal protein S20	MAFKDTGKTP	AFKDTGKTPV	A	98.4 ± 1.2	98.6 ± 0.9	0.2	1.002
Q9Z160	COG1_MOUSE	Conserved oligomeric Golgi complex subunit 1	MAAATASSAL	AAATASSALK	A	99.5 ± 0.5	99.7 ± 0.5	0.1	1.001
P61255	RL26_MOUSE	60S ribosomal protein L26	MKFNPFVTSD	MKFNPFVTSD	C	0.4 ± 0.5	0.5 ± 0.4	0.1	1.201
Q8BGA5	KRR1_MOUSE	KRR1 small subunit processome component homolog	MATSAEAPAK	ATSAEAPAKE	A	98.4 ± 0.7	98.6 ± 0.5	0.2	1.002
D3YXK2	SAFB1_MOUSE	Scaffold attachment factor B1	MAETLSGLGD	AETLSGLGDA	A	99 ± 1.3	99.3 ± 0.3	0.3	1.003
E9Q1P8	I2BP2_MOUSE	Interferon regulatory factor 2-binding protein 2	MAAAVAVAAA	AAAVAVAAAS	A	99.9 ± 0	99.9 ± 0.1	0.0	1.000
Q6PDM2	SRSF1_MOUSE	Serine/arginine-rich splicing factor 1	MSGGGVIRGP	SGGGVIRGPA	A	100 ± 0	100 ± 0	0.0	1.000
P20444	KPCA_MOUSE	Protein kinase C alpha type	MADVYPANDS	ADVYPANDST	A	99.2 ± 0.6	99.3 ± 0.6	0.1	1.001

Table A2: N-terminome analysis of WT and Naa20$^{-/-}$ MEF cells (cont).

UniProt Accession	Entry Name	Protein Description	Theoretical N-ter Sequence	Observed N-ter Sequence	NAT type (observed)	WT %NTA	Naa20$^{-/-}$ %NTA	%NTA Difference (Naa20$^{-/-}$-WT)	Ratio %NTA (Naa20$^{-/-}$/WT)
P52480	KPYM_MOUSE	Pyruvate kinase PKM)	MPKPHSEAGT	PKPHSEAGTA	?	1.3 ± 1	1.5 ± 0.8	0.1	1.112
Q62189	SNRPA_MOUSE	U1 small nuclear ribonucleoprotein A	MATIATMPVP	ATIATMPVPE	A	99.4 ± 0.6	99.3 ± 0.8	-0.1	0.999
P56391	CX6B1_MOUSE	Cytochrome c oxidase subunit 6B1	MAEDIKTKIK	AEDIKTKIKN	A	99 ± 0.9	98.6 ± 0.6	-0.4	0.996
Q8R5H1	UBP15_MOUSE	Ubiquitin carboxyl-terminal hydrolase 15	MAEGGAADLD	AEGGAADLDT	A	99.7 ± 0.5	99.6 ± 0.3	-0.1	0.999
Q91WM3	U3IP2_MOUSE	U3 small nucleolar RNA-interacting protein 2	MSTAVATRKR	STAVATRKRA	A	9.9 ± 4.9	11.9 ± 3.4	2.0	1.207
Q8R3F9	STPAP_MOUSE	Speckle targeted PIP5K1A-regulated poly(A) polymerase	MAAVDSDVVS	AAVDSDVVSL	A	98.9 ± 0.7	99.2 ± 0.8	0.2	1.002
Q78PY7	SND1_MOUSE	Staphylococcal nuclease domain-containing protein 1	MASSAQSSGS	ASSAQSSGSS	A	99.5 ± 0.4	99.4 ± 0.6	-0.1	0.999
Q8BJF9	CHM2B_MOUSE	Charged multivesicular body protein 2b	MASLFKKKTV	ASLFKKKTVD	A	99.3 ± 0.5	99 ± 1.2	-0.3	0.997
O08529	CAN2_MOUSE	Calpain-2 catalytic subunit	MAGIAIKLAK	AGIAIKLAKD	A	99 ± 1.1	99.3 ± 1.3	0.2	1.002
Q8BGB5	LIMD2_MOUSE	LIM domain-containing protein 2	MFQAAGAAQA	MFQAAGAAQA	C	98.3 ± 0.2	98.2 ± 0.4	-0.1	0.999
Q8CEC6	PPWD1_MOUSE	Peptidylprolyl isomerase domain and WD repeat-containing protein 1	MATESGSDSQ	ATESGSDSQL	A	99.2 ± 1	99.3 ± 0.6	0.2	1.002
Q91V61	SFXN3_MOUSE	Sideroflexin-3	MGDLPLNINI	GDLPLNINIQ	A	99.6 ± 0.5	99.7 ± 0.2	0.1	1.001
O08738	CASP6_MOUSE	Caspase-6	MTETDGFYKS	TETDGFYKSR	A	98.4 ± 0.2	98 ± 1.6	-0.3	0.997
P50580	PA2G4_MOUSE	Proliferation-associated protein 2G4	MSGEDEQQEQ	SGEDEQQEQT	A	99.1 ± 0.1	98.8 ± 1	-0.3	0.997
O08550	KMT2B_MOUSE	Histone-lysine N-methyltransferase 2B	MAAAAGGGSC	AAAAGGGSCP	A	98.3 ± 0.3	98.5 ± 0.9	0.2	1.002
P58252	EF2_MOUSE	Elongation factor 2	MVNFTVDQIR	VNFTVDQIRA	A	0.3 ± 0.2	0.3 ± 0.2	0.0	0.913
P97314	CSRP2_MOUSE	Cysteine and glycine-rich protein 2	MPVWGGGNKC	PVWGGGNKCG	?	11.9 ± 15.1	17.1 ± 16.2	5.2	1.439
P62874	GBB1_MOUSE	Guanine nucleotide-binding protein G(I)/G(S)/G(T) subunit beta-1	MSELDQLRQE	SELDQLRQEA	A	98.6 ± 2.2	99 ± 1.7	0.4	1.004
Q91YT7	YTHD2_MOUSE	YTH domain-containing family protein 2	MSASSLLEQR	SASSLLEQRP	A	97.5 ± 0.3	97.4 ± 0.9	-0.2	0.998

Table A2: N-terminome analysis of WT and Naa20$^{-/-}$ MEF cells (cont).

UniProt Accession	Entry Name	Protein Description	Theoretical N-ter Sequence	Observed N-ter Sequence	NAT type (observed)	WT %NTA	Naa20$^{-/-}$ %NTA	%NTA Difference (Naa20$^{-/-}$-WT)	Ratio %NTA (Naa20$^{-/-}$/WT)
Q99J36	THUM1_MOUSE	THUMP domain-containing protein 1	MATTAQQSPQ	ATTAQQSPQP	A	99.2 ± 0.9	99.1 ± 0.8	-0.1	0.999
Q6ZWY9	H2B1C_MOUSE	Histone H2B type 1-C/E/G	MPEPAKSAPA	AVTKAQKKDG	A?	2.3 ± 0.9	2.1 ± 0.8	-0.1	0.943
P26883	FKB1A_MOUSE	Peptidyl-prolyl cis-trans isomerase FKBP1A	MGVQVETISP	GVQVETISPG	A	0.9 ± 0.3	0.8 ± 0.4	0.0	0.944
Q8CHW4	EI2BE_MOUSE	Translation initiation factor eIF-2B subunit epsilon	MAATAAVPGA	AATAAVPGAA	A	99.3 ± 1.1	99.4 ± 0.3	0.1	1.001
Q9Z2R6	U119A_MOUSE	Protein unc-119 homolog A	MKVKKGGGGT	MKVKKGGGGT	C	3.4 ± 2	3.8 ± 0.9	0.5	1.143
P70122	SBDS_MOUSE	Ribosome maturation protein SBDS	MSIFTPTNQI	SIFTPTNQIR	A	95.3 ± 2.7	94.7 ± 3	-0.5	0.994
Q05816	FABP5_MOUSE	Fatty acid-binding protein 5	MASLKDLEGK	ASLKDLEGKW	A	99 ± 0.8	99.2 ± 0.8	0.1	1.001
Q3U7R1	ESYT1_MOUSE	Extended synaptotagmin-1	MEHSPEEGAS	MEHSPEEGAS	B	98.5 ± 1.4	98.2 ± 1.4	-0.2	0.997
Q99N96	RM01_MOUSE	39S ribosomal protein L1	MAAAVRCLRR	AAAAAATKPA	A?	0.8 ± 0.8	1 ± 1	0.1	1.173
Q91YT0	NDUV1_MOUSE	NADH dehydrogenase [ubiquinone] flavoprotein 1. mitochondrial	MLAARHFLGG	SSGTTAPKKT	A?	1.3 ± 0.6	1.5 ± 1.1	0.2	1.161
P60229	EIF3E_MOUSE	Eukaryotic translation initiation factor 3 subunit E	MAEYDLTTRI	AEYDLTTRIA	A	99.5 ± 0.8	99.6 ± 0.7	0.1	1.001
Q8BR90	CE051_MOUSE	UPF0600 protein C5orf51 homolog	MAAAVSGVVR	AAAVSGVVRR	A	98.3 ± 0.6	97.9 ± 2.1	-0.4	0.996
Q3UFK8	FRMD8_MOUSE	FERM domain-containing protein 8	MEGAEGNAGQ	MEGAEGNAGQ	B	99.4 ± 1	99.3 ± 0.4	-0.1	0.999
Q62448	IF4G2_MOUSE	Eukaryotic translation initiation factor 4 gamma 2	MESAIAEGGA	MESAIAEGGA	B	99.8 ± 0.3	99.7 ± 0.4	0.0	1.000
Q9WUK2	IF4H_MOUSE	Eukaryotic translation initiation factor 4H	MADFDTYDDR	ADFDTYDDRA	A	99.7 ± 0.4	99.7 ± 0.3	0.0	1.000
P35282	RAB21_MOUSE	Ras-related protein Rab-21	MAAAGGGAAA	AAAGGGAAAA	A	99.3 ± 0.5	99.4 ± 0.5	0.1	1.001
Q9WUL7	ARL3_MOUSE	ADP-ribosylation factor-like protein 3	MGLLSILRKL	GLLSILRKLK	A	0.3 ± 0.5	0.4 ± 0.5	0.1	1.306
Q8CI94	PYGB_MOUSE	Glycogen phosphorylase. brain form	MAKPLTDSER	AKPLTDSERQ	A	97.5 ± 2	97.9 ± 2.2	0.4	1.004
Q9CQI6	COTL1_MOUSE	Coactosin-like protein	MATKIDKEAC	ATKIDKEACR	A	99.6 ± 0.4	99.5 ± 0.5	-0.1	0.999

Table A2: N-terminome analysis of WT and Naa20$^{-/-}$ MEF cells (cont).

UniProt Accession	Entry Name	Protein Description	Theoretical N-ter Sequence	Observed N-ter Sequence	NAT type (observed)	WT %NTA	Naa20$^{-/-}$ %NTA	%NTA Difference (Naa20$^{-/-}$-WT)	Ratio %NTA (Naa20$^{-/-}$/WT)
P46978	STT3A_MOUSE	Dolichyl-diphosphooligosaccharide–protein glycosyltransferase subunit STT3A	MTKLGFLRLS	MTKLGFLRLS	C	5.5 ± 1.7	5.9 ± 1.7	0.4	1.069
Q9JLJ2	AL9A1_MOUSE	4-trimethylaminobutyraldehyde dehydrogenase	MSTGTFVVSQ	STGTFVVSQP	A	96 ± 1.6	95.7 ± 2.6	-0.3	0.997
P17225	PTBP1_MOUSE	Polypyrimidine tract-binding protein 1	MDGIVPDIAV	MDGIVPDIAV	B	99.6 ± 0.5	99.6 ± 0.5	0.1	1.001
P63158	HMGB1_MOUSE	High mobility group protein B1	MGKGDPKKPR	GKGDPKKPRG	A	1.6 ± 0.4	1.5 ± 0.5	0.0	0.970
P21550	ENOB_MOUSE	Beta-enolase	MAMQKIFARE	AMQKIFAREI	A	98.6 ± 1.9	98.2 ± 1.8	-0.5	0.995
Q9WV95	PHLA3_MOUSE	Pleckstrin homology-like domain family A member 3	MTAAATVLKE	TAAATVLKEG	A	99.5 ± 0.3	99.5 ± 0.4	-0.1	0.999
P16858	G3P_MOUSE	Glyceraldehyde-3-phosphate dehydrogenase	MVKVGVNGFG	VKVGVNGFGR	A	1.2 ± 0.6	1.1 ± 0.5	-0.1	0.955
Q7TPV4	MBB1A_MOUSE	Myb-binding protein 1A	MAEMKSPTKA	AEMKSPTKAE	A	99.8 ± 0.2	99.8 ± 0.2	0.0	1.000
Q9JJW6	ALRF2_MOUSE	Aly/REF export factor 2	MADKMDMSLD	ADKMDMSLDD	A	99.8 ± 0.2	99.8 ± 0.2	0.0	1.000
Q9CZD3	GARS_MOUSE	Glycine–tRNA ligase	MPCLLPSLLR	MDSAEELLAP	?	99.9 ± 0.2	99.8 ± 0.2	0.0	1.000
P80317	TCPZ_MOUSE	T-complex protein 1 subunit zeta	MAAVKTLNPK	AAVKTLNPKA	A	99.5 ± 0.5	99.5 ± 0.5	0.0	1.000
P22907	HEM3_MOUSE	Porphobilinogen deaminase	MSGNGGAATT	SGNGGAATTA	A	99.1 ± 1.1	99.3 ± 0.7	0.1	1.001
P61965	WDR5_MOUSE	WD repeat-containing protein 5	MATEEKKPET	ATEEKKPETE	A	99.2 ± 1.1	99.4 ± 1.2	0.1	1.001
Q3UZ39	LRRF1_MOUSE	Leucine-rich repeat flightless-interacting protein 1	MTSPEGAQNK	TSPEGAQNKE	A	99.1 ± 0.7	99 ± 1.2	-0.1	0.999
P63094	GNAS2_MOUSE	Guanine nucleotide-binding protein G(s) subunit alpha isoforms short	MGCLGNSKTE	GCLGNSKTED	A	5.7 ± 4.6	5 ± 6.5	-0.7	0.871
Q3URQ7	MTHSD_MOUSE	Methenyltetrahydrofolate synthase domain-containing protein	METQEGVSKQ	METQEGVSKQ	B	99.8 ± 0.1	99.8 ± 0.3	0.0	1.000
P17742	PPIA_MOUSE	Peptidyl-prolyl cis-trans isomerase A	MVNPTVFFDI	MVNPTVFFDI	C	99.5 ± 0.2	99.5 ± 0.2	0.0	1.000
P53996	CNBP_MOUSE	Cellular nucleic acid-binding protein	MSSNECFKCG	SSNECFKCGR	A	99.5 ± 0.5	99.5 ± 0.5	0.0	1.000
P62900	RL31_MOUSE	60S ribosomal protein L31	MAPAKKGGEK	APAKKGGEKK	A	1.1 ± 0.3	1.1 ± 0.2	0.0	0.978
P26350	PTMA_MOUSE	Prothymosin alpha	MSDAAVDTSS	SDAAVDTSSE	A	96.9 ± 1.2	96.6 ± 2.4	-0.3	0.997

Table A2: N-terminome analysis of WT and Naa20$^{-/-}$ MEF cells (cont).

UniProt Accession	Entry Name	Protein Description	Theoretical N-ter Sequence	Observed N-ter Sequence	NAT type (observed)	WT %NTA	Naa20$^{-/-}$ %NTA	%NTA Difference (Naa20$^{-/-}$-WT)	Ratio %NTA (Naa20$^{-/-}$/WT)
Q9DCT2	NDUS3_MOUSE	NADH dehydrogenase	MAAAAARVWC	ESAAADKRPT	?	0.1 ± 0	0.1 ± 0	0.0	1.074
P51410	RL9_MOUSE	60S ribosomal protein L9	MKTILSNQTV	MKTILSNQTV	C	0.5 ± 0.1	0.5 ± 0.1	0.0	0.960
P62317	SMD2_MOUSE	Small nuclear ribonucleoprotein Sm D2	MSLLNKPKSE	SLLNKPKSEM	A	99.4 ± 0.7	99.4 ± 0.5	0.1	1.001
Q8BTM8	FLNA_MOUSE	Filamin-A	MSSSHSRCGQ	PATEKDLAED	?	1.9 ± 0.1	1.8 ± 0.5	-0.1	0.958
P97470	PP4C_MOUSE	Serine/threonine-protein phosphatase 4 catalytic subunit	MAEISDLDRQ	AEISDLDRQI	A	99.9 ± 0.1	99.8 ± 0.3	0.0	1.000
P47757	CAPZB_MOUSE	F-actin-capping protein subunit beta	MSDQQLDCAL	SDQQLDCALD	A	99.5 ± 0.5	99.6 ± 0.5	0.0	1.000
P97310	MCM2_MOUSE	DNA replication licensing factor MCM2	MAESSESLSA	AESSESLSAS	A	98.9 ± 0.9	98.8 ± 0.8	-0.1	0.999
Q8K2C9	HACD3_MOUSE	Very-long-chain (3R)-3-hydroxyacyl-CoA dehydratase 3	METQVLTPHV	METQVLTPHV	B	99.9 ± 0.1	99.9 ± 0.1	0.0	1.000
Q99J77	SIAS_MOUSE	Sialic acid synthase	MPLELELCPG	PLELELCPGR	?	0.4 ± 0.3	0.4 ± 0.2	0.0	1.055
Q9WV80	SNX1_MOUSE	Sorting nexin-1	MASGGGGCSA	ASGGGGCSAS	A	100 ± 0	100 ± 0	0.0	1.000
O35129	PHB2_MOUSE	Prohibitin-2	MAQNLKDLAG	AQNLKDLAGR	A	99.4 ± 0.4	99.5 ± 0.5	0.0	1.000
P14733	LMNB1_MOUSE	Lamin-B1	MATATPVQQQ	ATATPVQQQR	A	99.4 ± 0.7	99.3 ± 0.8	-0.1	0.999
Q00612	G6PD1_MOUSE	Glucose-6-phosphate 1-dehydrogenase X	MAEQVALSRT	AEQVALSRTQ	A	99.7 ± 0.4	99.7 ± 0.2	0.0	1.000
P61804	DAD1_MOUSE	Dolichyl-diphosphooligosaccharide–protein glycosyltransferase subunit DAD1	MSASVVSVIS	SASVVSVISR	A	91.8 ± 3.3	92 ± 3.1	0.2	1.002
Q8K3I9	GLCI1_MOUSE	Glucocorticoid-induced transcript 1 protein	MSTASSSSSQ	STASSSSSQT	A	99.7 ± 0.1	99.7 ± 0.3	0.0	1.000
P19324	SERPH_MOUSE	Serpin H1	MRSLLLGTLC	AEVKKPLEAA	A?	1.1 ± 0.1	1.1 ± 0.3	0.0	0.977
P49312	ROA1_MOUSE	Heterogeneous nuclear ribonucleoprotein A1	MSKSESPKEP	SKSESPKEPE	A	99.2 ± 0.4	99.2 ± 0.6	0.0	1.000
O88485	DC1I1_MOUSE	Cytoplasmic dynein 1 intermediate chain 1	MSDKSDLKAE	SDKSDLKAEL	A	99.5 ± 0.5	99.5 ± 0.6	0.0	1.000
O35343	IMA3_MOUSE	Importin subunit alpha-3	MADNEKLDNQ	ADNEKLDNQR	A	99.6 ± 0.4	99.6 ± 0.4	0.0	1.000

Table A2: N-terminome analysis of WT and Naa20$^{-/-}$ MEF cells (cont).

UniProt Accession	Entry Name	Protein Description	Theoretical N-ter Sequence	Observed N-ter Sequence	NAT type (observed)	WT %NTA	Naa20$^{-/-}$ %NTA	%NTA Difference (Naa20$^{-/-}$-WT)	Ratio %NTA (Naa20$^{-/-}$/WT)
P63085	MK01_MOUSE	Mitogen-activated protein kinase 1	MAAAAAAGPE	AAAAAAGPEM	A	99.4 ± 0.8	99.4 ± 0.7	0.0	1.000
Q3UDR8	YIPF3_MOUSE	Protein YIPF3	MATPAAPASG	ATPAAPASGV	A	96.9 ± 1.8	97 ± 0.6	0.1	1.001
P08030	APT_MOUSE	Adenine phosphoribosyltransferase	MSEPELKLVA	SEPELKLVAR	A	99.5 ± 0.6	99.4 ± 0.8	0.0	1.000
Q8CBY8	DCTN4_MOUSE	Dynactin subunit 4	MASLLQSERV	ASLLQSERVL	A	99.4 ± 0.7	99.5 ± 0.5	0.1	1.001
Q9CX34	SGT1_MOUSE	Protein SGT1 homolog	MAAAAAGPAS	AAAAAGPASS	A	99.5 ± 0.4	99.5 ± 0.4	0.0	1.000
Q923T9	KCC2G_MOUSE	Calcium/calmodulin-dependent protein kinase type II subunit gamma	MATTATCTRF	ATTATCTRFT	A	100 ± 0	100 ± 0	0.0	1.000
Q9JKP8	CHRC1_MOUSE	Chromatin accessibility complex protein 1	MADAAVGKEK	ADAAVGKEKC	A	99.3 ± 0.5	99.4 ± 0.6	0.0	1.000
P17932	RL32P_MOUSE	Putative 60S ribosomal protein L32'	MAALRPLVKP	AALRPLVKPK	A	2.2 ± 0.6	2.3 ± 0.6	0.0	1.017
Q91VI7	RINI_MOUSE	Ribonuclease inhibitor	MSLDIQCEQL	SLDIQCEQLS	A	99.4 ± 0.6	99.5 ± 0.5	0.0	1.000
P46978	STT3A_MOUSE	Dolichyl-diphosphooligosaccharide–protein glycosyltransferase subunit STT3A	MTKLGFLRLS	TKLGFLRLSY	A	1.2 ± 0.9	1.2 ± 0.8	-0.1	0.953
Q6PGH2	JUPI2_MOUSE	Jupiter microtubule associated homolog 2	MFQGADSQAG	MFQGADSQAG	C	99.5 ± 0.5	99.6 ± 0.8	0.0	1.000
P09411	PGK1_MOUSE	Phosphoglycerate kinase 1	MSLSNKLTLD	SLSNKLTLDK	A	99.8 ± 0.3	99.8 ± 0.1	0.0	1.000
P17225	PTBP1_MOUSE	Polypyrimidine tract-binding protein 1	MDGIVPDIAV	SSSASAANGN	A?	98.9 ± 1.2	98.9 ± 1	0.0	1.000
O88543	CSN3_MOUSE	COP9 signalosome complex subunit 3	MASALEQFVN	ASALEQFVNS	A	99.6 ± 0.5	99.6 ± 0.5	0.0	1.000
Q9Z175	LOXL3_MOUSE	Lysyl oxidase homolog 3	MRAVSVWYCC	SPSPSISPEK	A?	1.1 ± 0.2	1 ± 0.8	-0.1	0.951
Q9Z1Q9	SYVC_MOUSE	Valine–tRNA ligase	MSILYVSPHP	SILYVSPHPD	A	99.4 ± 0.2	99.4 ± 0.1	0.0	1.000
O35143	ATIF1_MOUSE	ATPase inhibitor	MAGSALAVRA	DSSDSMDTGA	?	0.2 ± 0.1	0.2 ± 0.1	0.0	0.985
Q8CF66	LTOR4_MOUSE	Ragulator complex protein LAMTOR4	MTSALTQGLE	TSALTQGLER	A	99.3 ± 0.3	99.3 ± 0.4	0.0	1.000
Q9CZY3	UB2V1_MOUSE	Ubiquitin-conjugating enzyme E2 variant 1	MAATTGSGVK	AATTGSGVKV	A	99.4 ± 0.8	99.4 ± 0.6	0.0	1.000
Q9D8N0	EF1G_MOUSE	Elongation factor 1-gamma	MAAGTLYTYP	AAGTLYTYPE	A	99.2 ± 0.4	99.2 ± 0.5	0.0	1.000

Table A2: N-terminome analysis of WT and Naa20$^{-/-}$ MEF cells (cont).

UniProt Accession	Entry Name	Protein Description	Theoretical N-ter Sequence	Observed N-ter Sequence	NAT type (observed)	WT %NTA	Naa20$^{-/-}$ %NTA	%NTA Difference (Naa20$^{-/-}$-WT)	Ratio %NTA (Naa20$^{-/-}$/WT)
P18760	COF1_MOUSE	Cofilin-1	MASGVAVSDG	ASGVAVSDGV	A	99.8 ± 0.2	99.8 ± 0.1	0.0	1.000
Q91WV0	NC2B_MOUSE	Protein Dr1	MASSSGNDDD	ASSSGNDDDL	A	99.3 ± 0.6	99.2 ± 0.3	0.0	1.000
P08113	ENPL_MOUSE	Endoplasmin	MRVLWVLGLC	DDEVDVDGTV	?	0.4 ± 0.2	0.4 ± 0.2	0.0	1.010
P62908	RS3_MOUSE	40S ribosomal protein S3	MAVQISKKRK	AVQISKKRKF	A	99.3 ± 0.7	99.3 ± 0.7	0.0	1.000
Q9R0P3	ESTD_MOUSE	S-formylglutathione hydrolase	MALKQISSNR	ALKQISSNRC	A	99.2 ± 0.7	99.2 ± 0.9	0.0	1.000
P29758	OAT_MOUSE	Ornithine aminotransferase	MLSKLASLQT	TSVATKKTEQ	A?	0.7 ± 0.6	0.7 ± 0.3	0.0	0.992
Q3THW5	H2AV_MOUSE	Histone H2A.V	MAGGKAGKDS	AGGKAGKDSG	A	3.3 ± 1.6	3.2 ± 1.6	0.0	0.993
Q9EP72	EMC7_MOUSE	ER membrane protein complex subunit 7	MAGALWGFFS	SEVPGAAAEG	A?	0.3 ± 0.2	0.3 ± 0.2	0.0	0.993
Q9CQ49	NCBP2_MOUSE	Nuclear cap-binding protein subunit 2	MSGGLLKALR	SGGLLKALRS	A	99.6 ± 0.3	99.6 ± 0.4	0.0	1.000
Q9D8B3	CHM4B_MOUSE	Charged multivesicular body protein 4b	MSVFGKLFGA	SVFGKLFGAG	A	99 ± 0.9	99 ± 0.8	0.0	1.000
O35143	ATIF1_MOUSE	ATPase inhibitor	MAGSALAVRA	VSDSSDSMDT	A?	0.2 ± 0.1	0.2 ± 0.2	0.0	1.003
Q6ZPY7	KDM3B_MOUSE	Lysine-specific demethylase 3B	MADAAASPVG	ADAAASPVGK	A	100 ± 0	100 ± 0	0.0	1.000